CATÓLICA
ESCOLA SUPERIOR DE BIOTECNOLOGIA
PORTO

DESIGN OF PAPER-BASED ANALYTICAL DEVICES FOR CHEMICAL AND BIOCHEMICAL ASSAYS OF BIOMARKERS IN BIOLOGICAL FLUIDS OF NON-INVASIVE COLLECTION

Thesis submitted to Universidade Católica Portuguesa to attain the degree of PhD in Biotechnology, with specialization in Chemistry

Francisca Teixeira Soares da Mota Ferreira

February of 2025

CATÓLICA
ESCOLA SUPERIOR DE BIOTECNOLOGIA
PORTO

DESIGN OF PAPER-BASED ANALYTICAL DEVICES FOR CHEMICAL AND BIOCHEMICAL ASSAYS OF BIOMARKERS IN BIOLOGICAL FLUIDS OF NON-INVASIVE COLLECTION

Thesis submitted to Universidade Católica Portuguesa to attain the degree of PhD in Biotechnology, with specialization in Chemistry

Francisca Teixeira Soares da Mota Ferreira

Supervisor: Raquel B. R. Mesquita, Ph.D.
Co-supervisor: António O. S. S. Rangel, Full Professor

February of 2025

To my parents,
for all the support and encouragement throughout my entire life,
but most of all for always believing in me!

Abstract

Abstract

Ensuring basic healthcare access around the world remains a challenge, particularly in low-income regions. In response, international initiatives such as the Sustainable Development Goals (SDGs) and the World Health Organization (WHO) guidelines emphasize the need to develop innovative, accessible, and cost-effective diagnostic tools. Point-of-care testing has emerged as an ideal solution, enabling rapid and decentralized analysis. Among these type of devices, microfluidic paper-based analytical devices (μPADs) have gained attention due to their affordability, portability, and ease of use, making them a particularly valuable tool in resource-limited locations.

The purpose of the work presented throughout this thesis was to design and develop innovative point-of-care methodologies based on the μPAD approach for the determination of several health-related parameters, that could serve as an adding tool in the diagnosis and monitoring of several health conditions. The use of biological samples of non-invasive collection, such as saliva and urine, enhances diagnostic accessibility, particularly in point-of-care settings where traditional sample collection may be impractical or even impossible. Additionally, this thesis also explores the use of colorimetric detection methods, a straightforward approach to quantifying the targeted analytes by producing visible colour changes. To further improve the specificity and accuracy of these diagnostic tools, enzymatic reactions were incorporated into some of the developed μPADs.

The first developed device was dedicated to the quantification of total iron in urine samples by using the colorimetric reaction of bathophenanthroline with iron (II) coupled with hydroxylamine, a well-known reducing agent capable of converting iron (III) in iron (II). To handle the potential colour of the urine samples, a sample blank was included in the device. This feature was vital to ensure the applicability of the developed μPAD, as urine may present a wide variability of colour range, from light yellow to brownish.

The determination of nitrate was also accomplished in urine samples with a newly developed μPAD. This device included the enzymatic reaction of nitrate reductase to perform the conversion of nitrate to nitrite and the Griess reagent which provided the colorimetric detection of the resulting nitrite. In order to delay the vertical flow and increase the extent of the enzymatic reaction, a hydrophilic membrane layer was also incorporated into the device. The small porosity of this membrane also led to the retention of the compound responsible for the colour of urine, enabling a direct analysis of the samples.

The next devices developed performed the quantification of NH_X and urea in saliva samples but with a more complex approach. Not only were the devices composed of four layers, but the detection relies on the diffusion of NH_3 (g) through a gas-diffusion membrane to produce a colorimetric change of a pH indicator. The hydrophobicity of this membrane also helped eliminate possible interferences of the saliva sample in the colorimetric reaction, since it did not allow the sample to pass through the membrane and reach the colour reagent.

The urea determination was accomplished by including urease in the device, since it selectively catalyzes the dissociation of urea in ammonia and carbon dioxide. The urease activity determination

was accomplished using a similar structure and reactions to the one used for the urea μPAD. However, the determination itself was achieved using the kinetic capabilities of the enzyme by correlating to the urease activity with the variation of the signal obtained between two different enzymatic reaction times. This strategy not only allowed a more accurate quantification but also suppressed the influence of NH_X already present in the samples.

The last device developed using the μPAD structure approach was to quantify glucose in saliva samples. With only two layers in its composition, this device uses a combination of two enzymatic reactions. First, glucose oxidase converts glucose into gluconic acid and hydrogen peroxide, then followed by the release of oxygen from hydrogen peroxide performed by peroxidase. The colorimetric detection is accomplished with the oxidation of o-dianisidine. In this work, a correlation between the concentration of glucose in saliva and blood was also successfully established, using #5 saliva samples of diabetic patients and the correspondent glucometer measurements provided by the patients.

A rather different approach was used to perform the semi-quantitative analysis of *E. coli* DNA. Instead of developing a μPAD, an option was made to design a barcode-style lateral flow strip that would allow the semi-quantitative detection of *E. coli*. The amplification of the DNA in the sample was performed using the Loop-Mediated Isothermal Amplification (LAMP) technique since it can be performed at a constant temperature and provides high sensitivity and specificity results. The developed methodology, although requiring further optimization, showed reliable performance and offers a rapid, cost-effective method for *E.* coli detection.

Overall, this thesis demonstrates the potential of microfluidic paper-based analytical devices and lateral flow assays as innovative, cost-effective diagnostic tools for point-of-care applications. By addressing critical challenges such as sample complexity, reagent stability, and measurement accuracy, the developed devices enhance accessibility to reliable testing, particularly in resource-limited settings. Their affordability and ease of use further emphasize their role in expanding diagnostic capabilities outside traditional laboratory environment.

Keywords: microfluidic analytical tools; colorimetric detection; point-of-care analysis; saliva and urine samples.

Resumo

Resumo

Garantir o acesso a cuidados básicos de saúde em todo o mundo continua um desafio, especialmente em regiões com baixos rendimentos. Em resposta, iniciativas internacionais como os Objetivos de Desenvolvimento Sustentável (ODS) e as diretrizes da Organização Mundial da Saúde (OMS) enfatizam a necessidade de desenvolver metodologias de diagnóstico inovadoras, acessíveis e económicas. Os testes "point-of-care" surgiram como uma solução ideal, permitindo análises rápidas e realizadas fora do laboratório. Entre este tipo de testes, os dispositivos analíticos microfluídicos baseados em papel (μPADs) têm ganho atenção devido à sua acessibilidade, portabilidade e facilidade de uso, tornando-os uma ferramenta particularmente valiosa em locais em que os recursos são limitados.

O objetivo do trabalho apresentado ao longo desta tese foi delinear e desenvolver metodologias inovadoras "point-of-care" com base na metodologia dos μPADs para a determinação de vários parâmetros importantes para a saúde, que podem servir como uma ferramenta adicional no diagnóstico e monitorização de várias doenças. O uso de amostras biológicas de colheita não invasiva, como saliva e urina, aumenta a acessibilidade diagnóstica, especialmente em ambientes de ponto de atendimento onde a coleta tradicional de amostras pode ser impraticável ou mesmo impossível. Além disso, esta tese também explora o uso de métodos de deteção colorimétrica, uma abordagem direta para quantificar os analitos produzindo mudanças de cor visíveis. Para melhorar ainda mais a especificidade e a precisão dessas ferramentas de diagnóstico, reações enzimáticas foram incorporadas em alguns dos μPADs desenvolvidos.

O primeiro dispositivo desenvolvido foi dedicado à quantificação de ferro total em amostras de urina usando a reação colorimétrica da batofenantrolina com ferro (II) juntamente com hidroxilamina, um conhecido agente redutor capaz de converter ferro (III) em ferro (II). Para lidar com a cor das amostras de urina, um branco de amostra foi incluído no dispositivo. Esta estratégia foi vital para garantir a aplicabilidade do μPAD desenvolvido, pois a urina pode apresentar uma ampla variabilidade de cor, de amarelo claro a acastanhado.

A determinação de nitrato também foi realizada em amostras de urina com um μPAD desenvolvido. Este dispositivo incluiu a reação enzimática da nitrato redutase para realizar a conversão de nitrato em nitrito, e o reagente de Griess que permitiu a deteção colorimétrica do nitrito resultante. Para atrasar o fluxo vertical e aumentar a extensão da reação enzimática, uma camada de membrana hidrofílica também foi incorporada no dispositivo. A baixa porosidade desta membrana também permitiu a retenção dos compostos responsáveis cor à urina, permitindo asimm uma análise direta das amostras.

Os seguintes dispositivos desenvolvidos efetuaram a quantificação de NH_X e ureia em amostras de saliva, mas com uma abordagem mais complexa. Além dos dispositivos serem compostos de 4 camadas, a deteção depende da difusão de NH_3 (g) através de uma membrana de difusão de gás para produzir uma mudança colorimétrica do indicador de pH. A hidrofobicidade desta membrana também ajudou a eliminar possíveis interferências da amostra de saliva na reação

colorimétrica, uma vez que não permitiu que a amostra passasse através da membrana e atingisse o reagente de cor. A determinação da ureia foi conseguida incluindo urease no dispositivo, uma vez que catalisa seletivamente a dissociação da ureia em amoníaco e dióxido de carbono.

A determinação da atividade da urease foi realizada usando uma estrutura e reações semelhantes às usadas para o μPAD da ureia, no entanto, a determinação em si foi realizada usando as capacidades cinéticas da enzima, estabelecendo uma relação entre a atividade da urease e a variação do sinal obtido entre dois tempos de reação enzimática diferentes. Essa estratégia não só permitiu uma quantificação mais precisa, mas também suprimiu a influência do NH_X já presente nas amostras.

O último dispositivo desenvolvido usando a abordagem de μPAD foi para quantificar glucose em amostras de saliva. Com apenas duas camadas na sua composição, este dispositivo usa uma combinação de duas reações enzimáticas. Primeiro, a glucose oxidase converte glucose em ácido glucônico e peróxido de hidrogênio, seguido pela liberação de oxigênio do peróxido de hidrogênio realizada pela peroxidase. A deteção colorimétrica é realizada com a oxidação de o-dianisidina. Neste trabalho, uma correlação entre a concentração de glucose na saliva e no sangue também foi estabelecida com sucesso, usando #5 amostras de saliva de pacientes diabéticos e as correspondentes medições do glicosímetro fornecidas pelos pacientes.

Foi usada uma abordagem bastante diferente para realizar a análise semi-quantitativa do DNA de *E. coli.* Em vez de desenvolver um μPAD, optou-se por desenvolver uma tira de fluxo lateral em estilo de código de barras que permitisse a deteção semi-quantitativa de *E.* coli. A amplificação do DNA na amostra foi realizada usando a técnica de amplificação isotérmica mediada por loop (LAMP), pois pode ser realizada a uma temperatura constante e produz resultados de alta sensibilidade e especificidade. A metodologia desenvolvida, embora necessite de maior otimização, mostrou um bom desempenho e podendo ser considerado como um método rápido e económico para deteção de *E. coli*.

No geral, esta tese demonstra o potencial tanto de dispositivos analíticos baseados em papel como de testes de fluxo lateral, como ferramentas de diagnóstico inovadoras e económicas para aplicações point-of-care. Ao encarar desafios críticos como complexidade da amostra, estabilidade dos reagentes e precisão da medição, os dispositivos desenvolvidos aumentam a acessibilidade a testes de confiança, especialmente em zonas com recursos limitados. Sua acessibilidade e facilidade de uso enfatizam ainda mais seu papel na expansão das capacidades de diagnóstico fora dos ambientes laboratoriais tradicionais.

Palavras-Chave: ferramentas analíticas de microfluxo; deteção colorimétrica; análise point-of-care; amostras de saliva e urina.

Acknowledgements

Acknowledgements

To Escola Superior de Biotecnologia – _Universidade Católica Portuguesa for receiving me first as a graduation, then as a master student and finally as a PhD student, providing all the necessary conditions to accomplish all the work I developed. A special thanks for giving me the opportunity of teaching undergraduate students, it truly was an enrichment experience.

To Fundação para a Ciência e a Tecnologia (FCT) for the grant awarded (SFRH/BD/144962/2019) and the financial support which allowed me to do this work.

To my supervisor Dr. Raquel Mesquita and co-supervisor Prof. Dr. António Rangel. I cannot put into words how grateful I am for your support. This PhD adventure began many years ago when you first accepted me to do my master thesis in your laboratory and, without that, I am sure I would not be where I am today, both personally and professionally. I want to thank you for all the opportunities you have given me, like encouraging me to present my work in multiple conferences, letting me be part of the organisation committee of the 11th Meeting of the Analytical Chemistry Division, and inviting me to teach undergraduate students. I have learned immensely with all those experiences. I will be forever grateful for the insightful discussions, the challenges, the constructive criticism, the motivation, the kindness and care you have offered all these years, that made me grow and that have helped shape who I am today.

To Dr. Julien Reboud, from University of Glasgow, for receiving me in his lab at the Mazumdar-Shaw Advanced Research Center. Thank you for giving me freedom to explore other methodologies and techniques, while also giving guidance and support.

To Pawel Jajesniak, for his constant guidance and help in work developed in my stay in Glasgow.

To everyone in the Mazumdar-Shaw Advanced Research Center for their hospitality and friendship, in particular Giulia and Ella.

Another special thank you to Ana Machado, for her valuable help not only in validation the device for determination of glucose, but also in the writing stage of the *E. coli* determination work.

To my colleagues and friends, who have put a smile in my face every single day, even in the bad ones: Juliana Aguiar, Mafalda Pereira, Maria Melo, Raquel Teixeira, Tânia Ribas. Thank you for your friendship, help and support, always.

Acknowledgements

To all my friends at home and in ballet class, for their patience, support and friendship. A special thank you to Mariana and Sara for their true friendship, and Carolina Araújo, the ballet teacher who was always there with kind advice and support.

A very special thank you to my family: my grandmother, my godmother, my goddaughter, my brother, but most of all my parents for all their love and support, every single day. It was your faith in me that enabled me to believe I could ever achieve this.

To João, the one that held my hand through the ups and downs, thank you for all the patience during these years, and for being always by my side encouraging me.

Table of Contents

Table of Contents

Chapter 1. General Introduction

1.1. Analytical Tools in Today's World

Medical innovations have occurred throughout history, and with the advancements in medical and technological knowledge, the ability to treat complex diseases has increased. For example, the discovery of penicillin in 1928 revolutionized the treatment of infectious diseases, while more recent innovations such as immunotherapy and mRNA vaccines have transformed how we address cancer and pandemics like COVID-19 (1,2). Still, according to the World Health Organization (WHO), in the 21st century more than half of the world's population does not have access to essential basic health care, and this is particularly observed in more impoverished and secluded communities (3,4).

To achieve a more peaceful and prosperous future for the people and the planet, in 2015 the United Nations released the 17 Sustainable Development Goals (SDGs). Among them, goals 3 and 10 highlight the need to ensure health and well-being for all, and the need to reduce inequalities within and among countries (5). However, even though health service coverage has generally expanded, progress began to decelerate after 2015, which coincides with the adoption of the Sustainable Development Goals (4). While substantial strides have been made in providing services for infectious diseases, coverage for other diseases has shown minimal advancement (4). Chronic conditions such as diabetes and hypertension remain underserved in many low-income countries due to limited resources and a lack of trained medical personnel (6,7). As reported by WHO, in 2021 approximately 4.5 billion people lacked access to essential health services (4).

To guide research to the development of new diagnoses and treatment techniques that could respond to the identified needs, in 2006 the WHO outlined the ASSURED guidelines. These guidelines indicate that these techniques should be affordable, sensitive, specific, user-friendly, rapid and robust, equipment-free, and deliverable to end users (8,9). Recently, two additional guidelines were proposed: R for Real-time connectivity and E for Ease of specimen collection and environmental friendliness, making the final acronym REASSURED (10). These guidelines have already demonstrated their utility in real-world applications. Rapid diagnostic tests (RDTs) for malaria have helped reduce malaria-related mortality in Sub-Saharan Africa by being portable, low-cost, and easy to use (11,12). Similarly, COVID-19 antigen tests exemplify REASSURED principles through their real-time reporting capabilities and minimal environmental impact. These added guidelines ensure the adaptation to modern innovations in technology while also addressing the growing emphasis on environmental responsibility. However, despite the global emphasis on SDGs, inequalities in healthcare persist. For example, life expectancy disparities highlight ongoing inequities: high-income countries report averages of over 80 years, while life expectancy in some low-income nations is still below 60 years (13). Addressing these inequalities requires not only technological innovation but also substantial policy reforms. By incorporating these strategies and leveraging frameworks like REASSURED, the global health community can work toward reducing the 4 billion gap in essential healthcare access and achieving the vision outlined by the Sustainable Development Goals. To help bridge this gap it is necessary to invest in the development of innovative diagnostic solutions with enhance accessibility and efficiency.

1.2. Point-of-Care Devices

Point-of-care devices are an interesting tool for medical diagnosis and monitoring since they comply with most, if not all, of the guidelines outlined by WHO. As indicated by its name, these devices are portable and used on-site of care, which is a considerable advantage in areas where nearby care is not available. Furthermore, the improved microfluidics, miniaturization, and data processing techniques available allow a quick detection and quantification of biochemical markers with a reasonable sensitivity and selectivity, making it a reliable alternative to laboratory-based methodologies (14). This is why in the last few years there has been a consistent increase in the number of publications related to point-of-care devices, as shown in Figure 1.1.

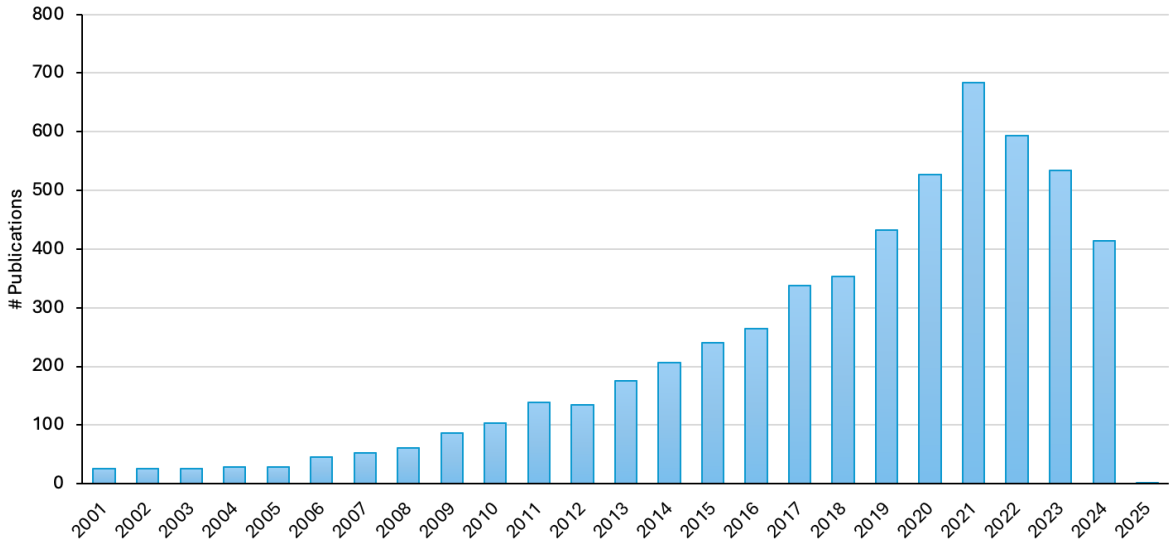

Figure 1.1 – Evolution of the number of publications on point-of-care devices throughout the years; Web of Science search performed on 17/10/2024 ("point-of-care device(s)" or "point-of-care test(s)").

The recent COVID pandemic is an example of the importance of rapid, point-of-care testing, since the self-testing COVID test allows the detection of the disease with decent accuracy, consequently reducing the demand for hospital/laboratory testing (14). However, there are other examples of commonly used devices, such as pregnancy tests, heart rate sensors, and pulse oximeters.

Paper-based devices are a point-of-care technique that not only fulfils the requirements outlined by WHO but have also been responsible for a big revolution in self-diagnosis as we currently know it (15). Paper is the most used platform for the development of point-of-care devices because it holds several characteristics that are considered advantageous (16). Paper is low-cost, lightweight, easy to obtain, store, and transport, while also being disposable and environmentally friendly, which aligns with the needs of point-of-care devices and guidelines of WHO (15,17). Furthermore, this material can be obtained in different colours, sizes, shapes, thicknesses, porosities, and treatments, which allows a detailed tailoring of the material and its characteristics such as hydrophobicity, permeability, conductivity, colour distribution, and overall reactivity (15,18).

Paper can also undergo different modification processes including cutting, coating, printing, and lamination, which further increases its versatility (15). However, the main characteristic that makes paper a suitable platform for point-of-care devices is the microporous structure, provided by its cellulose matrix, which allows the absorption and drive of fluids by capillary force, without the need for additional external pumping devices (9,15,17,18). Additionally, the cellulose matrix can also act as a filter for the separation of larger unwanted compounds, performing a rudimentary pre-treatment of the sample (17). Nevertheless, the use of paper for analytical procedures is not recent. It dates back to 1952, with the paper-based chromatography that won a Nobel Prize in Chemistry for Martin and Synge (9,16). From that time, the use of paper as a platform for analysis has continuously developed across areas of application, particularly in point-of-care devices (19).

Among the paper-based point-of-care devices, two types stand out: lateral flow assay devices (LFAs) and microfluidic paper-based analytical devices (μPADs). This categorization is mainly due to the use of different materials and design techniques. For example, while LFA are typically prepared with nitrocellulose membrane as its platform, μPADs on the other hand, usually use filter paper (cellulose). The characteristics and applications of these types of devices are further described in the following sections.

1.2.1. Lateral Flow Assays

The LFA is one of the most common methodologies in point-of-care diagnosis in the world since it allows the detection of the analytes within a few minutes (20). It can be used in a variety of applications from clinical diagnosis to food safety or even environmental monitoring.

Nevertheless, it is not a recently developed method, it actually dates back to the 1940s when Martin and Synge first reported paper chromatography (17,18). From then, several diagnosis kits were developed, one of the first being the semi-quantitative test developed in 1956 by Plotz for the detection of glucose in urine (18). However, only in 1984, LFA tests were made commercially available, with the urine-based pregnancy test (18). Currently several other tests are commercialized, such as for the detection of malaria, human immunodeficiency virus (HIV), and influenza A/B, but to this day, the LFA pregnancy test is one of the most used (21). In 2020, the COVID-19 pandemic brought the LFAs to the spotlight once again (18). The need for simple, rapid, on-hand diagnosis on a global scale led to the use of over 3 billion tests by late 2022, which removed a great amount of pressure from the healthcare testing facilities (18,21).

The conventional LFA strip is usually composed of four main components (Figure 1.2(A)): the sample pad, the conjugate pad, the reaction membrane, and the absorption pad (17,18,22,23). To initiate the test, the sample is placed on the sample pad (Figure 1.2(B)), which is generally composed of cellulose or glass fiber, and it has the purpose of evenly transporting the sample to the conjugate pad (18,20,24). Usually, this component contains buffer salts, proteins, and other substances that facilitate the control of the flow in the device and help in the interaction with the other components (20,23). Furthermore, this component can also be used to perform sample pre-treatment, such as component separation or interference elimination (18,24).

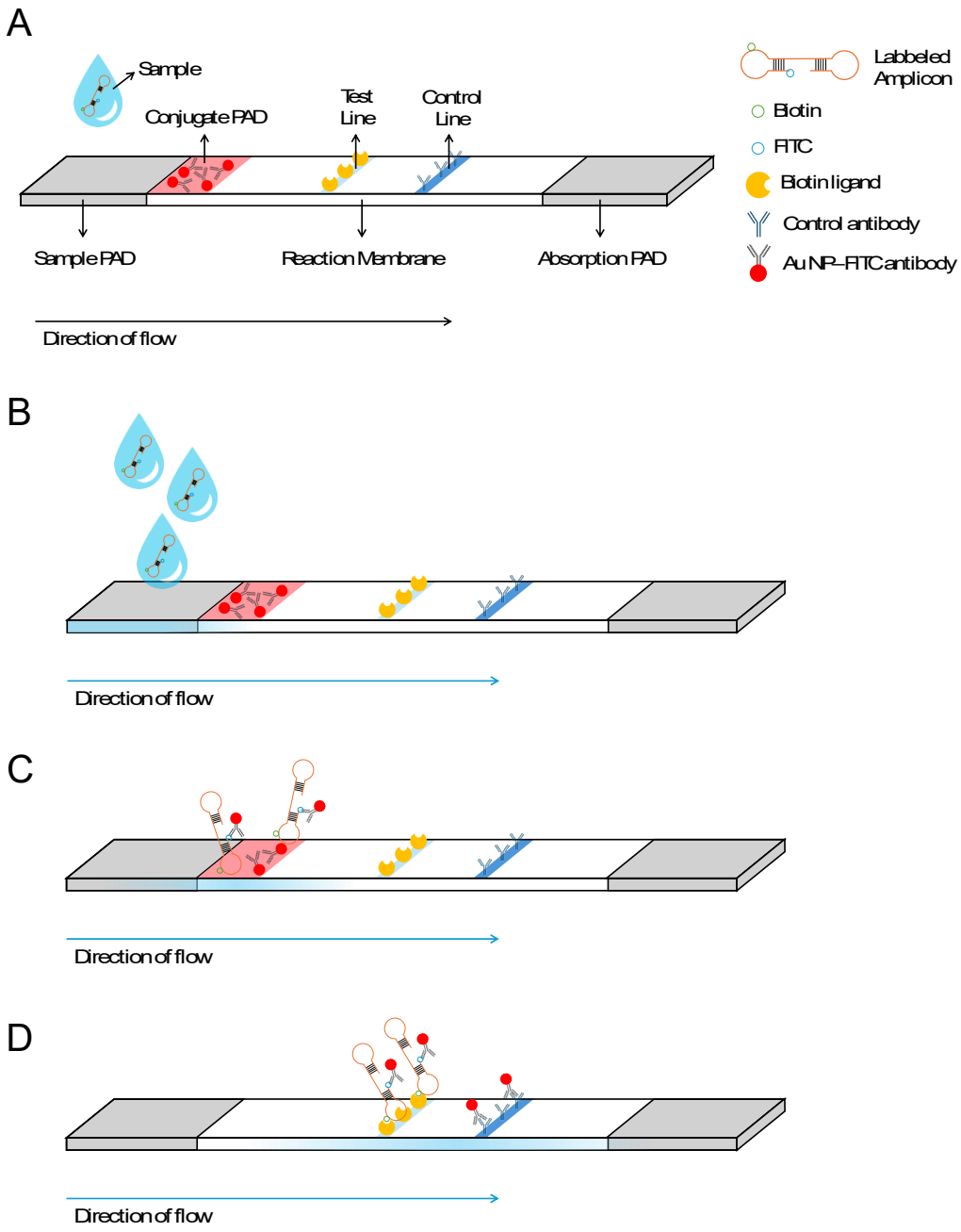

Figure 1.2 – Schematic representation of (A) LFA strip composition and (B-D) the main steps of the detection procedure.

The component that follows the sample pad is the conjugate pad, which can be composed of several materials such as cellulose, glass fiber, polyesters, among others (18,24). This pad is previously impregnated with antibodies that are specifically blind to the target analyte (Figure 1.2(C)). Additionally, these antibodies are conjugated with coloured or fluorescent particles to allow posterior detection (20,23). The main goal of the conjugate pad is to hold these detection particles and ensure their stability and performance until the test is performed, which is why it usually contains a conjugate buffer and carbohydrates, to allow this preservation (20).

After interacting with the conjugate pad, the sample flows through the reaction membrane where the detection occurs. This membrane is usually composed of nitrocellulose and it is possibly the most critical component (20,23). The target analyte binds to the test line making it visible, while the remaining conjugates bind to the control line independently of the presence of the analyte (17,23,24) (Figure 1.2(D)). While the role of the test line is to indicate the presence or absence of the analyte, the visibility of the control line is evidence of the correct functioning of the device, avoiding false negatives (17,18,24). Finally, the processed fluid completes the flow through the strip when it reaches the final component, the absorption pad (18,20,23). This component is usually composed of cellulose fibers and has a large bed volume, allowing the use of large volumes of sample and avoiding backflow of the fluid (18,20,23).

The strip is usually encased in a plastic casing with openings for sample placement (sample well) and for the visual reading of the result (reading window) as exemplified in Figure 1.3. Besides protecting the strip, this casing also provides pressure to ensure contact between the different components and consequently a better flow of the fluids through the strip (24).

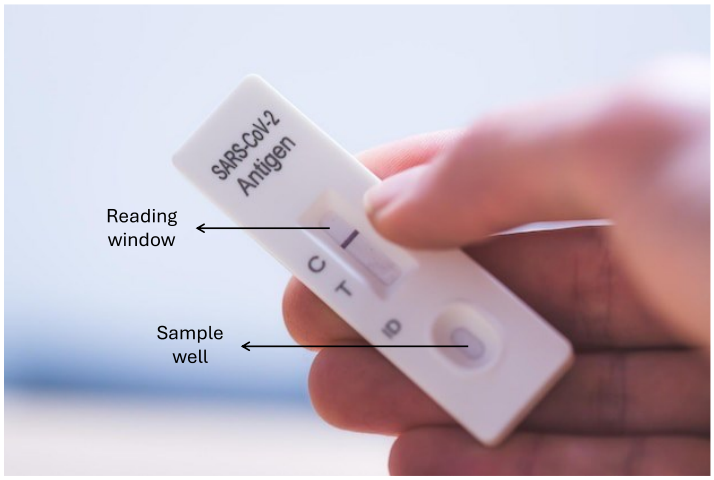

Figure 1.3 – Exemplification of a casing involving a LFA strip.

The manufacturing of LFA is a relatively simple process (Figure 1.4) since few equipment and techniques are involved. The assembly of this type of device relies on combining the different components of the strip in the structure previously described using lamination (18). The process starts with the laminated card as the base structure, on top of which the nitrocellulose reaction membrane is positioned. Then, the test and control lines are drawn in the reaction membrane, usually using a dispenser, and dried at 37 ºC (18,25). Next comes the preparation of the sample pad, which is achieved by soaking the pad in a solution of buffer salts, proteins, and other relevant substances. The sample pad is then dried also a 37ºC. The conjugate pad, on the other hand, is usually prepared by spraying the antibodies conjugated with the detection particles in the conjugate pad, which is then vacuum-dried (18,25). Then, the absorbent, the conjugate, and the sample pad are positioned in the laminated card in their respective place and order, and although this assembly is simple, it is important to ensure the contact between all components in order to guarantee the effective flow of the fluid through the entire strip. Finally, the strips are cut and inserted into their plastic casing (18,25).

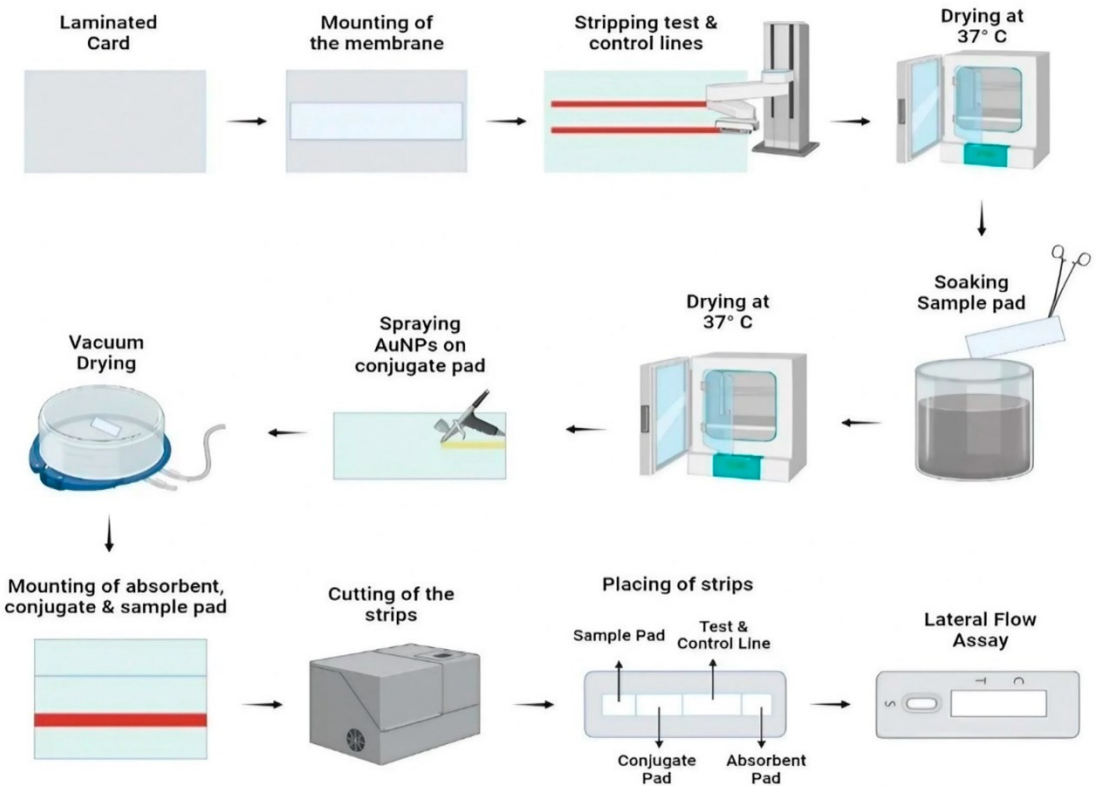

Figure 1.4 – Schematic procedure of fabrication of LFA strips; Image from (18)

As far as detection methods are concerned, the LFA can employ different techniques that can be grouped as optical and electrochemical detection (15). In the optical detection methods can be included the colorimetric, the bio-chemiluminescence, and the fluorescence detection. Of these three, the colorimetric assay is one of the most common, because it allows visual assessment of the results, and consequently a simpler, faster, and economical approach (15). In the electrochemical methods can be included the amperometric, the voltammetric, the conductometric, and the impedimetric detection (15).

Still, in the detection method category, there are three types of detection that can be performed. The qualitative detection is possibly the one that is most commonly associated with the LFA, due to tests like COVID-19 or pregnancy tests that are very well-known by the general population (22,25). The tests allow the evaluation of certain conditions by the presence or absence of a test line, respectively, and are therefore useful in scenarios where the specific amount of the biomarker present is not relevant, such as COVID-19 (Figure 1.5(A)) (20,25).

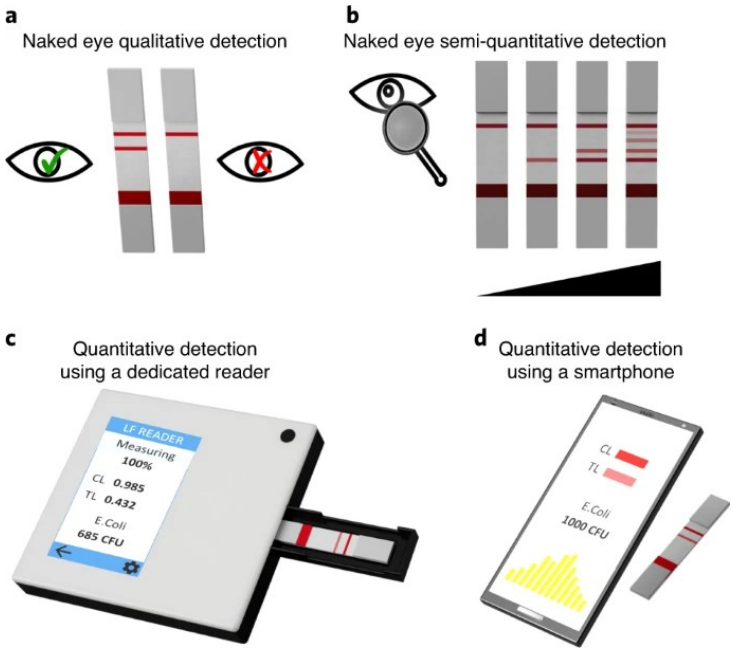

Figure 1.5 – Types of detection using LFA strips with different approaches; Image from (25)

The semi-quantitative approach is suitable for scenarios where some information about the quantity of the analyte is required, for example, if the amount of the analyte has to be above or below a certain threshold to be considered abnormal (25). The LFA developed for this purpose, usually use the barcode-style design, where multiple lines are present in the strip and the number of visible lines or even the intensity of their colour can be associated with a concentration of the analyte (Figure 1.5(B)) (20,25). In more recent years, LFA with quantitative analysis have been reported with the help of digital readers or smartphones (Figure 1.5(C) and (D)). In this type of detection, not only an accurate calibration curve is needed, but it is also important to ensure the reproducibility of the strips in order to obtain accurate results (20,22,25).

The recurrent use of LFAs throughout the years can be justified by an extensive list of advantages. Not only is this a one-step, simple, and easy-to-use assay, but it also provides fast, low-cost, mostly qualitative results using a low sample volume. Furthermore, the devices are easy to prepare and transport and have a long shelf life without requiring complex storage conditions, which makes them not only a good point-of-care tool but also easy to produce and commercialize (18,20,23,24). However, as with all other methods, LFA also has some drawbacks. Inaccurate sample volume, for example, can be a problem since it reduces the precision of the assay.

For samples other than fluids, sample pretreatment is required, a process that is usually time-consuming. Poor affinity of the biomolecules for the specific analyte can also be a problem, leading to decreased accuracy. Good antibody preparation is essential during the manufacturing process to obtain good repeatability. Intrinsic characteristics of the sample such as viscosity heavily impact not only the analysis time but also the flow throughout the strip, therefore influencing the correct functioning of the test (18,20,23,24). Still, most of the time, the advantages of the LFA as a point-of-care tool outweigh the disadvantages, which is why it is still a heavily used aiding tool for diagnosis and monitoring worldwide.

1.2.2. Microfluidic Paper-based Analytical Devices

Even though the use of paper for analytical purposes originated several decades before, in 2007 Martinez et al reignited the interest in paper microfluidics by using patterned paper to design a new low-volume, portable, and inexpensive platform for the quantification of protein and glucose in urine samples (17,19,23). Due to its composition, materials, and applications, this new technique was named microfluidic paper-based analytical device (μPAD) and has gained a lot of attention ever since it was first reported (Figure 1.6).

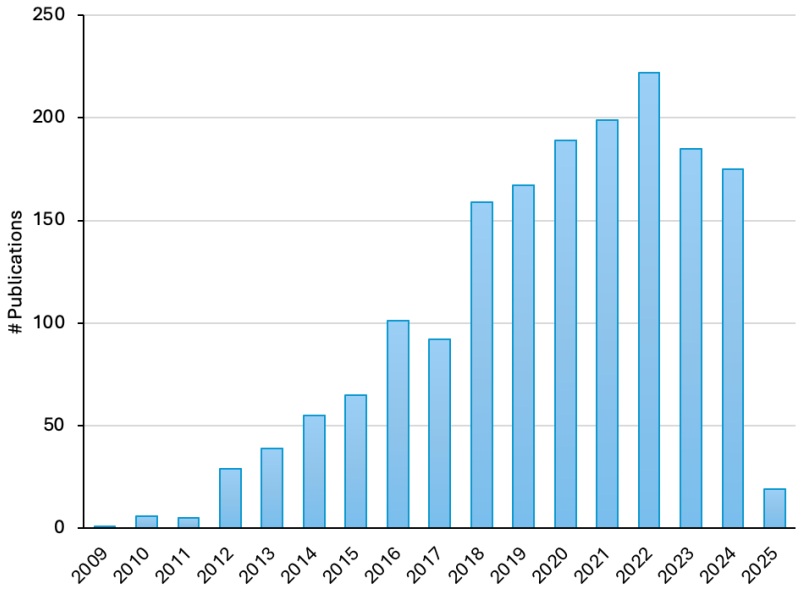

Figure 1.6 – Evolution of number of publications on microfluidic paper-based analytical devices throughout the years; Web of Science search performed on 04/02/2025 ("microfluidic paper-based analytical device(s)" or "microfluidic paper-based device(s)" or "paper-based analytical device(s)").

μPADs are usually a combination of two areas: the hydrophilic area and the hydrophobic area. The hydrophilic area is typically composed of paper and is the platform for the reactions (26). The hydrophobic area, on the other hand, serves as a barrier that, not only establishes the flow path but also contains the flow of the fluids and limits the reaction zone (17,26–28). These hydrophobic barriers can be generated using numerous techniques. Some of the most used ones are described in Table 1.1. Of those, wax printing, inkjet printing, photolithography, and flexographic printing, will be further discussed below.

Table 1.1 – Common methodologies for design and fabrication of the hydrophobic area and respective required materials and equipment; Adapted from (29).

Method	Materials	Equipment
Wax printing	Wax	Wax printer
Inkjet printing	Alkyl ketene dimer/UV-curable ink	Inkjet printer
Photolithography	Photoresist and developer, photomask	Photolithography equipment
Flexographic printing	Polystyrene ink/PDMS ink	Roll-to-roll flexography units
Plasma treatment	Alkyl ketene dimer/octadecyltrichlorosilane/ pentafluoroethane monomer, metal mask	Vacuum plasma reactor
Cutting and shaping	Adhesive sheet	Knife plotter or digital craft cutter
3D printing	Paraffin wax/photocurable resin	3D printer with a custom-made extruder

The first μPAD, reported by Martinez et al in 2007, described the use of photolithography to create the hydrophobic barriers (30,31). This is a high-precision technique that uses a pattern created on an optical mask and transfers it to a light-sensitive photoresist material in the paper using a beam of protons (Figure 1.7) (16,19,30,31). The high precision offered by this method allows the design of small channels and is a very attractive option for researchers that already have the knowledge and access to the equipment. However, for those that are not familiar with the technique, a few disadvantages are the cost of the fabrication equipment and the complexity of the procedure (30,32). Additionally, the solvent used to maintain the hydrophilic area can reduce paper flexibility and even interfere with some reactions (32).

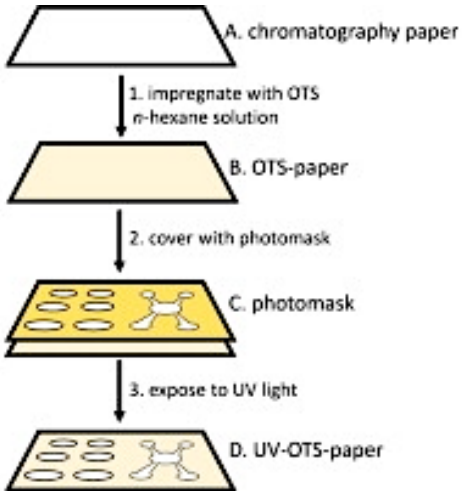

Figure 1.7 – Schematic representation of the formation of the hydrophobic area with photolithography; Image from (33).

Wax printing is another fabrication technique that is commonly used in μPADs design due to its non-toxic, low-cost, simple, and fast procedure (16,30,31).

In this method, a wax printer is used to dispense wax in a specific pattern on the surface of the paper. Then the paper is heated to allow the wax to melt and flow through the thickness of the paper, creating an impermeable pattern within the paper porous structure (Figure 1.8) (16,30,31). Some of the main disadvantages of this technique are high initial equipment cost, poor pattern resolution after melting the wax, limited availability of the printers in some countries (30,31).

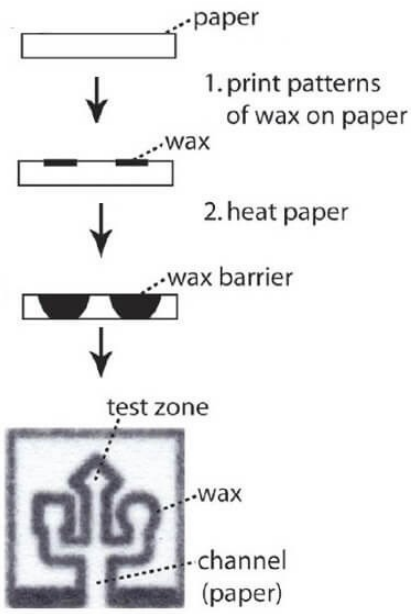

Figure 1.8 – Schematic representation of the formation of the hydrophobic area with the wax printing method; Image from (34).

The inject printing methodology was first reported in 2013 by Maejima et al and consists of printing onto the paper either a solvent or a UV-curable ink (additional need of UV light source) (30,31). This is also a popular choice of fabrication technique since the printers are inexpensive when compared to others and they are widely available (30). Furthermore, this methodology also allows the possibility of adding reagents during the printing process (31). Nevertheless, some disadvantages are the high cost of some inks, and the maintenance of the printer since some organic solutions can degrade the printer itself (31).

Flexographic printing was first applied to the fabrication of μPADs in 2010 by Olkkonen and it involves the use of print presser units to pattern the paper (30–32). This is well-suited to large-scale production since it can be adapted to the roll-to-roll processing technique (Figure 1.9) (30,32). Although being a rapid multi-step method, the flexographic printing still has two major drawbacks, namely the lower resolution of the pattern and the inability of the penetration of the ink through the paper, staying only on the surface (31,32). The choice of the technique used to create the hydrophobic barriers, should be carefully considered and take into account aspects such as the reactions and reagents to be used, the type of sample, applicability of the device, among others.

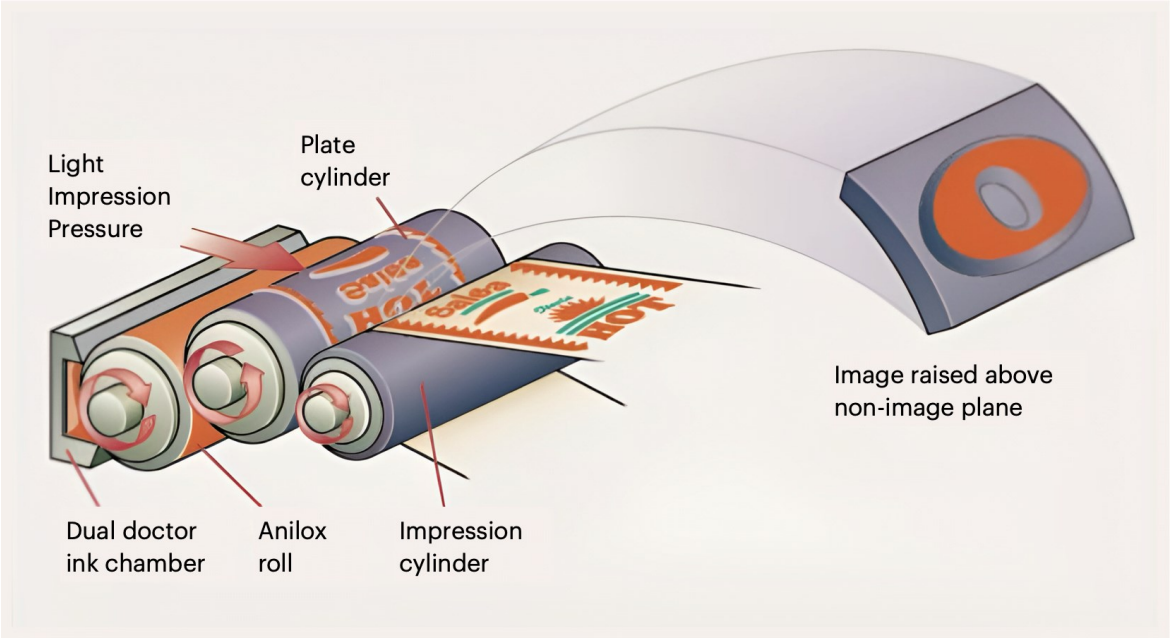

Figure 1.9 – Schematic representation of flexographic printing method using roll-to-roll technique; Image from (35).

In addition to the varying techniques used for the fabrication of the hydrophobic areas, μPADs can also be designed with types of configurational structures: the 2D structure and the 3D structure (31,36,37). As the name indicates, 2D μPADs have a simple two-dimensional structure in which the flow of the fluids occurs in the horizontal xy plane of only one layer of paper (37,38). This type of flow is usually referred to as lateral flow. The manipulation of the fluids in this type of devices relies on the size and geometry of the channels created by the hydrophobic areas/barriers in the paper. Parameters such as flow speed could be influenced by the width of the channel, for example (29,38).

3D-μPADs, on the other hand, have a more complex three-dimensional structure composed of several layers of paper, in which the flow of fluids can occur not only horizontally (lateral flow) in each layer but also vertically through the layers (vertical flow) (17,29,36–38). This three-dimensional structure provides numerous advantages over the 2D-μPADs. Not only does it facilitate more complex multi-step analysis, but it also provides faster and more accurate determinations (29,31,38). Furthermore, the vertical flow also leads to a decrease in the loss of fluids in the paper, consequently having better control of the flow of the fluids and reducing the minimal volumes required of both sample and reagents (36,38). The versatility of the 3D-μPAD also allows the possibility of introducing in the devices a layer for pre-treatment steps such as filtration or removal of interferences.

The assembly of the 3D-μPADs can be achieved generally with one of two techniques: folding or stacking (37,38). In the folding technique, the patterning of the channels and chambers is all performed in one layer of paper, and, using the origami concept, this layer is folded in a way that the channels and chambers connect and allow the three-dimensional flow of the fluids (Figure 1.10) (37–39). This methodology has a very simple and easy-to-reproduce fabrication procedure, reducing assembly errors (17,38). Furthermore, it also allows the possibility of disassembling and individually analysing the chambers or channels (38).

On the other hand, the stacking technique of assembling the devices, as the name implies, consists of stacking paper layers, layer by layer, to achieve the 3D structure (37,38).

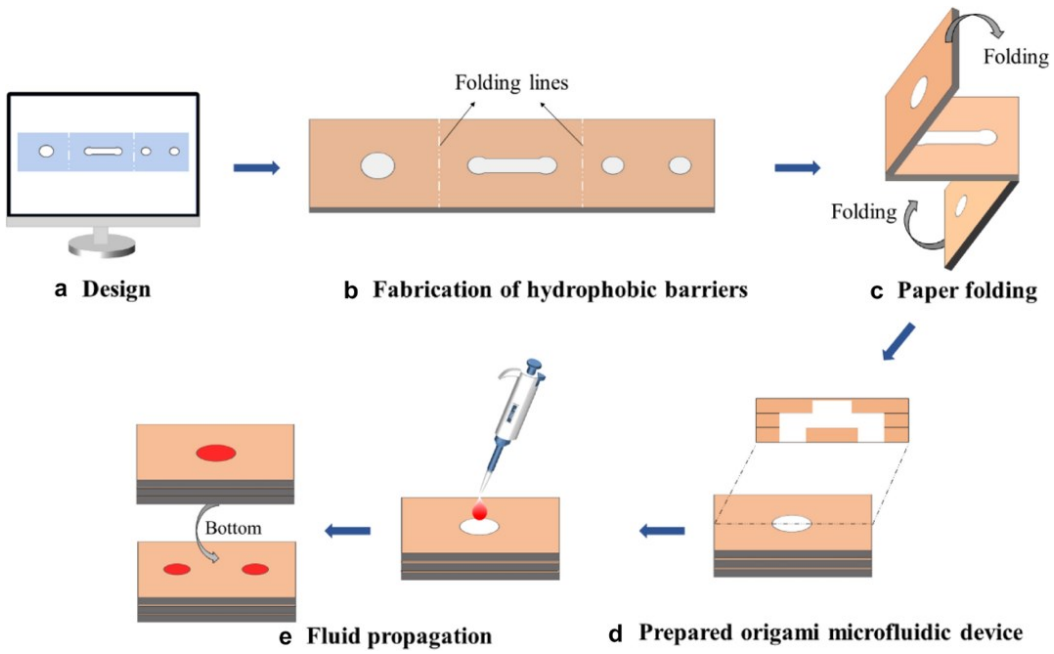

Figure 1.10 – Schematic representation of the assembly of a 3D-μPAD with the origami technique; Image from (39).

However, for both the folding and stacking techniques, the most critical step is keeping the layers connected during the placement of the sample in order to avoid cross-contamination in the device (37). Clamps, adhesive tape, or even glue, are a few of the tools that can be used to connect the layers of the device.

Even though adhesive tape and glue provide the strongest bonding between layers, it also eliminates the unfolding capability of the origami devices (39). The tool used should be carefully chosen taking into consideration the objective of the device. Almost all patterning methods used in the 2D device fabrication can be adapted to the 3D μPADs, still, the most commonly used is wax printing for origami 3D μPADs (39).

Overall, microfluidics paper-based devices, whether it be with a 2D or 3D structure, offer a large set of advantages, particularly for the point-of-care application (38). One of the biggest advantages that arise when talking about μPADs is their affordability (38,40). The low cost that is usually associated with these types of devices is related not only to the affordability of the materials used in its fabrication such as paper, but also to the very low volumes of reagents used for the determination in comparison with other methodologies, and the wide array of low-cost fabrication techniques that can be used (16,23,40). Additionally, these devices are very simple and easy to use, providing fast and sufficiently accurate measurements without needing complex expensive equipment or specialized training to be used. This little-to-no equipment need, in addition to the characteristic small size of the microfluidic devices, leads to a portable tool that can achieve sensitive analytical determinations in a wide array of applications (16,40). All these advantages go hand-in-hand with the WHO guidelines, making them a promising tool for point-of-care testing.

Currently, the main drawbacks of μPADs are related to logistical problems. Most of the time it is difficult to perform a large scale-up of production of the devices that can fulfil the demand of the population while maintaining the cost-effectiveness of the process (41,42). Additionally, the majority of the developed μPADs lack studies on the stability of the device or its performance under varying field conditions (30). Without these studies it is impossible to predict if the devices will maintain their accurate performance when used in a point-of-care setting (30,41).

1.2.3. Detection Methods

The detection method is another parameter that should be carefully considered when developing a microfluidic paper-based analytical device. Currently, several detection methods have been applied to μPADs, each of them with its pros and cons. The detection can be performed by one of four methodologies: colorimetry, electrochemistry, chemiluminescence, and fluorescence.

The colorimetric detection method is by far the most widely used, especially in point-of-care devices (27,40,43,44). This method relies on a chemical or enzymatic reaction with the intended analyte, that leads to the formation of a product with a different colour or different colour intensity (40,44). The main reason why this is the preferred readout method among point-of-care devices is its simplicity (27). Not only is easy to visually see the results but it is also simple to use and does not require complex or expensive equipment (43). Also, paper has the ideal white, high-contrast background for colorimetric detection (27). Furthermore, this approach offers a choice between a qualitative, semi-quantitative, or quantitative analysis based on the instrumentation used (40).

While a visual interpretation of the results by the naked eye would provide qualitative analysis, the use of colour charts or colour calibration tables for comparison would lead to more accurate

results, hence providing a semi-quantitative analysis (27,29,40). For the most accurate analysis, additional instrumentation is needed, such as a scanner or a camera, to record the image and analyse it with image processing software (27,29,40,43). For image analysis, the images are usually converted into a specific colour space (RGB, CMYK, HSV, among others), RGB being the most commonly used since it can achieve multiple shades of colours by the superposition of only three: Red, Green, and Blue (Figure 1.10) (40).

Even though colorimetry has a wide array of advantages, it also has some limitations. Colorimetric detection is often associated with low sensitivity and selectivity (27,43). Low reproducibility is also commonly reported due to the sometimes non-uniform distribution of colour in the paper (44). Several strategies have already been reported to minimize these limitations, such as using nano-particles or enzymes to further enhance sensitivity and selectivity or performing several replicates to minimize error due to the non-uniform distribution of colour (27).

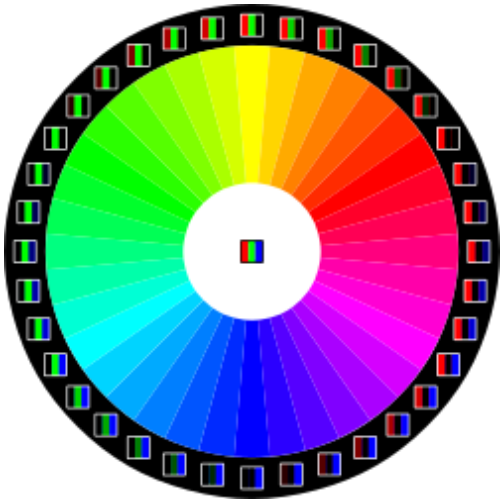

Figure 1.11 – Schematic representation of the colour wheel with the RBG superposition of colours; Image from (45).

Electrochemical detection consists of the conversion of the chemical signals of the analyte into electrical signals using electrodes placed in the device, typically using the screen-printing technique (40,43). Usually, electrochemical detection requires three electrodes for the voltametric measurements: the working electrode, the reference electrode, and the counter electrode (Figure 1.12) (40,43). The working and the counter electrode form a loop where the redox reactions occur, while the reference electrode provides a standard value for the potential measurements (40,43). µPADs that employ this detection method can also be named ePADs and provide faster and more sensitive measurements when compared to other techniques (17,27,43). The advances in technologies and miniaturization allow the placement of the electrodes without compromising the size or portability of the devices (27).

The main drawbacks of this detection method when compared to the colorimetric detection, are the higher cost, more complex fabrication procedure, and less intuitive reading and analysis of results (17,43).

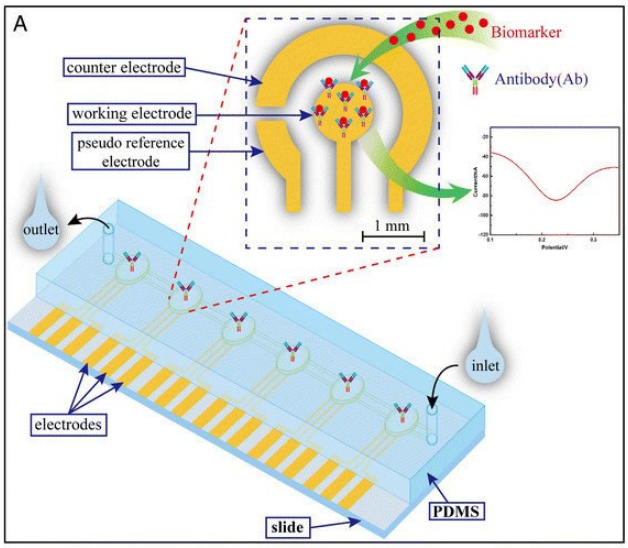

Figure 1.12 – Example of μPAD with electrochemical detection; Image from (46).

The chemiluminescence detection consists of the correlation of radiation emitted by an analyte and its concentration (40). When a molecule in a ground state absorbs energy released in a chemical reaction, it transits to an excited state. However, due to the instability of the excited state, the molecule returns to the ground state and emits radiation, which is then measured and correlated to the concentration of the substance (40). The most commonly used chemiluminescence system in μPADs is the reaction of luminol and peroxide (40). This detection method provides highly sensitive and selective results; however, it requires a chemiluminescence reader, and the measurements have to be performed in the dark, which complicates the analysis process (29,40,43). Additionally, because the signal obtained in this method is very dynamic, reproducibility can also be an issue (43).

Fluorescence is another detection method that has been used in μPADs, due to its high sensitivity and consequent low limits of detection. The mechanism is similar to the one of chemiluminescence, but in this method, the excitation of the molecules occurs due to an external light source (40,44). Besides the additional instrumentation needed, the main limitation of this detection method is the high background signals. This happens due to the fact that commercial paper used in the devices often contains additives that auto-fluorescence (40).

1.3. Biological Samples of Non-Invasive Collection

Biological samples play a crucial role in the current diagnostics and monitoring of a wide array of diseases. While blood still is considered the standard sample for diagnosis, the invasive nature of its collection is a major drawback (26,47). Blood sampling typically requires skilled healthcare professionals, sterile environments, and specialized equipment, which makes it more expensive, time-consuming, and inaccessible, particularly in remote areas with limited resources. Additionally, the process can be uncomfortable or painful for patients, particularly children or elderly individuals (26,47).

In response to these challenges, there has been a growing interest in non-invasive collection samples, such as saliva and urine. These types of samples offer several advantages over blood. They are easily accessible and can often be collected without the need for trained personnel or sophisticated equipment, reducing costs and expanding access to diagnostic tools in underserved populations. More importantly, non-invasive collection of these types of samples are painless, reducing patient anxiety and improving compliance, particularly when repeated testing is needed.

1.3.1. Saliva

Saliva is a viscous slightly acidic fluid (pH = 6 – 7) that is produced in the oral cavity by the parotid, submandibular, and sublingual salivary glands (17,47). It is composed of 94% to 99% water, with the remaining percentage being a wide range of enzymes, proteins, and other organic and inorganic substances (17,47). A healthy adult produces on average 500 to 1500 mL per day; however, saliva's composition varies throughout the day. During the day, the parasympathetic nerve induces the parotid gland to produce a waterier saliva; during episodes of fear or stress, the sympathetic nerves activate the production of a more viscous saliva by the sublingual and submandibular glands (48,49).

The main purposes of this fluid are to help the digestion, keep the mouth moist, and eliminate harmful bacteria that may enter the mouth (47). However, because the salivary glands are densely irrigated by blood vessels, many blood substances can be also found in saliva (48). If there are high levels of a certain biomarker in blood, then it is probable that this excess is excreted through saliva (47). This supports the idea that saliva can be used as an indicator of the general health of an individual (16,17,38,48,49).

Figure 1.13 shows the evolution of publications related to the use of saliva as a sample. The number of publications, as shown, has been increasing consistently for several years. This could be justified by the several advantages the use of saliva entails. This biological fluid has an easier, safer, and simpler collection, that does not require specific equipment or specialized technicians (17,48). Furthermore, the saliva collection is not invasive and consequently not painful, with less risk of contamination and simple enough to be performed by the patient itself (17,48).

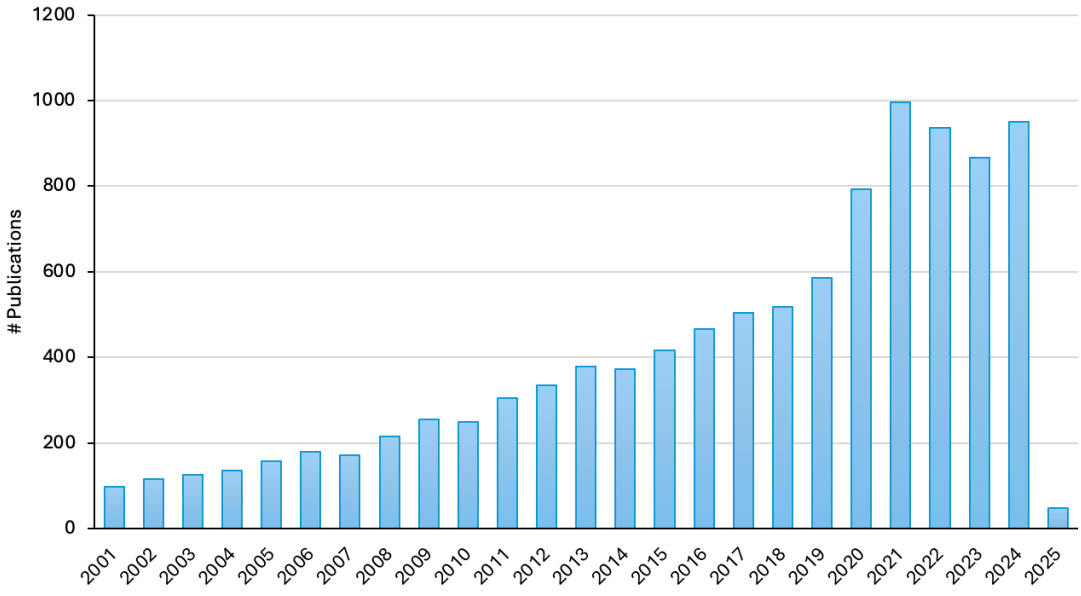

Figure 1.13 – Evolution of number of publications related to saliva samples throughout the years; Web of Science search performed on 27/01/2025 ("saliva sample(s)" or "sample(s) of saliva").

Currently, the most used method for the collection of this biological sample is passive drooling. This method consists of asking the patient to tilt their head down and simply let saliva drip from the mouth to the collection tube (48). Although simple, this method can be time-consuming, since some individuals may have difficulty producing the necessary amount of sample in a short period of time. An alternative method consists of placing a liquid in the mouth and swishing. This, however, has the disadvantage of diluting the sample, possibly making the quantification of the analyte more difficult. Additionally, both these methodologies cannot be easily used in small children. To try to overcome these limitations, researchers have been reporting alternative methodologies for the collection of this biological fluid. One of the strategies reported is the use of an absorbent material (such as cotton or gauze) that could be placed in the mouth and absorb the saliva (26,50,51).

Nevertheless, there are also a few limitations associated with this biological sample. The majority of biomarkers in saliva are typically present in very low concentrations, making it very difficult to perform an accurate quantification (48). Additionally, the varying composition of the sample throughout the day can also make more difficult the diagnosis process since it can affect not only the concentration of the targeted analyte but also the viscosity of the sample and the concentrations of other substances that could interfere in the determination (48).

Regardless of the mentioned limitations, saliva remains a more viable option for biological samples for point-of-care applications, especially when compared to traditional blood-based diagnostics. As the advancements in analytical methodologies continue to improve, the sensitivity and specificity of saliva-based tests will too, further reinforcing its importance in modern healthcare.

1.3.2. Urine

Urine is a biological fluid produced by the kidneys, which is responsible for filtering the blood and maintaining homeostasis. The process of urine production be resumed in three main steps: filtration, reabsorption, and excretion. First, the blood is filtered in the kidneys, in order to remove waste products and excess ions. Then, some useful substances such as glucose, amino acids, and certain electrolytes are reabsorbed into the bloodstream to prevent excessive loss. Finally, the remaining waste products, excess ions, and toxins are secreted into the urine, which is then transported to the bladder for temporary storage before being expelled from the body through the urethra. Therefore, the primary purpose of urine production is to eliminate metabolic waste products, regulate the body's fluid and electrolyte balance, and maintain acid-base homeostasis (52).

This fluid consists of over 90% water, with the remaining components being a variety of organic compounds, organic ammonium salts, inorganic salts, and urea (53). Since urine reflects kidney function and systemic metabolism, it is a suitable biological sample for assessing overall health. Figure 1.14 shows the positive evolution of the number of publications related to urine as a sample.

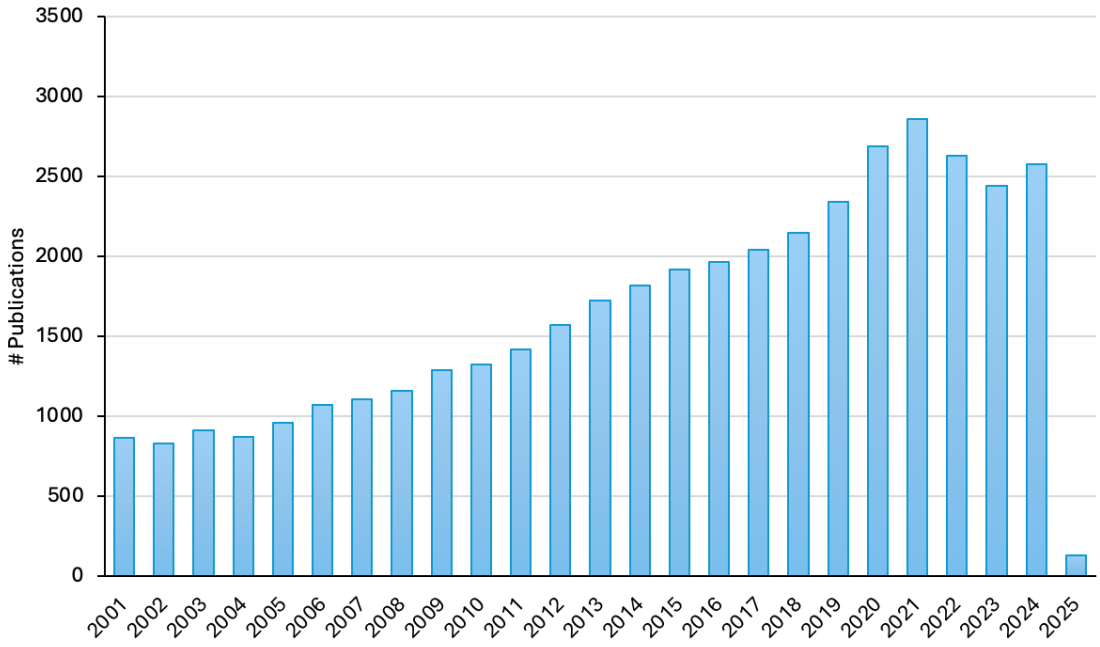

Figure 1.14 – Evolution of number of publications related to urine samples throughout the years; Web of Science search performed on 27/01/2025 ("urine sample(s)" or "sample(s) of urine").

Furthermore, because of its non-invasive and easy collection, urine is also a promising option for biological samples to be used in point-of-care testing (53). Urine-based diagnostic devices have been successfully developed for detecting a variety of health conditions (53,54). One of the most recognized tests performed with urine is the pregnancy test which detects the presence of the human chorionic gonadotropin hormone (53).

Alongside the many advantages associated with the non-invasive collection of urine already mentioned, urine is less influenced by factors like stress or meal consumption, unlike saliva, and it can be stored for extended periods without significant degradation (53). Despite these advantages, there are also some challenges and limitations worth mentioning. The biggest limitations currently are the urine's complex composition and the inter-individual variability (54). This variability can be associated with several factors such as hydration levels, diet, and medications (53). Furthermore, the intrinsic yellow colour of urine and the variability of shades could also pose a problem, particularly in the devices that used colorimetric detection (44). To prevent some of these interferences, some of the reported devices already include an integrated sample pre-treatment (44).

Nevertheless, ongoing research and technological advancements continue to address these limitations, further solidifying urine's role as a valuable biological fluid for point-of-care analysis (54). Overall, urine's rich biomarker composition, accessibility, ease of collection, and broad diagnostic potential make it a promising alternative to blood in point-of-care applications.

1.4. Application of µPADs to Biological Samples of Non-Invasive Collection

Microfluidic paper-based analytical devices have several advantages as mentioned before for point-of-care. These devices are not only portable and affordable but also do not require complex equipment or training to provide sufficiently accurate analytical measurements that could aid in the diagnosis or monitoring of several health conditions outside of the lab. This is particularly useful in more remote or underserved areas, that do not have access to health care, whether it be for lack of conditions or for economic reasons. When combined with the use of biological samples of non-invasive collection, it becomes the perfect tool for diagnosis and monitoring of multiple diseases since the measurements could be obtained using a sample that is easier, safer, and painless to collect. A Web of Science search (parameters in Appendix A) of the microfluidic paper-based test developed that reported the application to either urine or saliva samples revealed a total of 76 articles published from 2014 to 2025 (Figure 1.15(A)) among which 83 analytical determinations were performed. The majority of these publications were placed by Web of Science in the categories of chemistry or related to chemistry (Biochemistry, Electrochemistry,…) (Figure 1.15(B)).

Moreover, a summary of some features of the analytical determinations and devices reported in the Web of Science search performed is shown in Table 1.2. The not-yet-published work presented in this thesis that fitted the criteria of the search performed (work presented in Chapter 7) was also included in the table. This table lists by alphabetic order of analyte, characteristics such as dynamic range, the limit of detection, fabrication structure of the device (2D or 3D) and technique used for 3D structures (folding or stacking), detection method, and type of biological sample to which the analysis is performed.

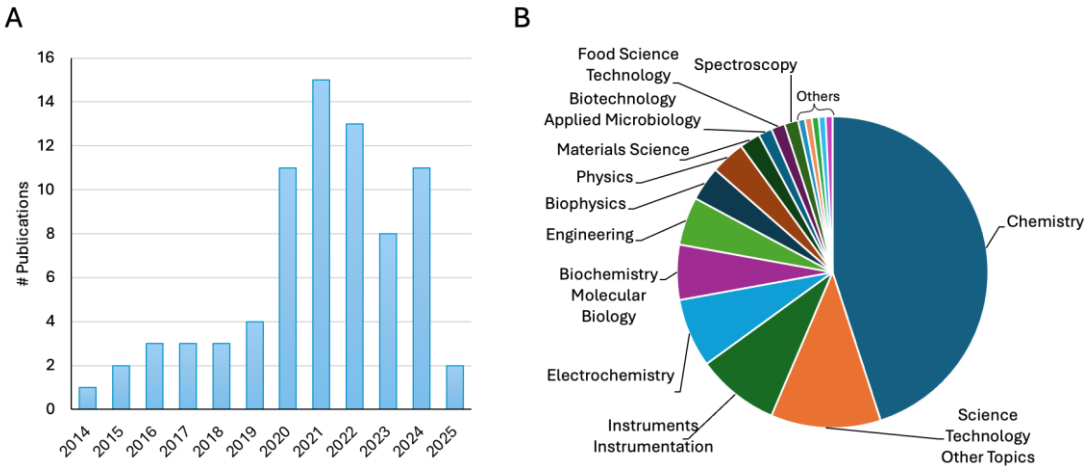

Figure 1.15 – (A) Evolution of number of publications reporting microfluidic paper-based devices applied to saliva or urine samples throughout the years; (B) Category distribution by Web of Science of the publications in the performed search; Web of Science search performed on 04/02/2025.

Because Table 1.2 is listed by alphabetic order of analyte, the first and most obvious observation is the number of publications reporting the determination of each analyte. Figure 1.16 shows the distribution by analyte of all analytical determinations mentioned in Table 1.2. At first glance, it is easy to observe that three analytes are considerably more reported in comparison to all others. Tied for first place are creatinine and glucose with 11 reported publications, followed by uric acid with 10 reported publications. All analytes that were reported only once were included under others in Figure 1.16.

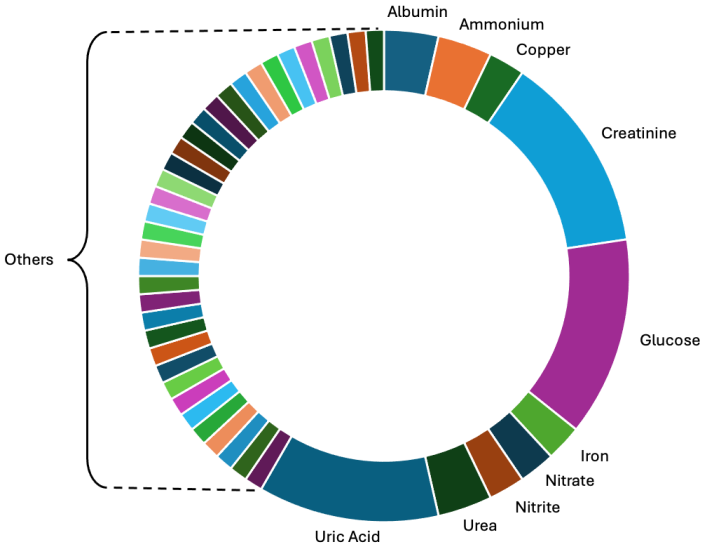

Figure 1.16 – Distribution of analytes among all determinations listed in Table 1.2.

Table 1.2 – Microfluidic paper-based devices and sensors applied to the analysis of saliva and urine samples.

Analyte	Dynamic Range	LOD	2D vs 3D µPAD	Detection Method	Sample	Reference
β-amyloid	0.50 – 10.0 ng/mL	0.20 ng/mL	2D	Colorimetric	Urine	(55)
3-nitrotyrosine (3-NT)	500 nM – 1 mM	22.3 nM	2D	Electrochemical	Urine	(56)
Albumin	0.2 – 10 µM	0.47 µM	2D	Fluorescence	Urine	(57)
Albumin	1 – 500 mg/dL	0.072 mg/dL	3D folding	Electrochemical	Urine	(58)
Albumin	0 – 1000 mg/L	-	2D	Colorimetric	Urine	(59)
Aldehydes	20.4 – 114 µM	6.1 µM	3D folding	Colorimetric	Saliva	(60)
Ammonium	0.5 – 20 mM	290.1 µM	2D	Electrochemical	Urine	(61)
Ammonium/Ammonia	15 -150 mg/L	11.3 mg/L	3D stacking	Colorimetric	Saliva	(62)
Ammonium/Ammonia	0.10 – 5.0 mM	0.032 mM	3D stacking	Colorimetric	Saliva	Chapter 5 of this work
Ascorbic Acid	20 – 700 µM	3.20 µM	3D folding	Electrochemical	Urine	(63)
Bilirubin	5 – 1000 mg/L	1.0 mg/L	2D	Colorimetric	Urine	(64)
Calcium	0.27 – 4.50 mM	78 µM	3D stacking	Colorimetric	Saliva	(50)
Cyanide	26 – 286 µg/L	5 µg/L	2D	Colorimetric	Urine	(65)
Citrate	5 – 150 mg/L	2.9 mg/L	2D	Colorimetric	Urine	(66)
Copper (II)	0.01 – 1 mg/L	0.01 mg/L	2D	Fluorescence/Colorimetric	Urine	(67)
Copper (II)	0.001 – 5 mg/L	0.1 mg/L	2D	Fluorescence/Colorimetric	Urine	(68)

Table 1.2 – Microfluidic paper-based devices and sensors applied to the analysis of saliva and urine samples. (continuation)

Analyte	Dynamic Range	LOD	2D vs 3D μPAD	Detection Method	Sample	Reference
Creatinine	2.20 – 35.0 mg/dL	0.66 mg/dL	3D stacking	Colorimetric	Urine	(69)
Creatinine	0.5 – 4 mM	500 μM	2D	Electrochemical	Urine	(61)
Creatinine	0.03 – 0.50 mM	0.022 mM	2D	Colorimetric	Urine	(70)
Creatinine	1.05 – 20 mM	0.35 mM	3D folding	Colorimetric	Urine	(71)
Creatinine	0.82 – 10 mM	0.27 mM	3D folding	Colorimetric	Urine	(71)
Creatinine	1 .250 mg/L	0.72 mg/L	2D	Fluorescence/Colorimetric	Urine	(72)
Creatinine	0 – 3000 mg/L	-	2D	Colorimetric	Urine	(59)
Creatinine	50 – 1000 mg/L	16.9 mg/L	2D	Colorimetric	Urine	(73)
Creatinine	0.010 – 3.0 μM	3.7 nM	2D	Electrochemical	Urine	(74)
Creatinine	50 – 600 mg/L	15.7 mg/L	2D	Colorimetric	Urine	(75)
Creatinine	2.5 – 25 mg/dL	2.0 mg/dL	2D	Colorimetric	Urine	(76)
Cysteine	1 – 100 μM	1.5 μM	2D	Colorimetric	Urine	(77)
Dapoxetine	0.01 μM – 1 mM	0.01 μM	2D	Colorimetric	Urine	(78)
Diazepam	3.5 nM – 3.5 mM	1.5 nM	2D	Electrochemical	Urine	(79)
Dipropylamine	1 – 250 mg/L	0.80 mg/L	2D	Fluorescence/Colorimetric	Urine	(72)
Dopamine	20 – 1000 μM	2.19 μM	3D folding	Electrochemical	Urine	(63)

Table 1.2 – Microfluidic paper-based devices and sensors applied to the analysis of saliva and urine samples. (continuation)

Analyte	Dynamic Range	LOD	2D vs 3D µPAD	Detection Method	Sample	Reference
E. coli	5.0×10^2 - 5.0×10^5 CFU/mL	2.0×10^2 CFU/mL	2D	Colorimetric	Urine	(80)
Ethanol	1 – 20 %(v/v)	0.22 %(v/v)	3D stacking	Colorimetric	Saliva	(81)
Folic Acid	1 – 300 µM	0.28 µM	2D	Fluorescence	Urine	(82)
Fructose	1.55 – 100 µM	0.51 µM	2D	Fluorescence/Colorimetric	Urine	(83)
Glucose	0.095 – 1.1 mM	0.028 mM	3D stacking	Colorimetric	Saliva	Chapter 7 of this work
Glucose	2 – 200 µM	1 µM	2D	Colorimetric	Urine	(84)
Glucose	0.1 – 50 mM	0.026 mM	2D	Fluorescence	Urine	(85)
Glucose	0 – 10 mM	1.65 mM	2D	Colorimetric	Urine	(86)
Glucose	5 – 400 µM	1.27 µM	2D	Colorimetric	Urine	(87)
Glucose	0.01 – 10 mM	3 µM	3D folding	Colorimetric	Urine	(88)
Glucose	2.68 – 200 µM	0.80 µM	2D	Fluorescence/Colorimetric	Urine	(83)
Glucose	0.01 – 30 mM	5 µM	2D	Electrochemical	Urine	(89)
Glucose	0 – 180 mg/dL	0.84 mg/dL	2D	Colorimetric	Saliva	(90)
Glucose	0 – 10 mM	0.35 mM	2D	Electrochemical	Urine	(91)
Glucose	0 – 20 mM	2.47 mM	2D	Colorimetric	Urine	(92)
Hexylamine	1 – 300 mg/L	0.75 mg/L	2D	Fluorescence/Colorimetric	Urine	(72)

Table 1.2 – Microfluidic paper-based devices and sensors applied to the analysis of saliva and urine samples. (continuation)

Analyte	Dynamic Range	LOD	2D vs 3D µPAD	Detection Method	Sample	Reference
Histidine	1 – 90 µM	0.5 µM	2D	Colorimetric	Urine	(77)
Human Chorionic Gonadotrophin	10 – 500 ng/mL	10 ng/mL	2D	Colorimetric	Urine	(93)
Iron	0.07 – 1.2 mg/L	20 µg/L	3D stacking	Colorimetric	Urine	Chapter 3 of this work
Iron (III)	0.01 – 1 mg/L	0.01 mg/L	2D	Fluorescence/Colorimetric	Urine	(67)
L-cysteine	0.1 – 250 µM	0.02 µM	2D	Electrochemical	Urine	(94)
Lead (II)	10 – 500 µg/L	9 µg/L	2D	Electrochemical	Urine	(95)
Leukocyte Esterase	55 – 108 µg/L	3.75 µg/L	2D	Colorimetric	Urine	(96)
Magnesium	82 – 247 µM	62 µM	3D stacking	Colorimetric	Saliva	(51)
MicroRNA-21	10 - 1000 pM	4.1 pM	2D	Colorimetric	Urine	(97)
Nitrate	0.14 – 1.0 mM	0.04 mM	3D stacking	Colorimetric	Urine	Chapter 4 of this work
Nitrate	0.27 – 1.2 mM	80 µM	3D stacking	Colorimetric	Saliva	(26)
Nitrite	0.20 – 2.0 µM	0.18 µM	2D	Colorimetric	Urine	(80)
Nitrite	5 – 250 µM	0.05 µM	3D stacking	Colorimetric	Saliva	(26)
Oxalate	2 – 40 mg/L	0.6 mg/L	2D	Colorimetric	Urine	(66)
Phenylalanine	60 – 2400 µM	60 µM	2D	Colorimetric	Urine	(98)

Table 1.2 – Microfluidic paper-based devices and sensors applied to the analysis of saliva and urine samples. (continuation)

Analyte	Dynamic Range	LOD	2D vs 3D µPAD	Detection Method	Sample	Reference
Putresceine	5 – 150 mg/L	1.7 mg/L	2D	Fluorescence/Colorimetric	Urine	(72)
Pyridine	5 – 75 mg/L	1.4 mg/L	2D	Fluorescence/Colorimetric	Urine	(72)
Sarcosine	2 – 500 µM	1 µM	2D	Colorimetric	Urine	(84)
Serotonin	0.01 – 1000 µM	0.002 µM	3D folding	Electrochemical	Urine	(99)
Tetrahydrocannabinol	1 – 100 ppm	0.24 ppm	3D stacking	Colorimetric	Saliva	(81)
Thiocyanate	0 – 40 mM	0.06 mM	2D	Colorimetric	Saliva	(100)
Urea	0.5 – 6 mM	500 µM	2D	Electrochemical	Urine	(61)
Urea	0.16 – 5.0 mM	0.049 mM	3D stacking	Colorimetric	Saliva	Chapter 5 of this work
Urea	0.5 – 5.0 mM	0.27 mM	2D	Colorimetric	Urine	(101)
Urease Activity	0.041 – 0.750 U/mL	0.012 U/mL	3D stacking	Colorimetric	Saliva	Chapter 6 of this work
Uric Acid	25 – 1000 µM	10 µM	3D stacking	Colorimetric	Saliva	(102)
Uric Acid	2 – 500 µM	1 µM	2D	Colorimetric	Urine	(84)
Uric Acid	5 – 45 mg/L	3.1 mg/L	2D	Colorimetric	Urine	(66)
Uric Acid	0.01 – 1 mM	1.1 µM	3D folding	Electrochemical	Urine	(103)
Uric Acid	0.01 – 5 mM	4 µM	3D folding	Colorimetric	Urine	(88)
Uric Acid	0.05 – 15 mM	20 µM	2D	Electrochemical	Urine	(89)

Table 1.2 – Microfluidic paper-based devices and sensors applied to the analysis of saliva and urine samples. (continuation)

Analyte	Dynamic Range	LOD	2D vs 3D µPAD	Detection Method	Sample	Reference
Uric Acid	0.010 – 3.0 µM	8.4 nM	2D	Electrochemical	Urine	(74)
Uric Acid	20 – 1000 µM	1.80 µM	3D folding	Electrochemical	Urine	(63)
Uric Acid	50 – 500 mg/L	16.5 mg/L	2D	Colorimetric	Urine	(75)
Uric Acid	0 – 2 mM	0.08 mM	2D	Electrochemical	Urine	(91)
Vanadium (V)	0.01 – 1 mg/L	0.01 mg/L	2D	Fluorescence/Colorimetric	Urine	(67)

After taking a closer look at the three most frequent analytes reported, it was possible to observe that for all analytes the most common biological sample used was urine (Figure 1.17). In the publications reporting creatinine determination, all devices were developed for application in urine samples. This was expected since creatinine is a well-known biomarker found in urine that allows the evaluation of kidney function (104). In the publications reporting glucose determination, nine of the 11 devices were developed for application in urine samples, while the remaining two were applied to saliva samples. One of the two reports of glucose determination in saliva samples is the work reported in Chapter 7 of this thesis. Glucose is a very important nutrient since it is the body's main source of energy (105). Elevated levels of glucose in saliva or urine can be an indicator of hyperglycemia and even diabetes. Finally, in the publications reporting uric acid determination, only one of the 10 devices reported were applied to saliva samples. The predominance of devices developed for urine determination of uric acid was also expected since it is also a common biomarker of kidney function (106).

Figure 1.17 – Distribution of the devices by type of biological sample for the determinations of creatinine, glucose, and uric acid reported.

With the clear prevalence of urine analysis of the three most common analytes, it seemed relevant to analyse the distribution by type of biological sample of all analytical determinations reported in Table 1.2. The results are shown in Figure 1.18(A), and it was possible to observe that over 80% of the analytical determinations were performed in urine samples. This seems to lead to the conclusion that urine is considered by the research community to be a much more established and reliable biological sample.

To further analyse the evolution of the use of these types of samples in point-of-care, the progression of the reports related to each type of sample throughout the years was also evaluated (Figure 1.18(B)). When analysing the results, at first glance, a clear correlation between the choice of saliva as a biological sample and more recent publications was not observed. However, the publications that reported the use of saliva as a biological sample between 2020 to 2025 correspond to 80% of the total publications related to saliva, therefore indicating that the use of saliva as a biological sample in point-of-care testing is not as predominant as urine, because it is a more recent and unexplored sample source. A possible cause for this increase in 2020 could be the COVID-19 pandemic. The widely used COVID rapid self-tests could be the trigger that sparked the researcher´s' interest in using saliva samples in point-of-care testing.

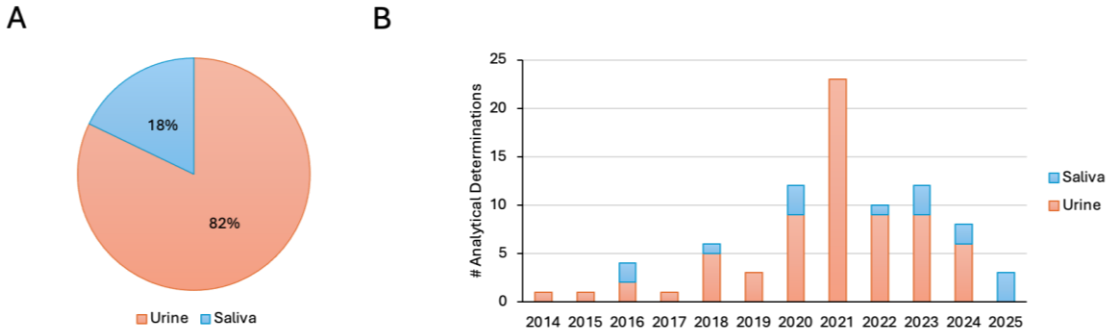

Figure 1.18 – (A) Distribution of all the analytical determinations by type of biological sample; (B) Evolution of analytical determinations applied to saliva or urine samples throughout the years.

Regarding the microfluidic device itself, two main characteristics were identified in all reports in Table 1.2, namely the type of structure of the device and the detection method used. In terms of structure, the devices can be fabricated with a 2D or a 3D structure.

As mentioned before the 2D devices are usually composed of only one layer of paper, and therefore use the lateral flow through that layer. The 3D devices, on the other hand, are composed of two or more layers consequently using the vertical flow through those layers. This 3D structure can be achieved either by folding or by stacking layers of paper.

After analysing the results obtained in the Web of Science search, it was possible to conclude that almost 70% of the microfluidic devices developed for analysis in saliva or urine samples, consisted of a 2D structure (Figure 1.19(A)). Of the remaining 26 analyte determinations achieved using 3D devices, 11 used the folding techniques and 15 used the stacking technique.

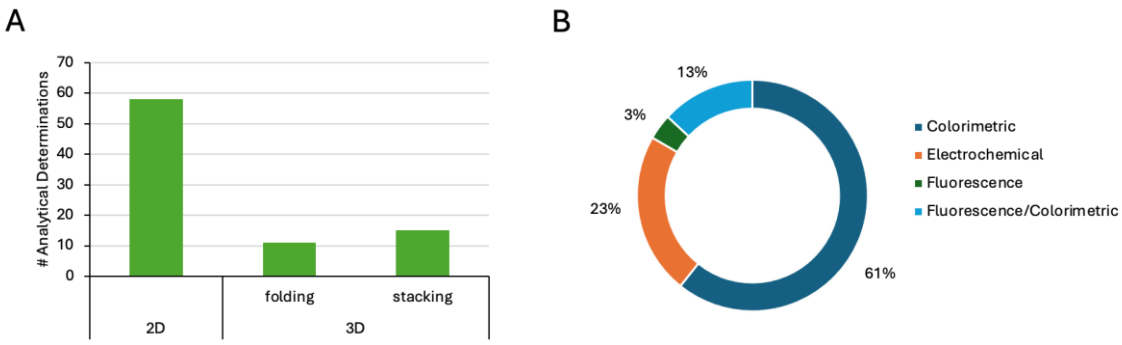

Figure 1.19 – Distribution of all the analytical determinations in Table 1.2 by (A) type of structure of the devices and (B) by detection method used.

Although, at first glance, the stacking technique might seem the more popular, in reality, six of the 15 devices reported with 3D structure consist of the work presented in this thesis in Chapters 3 to 7. Furthermore, another six reported devices were developed by colleague researchers from our laboratory. These use an innovative technique, similar to the one reported in this thesis, that was invented within the research group. So, of the initial 15 reports, only three analytical determinations using 3D μPADs assembled by stacking were reported by researchers of other research groups.

Srisomwat C. et al reported in 2024, a 3D device for the simultaneous determination of Δ9-tetrahidrocannabinol and ethanol in saliva samples, and Tong et al reported in 2025 the development of a 3D device for the determination of uric acid also in saliva samples (81,102).

The detection method is a very important choice when developing a point-of-care device. Among the most commonly used in μPADs are the colorimetric, the electrochemical, and the fluorescent detection. The colorimetric is usually the most common of them since it allows a visual perception of the results, which could be captured with a smartphone, a camera, or a regular scanner.

Of all the analytical determinations in Table 1.2, over 60% rely on colorimetric detection. In second place, but with a considerable distance, is the electrochemical detection, which was used in 23% of the determinations. The fluorescence was the least used detection method of the three, being applied in only 3% of the reports in Table 1.2. The remaining 13% correspond to devices that used a combination of the fluorescent and colorimetric methods. These devices relied on the fluorescent reaction that usually provide higher sensitivities, but the recording of the results was performed by capturing the signal with smartphones or cameras and the images were analysed with image processing software, similar to colorimetric detection.

Nevertheless, as expected, the colorimetric detection is the widely preferred detection method, as it provides numerous advantages like simplicity and little-to-no equipment requirement, that far outweigh the few limitations that are associated with it.

1.5. Objectives

The purpose of the work presented throughout this thesis was to design and develop innovative point-of-care methodologies based on the microfluidic paper-based analytical device approach for the determination of several health-related parameters, that could serve as an adding tool in the diagnosis and monitoring of several health conditions.

This work also aimed to highlight the use of biological samples of non-invasive collection, such as saliva and urine, as viable alternatives to traditional diagnostics using blood samples. The collection of these samples is painless, does not require specialized training or equipment, and reduces the risks associated with invasive procedures, such as infections or patient discomfort. By combining non-invasive sampling methods with microfluidic paper-based analytical devices, this research aimed to enhance diagnostic accessibility, particularly in point-of-care settings where traditional sample collection may be impractical or even impossible.

In order to achieve reliable and easy-to-interpret results, this thesis also aimed to explore the use of colorimetric detection methods, which allow for rapid visual analysis without the need for complex instrumentation or training.

To further improve the specificity and accuracy of these diagnostic tools, this work intended to incorporate enzymatic reactions into some of the developed μPADs. The use of enzymatic reactions should enhance selectivity by enabling highly specific biochemical interactions, reducing interference from non-target substances, and ultimately increasing the accuracy of the results.

Overall, this research aimed to close the gap between advanced diagnostic methodologies and real-world healthcare needs by developing innovative, cost-effective, and accessible point-of-care testing solutions. Combining microfluidic paper-based analytical devices, non-invasive sample collection, and optimized detection strategies, this work intended to contribute to the ongoing efforts to improve early disease detection, patient monitoring, and healthcare accessibility, particularly in isolated areas with little to no resources.

1.6. Structure of thesis

This thesis was organized in a total of ten chapters.

In Chapter 1, a general introduction is presented. The main concepts of point-of-care devices, μPADs and its application to biological samples of non-invasive collection, is also discussed.

In Chapter 2, a brief presentation of the general material and methods used throughout the experimental work, is presented. However, material and methods specificities of the developed devices are referred in the respective chapter.

In the subsequent six chapters (from Chapter 3 to Chapter 8), a detailed description of the developed microfluidic paper-based devices developed for point-of-care analysis is presented. In each chapter, the results, their discussion and respective conclusions of the developed methodology, is also described. Chapters 3 to 7 are devoted to the development of microfluidic paper-based analytical devices for analysis of biomarkers present in biological samples of non-invasive collection and, in Chapter 8, a novel methodology of semi-quantification of *Escherichia coli* for public health monitorization.

The developed work that is published in international scientific periodicals with peer review are identified in each chapter. The information presented in this thesis corresponds to the published information. However, an option was made to present it in the format of a thesis.

In Chapter 3, the work entitled “New microfluidic paper-based analytical device for iron determination in urine samples” is presented. This work is published in Analytical and Bioanalytical Chemistry, Volume 413, 7463–7472 (2021).

In Chapter 4, the work entitled “Design and functionalization of a μPAD for the enzymatic determination of nitrate in urine” is presented. This work was published in Molecules, Volume 26, 6355 (2022).

Chapter 5 presents the work: “On-hand tool for ammonium and urea determination in saliva to monitor chronic kidney disease – design of a couple of microfluidic paper-based devices”. This work was published in Microchemical Journal, Volume 193, 109102 (2023).

In Chapter 6, a description of the work entitled “A microfluidic paper-based device for monitoring the urease activity in saliva” is presented. This work was published in Biosensors, Volume 15, 48 (2025).

In Chapter 7, a description of the work entitled “Alternative diabetes monitorization tool: development of microfluidic paper-based device for glucose determination in saliva samples.” is presented. This work is now in preparation for publication.

In Chapter 8, a description of the work entitled “Newly designed lateral flow strips for a semi-quantitative analysis of *E. coli*.” is presented. This work is now in preparation for publication.

The final chapter (Chapter 9) is devoted to the general conclusions of the developed work and some possible future work.

Chapter 2. General Materials and Methods

2.1. Reagents and Solutions

All chemicals used in this thesis were of analytical grade and no further purification was applied. Milli-Q water with a resistivity of under 18 MΩ·cm was used throughout most of the work presented (Chapters 4-7); however, in Chapter 3 deionized water with specific conductance under 0.1 mS/cm was used.

Standard stock solutions were prepared by either weighing the respective solid in a analytical balance (Mettler Toledo AG204) followed by dissolution in appropriate solutions, or by rigorous dilution from a concentrated solution. The working standard solutions were prepared by rigorous dilution of the stock solutions using glass volumetric pipettes and volumetric flasks (class A) of different volumes.

Synthetic saliva used in this thesis was prepared based on concentrations reported by Batista et al. (107): [KCl] = 2237 mg/L; [KH_2PO_4] = 544.3 mg/L; [HEPES] = 4766 mg/L; [$CaCl_2 \cdot 2H_2O$] = 77.69 mg/L; [MgCl] = 19.04 mg/L; [Bovine Serum Albumin] = 2700 mg/L.

Synthetic urine used in this thesis was prepared based on concentrations reported by Machado et al. (108): [Urea] = 10 g/L; [Uric Acid] = 0.07 g/L; [Creatinine] = 0.8 g/L; [NaCl] = 5.2 g/L; [Latic Acid] = 0.1 g/L; [Citric Acid] = 0.4 g/L; [$CaCl_2 \cdot 2H_2O$] =0.37 g/L; [$MgSO_4 \cdot 7H_2O$] = 0.49 g/L; [Na_2SO_4] = 1.41 g/L; [KH_2PO_4] = 1.2 g/L; [Glucose] = 0.49 g/L.

When required, the pH of solutions was measured using a combined glass pH electrode (Crison 52-02) and a Crison (model 2002) potentiometer.

2.2. µPAD Assembly Materials

To assemble the microfluidic devices reported in Chapters 3 through 7, plastic laminating pouches were used as the hydrophobic area and filter paper discs were used as hydrophilic area (Figure 2.1(A)). All pouches were previously perforated with either a puncher (KNIPEX; Chapter 3) or a laser cutting machine (FDA, Model 3040; Chapters 4 – 7), in a column and row grid distribution, to allow the posterior sample insertion in the device (Figure 2.1(A)). The size of the pouches and of the holes varied throughout the developed work, which consequently changed column x row distribution. In Chapter 3, a 75 x 110 mm plastic pouch (glossy, 125 microns, Q-Connect) was perforated with a total of 20 holes of 5 mm diameter, in a 4 column and 5 row distribution. In the work reported in Chapters 4 and 7, the same 75 x 110 mm pouch was used but with a 4 column and 6 rows distribution of 3 mm diameter holes, to a total of 24 holes. In Chapters 5 and 6, the devices were assembled with A6 size plastic laminating pouch (125 µm, Leitz) perforated with 32 holes of 3 mm diameter, in a 4 column and 8 row distribution.

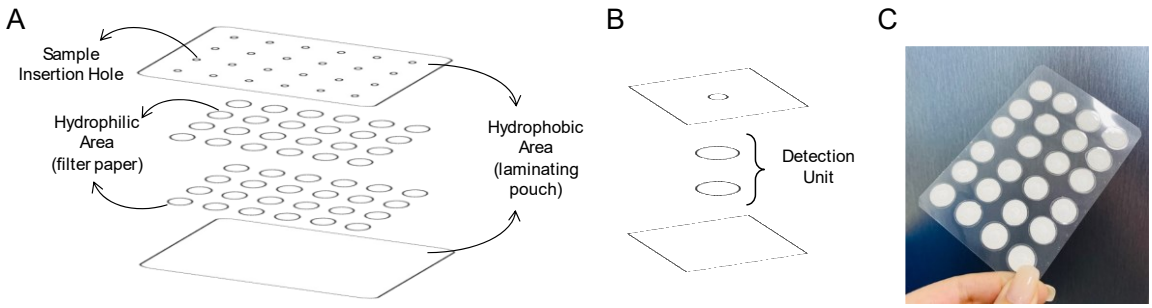

Figure 2.1 – Schematic representation of: (A) the general structure and components of a μPAD; (B) of a detection unit; and (C) photograph of a μPAD after lamination.

The hydrophilic area of the devices was composed of multiple layers of filter paper discs embedded with the different reagents, stacked on top of each other. Each stack was called a detection unit and was aligned under each of the holes in the laminating pouch (Figure 2.1(B)). The size of the discs and the type and porosity of filter paper varied not only within the layers of the device but also among the different devices reported. Furthermore, all discs with embedded solutions were dried in the oven at a specific temperature and for a set amount of time, depending on the stability requirements of the solution, on the reaction and on the objective of the device itself.

After the alignment of the detection units inside the plastic laminating pouch, the lamination process was performed which consisted in passing the pouches through the laminator (United Office – ULG 300 B1 in Chapters 3-6; A3-330C Laminator in Chapter 7) to melt the plastic and seal the devices, thus creating a solid barrier in between the detection units (Figure 2.1(C)). After the lamination the devices were ready to be used.

2.3. General Determination Procedure

To initiate the determination procedure, the sample or standard was introduced into the devices through the sample insertion holes. In the devices developed for determination of urea and urease, in Chapters 5 and 6 respectively, and additional step of placing NaOH in the devices is required. Afterwards, in all devices developed and reported in Chapters 3 to 7, the sample insertion holes were covered with adhesive tape to prevent possible evaporation and/or contaminations when handling the biological samples. When the sample or standards comes in contact with the reagents embedded in the device, a set of reactions are prompted, including a colorimetric reaction, which leads to either the formation of a colorimetric product or a change of colour of one of the reagents. To capture the colour, all the devices developed were scanned with a portable scanner (Cannon LiDE 120).

In Chapters 3, 4 and 5, because the reactions involved in the determination occur continuously, only the time between the sample/standard introduction and the scanning of the μPAD is controlled, and it was named reaction time (RT).

However, in Chapters 5 and 6, an additional solution of NaOH is placed in the device, so the time between the sample/standard introduction and the placement of NaOH was called enzymatic reaction time (ERT), and the time following the placement of NaOH up until scanning the device was named colorimetric reaction time (CRT).

The scanned images were then processed using the image processing software ImageJ (National Institutes of Health, USA). First, the images, which are obtained in RGB format, were separated in its three components: Red, Green and Blue (Figure 2.2(A)). Then the average intensity of colour of the pixels is measured in one of the RGB components (Figure 2.2(B)). This choice of RGB component depends on the colour of the coloured product that was being measured. Most chemicals exhibit colour due to their ability to absorb specific wavelengths of light while reflecting others. Consequently, the colour that is perceived is typically the complementary to the light it absorbs. The colour wheel is a tool that illustrates these oppositional relationships between colours and consequently can be used to accurately select of RGB component that would allow a highest absorbance based on the observed colour (Figure 2.2(C)).

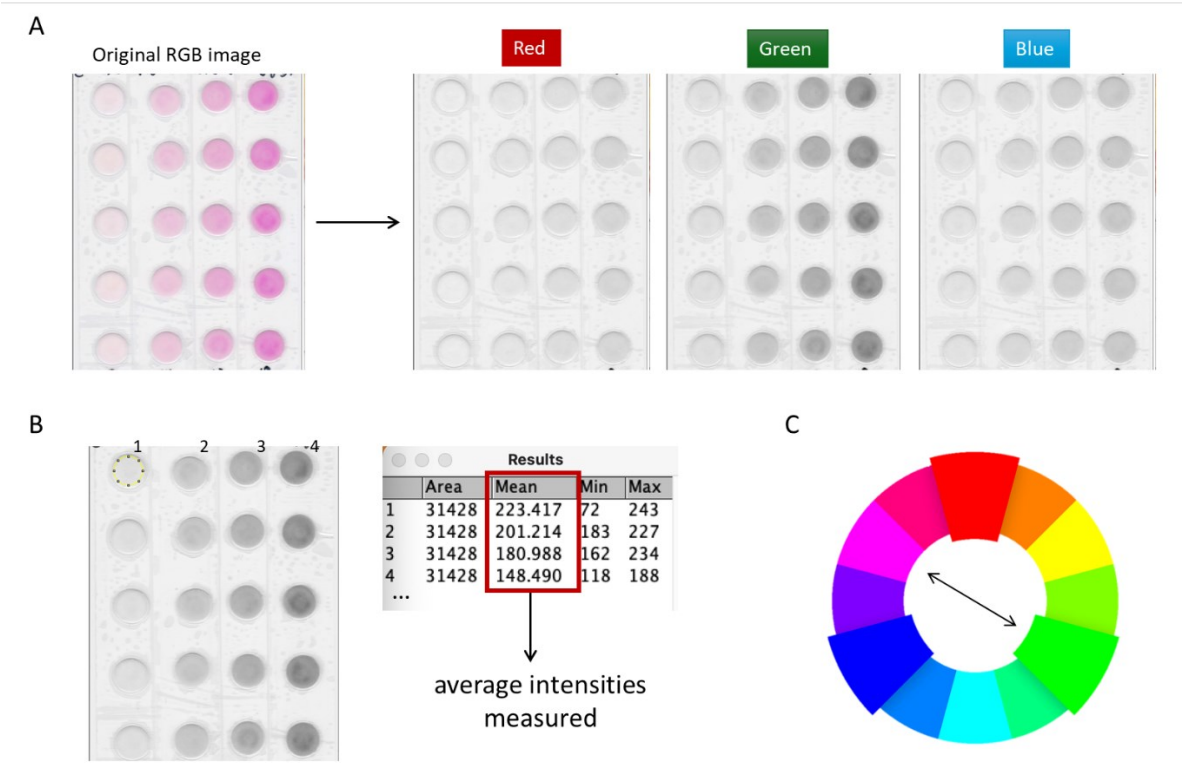

Figure 2.2 – Exemplification of the image analysis steps: (A) choice of RGB component and (B) measurement of intensities of each detection unit; (C) Colour wheel scheme with exemplification of complementary colours: pink and green.

In the work developed in Chapters 3 to 7, the RGB component chosen was the one that was closest to the complementary colour of the coloured product. Furthermore, the measurements of intensity of colour were obtained using the circular selection tool, however the size of this selection tool varied according to variables such as size of paper discs or size of the sample insertion hole of the device been analysed.

The intensities of colour of the pixels in the image were then converted into pseudo-absorbance values using the following formula:

$$A = \log_{10} (I_B / I_S)$$

where I_B is the intensity of colour of the blank signal, obtained when loading water (Chapters 3, 4, 5 and 7) or synthetic saliva (Chapter 6), and I_S is the intensity of colour obtained when loading the sample or standard solution into the device.

Calibration curves were established using the concentration of the analyte and the corresponding absorbance signal. The concentration of the analyte in the samples was calculated interpolating its absorbance value in the calibration curve.

For each reading of blank, standard or sample, several measurements were obtained, and outliers were removed when necessary. The remaining replicates were used in average calculations.

2.4. Optimization Process (for the devices' development)

For the development and optimization of a μPAD, first some parameters, such as reagent concentration and volumes, were roughly chosen on a trial-and-error basis and tested in a batchwise procedure to perform the determination between the expected concentration limits. Then, the determination was scaled down in proportion to the expected volumes usually accommodated by the devices.

After this initial prototype of device is achieved, the several parameters were optimized in order to obtain the highest sensitivity and lowest limits of detection and quantification possible. To achieve this optimization, each parameter was varied within certain interval, and the sensitivities of the calibration curves obtained were compared by calculating the relative deviation, %RD, as follows:

$$\%RD = [(S_{Ob} – S_{Ref}) / S_{Ref}] \times 100$$

in which S_{Ob} is the sensitivity of the calibration curved obtained with the tested parameter, and S_{Ref} is the sensitivity of the reference calibration curved obtained up until that testing point. A %RD below or equal to 10% was considered non-significant.

After optimization, the developed μPADs were characterized in terms of dynamic range, average calibration curve, limits of detection and quantification and repeatability.

The dynamic range was established by inserting a set of working standard solutions with different concentrations and assessing the range in which the absorbance signal was linearly correlated to the concentration of the analyte.

The average calibration curve was obtained by calculating the mean and standard deviation of the slopes, the intercepts and of the correlation values of several calibration curves.

The limit of detection (LOD) was calculated according to IUPAC recommendations (109). When expressed in concentration units, it represents the concentration corresponding to the smallest measurement that can be detected with a reasonable certainty with the developed device (X_{LOD}) and was calculated as follows:

$$X_{LOD} = 3 \times SD_{intercept}$$

where SD represents the standard deviation of the intercept of the calibration curve, and 3 is a numerical factor determined assuming a 95% confidence interval.

The limit of quantification (LOQ) was also calculated according to IUPAC recommendations using a similar procedure and also expressed in concentrations units (109). The calculated value derived from the smallest measure (X_{LOQ}) that can be quantified with reasonable certainty with the developed µPAD, and was calculated as follows:

$$X_{LOQ} = 10 \times SD_{intercept}$$

where SD represents the standard deviation of the intercept of the calibration curve, and 10 is a default value by IUPAC that represents a 10% relative standard deviation.

In Chapter 5, the repeatability of the developed µPADs was obtained by calculating the relative standard deviation (RSD) of a sample measurement, by dividing the standard deviation of the sample measurements by the average of those values. In the remaining chapters (3, 4, 6 and 7) the repeatability of the µPADs was evaluated by the determination of the relative standard deviation of the slopes of a set number of calibration curves. In some of the works presented in this thesis, an additional distinction between intraday repeatability and interday repeatability is performed. The intraday repeatability is calculated using the slope of calibration curves prepared within the same day, while interday repeatability is calculated considering calibration curves prepared in different days.

2.5. Stability Assessment

In the development of all the reported µPADs (Chapters 3-7), stability studies were performed in order to evaluate its potential field application. Storage stability studies and the stability of the coloured product formed were both performed for all devices developed.

The storage stability studies allowed to evaluate the performance of the devices when stored in different atmospheric conditions and/or at different temperatures, for several periods of time. To perform these studies, several devices were prepared, wrapped in aluminium foil (protected from light) and stored in plastic bags (Lacor, 69053) (Figure 2.3). Two atmospheric conditions were used consistently throughout the thesis: air and vacuum, the latter obtained using a vacuum packaging machine (Henkovac – MINI/120-ST ECO).

Different periods were tested for each condition and at every studied period the stored μPAD was used to perform a calibration curve and compared to calibration curve of a freshly assembled μPAD with the same set of standards. A relative deviation below 10% was considered non-significant.

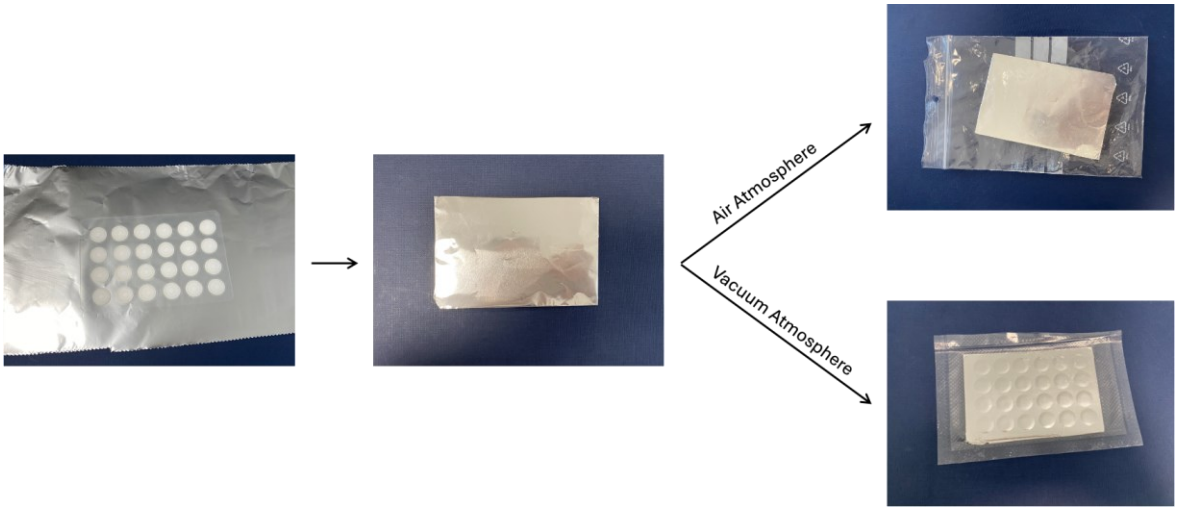

Figure 2.3 – Schematic representation of the procedure steps of the storage stability assessment under two different atmospheric conditions.

The studies of colour product stability evaluate the colour development in the device and its influence in the sensitivity obtained. This, consequently, directly influences the reported optimal time for scanning the devices. To perform these studies a μPAD is prepared, standard solutions are placed, and the device is scanned at several periods. The slopes of the calibration curves obtained with the different scanning times were compared and a relative deviation below 10% was considered non-significant.

2.6. Sample Collection and Preparation

Since two different types of samples were used throughout this thesis, the collection of each type of sample was performed differently, however, all samples were collected as “blind samples” from volunteers with their informed consent.

The urine samples used in both Chapter 3 and 4 were collected by the volunteers and stored in the freezer at -20 ºC until use.

The saliva samples used in Chapters 5 – 7 were collected with a general procedure for collection of saliva samples (Figure 2.4) consisting of first placing a 5 x 5 cm sterile gauze in the mouth; then, after 2 minutes, removing the gauze from the mouth and placing it in a 5 mL sterile syringe; and finally, squeezing the gauze into a 5 mL plastic tube to remove the saliva and obtain the final sample. In Chapter 5, additional methodologies for collecting saliva samples were tested and reported.

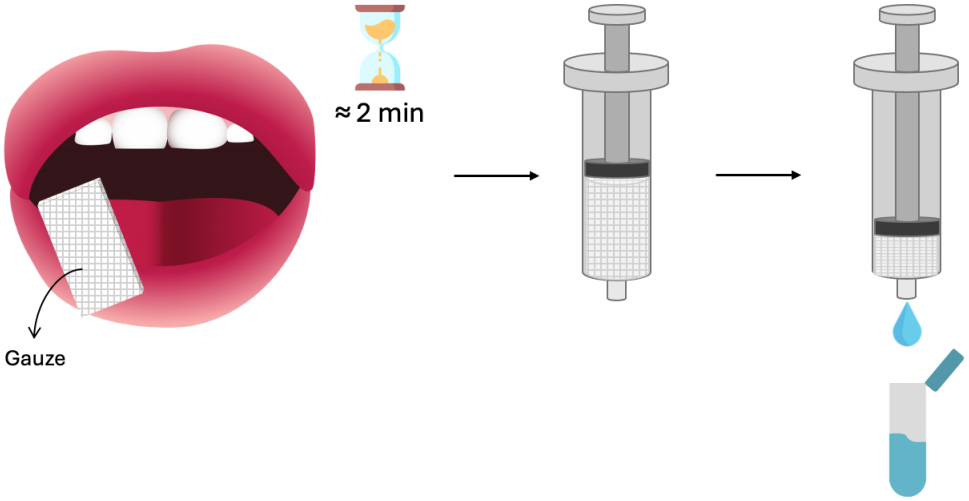

Figure 2.4 – Schematic representation of the generally used saliva collection procedure.

2.7. Validation

The accuracy of the developed devices was evaluated by comparing the results obtained by the proposed μPAD ($C_{\mu PAD}$) with those obtained by a corresponding reference procedure (C_{REF}). The results obtained were plotted and a linear regression was established between the two variables (Figure 2.5). The regression line intercept (C_0) and slope (S) were calculated, and a perfect agreement of the methods would mean a C_0 equal to 0 and S equal to 1. So, the methods were considered to be statistically comparable when C_0 and S did not differ significantly from 0 and 1, respectively. This was verified by estimating the error in the intercept and slope values through calculation of their confidence limits at 95% significant level (110).

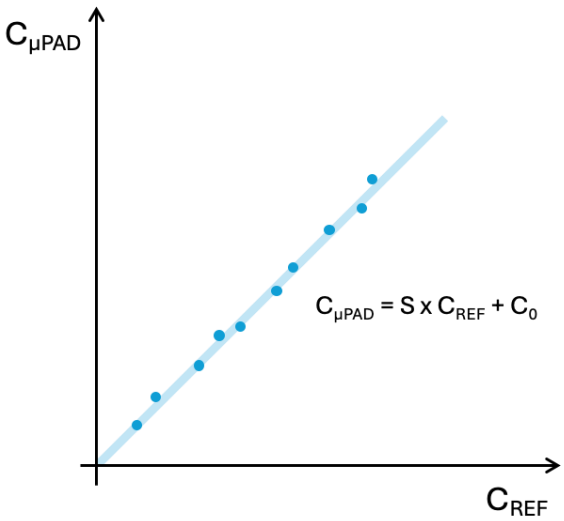

Figure 2.5 – Schematic representation of the correlation established between the concentrations obtained with the μPAD ($C_{\mu PAD}$) and with the reference method (C_{REF}).

The relative deviation (RD) values, expressed as percentage, were calculated based on the expression:

$$\%RD = [(C_{\mu PAD} - C_{REF})/C_{REF}] \times 100$$

In Chapter 4, the accuracy of the developed device was assessed by recovery studies. The sample was analysed before and after a standard addition of analyte and the recovery was calculated, according to IUPAC (2002) (111), as follows:

$$R_A = [Q_A(O+S) - Q_A(O)] / Q_A(S)$$

where $Q_A(O)$ the quantity of the original sample, $Q_A(S)$ is the quantity of analyte A added (spiked value), and $Q_A(O+S)$ the quantity of A recovered from the spiked sample.

The recovery value was then presented in percentage and a significant test known as a null hypothesis (110) was used to evaluate if the percentages were statistically different from 100%. So, in order to decide if the average of the results (the recovery percentages) was different from 100%, the following expression was used:

$$t = \frac{(\bar{X} - \mu)}{\frac{s}{\sqrt{n}}}$$

where $\bar{X}$ is the average of the recovery percentages, n is the number of samples, s is the standard deviation of those results and μ is the value to be compared with, in this case 100%. The value of t calculated is compared with the critical value listed in the t-distribution tables. If the calculated value, $|t|$, is below the $t_{critical}$ it means that the recovery percentages are not statistically different from 100%; if the calculated value exceeds the $t_{critical}$ it means that there is a systematic error in the results.

2.8. E. coli – Lateral Flow Strip

In chapter 8, the development of a lateral flow strip test (LFS) is reported. This work was a result of a mobility to the Mazumdar-Shaw Advanced Research Center – University of Glasgow in Scotland. Since this work uses very different materials and methodologies to the ones used in the remaining work reported here, the detailed information of the solutions, materials and methodologies is described in Chapter 8.

Chapter 3. Total Iron in Urine Samples

Chapter based on the paper published in

Analytical and Bioanalytical Chemistry

Volume 413, 7463–7472 (2021)

https://doi.org/10.1007/s00216-021-03706-9

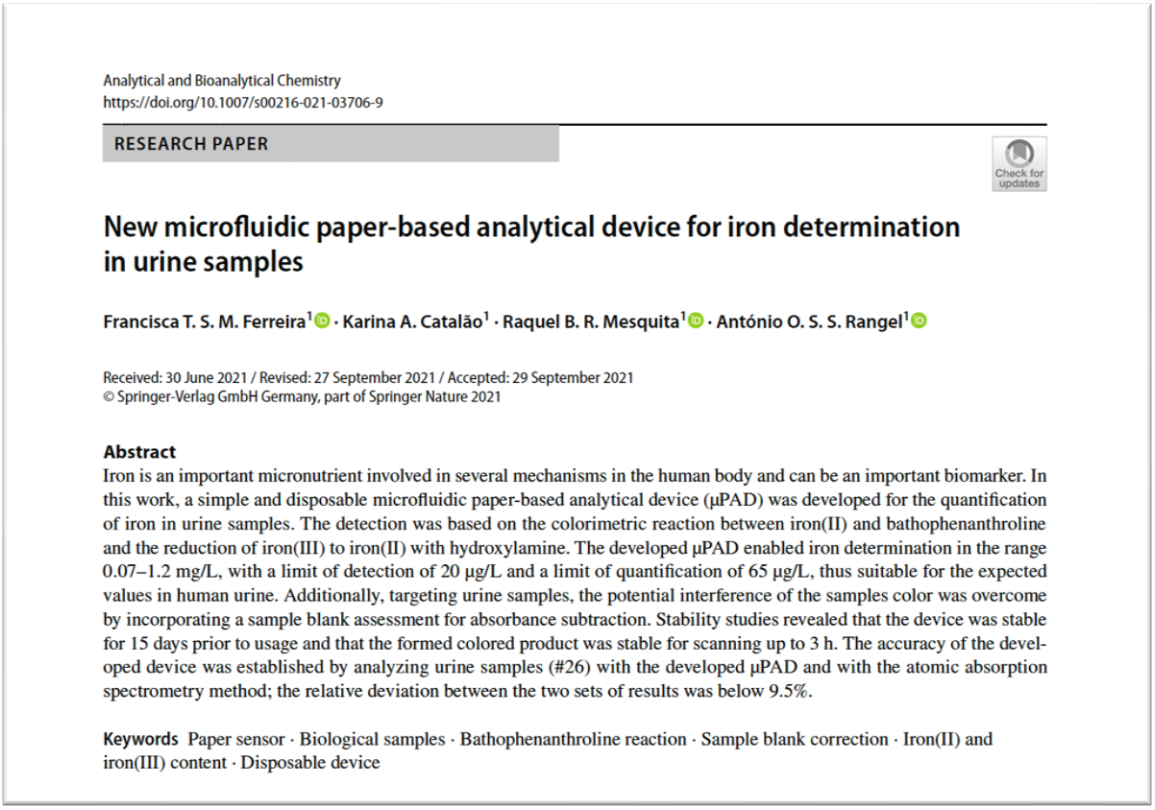

Analytical and Bioanalytical Chemistry
https://doi.org/10.1007/s00216-021-03706-9

RESEARCH PAPER

New microfluidic paper-based analytical device for iron determination in urine samples

Francisca T. S. M. Ferreira[1] · Karina A. Catalão[1] · Raquel B. R. Mesquita[1] · António O. S. S. Rangel[1]

Received: 30 June 2021 / Revised: 27 September 2021 / Accepted: 29 September 2021

Abstract
Iron is an important micronutrient involved in several mechanisms in the human body and can be an important biomarker. In this work, a simple and disposable microfluidic paper-based analytical device (μPAD) was developed for the quantification of iron in urine samples. The detection was based on the colorimetric reaction between iron(II) and bathophenanthroline and the reduction of iron(III) to iron(II) with hydroxylamine. The developed μPAD enabled iron determination in the range 0.07–1.2 mg/L, with a limit of detection of 20 μg/L and a limit of quantification of 65 μg/L, thus suitable for the expected values in human urine. Additionally, targeting urine samples, the potential interference of the samples color was overcome by incorporating a sample blank assessment for absorbance subtraction. Stability studies revealed that the device was stable for 15 days prior to usage and that the formed colored product was stable for scanning up to 3 h. The accuracy of the developed device was established by analyzing urine samples (#26) with the developed μPAD and with the atomic absorption spectrometry method; the relative deviation between the two sets of results was below 9.5%.

Keywords Paper sensor · Biological samples · Bathophenanthroline reaction · Sample blank correction · Iron(II) and iron(III) content · Disposable device

Submission received: 30 June 2021

Revised: 27 September 2021

Accepted: 29 September 2021

Published: 15 October 2021

3.1. Introduction

Iron is one of the most studied micronutrients on Earth and it is crucial for the existence of life. This metal is associated to several important roles such as the transport, storage and use of oxygen, the correct function of hundreds of proteins and enzymes, the DNA synthesis, among others (112). Because it is present in several biological mechanisms, iron metabolism is very tightly regulated and, both deficiency and overload of this metal can cause severe damages. The majority of the iron a human individual requires is achieved by recycling it from senescent blood cells, the remaining comes from diet intake (112,113). When it exceeds the normal concentration, the excretion occurs in urine (113). The normal excretion rate is of approximately 100 µg/day to 300 µg/day. In case of deficit or excess of the ingested iron, excretion will be less or more than normal, respectively (114). A few common diseases associated with the deregulation of iron are anemia, hemochromatosis (> 20 mg/day), cancer and neurodegenerative diseases (112,114). Because of all the relevant roles and common diseases related to iron regulation in the human body, it is essential to have simple, rapid, and effective monitoring tool. Currently, urinary iron is mostly determined by inductively coupled plasma (ICP) combined with either mass or optical emission spectrometry; however, these techniques require costly and complex equipment (114–116).

In the human body, iron is present in two different oxidation states, the divalent ferrous (Fe^{2+}) and the trivalent ferric (Fe^{3+}), and it changes its state in order to participate in several biological reactions (117). At the physiological pH, iron is usually present in the ferric state, Fe(III), although it is only absorbed as Fe(II) (118). The determination of iron in biological fluids, namely urine, has then the potential of being useful for health diagnosis. However, although there are some reported works describing paper-based devices for iron determination, only the work by Kamlesh Shrivas (2020) targets the analyses of biological fluids (blood), in addition to water samples (119–121).

In this context, the aim of this work was to develop a new microfluidic paper-based analytical device (µPAD) capable of performing on-hand quantification of iron in human urine samples, enabling to overcome potential sample colour interference. Since iron can be present in both forms, an option was made to perform the determination of total iron. The assembly of the µPAD relied in an innovative approach and the detection was based on the colorimetric reaction of bathophenanthroline with iron (II), a selective and sensitive methodology (26,122,123). To attain the determination of total iron, bathophenanthroline (BPS) was combined with hydroxylamine, a well-known reducing agent capable of converting Fe (III) in Fe (II) (123) (Schemes 3.1 and 3.2).

Scheme (3.1) $2Fe^{3+} + 2NH_2OH \longrightarrow 2Fe^{2+} + N_2 + 2H^+ + 2H_2O$

Scheme (3.2) $Fe^{2+} + BPS \longrightarrow BPS$ (Colourless) → (Pink)

To handle the potential colour of the urine samples, sample intrinsic absorption, a sample blank approach was considered. As far as we know, it was the first time this approach was used in a paper-based platform. This feature was highly important to ensure the applicability of the developed µPAD,

as urine may present a wide variability of colour range, from light yellow to brownish. In the end, this innovative solution enabled the determination of total iron in several urine samples with the developed disposable device in an in-situ approach.

3.2. Materials and Methods

3.2.1. Reagents and Solutions

A standard stock solution of 50 mg/L iron was monthly prepared by dilution of the iron atomic absorption standard solution (1000 mg/L) (Fluka, 16596-250 mL). The working standards were weekly prepared from the stock solution in the dynamic range of 0.1 – 1.2 mg/L Fe (III) in 5 mM of nitric acid.

A 1 g/L bathophenanthroline solution (BPS) was monthly prepared by dissolving 20 mg of bathophenanthroline disulfonic acid disodium salt hydrate (Alfa Aesar) in 20 mL of deionized water and stored in a dark bottle.

The hydroxylamine solution was prepared by dissolving 0.75 g of the solid (Sigma-Aldrich) in 7 mL of HCl 6 M and then completed to 50 mL with deionized water to final concentrations of 15 g/L hydroxylamine in 0.84 M of HCl. The 6 M HCl solution used was obtained from hydrochloric fuming acid (d = 1.19, 37%, Merck).

The working reagent solution (BPSh) was daily prepared by mixing 1 mL of BPS solution and 400 mL of hydroxylamine solution and it was stored in a dark bottle and shielded from the light.

3.2.2. Assembly of the µPAD and Analytical Procedure

The developed µPAD (Figure 3.1(A)) consisted in 20 filter paper units, as hydrophilic area, aligned in a 4 columns and 5 rows distribution, inside of a laminating pouch, as hydrophobic area (L1 and L2 – Figure 3.1(A)). The paper units were placed under 5 mm holes, previously perforated using a puncher for the sample insertion (L1 – Figure 3.1(A)).

Each unit (Figure 3.1(B)) consisted of two layers: top layer R1, the reagent layer, a paper disc Whatman Grade 1 filter, 9.5 mm diameter; and E1, an empty layer, a paper disc Whatman Grade 3 filter, 12.7 mm diameter. The reagent paper discs were prepared by adding 10 µL of the working reagent solution (BPSh) to the discs and then dried it in the oven for 15 min at 50 °C.

After the alignment of the paper units with the sample insertion holes of the laminating pouch they were passed through the laminator (United Office – ULG 300 B1), where the plastic sheets of the pouch sealed around the paper units, creating a strong physical barrier between the units (Figure 3.1(C)).

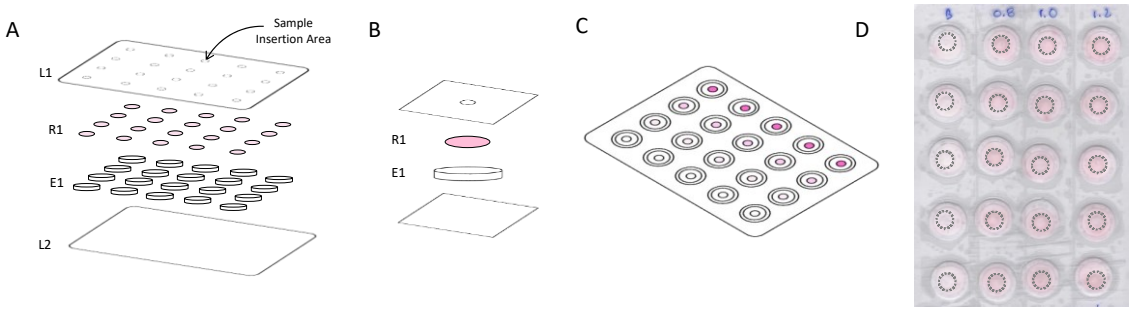

Figure 3.1 – Schematic representation of the μPAD assembly for iron determination; (A) Indication of the layers alignments: L1, perforated top layer of the laminating pouch for sample/standard insertion; R1, reagent layer; E1, empty layer; L2, bottom layer of the laminating pouch; (B) Schematic representation of one unit of detection. (C) Schematic illustration of the top view of the μPAD after standard placement; (D) Scanned image of the μPAD (top view) with indication of the selected area for intensity measurement (dotted circles).

To perform the measurements, after assembly of the μPAD, 40 μL of sample/standard were inserted through the μPAD sample hole. It was established to have five units for each standard/sample (corresponding to one column), to enable the exclusion of outliers (if necessary) and still have replicates. Once the sample/standard was completely absorbed, the sample holes were covered with adhesive tape, to prevent possible contaminations when handling the targeted biological samples.

The iron in the sample/standard reacts with the BPS and hydroxylamine mixture (BPSh) while going through the reagent layer (layer R1) forming a pink colour product. The intensity of pink colour is directly proportional to the concentration of iron in the sample. To measure the intensity of the colour, the top layer of the μPADs was scanned and the images processed using an image software.

The time between the sample/standard introduction and the scanning of the μPAD, named reaction time (RT), was set to 20 minutes. In the ImageJ program, images were converted into RGB plots, and the green component used to measure the intensity, since the expected coloured product of the BPS reaction with iron is pink (from which the complementary colour is green). For each unit, an option was made to do the measurements in the sample insertion hole where the coloured product was concentrated (5 mm diameter) corresponding to a circular selection of 100 × 100 pixels, (Figure 3.1(D)). The intensity values were then converted into absorbance values.

3.2.2.1. Urine sample μPAD - the design adjusted to include sample blank

As the colour measurement is based on a RGB filter selection (not a specific wavelength), the potential interference of the colour of the urine sample was addressed. Urine has a highly variable colour, intrinsic absorption, so the strategy for eliminating its potential interference consisted in incorporating, in the μPAD card, the measurement of a sample blank. This measurement corresponded to the intensity values registered when loading the sample without the colour reagent.

For the absorbance calculation, a I_0 value is needed, so the sample µPAD card also needed to include one column (with five units) for the corresponding blank signal, without BPS and to be loaded with water.

Therefore, only the reagent layer of the sample µPAD was different from the reagent layer of the standards µPAD (Figure 3.1): two columns of the reagent layer included the colour reagent (BPS) and other two columns just had hydroxylamine (Figure 3.2 (A)).

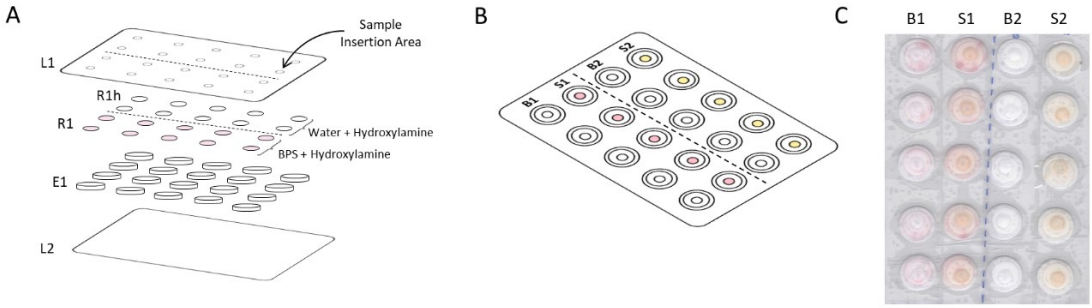

Figure 3.2 – Schematic representation of the sample µPAD for iron determination in urine samples; (A) Layers' assembly: L1, perforated top layer of the laminating pouch for sample/standard insertion; R1, BPSh reagent (BPS + hydroxylamine) layer; R1h, reagent without BPS (water + hydroxylamine) layer; E1, empty layer; L2, bottom layer of the laminating pouch; (B) Schematic representation (top view) of the placement of one urine sample with and without colour reagent (S1 and S2) and the respective blanks (B1, blank of the colour reaction and B2, blank of the urine colour); (C) Scanned image of the µPAD (top view).

To analyse the urine sample, the two columns with BPS were prepared as mentioned above; one column (B1 in Figure 3.2(B)) was loaded with 40 µL of water, another one (S1 in Figure 3.2(B)) loaded with 40 µL of sample for total absorbance (A_T) calculation. As for the two columns without BPS, the reagent layer (R1h) was prepared only with hydroxylamine solution (without the colour reagent BPS) and aligned on top of the empty layer (E1). Again, one column was loaded with water and one column loaded with sample (B2 and S2, respectively, Figure 3.2(B)); the calculated absorbance corresponded to the sample blank (A_{SB}). The iron concentration of the sample was calculated based on the absorbance corresponded to the absorbance value resulting from the colour reaction (A_{CR}): $A_{CR} = A_T - A_{SB}$.

3.2.3. Samples

The urine samples were collected as "blind samples" from volunteers with their informed consent and stored at − 20 °C until use. The samples that showed turbidity (suspended solids) were filtrated using disposable syringe filters with a pore size of 0.45 µm (Chromafil® Pet -45/25; polyester). All samples were acidified to 5 mM of nitric acid before being analysed.

3.2.4. Reference Procedure - Validation

To assess the accuracy of the developed µPAD for the iron determination in urine samples, a comparison was made between the results obtained with the µPAD and those obtained by atomic absorption spectrometry (AAS).

For the AAS procedure, a calibration curve in the range 0.1 – 1.5 mg/L was established with iron (III) standards according to the reference protocol (124). The urine samples were prepared as described in section 3.2.3.

3.3. Results and Discussion

3.3.1. Preliminary studies

Different colorimetric reactions for iron determination, namely with thiocyanate and bathophenantroline (BPS), were tested to select the best regent for the target concentration range. The results obtained in a batchwise approach, showed a significantly higher sensitivity (over 4-fold increase) for the reaction with BPS. The same comparison was performed on a paper approach using two layers of paper (Whatman 1 12.7 mm diameter) one layer with 12 µL of reagent, as the top layer, and an empty bottom layer. The results also showed a significantly better sensitivity when using BPS, so it was the reagent chosen.

Because BPS reacts with Fe(II), a reducing agent was needed to convert Fe(III) to Fe(II) (123). For the reduction, a 15 g/L hydroxylamine solution was chosen due to its proven efficiency in previous work (125). Therefore, the reagent solution used in the development of the µPAD for iron determination was a mixture of BPS and hydroxylamine (BPSh). Different proportions of BPS and hydroxylamine were tested, based on what was reported by Marczenko (123), in order to attain a higher sensitivity with total conversion of Fe(III) in Fe(II). This was verified by comparing the calibration curves obtain from Fe(III) and Fe(II) standards, and as the calibration curves overlapped (relative deviation, RD < 2%), it confirmed that the Fe(III) was completely reduced to Fe(II).

3.3.2. Physical Parameters – µPAD Assembly

First, the physical parameters of the µPAD were studied, and a basic structure composed by two layers of paper discs was used. The idea was to force the sample/standard through a reagent layer and to have an empty layer below to promote the vertical flow and to serve as reservoir. The top layer, reagent layer, consisted in 9.5 mm diameter discs and the bottom layer consisted in 12.7 mm diameter Whatman 1 empty discs. The different paper discs sizes facilitated the alignment. To prepare the reagent layer, 12 µL of the reagent, [BPS] = 100 g/L, was used and after 10 min oven drying (at 50 ºC), the discs was aligned on top of the empty disc and laminated between the two sheets of the plastic pouches.

This assembly enabled the insertion of 25 µL of standard and reaction time (RT) of 20 minutes. Filter papers with different paper treatments and porosities (Appendix B) were tested on the reagent layer evaluating its influence in the slope of the calibration curve (Figure 3.3).

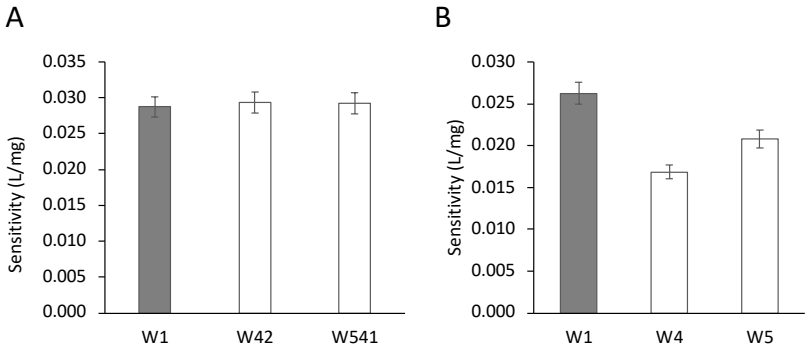

Figure 3.3 – Study of the influence in the calibration curve slope of different filter papers; (A) Papers with different treatments; (B) Qualitative filter papers with different porosities; the dark grey bars represent the chosen option; W1, Whatman 1 paper; W4, Whatman 4 paper; W5, Whatman 5 paper; W42, Whatman 42 paper; W541, Whatman 541 paper; the error bars represent 5% deviation of the measurements.

3.3.2.1. Filter Paper Type

When different paper treatments were being compared, Whatman 1, 42, 50 and 541, the calibration curves obtained were very similar (Figure 3.3(A)) except for the Whatman 50 paper, in which there was no full absorption of the standard and was excluded. As there were no significant differences in the sensitivities, Whatman 1 was chosen for being the paper without treatment (qualitative grade) and consequently being the most inexpensive.

3.3.2.2. Filter Paper Porosity

Using the chosen qualitative type, the influence of the paper porosity (Whatman 1, 4 and 5), was studied and the highest sensitivity resulted with Whatman 1, so it was the one chosen (Figure 3.3(B)).

Due to the manual assembly process, and with a RT of 20 min, it was observed that occasionally some units of the µPAD card were not fully dry. To guarantee that the entire µPAD was completely dry before scanning, a paper disk (Whatman 1) with diameter of 14 mm in the bottom (empty) layer was tested. Although there was no difference in the sensitivity (RD < 10%), the 14 mm discs did result in a more homogenous absorption in the entire µPAD card, so it was chosen.

So, after the physical parameters study, a two-layer µPAD with 9.5 mm and 14 mm Whatman 1 paper discs, for reagent and empty layer, respectively, was established.

3.3.3. Colorimetric Reaction – Iron Determination

After establishing the physical assembly of the µPAD, the influence of the BPS concentration was studied, to minimize consumption (batchwise studies were performed with a 100 g/L solution). The conditions used in this study were 12 µL of the reagent with 10 min oven dry (at 50º C), 25 µL of standard and reaction time (RT) of 20 minutes.

To guarantee reagent excess, the lowest concentration of BPS to be studied was 0.5 g/L, corresponding to a BPS amount more than 5-fold the stoichiometric value of the highest iron standard. Consequently, for a 0.5 mg/L of iron standard, two BPS solutions with 0.5 g/L and 1 g/L were tested and the absorbance value increased 42% for the highest concentration. As a significant increase was observed, the BPS stock solution of 100 g/L was also tested, and the absorbance signal only increased 1%. This way, the BPS concentration of 1 g/L was set ensuring about a 10-fold excess over the stoichiometric value.

3.3.3.1. Reagent and Sample/Standard Volume

The studies of both the reagent and the sample/standard volumes were made by establishing calibration curves for each tested volume and comparing the obtained slopes. Different reagent volumes, from 8 to 18 µL, were loaded in the reagent layer and, as the highest sensitivity was obtained with 10 µL of reagent, this was the chosen volume (Figure 3.4(A)).

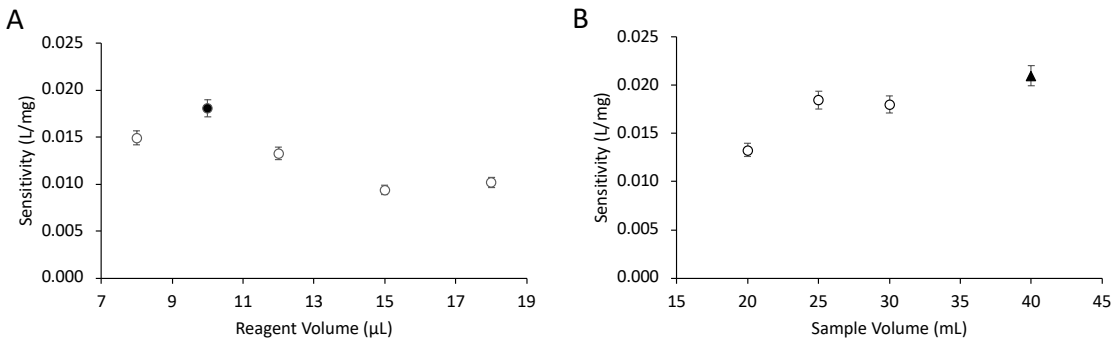

Figure 3.4 – Study of the influence in the calibration curve slope of the working volumes; (A) The reagent volume; (B) Sample volumes where the circles represent µPADs with W1/W1 units and triangle represents µPADs with W1/W3 units; the points in black represent the chosen values; the error bars represent 5% standard deviation of the measurements.

Then, sample volumes of 20, 25 and 30 µL were tested (Figure 3.4(B)). Although there was an increase up to 25 µL, no significant difference was observed from 25 to 30 µL (RD < 10%). This could be a result of exceeding the reservoir capacity and so, if a higher sample volume had to be tested, the absorption capacity would have to be increased. The empty layer was initially composed of a Whatman 1 paper disk of 14 mm (section 3.2); to enhance the reservoir capacity, a Whatman 3 filter paper was tested.

This filter paper is similar to Whatman 1, in respect to type and porosity (Appendix B), but presents a higher thickness (0.39 mm over 0.18 mm). With Whatman 3 in the empty layer, 40 µL of sample/standard could be used (triangle in Figure 3.4(B)) and a significant increase of the sensitivity (RD > 17%) was obtained, so 40 µL of sample was the volume chosen. Even though the µPAD card appeared to dry out in 15 min, the RT was kept at 20 min to guarantee complete dryness.

3.3.4. Stability Assessment

One of the main advantages of paper-based devices is the potential field application, so it is crucial to test both the storage stability of the µPAD before use, and the stability of the coloured product formed, after the sample/standard insertion.

3.3.4.1. Coloured Product Stability

To evaluate the colour product stability in the developed µPAD, a calibration curve was prepared and the µPADs scanned after the established RT = 20 min. Then, a new scanning was made every 10 min for one hour and every hour up to 4 hours (Figure 3.5(A)). The calibration curve slopes obtained with the different scanning times were compared and no significant differences were observed up to 3 hours (RD = 9%) but after 4 hours after the sample insertion, a decrease in the sensitivity of 11% was observed. Therefore, the developed µPAD presents a RT window from 20 min up to 3 hours.

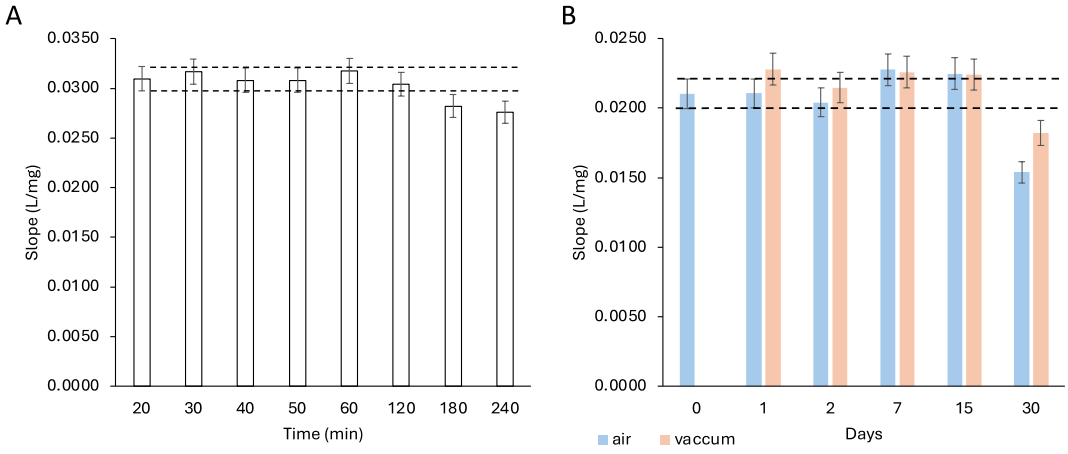

Figure 3.5 – Stability evaluation by comparing calibration curve slopes: (A) Coloured product stability from the chosen scanned time of 20 minutes up to 4 hours; the dashed lines represent the 10% deviation of the calibration curve slope attained at 20 minutes; (B) µPAD storage stability kept light protect and stored in the presence of air (blue bars) or in vacuum (orange bars); the dashed lines represent the 10% deviation of a freshly assembled µPAD calibration curve slope.

3.3.4.2. µPAD Stability

To test the stability of the µPADs, several devices were prepared and stored in plastic bags at room temperature (approximately 21 °C) and protected from light. Two atmospheric conditions were used: air and vacuum.

Different periods were tested for each of the atmospheric conditions, ranging from 1 to 30 days (Figure 3.5(B)). At every studied period the stored µPAD was used to perform a calibration curve and compared to calibration curve of a freshly assembled µPAD prepared with the same set of standards. A relative deviation below 10% was considered non-significant and the results showed that the devices were stable for a maximum of 15 days, in both atmospheric conditions.

3.3.5. Features of the Developed µPAD for Iron Determination

The main characteristics of the developed µPAD are summarized in Table 3.1, including the dynamic range, the limit of detection, the limit of quantification and repeatability.

Table 3.1 – Features of the developed µPAD for iron determination; LOD, limit of detection; LOQ, limit of quantification; RSD, relative standard deviation.

Dynamic Range (mg/L)	Calibration Curve [a] A = S × [Fe] + b	LOD (µg/L)	LOQ (µg/L)	Repeatability, RSD	
				Intraday [b]	Interday [c]
0.065 – 1.2	$A = 2.05 \times 10^{-2}(\pm 9 \times 10^{-4}) \times [Fe] + 3 \times 10^{-4}(\pm 1 \times 10^{-4})$ R^2=0.996±0.003	20	65	3%	6%

[a] n = 3; [b] n = 5; [c] n = 4.

The limit of detection (LOD) and the limit of quantification (LOQ) were calculated according to IUPAC recommendations (109) as the concentration corresponding to three (LOD) and ten-times (LOQ) the standard deviation of the intercept (n = 3). The µPAD repeatability was assessed by calculating the relative standard deviation (RSD) of the slope of five calibration curves in the same day, intraday RSD, and in consecutive days, interday RSD. The reagent consumption was calculated based upon the total volume of all reagent solutions used in the 20 discs of reagent layer of one µPAD, and corresponded to 0.143 mg BPS, 0.857 mg hydroxylamine and 1.75 mg HCl.

3.3.6. Interferences – Urine Matrix

Aiming for application to urine samples, the potential matrix interference was evaluated by comparing calibration curves slopes (sensitivity). Two sets of the developed µPAD were assembled to perform a couple of calibration curves: one using iron standards prepared in water and one using iron standards prepared in synthetic urine (SU).

The results showed a significant decrease in the calibration curve slope (Figure 3.6(A)), indicating that at least one component of the synthetic urine is causing interference.

Based upon the synthetic urine composition, we narrowed down the potential source of the interference to three components: lactic acid (LA), citric acid (CA), or phosphate (P). In order to find which one causes interference, different solutions of synthetic urine were prepared, one without the three components (InSU_0) and then with each of the components added individually (InSU_LA, InSU_CA and InSU_P). These solutions were used to prepare iron standards and calibration curves performed (Figure 3.6(A)).

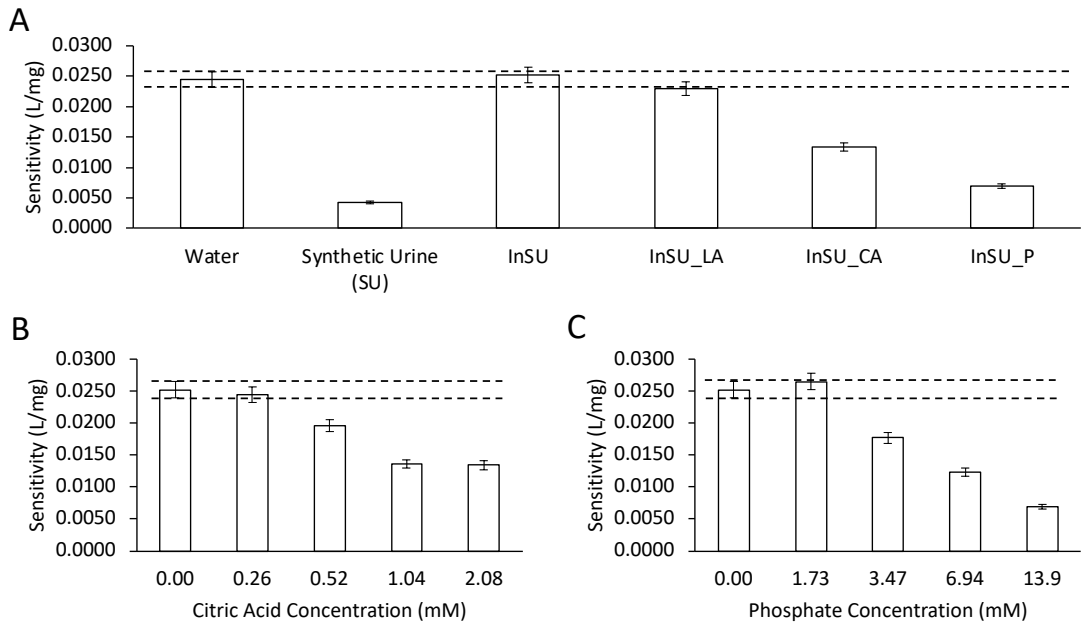

Figure 3.6 – Study of potential matrix interference on the calibration curve slope (sensitivity); (A) Iron standards prepared in water, synthetic urine (SU), incomplete synthetic urine (InSU_0), incomplete synthetic urine with lactic acid (InSU_LA), incomplete synthetic urine with citric acid (InSU_CA), and incomplete synthetic urine with phosphate (InSU_P); (B) Iron standards prepared in synthetic urine with different concentrations of citric acid; (C) Iron standards prepared in synthetic urine with different concentrations of phosphate; the error bars represent 5% standard deviation of the measurements.

It was possible to conclude that the other components in the synthetic urine (InSU_0) did not interfere with the assay, as well as lactic acid (InSU_LA), but that both citric acid (InSU_CA) and phosphate (InSU_P) caused a significant interference (Figure 3.6(A)). Then, to assess the maximum concentration possible to use without interference, calibration curves were established using iron standards prepared in synthetic urine with different concentrations of the citric acid (Figure 3.6(B)) and phosphate (Figure 3.6(C)). The maximum concentrations that did not display interference (RD < 5%) were 0.26 mM for citric acid and 1.73 mM for phosphate.

3.3.7. Application to Urine Samples

3.3.7.1. Sample Blank

Due to the urine potential intrinsic absorbance and the lack of a specific wavelength selection (detection based on RGB filter selection), some overlapping with the coloured product formed was expected. In fact, this would result in an increase in the measurement of pixels intensity and consequent absorbance calculation. To tackle this problem, a strategy was developed to include the measurement of a sample blank. The μPAD assembly was adapted to include measurements without the colour reagent, as described in section 3.2.2.(i), to calculate the sample intrinsic absorbance. Then, that intrinsic absorption was subtracted from the calculated absorption obtained with the colour reagent, according to the equation detailed also in section 3.2.2.(i).

3.3.7.2. Validation

To assess the accuracy of the developed μPAD for iron determination in urine samples, several samples (#26) were analysed and the results compared to those obtained by AAS, atomic absorption spectrophotometry (124). The relative deviation between the results obtained with the developed μPAD ($[Fe]_{\mu PAD}$) and the AAS method ($[Fe]_{AAS}$) was calculated (Table 3.2).

A linear relationship between the two set of results (Figure 3.7) was established: $[Fe]_{AAS}$ = 1.013 (±0.039) × $[Fe]_{\mu PAD}$ + 0.002 (±0.010), where the values in brackets correspond to the 95% confidence interval (of a t-student analysis). As the slope and the intercept were not statistically different from 1 and 0, respectively, there is no evidence for differences between the two sets of results and consequently the two methods.

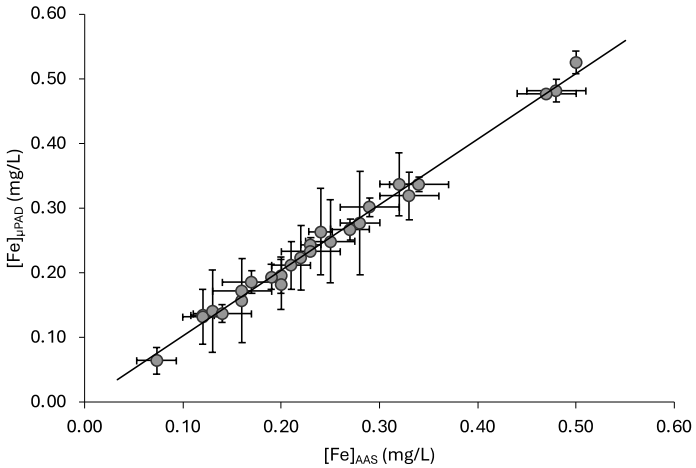

Figure 3.7 – Comparison between the results obtained for iron determination in urine samples (#26) with the developed μPAD and the atomic absorption spectrometry (AAS); the error bars represent the standard deviation of the measurements and the full line represents the linear trendline between the two sets of results.

Table 3.2 – Comparison between the iron concentration determined with the AAS method and the concentration determined with the developed µPAD; RD, relative deviation.

Sample ID	$[Fe]_{AAS}$ (mg/L)	$[Fe]_{\mu PAD}$ (mg/L)	RD (%)
US1	0.48 ± 0.03	0.48 ± 0.02	0.4
US2	0.24 ± 0.01	0.26 ± 0.07	10
US3	0.29 ± 0.03	0.30 ± 0.01	4.0
US4	0.25 ± 0.02	0.25 ± 0.06	-0.4
US5	0.34 ± 0.03	0.34 ± 0.01	-0.9
US6	0.16 ± N.D.	0.16 ± 0.07	-1.8
US7	0.12 ± 0.01	0.13 ± 0.01	12
US8	0.20 ± 0.00	0.20 ± 0.03	-1.7
US9	0.23 ± 0.01	0.24 ± 0.01	5.9
US10	0.47 ± 0.03	0.48 ± N.D.	1.5
US11	0.50 ± 0.00	0.53 ± 0.02	5.1
US12	0.33 ± 0.03	0.32 ± 0.04	-3.3
US13	0.19 ± 0.00	0.19 ± 0.02	1.9
US14	0.32 ± 0.02	0.34 ± 0.05	5.4
US15	0.16 ± 0.03	0.17 ± 0.00	7.3
US16	0.21 ± 0.02	0.21 ± 0.04	0.9
US17	0.22 ± 0.00	0.22 ± 0.05	1.8
US18	0.12 ± 0.02	0.13 ± 0.04	10
US19	0.13 ± 0.00	0.14 ± 0.06	8.7
US20	0.28 ± 0.02	0.28 ± 0.08	-1.0
US21	0.20 ± 0.00	0.18 ± 0.04	-8.7
US22	0.27 ± 0.02	0.27 ± 0.02	-1.0
US23	0.17 ± 0.03	0.19 ± 0.02	9.1
US24	0.23 ± 0.03	0.23 ± 0.01	1.5
US25	0.14 ± 0.03	0.14 ± 0.01	-2.2
US26	0.073 ± 0.017	0.065 ± 0.021	-7.5

Additionally, a t-test statistical analysis was made (Table 3.3) and, for a 95% significance level, the obtained t-value was higher than the significance level ($r = 0.882 > 0.05$), and the calculated t-value was 0.150 with a correspondent critical value of 2.01 (two-tail), indicating that the two sets of results are not statistically different. So, the results obtained with the developed µPAD proved not only to be comparable to the results of atomic absorption, but also that the working range was adequate for the analysis of the target samples.

Table 3.3 – Statistical t-test applied to the two sets of results, the developed µPAD and the atomic absorption spectrometry (AAS).

t-Test: Two-Sample Assuming Equal Variances	*Variable 1 (µPAD)*	*Variable 2 (AAS)*
Mean	0.248	0.243
Variance	0.013	0.012
Observations	26	26
Pooled Variance	0.0128	
Hypothesized Mean Difference	0	
df	50	
t Stat	0.150	
P(T<=t) two-tail	0.882	
t Critical two-tail	2.009	

3.4. Conclusions

In this work, a sensitive and portable microfluidic paper-based analytical device (µPAD) for iron determination in urine samples was developed. The device is capable of fast, on-hand measurements of iron in human urine samples without requiring pre-treatments. A range of 0.07 to 1.2 mg/L of iron, with a detection limit of 20 µg/L, proved suitable for all the analysed samples (#26) and comparable to the determination by atomic absorption spectrophotometry (RD < 9.5%). The application of paper-based devices for iron determination in biological samples has been reported only once by Kamlesh Shrivas (2020) (121) applied with water and blood plasma samples in a range of 50 to 900 µg/L, showing limits of detection and quantification of 20 µg/L and 65 µg/L, respectively. The described device in this work attains identical limits of detection and quantification, but was applied to a different biological sample, namely urine, handling with the intrinsic absorption of the sample.

The developed µPAD was envisioned to aid in health diagnosis, not only in healthcare facilities, but also in field application including remote areas. To meet the requirements for that, stability studies were performed, and the developed µPAD was stable for 15 days after assembling. After loading the sample, the device can be scanned within three hours, corresponding to the formed coloured product stability. After usage, the µPAD is disposable by incineration, which is not only environmentally friendly, but also an advantage when handling biological samples. The main drawback of the developed device is its manual and laborious assembly, namely the delicate lamination process (avoiding the shifting of the discs), making it susceptible for an uneven distribution, potentially affecting reproducibility. However, this difficulty can be minimized if a mechanical aid could be used. The potential effect of this problem in the intensity readings is minimized by the elimination of the outliners. The developed µPAD could ultimately be used as a screening option not only in healthcare facilities, but also as an aid in the diagnosis of some diseases and health conditions in field applications, including remote locations.

Chapter 4. Nitrate in Urine Samples

Chapter based on the paper published in

Molecules

Volume 26, 6355 (2021)

https://doi.org/10.3390/molecules26216355

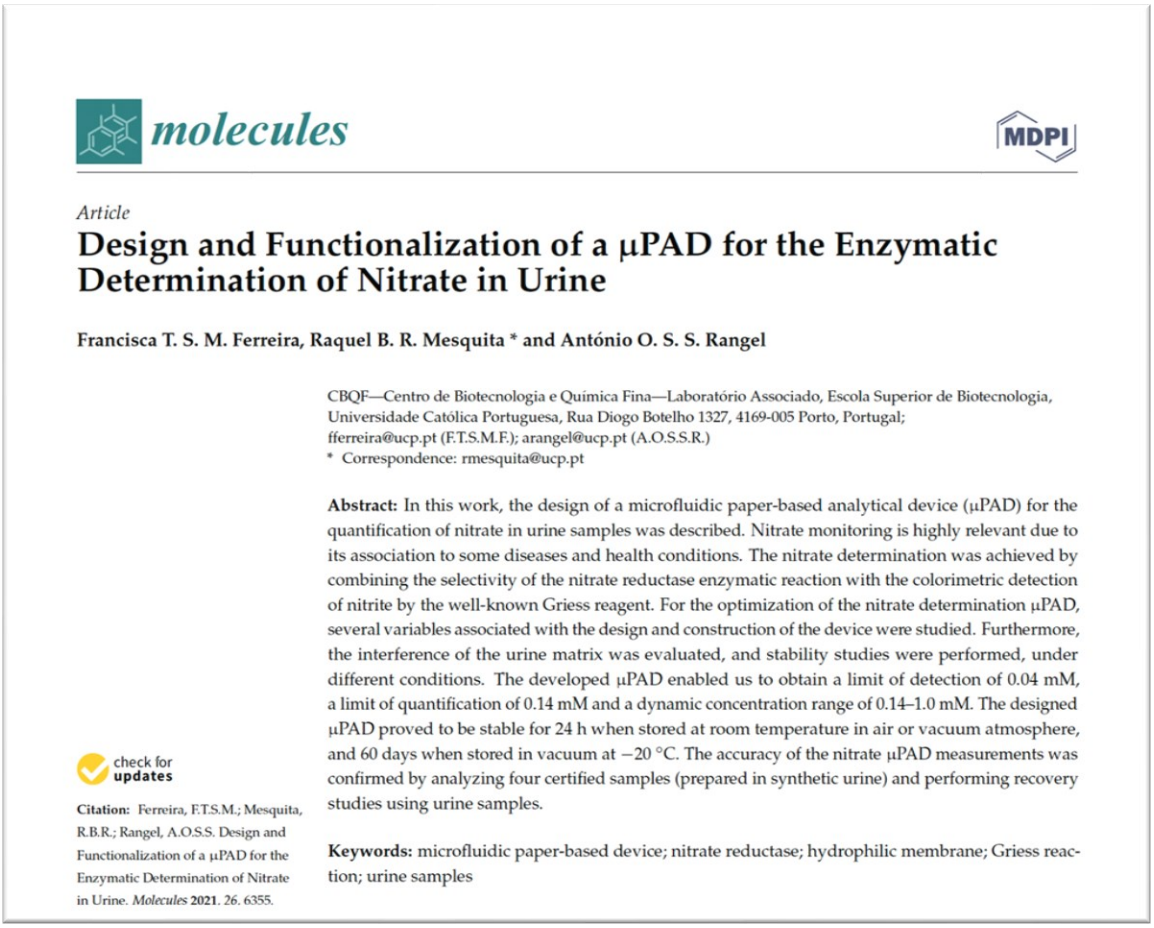

molecules

MDPI

Article

Design and Functionalization of a μPAD for the Enzymatic Determination of Nitrate in Urine

Francisca T. S. M. Ferreira, Raquel B. R. Mesquita * and António O. S. S. Rangel

CBQF—Centro de Biotecnologia e Química Fina—Laboratório Associado, Escola Superior de Biotecnologia, Universidade Católica Portuguesa, Rua Diogo Botelho 1327, 4169-005 Porto, Portugal; fferreira@ucp.pt (F.T.S.M.F.); arangel@ucp.pt (A.O.S.S.R.)

* Correspondence: rmesquita@ucp.pt

Abstract: In this work, the design of a microfluidic paper-based analytical device (μPAD) for the quantification of nitrate in urine samples was described. Nitrate monitoring is highly relevant due to its association to some diseases and health conditions. The nitrate determination was achieved by combining the selectivity of the nitrate reductase enzymatic reaction with the colorimetric detection of nitrite by the well-known Griess reagent. For the optimization of the nitrate determination μPAD, several variables associated with the design and construction of the device were studied. Furthermore, the interference of the urine matrix was evaluated, and stability studies were performed, under different conditions. The developed μPAD enabled us to obtain a limit of detection of 0.04 mM, a limit of quantification of 0.14 mM and a dynamic concentration range of 0.14–1.0 mM. The designed μPAD proved to be stable for 24 h when stored at room temperature in air or vacuum atmosphere, and 60 days when stored in vacuum at −20 °C. The accuracy of the nitrate μPAD measurements was confirmed by analyzing four certified samples (prepared in synthetic urine) and performing recovery studies using urine samples.

Keywords: microfluidic paper-based device; nitrate reductase; hydrophilic membrane; Griess reaction; urine samples

check for updates

Citation: Ferreira, F.T.S.M.; Mesquita, R.B.R.; Rangel, A.O.S.S. Design and Functionalization of a μPAD for the Enzymatic Determination of Nitrate in Urine. *Molecules* **2021**, *26*, 6355.

Submission received: 13 September 2021

Accepted: 19 October 2021

Published: 21 October 2021

4.1. Introduction

Nitrite and nitrate are both forms of nitrogen found in the human body either due to an endogenous production by the body or through ingestion of water and food, like vegetables and processed meats. (126) These ions have been often associated with cancer, especially nitrite, either from direct ingestion, or the nitrate reduction by bacteria in the digestive system (26,127). When nitrite reaches the acidic environment of the stomach, and combined with amine or amide, it may form toxic and carcinogenic compounds such as nitrosamines and nitrosamides (26). Furthermore, nitrite acts both as a substrate for the respiration of tumor cells and a signal molecule for their growth. So, even though it does not directly lead to cancer, it has been reported to accelerate the proliferation and malignant transformation of cancer cells (128). When absorbed to the bloodstream, nitrite can also cause methemoglobinemia, especially in infants. In this condition, nitrite reacts with the iron in hemoglobin, irreversibly converting it in methemoglobin and blocking the transport of oxygen (26,129). Because the human body is a complex cooperation of interconnected systems, the content of nitrate and nitrite in biological fluids such as blood, urine and saliva, reflect the transformation and metabolism of these ions in the entire body (128). For example, although the presence of nitrate in the human urine is to be expected, the presence of nitrite usually implies the existence of infection by bacteria that convert nitrate to nitrite (130). Therefore, monitoring is essential for the early detection of diseases like infections and cancer.

The focus of this work was to develop a simple microfluidic paper-based analytical device capable of performing the nitrate determination in human urine samples. The nitrate conversion to nitrite is ensured by the enzymatic reaction involving nitrate reductase and the co-factor NADPH (131,132) (Scheme. 4.1), with the detection of the resulting nitrite performed by the Griess reagent (131–133) (Scheme. 4.2). Enzymes are biological catalysts that usually present a high selectivity and specificity, which is why it is considered an important technique in the analysis of numerous analytes. (134) To effectively use the enzymatic reaction in a microfluidic paper device, a strategy to delay the vertical flow to enable a significant extent of the enzymatic reaction was designed. This was attained by incorporating a hydrophilic membrane layer, enabling to control the vertical flow rate and minimize potential interferences. The incorporation of a hydrophilic membrane also provided a physical separation between the sample insertion layer and the colour reaction layer, enabling to directly analyse coloured samples, namely urine. Additionally, the limitations of a previously reported (26) fabrication process of a device, namely the placement of the zinc powder on paper, were also tackled.

Scheme (4.1) $NO_3^- + NADPH + H^+ \xrightarrow{\text{Nitrate Reductase}} NO_2^- + NADP^+ + H_2O$

Scheme (4.2) NO_2^- + Sulfanilamide + N-(1-naphthyl)-ethylenediamine dihydrichloride ⟶ Azo Dye (Pink)

4.2. Materials and Methods

4.2.1. Reagents and Solutions

A standard stock solution of 10 mM potassium nitrate (Fluka) was prepared monthly by dissolving approximately 10 mg of previously dried solid (overnight at 100 °C) in 10 mL of water. The working nitrate standards were daily prepared from the stock solution in a range of 0.2–1.0 mM.

A phosphate buffer solution was prepared by dissolving 1.16 g of $K_2HPO_4 \cdot 3H_2O$ (Merck) and 3.5 mg of ethylenediamine tetraacetic acid (EDTA) (Merck) in 200 mL of water, and the pH adjusted to 7.4. The solution was stored in the refrigerator.

A 20 mM NADPH solution was prepared by dissolving 16.5 mg NADPH (tetrasodium salt, 98%, Roche) in 1 mL of water and stored in the refrigerator.

The nitrate reductase (NR) enzyme stock solution (from Aspergillus species, Roche) was prepared by adding 2 mL of water to the 20 U in the flask. This solution was separated in 100 µL aliquots and stored in a freezer. The 1.5 U/mL NR solution was prepared daily by dilution of the 10 U/mL stock solution.

The enzyme solution (ES) placed on the µPAD was prepared upon use by mixing 120 µL of NR 1.5 U/mL and 15 µL of NADPH 20 mM.

The modified Griess reagent was monthly prepared according to Teixeira et al. (133), by dissolving separately 0.4 g of sulfanilamide (Sigma- Aldrich) in 2 mL of 5 M orthophosphoric acid and 0.04 g of N-(1-naphthyl)-ethylenediamine dihydrichloride (N1NED) (Merck) in water. These two homogenized solutions were then mixed, and the volume was completed to 20 mL to final concentrations of 20 g/L of sulfanilamide and 2 g/L N1NED. This solution was stored in a dark bottle, shielded from the light.

4.2.2. Design of the Developed µPAD

To assemble the µPAD, 24 hydrophilic units (Figure 4.1(A)) were aligned under the 3 mm holes (L1) previously perforated in a laminating pouch (75 x 110 mm), in 4 columns and 6 rows distribution (Figure 4.1(B)). Each hydrophilic unit comprised 3 layers: the top layer, N, consists of a Whatman Grade 4 filter paper disc with 6.35 mm diameter loaded with enzymatic solution (ES); the middle layer, M, consists of a hydrophilic mixed cellulose ester membrane with 12.7 mm diameter (ME24 Whatman); and the bottom layer, G, consists of a Whatman Grade 50 filter paper disc with 9.5 mm diameter loaded with Griess reagent.

The ES disc from layer N was prepared by loading 5 µL of NR and NADPH mixture (enzymatic solution) in each disc and set to dry for 20 min in the oven at 37 °C. The paper disc from the G layer were prepared by adding 10 µL of the Griess reagent to the discs and placing them in the oven to dry, for 10 min at 50 °C.

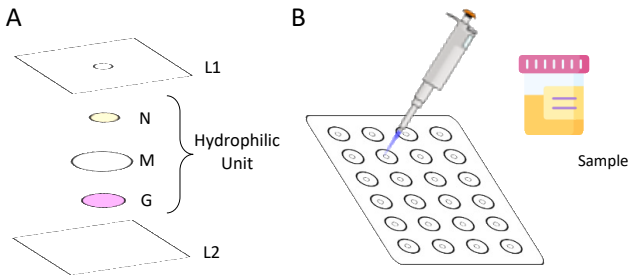

Figure 4.1 – Schematic representation of: A) the µPAD unit assembly and B) sample insertion.

After the alignment of the units, the laminating pouches were passed through the laminator, which forces the plastic pouch to melt and seal around the units creating a strong physical barrier, the hydrophobic area. After the lamination, the µPADs were ready to be use.

The lamination is a delicate part of the assembly process, and a poor distribution of the units may result in a low reproducibility. Avoiding the shifting of the discs and units is essential; however, it can still happen, and for that reason, it was established to have eight units for one standard/sample (and collect the data of three/four replicates) to account for possible outliers.

4.2.3. Determination Procedure

To measure the concentration of nitrate in urine samples, 20 µL of standard/sample were placed at the insertion hole of the assembled µPAD (L1 layer in Figure 4.1(A)), then the sample/standard enters the µPAD and nitrate interacts with the nitrate reductase enzyme and NADPH (layer N in Figure 4.1(A)), being nitrate converted into nitrite. The hydrophilic membrane (layer M in the Figure 4.1(A)) delays the flow of the sample and ensures that it is retained in the enzymatic layer enough time to attain the nitrate reduction. After its complete absorption, the holes were covered with adhesive tape to prevent evaporation and possible contaminations. After the nitrate reduction, the formed nitrite passes through the membrane to the bottom layer with the Griess reagent (layer G in Figure 4.1(A)), thus reacting and forming the pink colour product. The intensity of the colour was measured by scanning the bottom layer of the µPADs. The time lapse between the sample/standard introduction and the scanning (RT) was set to 20 minutes.

The scanned images were processed using ImageJ by separating them into the RGB components. Then, the green component was used to measure the intensity, since the expected coloured product of the Griess reaction is pink. For each unit, an option was made to do the measurements using a circular selection of 200 × 200 pixels, since it allowed a better adjustment to the area of the reagent disc.

The intensity values were then converted into absorbance values. For each reading of blank or standard/sample, eight measurements were made, and outliers were removed when necessary. The remaining replicates were used for the average absorbance calculation. The calculated absorbance values were then plotted against the concentration of nitrate.

4.2.4. Samples Collection

The urine samples were collected as “blind samples” from volunteers with their informed consent and stored in the freezer at − 20 °C until use.

4.2.5. Validation

To assess the accuracy of the µPAD measurements, a certified water sample was used, QC RW1 (VKI reference materials, DANAK) as it consists in a concentrate preparation ampoule to be diluted. Therefore, different dilutions were made in synthetic urine instead of water. The final nitrate concentrations of the dilutions were: 0.707 mM (AC1), 0.530 mM (AC2), 0.471 mM (AC3) and 0.354 mM (AC4). For further validation assessment, recovery percentages were calculated based on addition of 20/30 µL of 10 mM nitrate standard to 1 mL of the urine samples.

4.3. Results and Discussion

As above mentioned, the colour reaction chosen for the developed µPAD was the Griess reaction for nitrite determination, so the colour reaction layer (layer G in Figure 4.1(A)) was adapted from a previously reported work by Ferreira et al (26).

4.3.1. Preliminary Studies

To attain the nitrate determination based on the Griess colour reaction for nitrite, it required the reduction of nitrate to nitrite, for which the enzymatic reaction using nitrate reductase was chosen. The enzymatic reaction with consequent colorimetric reaction was tested in a batchwise study based on the enzymatic assay of nitrate reductase of SIGMA (EC 1.6.6.1).

4.3.1.1. Incubation period

According to the enzymatic protocol, there is an incubation step. To evaluate if this step could be avoided, the first study was to test the protocol with and without the incubation temperature. The studies were performed for different nitrate concentrations, 4.3 and 2.8 mM, using both the incubation temperature of reported in the protocol (30 ^{o}C) and ambient temperature (≈ 21 ^{o}C). As it was expected, lower temperature produced a decrease of the efficiency of the enzymatic reaction, which was higher for the highest concentration (-31%) than for the lower one (-23%). Nevertheless, because the incubation at 30 ^{o}C would impair the µPAD field application, and considering the target concentrations were below 2 mM, an option was made to carry out the determination at room temperature.

4.3.1.2. Enzymatic reaction conditions

In order to optimize the enzymatic reaction conditions, several combinations with different proportions of NR, NADPH, and nitrate were tested (Table 4.1 and Table 4.2). The first set of combinations (Table 4.1) were made using a nitrate standard of 12 mM, as recommended by the SIGMA protocol. Although this nitrate concentration was above the target range, these studies still enabled to conclude that, for the same amount of NR, increasing the NAPDH amount did not cause a significant signal increase (Figure 4.2(A)). However, for the same amount of NADPH, the increase of NR amount resulted in an increase of the absorbance signal.

Table 4.1 – Description of the different parameters tested in each condition and the resulting absorbance signal; 100 µL of a nitrate standard of 12 mM (1.2 µmol); concentration NADPH 2 mM; concentration of NR 0.4 U/mL.

Condition ID	***NADPH***		***NR***		***A***
	Vol. (µL)	µmol	Vol. (uL)	U	
1A	100	0.2	100	0.04	0.572
2A	50	0.1	100	0.04	0.626
3A	100	0.2	50	0.02	0.238
4A	50	0.1	50	0.02	0.238
5A	50	0.1	150	0.06	0.634
6A	50	0.1	200	0.08	0.742

Table 4.2 – Description of the different parameters tested in each condition and the resulting absorbance signal; 100 µL of a nitrate standard of 1.2 mM (0.12 µmol; concentration of NADPH 0.2 mM; concentration of NR 0.4 U/mL.

Condition ID	***NADPH***		***NR***		***A***
	Vol. (uL)	µmol	Vol. (uL)	U	
1B	50	0.01	100	0.04	0.101
2B	50	0.01	150	0.06	0.097
3B	50	0.01	200	0.08	0.091
4B	100	0.02	100	0.04	0.181
5B	150	0.03	100	0.04	0.275
6B	200	0.04	100	0.04	0.292
7B	150	0.03	150	0.06	0.270

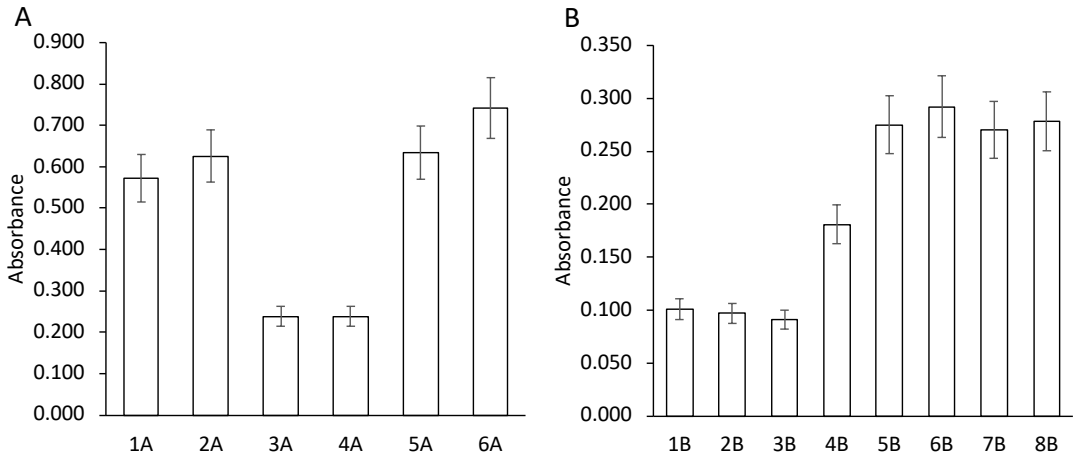

Figure 4.2 – Plotting of the studied conditions in Table 4.1 and Table 4.2 with: (A) a 12 mM nitrate standard; and (B) a 1.2 mM nitrate standard; the error bars represent 5% relative deviation.

As the top expected nitrate concentration in urine sample was 1.0 mM, the previous studies were repeated using a nitrate concentration of 1.2 mM (Table 4.2). The results showed that by increasing the NADPH amount, the absorbance slightly increase (Figure 4.2(B)). By increasing the NR amount, there was no significant variation in the absorbance. In the end, the chosen conditions for 100 µL of a 1.2 mM standard corresponded to: 150 µL of 0.2 mM NADPH and 100 µL of 0.4 U/mL NR.

4.3.2. µPAD Design – Membrane Incorporation

After having a better understanding of the enzymatic reaction conditions, the design of the µPAD was carried out. A vertical flow was chosen for the µPAD design and the enzymatic reaction had to occur before the colorimetric reaction, which would mean setting the first layer for the nitrate reduction prior to the colorimetric determination.

The nitrate in the sample would firstly have to be in contact with the NR and its cofactor, to enable the nitrate conversion to nitrite, which would then react with the Griess reagent layer to form a pink coloured product. Therefore, a strategy was made for separating the two reactions and, having into account that the enzymatic reduction may need more time to proceed at sufficient extent, an option was made to introduce an extra layer between enzymatic reaction layer and the colour reaction layer.

4.3.2.1. Separation Layer

As mentioned, to increase the efficiency of the enzymatic reduction, a strategy was designed to slow down the vertical flow by incorporating a membrane (hydrophilic membrane) between the enzymatic reaction layer and the colour reaction layer.

Then, the developed μPAD would be composed by three layers: the first layer, impregnated paper with enzymatic solution (a mixture of NR and NADPH); the second layer, a hydrophilic membrane to increase the residence time in the first layer and consequently the reaction time; and the third layer, an impregnated paper with Griess reagent for the colorimetric reaction. The proportion of the components in the enzymatic solution (ES) mixture used was based on the above-mentioned preliminary studies (section 4.3.1).

4.3.2.2. Membrane Selection

As mentioned, in order to increase the efficiency of the enzymatic reduction it was essential to ensure enough reaction time, so a hydrophilic membrane was placed in the second layer. The size of the membrane disk was set to 12.7 mm to ensure complete separation between the enzymatic reduction and colorimetric reaction layers.

Using the same nitrate standard, different membranes were tested (Table 4.3) to assess which one produced the highest absorbance value. A higher value would mean that a higher amount of nitrite had reached the reagent layer which in turn would mean that the membrane had caused a higher delay time in the first layer, thus promoting a higher reduction rate. The one that provided a higher absorbance signal was the CE20 membrane, so this was the chosen for further studies.

Table 4.3 – Tested hydrophilic membranes and their characteristics.

Membrane ID	***Material***	***Porosity (μm)***	***Supplier***
Ny45	Nylon	0.45	Whatman Nylon (7404-004)
CA45	Cellulose Acetate	0.45	Whatman OE67 (1040-4014)
CE20	Cellulose Ester	0.20	Whatman ME24 (1040-1714)
CN45	Cellulose Nitrate	0.45	Sartorius (11406)
CN20	Cellulose Nitrate	0.20	Sartorius (11407)
P20	Polyethersulfone	0.20	Gelman

4.3.3. μPAD Design – Enzymatic Reaction

After the optimization of the physical assembly of the μPAD, the concentration of the NR and NADPH used in the enzymatic solution mixture, were revisited and the sample volume studied.

4.3.3.1. Paper Selection

The filter paper type and porosity used on the enzymatic reduction layer (layer N from Figure 4.1(A)) was studied using two nitrate standards (0.5 and 1.5 mM (Figure 4.3).

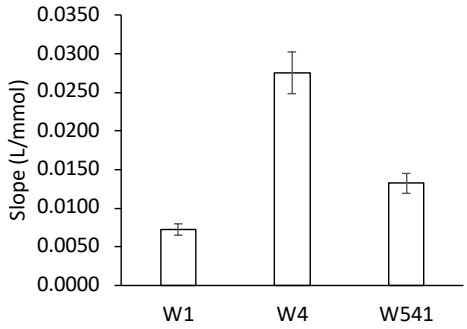

Figure 4.3 – Study of filter paper type and porosity influence on the enzymatic reduction reaction.

The most widely used and less expensive filter paper is the qualitative grade Whatman 1 (W1), so that it would always be the first choice. Then, Whatman 4 (W4) was tested, being the same qualitative grade, but with higher porosity (Appendix B) to facilitate the space arrangement of the enzymatic reaction.

Maintaining the higher pore size, a hardened ashless grade paper (W541) was also tested to assess if the paper treatment would benefit the enzymatic reaction. The paper that presented a significantly higher sensitivity (calibration slope) was the W4 (Figure 4.3), so this was the paper used on the layer N for the remaining of the studies.

4.3.3.2. Nitrate Reductase Concentration

The NR concentration used in the enzyme solution mixture had been based upon preliminary studies, but it was revisited in the μPAD approach. The study was performed using the highest nitrate standard (1.5 mM) and in the range of 0.5 – 2.5 U/mL of NR (Figure 4.4(A)).

The amount that resulted in a higher nitrate reduction would present a higher absorbance signal and the NR concentration that presented a significantly higher value of absorbance was 1.5 U/mL of NR.

4.3.3.3. NADPH Concentration

The NADPH concentration in the enzymatic mixture was also studied using the 1.5 mM nitrate standard (Figure 4.4(B)). From the studied range, 10 - 25 mM, the concentration of 20 mM resulted in the highest absorbance value, inferring a higher conversion of nitrate to nitrite.

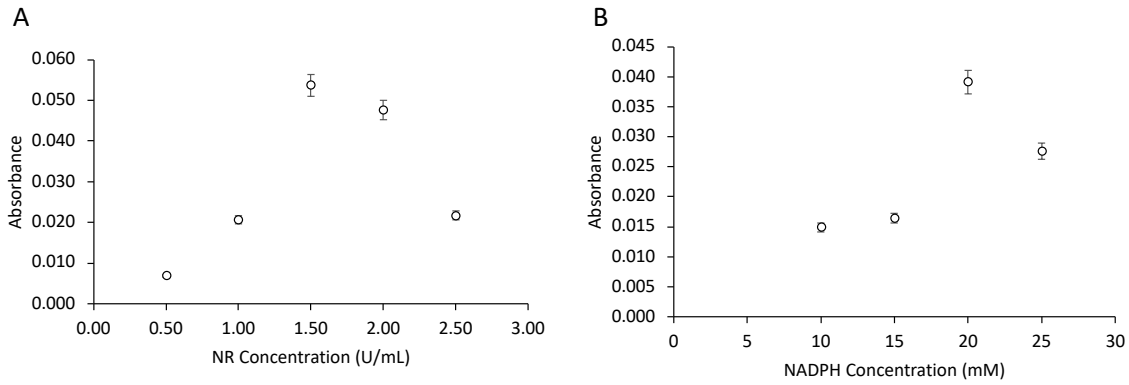

Figure 4.4 – Study of the influence of the NR concentration (A) and NADPH concentration (B) on the enzymatic reduction reaction by calculation of the absorbance signal obtained for a 1.5 mM nitrate standard.

4.3.3.4. Sample Volume

Trying to increase the sensitivity of the determination, a higher volume of sample, 25 µL, was tested. However, it was observed an incomplete absorption, even after 1 hour, which would not be compatible for field application. This led to believe that the maximum capacity of the µPAD had been reached with the 20 µL sample/standard, and so it was the chosen volume.

4.3.4. Features of the Developed Device

The main characteristics of the developed µPAD including dynamic range, limit of detection (LOD) and quantification (LOQ) and relative standard deviation (RSD), are summarized in Table 4.4.

Table 4.4 – Features of the developed µPADs for the determination of nitrate; LOD, limit of detection; LOQ, limit of quantification; RSD, relative standard deviation.

Dynamic Range (mM)	Calibration Curve[a] $A = S \times [NO_3^-] + b$	LOD[a] (mM)	LOQ[a] (mM)	Repeatability, RSD	
				Intraday[b]	Interday[c]
0.14 – 1.0	$y = 2.7 \times 10^{-2} (\pm 4 \times 10^{-3}) \times [NO_3^-] + 6 \times 10^{-4} (\pm 4 \times 10^{-4})$	0.04	0.14	8%	5%

[a] n=5; [b] n=2; [c] n=4.

The presented calibration curve was calculated as the average of 5 calibration curves (Figure 4.5(A)). The LOD and the LOQ were calculated as concentration corresponding to three and ten-times, respectively, the standard deviation of the intercept (n = 5) according to IUPAC recommendations (109). The repeatability of the developed µPADs was evaluated by calculating the RSD of the calibration curve slope, 2 calibration curves in the same day for the intraday repeatability and 4 calibration curves in consecutive days for the interday repeatability.

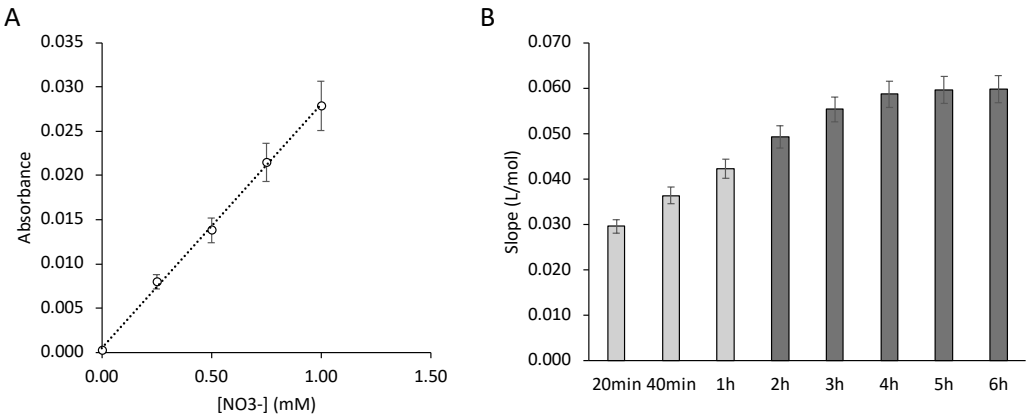

Figure 4.5 - Calibration curve for the nitrate determination obtained with the developed μPAD: (A) calibration curve plot; (B) calibration curve slope at increasing scanning times; light grey bars represent calibration curves with a correlation coefficient >0.99; the dark grey bars represent calibration curves with a correlation coefficient < 0.98.

4.3.4.1. Scanning Time Interval

The enzymatic reaction requires time, and the chosen approach to incorporate a hydrophilic membrane intended to increase the residence time in the enzymatic layer. However, the idea was to have enough reaction extension and yet a minimal time between sample insertion and digital scanning, named reaction time (RT), to ensure one of μPADs most attractive characteristics, real-time analysis.

For RT assessment, a calibration curve was prepared, and the μPADs scanned at several times after standard insertion, from 20 min up to 3 h (Figure 4.5(B)). As expected, the results showed that the sensitivity increased from the set RT of 20 min to 40 min (14%) and up to 1 h (≈ 30%) as a consequence of more nitrite being formed and reaching the reagent layer. After 1 h, there was no further increase in the sensitivity and there was a significant decrease in linearity (Figure 4.5(B)), indicating that no more nitrite was reaching the bottom layer and that some degradation of the coloured product might be occurring.

4.3.4.2. Assessment of μPAD Stability

To evaluate the robustness of the developed μPAD, the stability of the developed device was tested when stored. The μPADs were stored in plastic bags, under two different atmospheric conditions (air and vacuum), and at two temperatures, room temperature (approximately 21 °C) and in a freezer (approximately -20 °C). All stored μPADs were shielded from light. Different periods of time were assessed for each of the atmospheric conditions and temperature.

The sensitivity of the average calibration curves obtained from freshly prepared μPADs, was then compared with the sensitivities obtained with μPADs under different storage conditions; then, a relative deviation (RD) below 10% was considered non-significant.

The calibration curves obtained with the devices stored for 24 h in air and vacuum at room temperature showed no significant difference when compared to the calibration curves average (RD < 7%). The calibration curves obtained with the devices stored for 30 days in a freezer and in vacuum, still presented a similar sensitivity to the average of calibration curves (RD < 1%) which confirmed that the developed μPADs can be efficiently stored for that time period.

4.3.5. Interferences Assessment

To assess potential interferences from the urine matrix, a set of μPADs were prepared to perform two calibration curves, one using standards prepared in water, and another using standards prepared in synthetic urine.

There was no significant difference on the calibration curves slopes (relative deviation < 10%) thus indicating that no significant matrix interferences occurred. Therefore, to reduce the reagents consumption, the standards preparation in water was kept.

4.3.6. Application to Urine Samples – Validation

To evaluate the accuracy of the developed μPAD for nitrate measurements, four dilutions in synthetic urine of a certified sample were used (Table 4.5).

Table 4.5 – Analysis of certified samples performed with the nitrate μPAD; CI, confidence interval at 95%; SD, standard deviation; RD, relative deviation.

Certified sample dilution	Certified Value, $[NO_3^-]$ ± CI [mM)	μPAD $[NO_3^-]$ ± SD [mM)	RD (%)
AC1	0.707 ± 0.011	0.717 ± 0.056	1.0
AC2	0.530 ± 0.008	0.491 ± 0.030	-7.4
AC3	0.471 ± 0.007	0.483 ± 0.067	2.5
AC4	0.354 ± 0.006	0.346 ± 0.020	-2.1

A linear relationship between the two set of results was established: $[NO_3^-]_{\mu PAD}$ = 1.03 (± 0.30) × $[NO_3^-]_{CV}$ - 0.022 (± 0.163) where the values in brackets represent the 95% confidence interval (t-student analysis). As the slope and the intercept are not statistically different from 1 and 0, respectively, there was no statistical difference between the certified value and the μPAD measurement.

To further assess the accuracy, recovery studies were performed by spiking the samples with 20 μL and 30 μL of the nitrate standard stock solution of 10 mM in 1 mL of the urine sample. The calculation of the recovery percentages were made (($[NO_3^-]_{found}$ – $[NO_3^-]_{initial}$) / $[NO_3^-]_{added}$) according to IUPAC (111) and listed in Table 4.6.

Table 4.6 – Recovery percentages studies; Standard deviation (SD); Relative standard deviation (RSD).

Sample ID	*Inicial*			*Added [NO_3^-] (mM)*	*Found*			*Recovery (%)*
	[NO_3^-] ± SD (mM)		**RSD (%)**		**[NO_3^-] ± SD (mM)**		**RSD (%)**	
U1	0.79	0.05	6.6	0.300	1.09	0.06	5.9	100
U2	0.55	0.03	5.5	0.200	0.76	0.05	7.0	103
U3	0.23	0.03	15	0.200	0.44	0.03	7.2	101
U4	1.38	0.04	2.7	0.200	1.55	0.13	8.1	85
U5	< LOD			0.200	0.21	0.02	8.7	81
U6	0.096	0.011	11	0.200	0.29	0.03	12%	95
U7	0.316	0.016	5.1%	0.200	0.53	0.05	8.5	106

The average of the calculated recoveries was 99% with a standard deviation of 7%. A statistical test (t-test) was used to evaluate if the mean recovery value did significantly differ from 100%. For a 95% significance level, the calculated t-value was 0.25 with a correspondent critical value of 2.97. The statistical results indicate the absence of multiplicative matrix interferences proving that the developed µPAD was applicable to urine samples.

4.3.6.1. Nitrite Testing

As mentioned above, the aim of the developed µPAD was to be applied to nitrate determination in urine samples, where nitrite is not supposed to be present. Nevertheless, a nitrite presence testing can be incorporated if in the same assembly the top layer (N layer in Figure 4.1(A)) is loaded only with NADPH and no NR.

In this case, the colour product formed is indicator of nitrite presence. If a quantification is intended, then a full calibration curve with nitrite standards and a µPAD without NR in the first layer would have to be established (Figure 4.6).

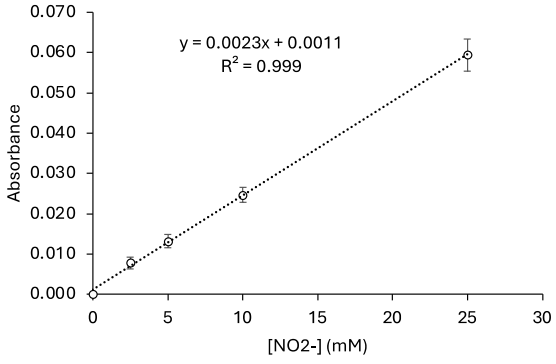

Figure 4.6 – Nitrite calibration curve; the error bars represent the standard deviation.

4.4. Conclusion

In this work, a novel microfluidic paper-based analytical device was developed for the quantification of nitrate in human urine samples. The use of the enzymatic reduction of nitrate, as opposed to using zinc powder (26), enabled a less laborious and easier to reproduce process of preparation and assembly of the device. Moreover, as far as we know, this is the first time the nitrate reductase enzyme is used in a μPAD platform. To slow down the vertical flow and thus promote the reduction reaction, a hydrophilic membrane was placed below the enzymatic layer which also enabled to overcome potential interferences. Among these was the intrinsic colour of urine, which was no longer a problem facilitating the application to urine samples. This innovative approach added significant advantages without compromising the analytical features and can be used in other analytical situations where these challenges occur. The previously reported μPADs for nitrate determination (Table 4.7) use either zinc or vanadium (III) as a reducing agent, which emphasizes the innovative approach of the developed μPAD. Additionally, there was no application to urine samples, probably due to the problem of potential colour interference, which was tackled in our work with the membrane approach.

Table 4.7 – Summary of the characteristics of the developed μPAD in comparison with previously described devices; LOD, limit of detection; LOQ, limit of quantification.

Sample	Dynamic Range (mM)	LOD (mM)	LOQ (mM)	Reduction Agent	Fabrication method	Reference
Water	0.05 - 1	0.019	0.048	Zinc	Inkjet printer	(135)
Food products	0.16 – 0.81	0.058	0.19	Zinc	Screen-printing	(136)
Food products	0.008 – 0.64	0.006	0.023	Vanadium (III)	Screen-printing	(137)
Saliva	0.27 – 1.2	0.08	0.27	Zinc	Cutting and Lamination	(26)
Urine	0.14 – 1.0	0.04	0.14	Nitrate Reductase	Cutting and Lamination	This work

Although a couple of works did present better LOD and LOQ, the dynamic range reported here was quite suitable for the determination of nitrate in the target samples with a more economic and environmentally friendly fabrication process. In terms of storage stability, the μPAD showed to be stable for 24 h when stored in air or vacuum atmosphere, and for 30 days when stored in vacuum at -20ºC. The characteristics of the developed μPAD for nitrate determination in urine make it suitable for point-of-care analysis.

Chapter 5. Ammonia Nitrogen and Urea in Saliva Samples

Chapter based on the paper published in

Microchemical Journal

Volume 193, 109102 (2023)

https://doi.org/10.1016/j.microc.2023.109102

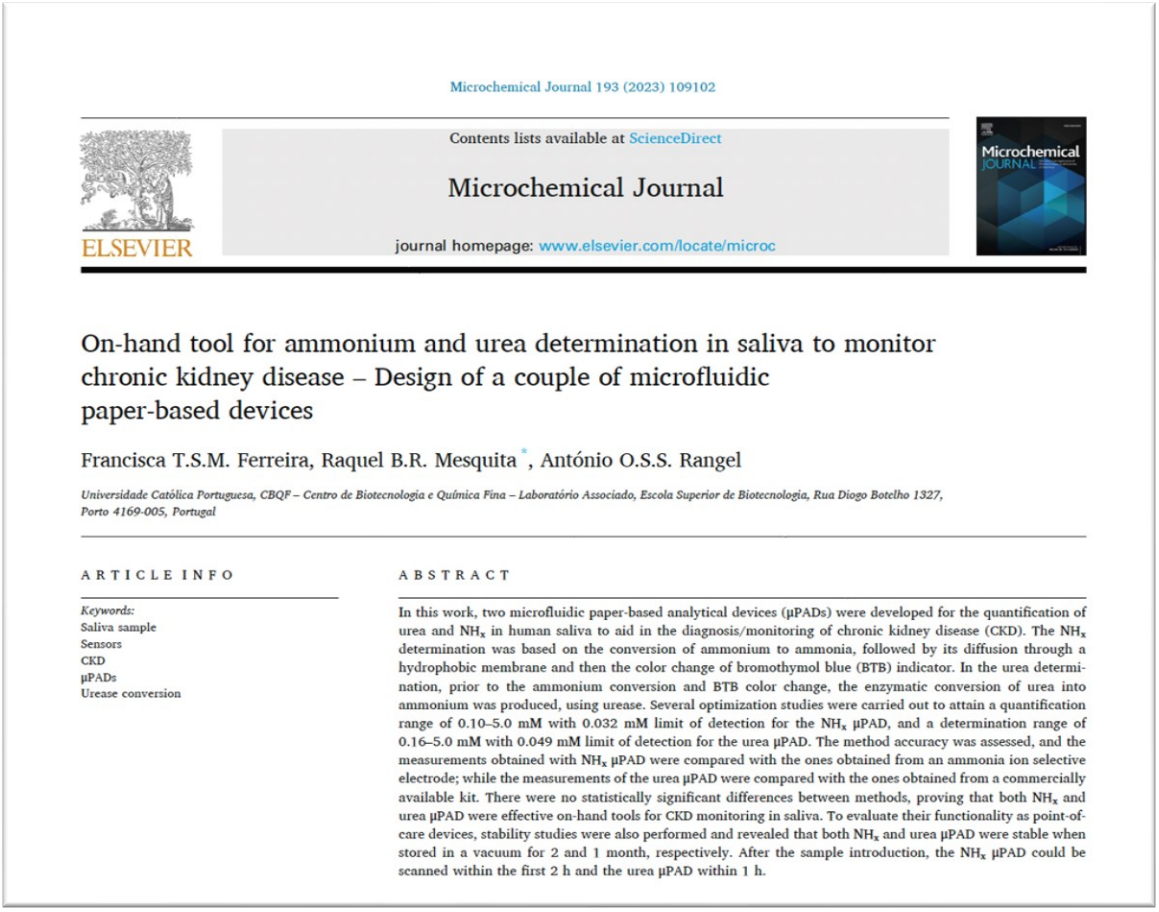

Microchemical Journal 193 (2023) 109102

Contents lists available at ScienceDirect

Microchemical Journal

journal homepage: www.elsevier.com/locate/microc

On-hand tool for ammonium and urea determination in saliva to monitor chronic kidney disease – Design of a couple of microfluidic paper-based devices

Francisca T.S.M. Ferreira, Raquel B.R. Mesquita *, António O.S.S. Rangel

Universidade Católica Portuguesa, CBQF – Centro de Biotecnologia e Química Fina – Laboratório Associado, Escola Superior de Biotecnologia, Rua Diogo Botelho 1327, Porto 4169-005, Portugal

ARTICLE INFO

Keywords:
Saliva sample
Sensors
CKD
μPADs
Urease conversion

ABSTRACT

In this work, two microfluidic paper-based analytical devices (μPADs) were developed for the quantification of urea and NH_x in human saliva to aid in the diagnosis/monitoring of chronic kidney disease (CKD). The NH_x determination was based on the conversion of ammonium to ammonia, followed by its diffusion through a hydrophobic membrane and then the color change of bromothymol blue (BTB) indicator. In the urea determination, prior to the ammonium conversion and BTB color change, the enzymatic conversion of urea into ammonium was produced, using urease. Several optimization studies were carried out to attain a quantification range of 0.10–5.0 mM with 0.032 mM limit of detection for the NH_x μPAD, and a determination range of 0.16–5.0 mM with 0.049 mM limit of detection for the urea μPAD. The method accuracy was assessed, and the measurements obtained with NH_x μPAD were compared with the ones obtained from an ammonia ion selective electrode; while the measurements of the urea μPAD were compared with the ones obtained from a commercially available kit. There were no statistically significant differences between methods, proving that both NH_x and urea μPAD were effective on-hand tools for CKD monitoring in saliva. To evaluate their functionality as point-of-care devices, stability studies were also performed and revealed that both NH_x and urea μPAD were stable when stored in a vacuum for 2 and 1 month, respectively. After the sample introduction, the NH_x μPAD could be scanned within the first 2 h and the urea μPAD within 1 h.

Submission received: 13 December 2022

Revised: 11 July 2023

Accepted: 16 July 2023

Published: 17 July 2023

5.1. Introduction

The human body is an intricate and complex ‘machine’ in which every organ has a purpose. The kidneys, among other functions, are responsible for blood filtration, removing wastes and toxins, and regulating blood chemicals that are essential to life (138).

Chronic Kidney Disease (CKD) is a condition in which the kidneys malfunction and are unable to properly filtrate blood, causing the accumulation of metabolic toxins and waste, harmful to the human body (139). Because there is no cure for CKD, early detection is key for slowing the disease progression, avoiding other complications, and maintaining the patients´ quality of life (138,140). Particularly in economically fragile countries with limited access to the required healthcare and where the lack of diagnosis is a possible death sentence (140,141). Even though advances in diagnosis and treatment technologies have significantly increased over the years, point-of-care affordable detection methods are still in need.

Urea is a nitrogenous product of the protein metabolism via the urea cycle, in which toxic NH_X is converted in urea (142–144). Since its primarily secreted by the kidneys, urea is one of the most used biomarkers for kidney failure (145,146). Furthermore, urea is present in several body fluids like blood, urine, and saliva (146). Although the standardized sample used for urea determination is blood, it requires a painful, time-consuming, invasive collection (144). Besides, CKD patients are more at risk of developing blood-borne diseases. (139). A viable alternative sample is saliva since it involves an easy, quick, painless, non-invasive collection. Furthermore, not only there are several studies that report a good correlation between blood and salivary concentrations of urea, but there are also studies that report a significant difference between the salivary urea concentration in healthy individuals and in CKD patients (139,144,145,147–149). With the increase of salivary urea, urease-producing microorganisms can significantly grow in the mouth, consequently leading to an increase of salivary ammonium. It has been previously reported that the average urea and ammonia concentrations found in CKD patients' saliva is 16.7 mM and 32.9 mM, respectively, as opposed to the urea and ammonia concentrations found in healthy individuals, 2.99 mM and 7.70 mM, respectively (149).

For ammonium and urea detection, several analytical methods have already been reported such as colorimetry, fluorometry, spectrophotometry, chromatography, among others. However, most of these conventional techniques are time consuming, require sample preparation, involve costly equipment, and require specialized personnel to perform the analysis (144,145). On the other hand, point-of-care devices have gained a great interest in the past decade, since they are capable of performing the analytical determinations in less time and with a more simple, economic and user-friendly procedure (146).

In this work, two microfluidic paper-based analytical devices using a vertical flow approach were developed for the determination of ammonia nitrogen (NH_X) and urea. In both devices, the detection relies on the diffusion of NH_3 (g) through a gas-diffusion membrane to produce a colorimetric change of a pH indicator. The use of vertical flow ensures that the sample (and/or standards) go through the paper disc with reagent and through the hydrophobic membrane, promoting the determination

specificity and the device accuracy. This feature resulted in a 3D structure (lateral flow within the paper disc coupled to vertical flow through the various layers). The urea determination was possible due to the use of urease, which is a nickel-dependent metallo-enzyme, commonly used in biosensors for urea determination, since it selectively catalyzes the dissociation of urea in ammonia (144,145) (Scheme 5.1). In an aqueous solution, ammonia is in equilibrium with ammonium (pK_a= 9.25) as shown in Scheme 5.2; however, because the enzymatic reaction occurs approximately at pH 7.0, the main form is NH_4^+. In order to convert NH_4^+ in gaseous NH_3, and consequently pass through the hydrophobic membrane, sodium hydroxide was also added to the devices. The pH indicator used for the colorimetric detection was bromothymol blue (Scheme 5.3), whose colour changes by converting gaseous NH_3 back to NH_4^+.

Scheme (5.1) $\quad Urea + H_2O \xrightarrow{Urease} H_2CO_3 + 2NH_3$

Scheme (5.2) $\quad NH_4^+ \rightleftharpoons NH_3 + H^+$

Scheme (5.3) $\quad$ Bromothymol Blue (pH<7 - Yellow) $\xrightarrow{NH_3 \rightarrow NH_4^+}$ Bromothymol Blue (pH>7 - Green/Blue)

5.2. Materials and Methods

5.2.1. Reagents and Solutions

Standard stock solutions of 10 mM ammonium chloride (Merck) and 10 mM of urea (Sigma) were prepared monthly by dissolving approximately 26.0 mg and 31.0 mg, respectively, of previously dried solids (overnight at 100 °C) in 50 mL of water. The working standards were weekly prepared from the stock solution in a range of 0.10 – 5.00 mM.

A 5 M sodium hydroxide stock solution was prepared by dissolving 20 g of the solid pellets in 100 mL of water. A fivefold dilution was prepared weekly to a final concentration of 1 M.

A 0.2 M phosphate buffer solution was prepared by dissolving 4.5 g of K_2HPO_4 $3H_2O$ (Merck) in 100 mL of water, and the pH was adjusted to 7. This solution was stored in the refrigerator at 2-8 ^oC.

The urease enzyme (from Canavalia ensiformis (Jack Bean), Sigma-Aldrich) solution of 125 U/mL was prepared by dissolving 32 mg of the lyophilized powder in 10 mL of phosphate buffer and was stored refrigerated at 2-8 ^oC.

The colour reagent, 2 mM bromothymol blue indicator (BTB) solution, was prepared by dissolving 12.5 mg of BTB powder (Merck) in 10 mL of ethanol (Panreac, 99.8% (v/v)) and the pH adjusted to 6.5.

5.2.2. Design of the Developed µPADs

The assembly of the developed µPADs consists of the alignment of 32 detection units (Figure 5.1) in a distribution of 4 columns x 8 lines, inside a laminating pouch A6 size. Each unit comprises four layers staked between the two sheets of the laminating pouch and aligned with the sample hole. The top sheet of the laminating pouch was perforated with 3 mm diameter holes prior to the laminating process, for posterior sample insertion (L1 in Figure 5.1).

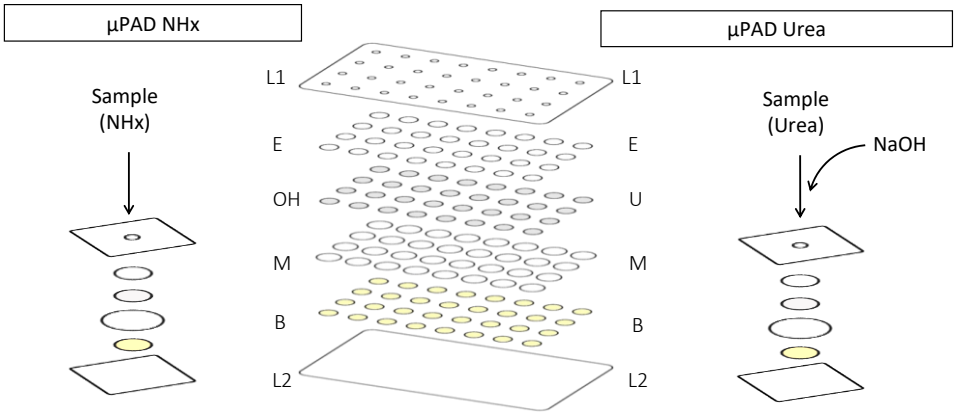

Figure 5.1 – Schematic representation of the assembly of the developed µPADs for NHx (left) and urea (right) determination; L1, top layer of the laminating pouch; L2, bottom layer of the laminating pouch; E, empty layer; OH, NaOH layer (15 µL per disc); U, urease layer (15 µL per disc); M, hydrophobic membrane layer; B, BTB layer (15 µL per disc).

In the µPAD for the NHx determination, the first layer below the sample hole consists of a 9.5 mm diameter of Whatman 4 (W4) filter paper disc without any reagent or solution (E in Figure 5.1). This layer was aligned on top of a 9.5 mm diameter W4 filter paper loaded with 15 µL of NaOH 1 M (OH in Figure 5.1) to attain the conversion of ammonium to ammonia. Both these layers were placed over a 1.27 cm diameter hydrophobic Durapore Membrane (0.45 µm porosity, Merck) promoting that only the formed gaseous ammonia would go through (M in Figure 5.1). The bottom layer (B in Figure 5.1) consisted of a 9.5 mm diameter of Whatman 1 (W1) filter paper loaded with 15 µL of BTB 2 mM (pH = 6.5).

The µPAD for urea determination consisted of the same E layer (9.5 mm W4 filter paper discs, without any reagent or solution) as the first layer but with a different second layer (U in Figure 5.1) consisting of a of 9.5 mm diameter W4 discs with 15 µL per disc of urease 125 U/mL. These two layers were also over the hydrophobic membrane, as the same M layer (1.27 cm diameter hydrophobic Durapore membrane with 0.45 µm porosity, Merck). The bottom layer (B in Figure 5.1) was also the same as for the NH_X determination µPAD (9.5 mm diameter W1 discs loaded with 15 µL per disc of BTB 2 mM). Before the alignment, all discs loaded with solutions/reagents were dried in an oven: the filter paper discs loaded with NaOH and BTB were dried at 50 ^{o}C for 20 min and 10 min, respectively and the filter paper discs loaded with urease were dried at 37 ^{o}C for 20 min. After the alignment, the laminating pouch passes through the laminator to melt and seal the plastic pouch.

5.2.3. Determination Procedures

For the NH_X determination, 25 µL of sample/standard were loaded through the sample hole and, after this volume is completely absorbed (< 1min), the holes were covered with adhesive tape to prevent contamination (of handling saliva) and possible ammonia loss by evaporation.

In contact with NaOH (OH in Figure 5.1) NH_4^+ is converted to dissolved gaseous NH_3 which diffuses through the hydrophobic membrane (M in Figure 5.1) to the BTB layer causing a colour change from yellow to green while being converted back to ammonium. The cover of the sample holes ensures that the dissolved gaseous NH_3 goes through the hydrophobic membrane and gets converted into ammonium, thus contributing to the selectivity of the method. To capture this colour change, the bottom side of the µPAD was scanned 15 minutes after the sample/standard placement.

In the urea determination, 20 µL of sample/standard were inserted into the sample hole and a waiting period of 15 minutes was accounted to enable the enzymatic conversion of urea into ammonium to occur (Enzymatic Reaction Time, ERT). Then, 10 µL of NaOH 1M was added to the µPAD also through the sample hole to promote the conversion of the formed ammonium to ammonia, so it can diffuse through the hydrophobic membrane to the BTB layer. Like the ammonium determination, the sample holes were covered with adhesive tape, and the bottom side of the device was scanned, 20 minutes after the NaOH placement (Colour Reaction Time, CRT).

The scanned images were processed through ImageJ by separating them into the RGB components and using the red component to measure the colour intensity. The use of the red component can be justified by the complementary colours wheel since red is the closest colour that is complementary of green obtained from the pH reaction.

For each unit, an option was made to do the measurements using a circular selection of 200 × 200 pixels, since it allowed a better adjustment to the BTB disc area. The intensity values were then converted into absorbance values. For each reading of blank or standard/sample, six measurements were obtained, and outliers were removed when necessary. The remaining replicates were used in the average calculations.

The concentration obtained from the urea determination µPAD corresponds to [NH_X+Urea], therefore the concentration of urea ([Urea]) was calculated by subtracting the concentration of NHx ([NH_X]) from the concentration obtained from the urea µPAD ([NH_X+Urea]).

5.2.4. Saliva Samples

The saliva samples used in this work were collected as “blind samples” from volunteers with their informed consent, and different collecting processes were used. Samples were analysed after collection (when possible) and stored in the freezer when not in use.

5.2.4.1. Saliva Collection using Gauze

Saliva samples were collected by placing a 5 × 5 cm sterile gauze (Wells) in the mouth for approximately 2 minutes. The gauze was then placed in a 5 mL sterile syringe and squeezed to remove the saliva from the gauze to a 5 mL plastic tube.

5.2.4.2. Saliva Collection by Swish

Saliva samples were collected by swishing 5 or 10 mL of deionized water for about 1 minute and retrieving the swished water into a plastic tube.

5.2.4.3. Saliva Collection by Spiting – CKD Patients

Saliva samples collected from patients with CKD undergoing peritoneal dialysis (PD) at least 1 h after eating or performing oral hygiene procedure, by spitting into a sterile tube for 5 minutes were supplied as blind samples. These samples were stored in the freezer and, due to the low quantity of sample supplied and the expected high content of the analytes, all samples were diluted 10 times with synthetic saliva (107) before analysis.

5.2.5. Comparison Methods – Validation Process

To assess the accuracy of the measurements provided by the NHx determination μPAD, 15 saliva samples were analysed both with the developed device and with an ammonia selective electrode (OrionTM, ThermoFisher Scientific, USA). The potentiometric determination was performed by mixing 10 mL of water with 1 mL of standard/sample and adding 250 μL of NaOH 5 M immediately before the measurement, as recommended by the manufacturer.

The accuracy of the urea determination μPAD was evaluated by comparing the measurements of #11 saliva samples obtained from the developed device, and the measurements of the samples obtained from a commercially available urea/ammonia determination kit (K-URAMR 04/20; Megazyme).

5.3. Results and Discussion

5.3.1. Ammonium/Ammonia µPAD

The µPAD assembly was based upon the work described by Thepchuay et al (62) which consisted of three-layer units including a hydrophobic membrane as the middle layer. The diameter of the paper discs (9.5 mm) and of a hydrophobic membrane (12.7 mm) were adopted from that work. Consequently, the volumes of the colour reagent, in the bottom layer, and of hydroxide, in the top layer, were also set from the published work as 15 µL (reported as the maximum volume for the 9.5 mm paper disc).

5.3.1.1. Design of the µPAD – Sample Volume

The work described by Thepchuay et al (62) reported the use of 12 µL of sample/standard volume, as the maximum amount to be absorbed. So, aiming to increase the sample volume, it was necessary to add a filter paper layer to the device. Therefore, a µPAD with four layers was prepared by adding an empty Whatman 1 filter paper disc (9.5 mm diameter) on top of the three layers described by Thepchuay et al (62). In the newly designed µPAD, with a four-layer structure, sample volumes of 15, 20, 25, and 30 µL (Figure 5.2) were tested. It was also possible to observe that there were no significant differences in sensitivity for the sample volumes of 15, 20 and 25 µL (overlapping of the 5% relative deviation intervals). However, when a 30 µL sample volume was placed in the device, a sensitivity decrease (relative deviation of the slope > 20%) was observed, probably because the sample was not completely absorbed. Therefore, to obtain the highest possible sensitivity, the sample volume chosen to continue the optimization studies was set at 25 µL.

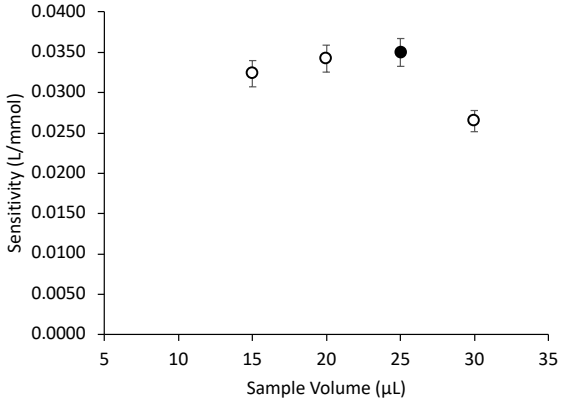

Figure 5.2 – Influence of the sample volume in the sensitivity of the calibration curves. The error bars correspond to a 5% deviation; the black bullet corresponds to the sample volume chosen.

5.3.1.2. Paper Selection

The porosity of the filter paper can affect the reactions on the microfluidic device, so among the Whatman qualitative paper variants, different pore sizes were tested: Whatman Grade 1 (W1) with 11 µm pore size, Whatman Grade 4 (W4) with 20-25 µm, and Whatman Grade 5 (W5) with 2.5 µm. The most widely used (and cheaper) filter paper is W1, so it was the base choice. Considering that the top layer of the designed µPAD was an empty layer, the first studies were made for the second layer (loaded with NaOH) keeping W1 in the empty top layer. The studies were performed by establishing calibration curves (#3 standards) and comparing the calibration curve slope; no standards were removed as outliers (Figure 5.3).

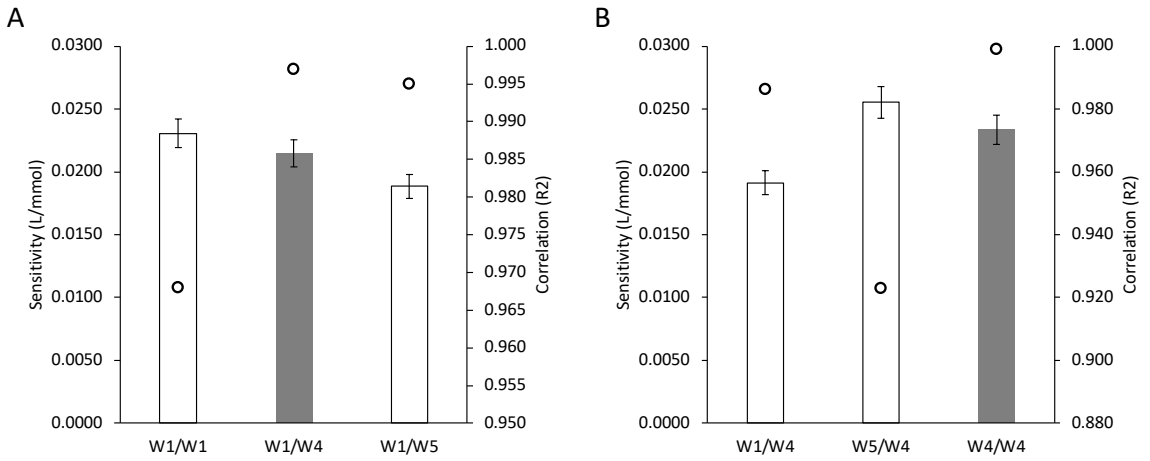

Figure 5.3 – Study of the influence of different filter paper porosities (W1: 11 µm; W4: 20 – 25 µm; W5: 2.5 µm) on the slope of the calibration curve (bars) and correlation factor (bullets) for the NH_x µPAD; A) study of the second layer loaded with NaOH; B) study of the top (empty) layer; the dark grey bar represents the chosen combination, and the error bars correspond to the 10% relative error.

When using either W1 and W4 in the second layer, there were no significant differences in the sensitivity (overlapping of the relative error intervals), but W4 presented a higher correlation factor (Figure 5.3(A)); so, the W4 was chosen as a compromise solution between sensitivity and correlation factor. Then, the first layer filter paper was also tested using the same filter papers W1, W4, and W5 (Figure 5.3(B)). Again, the paper that presented the best compromise solution, with high sensitivity and high correlation factor, was the W4 filter paper. In conclusion, the paper chosen for the first two layers of the µPAD was W4. This choice intended to ensure that they were not the limiting factor for the gas diffusion rate.

5.3.1.3. Hydrophobic Membrane

The hydrophobic membrane layer, the third layer of the device, is an essential layer for the device selectivity in the NH_4^+ determination, since it ensures that only the gaseous NH_3 diffuses to the detection layer (bottom layer).

Two hydrophobic membranes were tested, Mitex (5 µm porosity) and Durapore (0.45 µm porosity), preparing a µPAD with each membrane in order to obtain calibration curves. The results (Figure 5.4) showed that the sensitivity values were not statistically different (relative deviation of the slope < 10%), and so the Durapore membrane was chosen as a more economical choice.

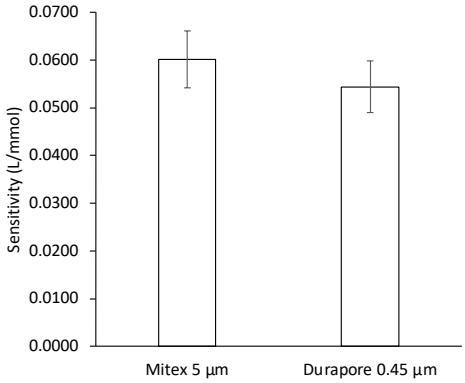

Figure 5.4 – Influence of the hydrophobic membrane porosity in the sensitivity of the calibration curves; the error bars correspond to a 10% deviation.

5.3.1.4. BTB and NaOH Concentration

The influence of the BTB concentration in the absorbance signal was evaluated and BTB concentrations of 1, 2, and 3 mM were prepared and used on the designed µPAD (Figure 5.5(A)). Then, the absorbance signal of a 1 mM ammonium standard was calculated for each BTB concentration, and it was possible to observe an over 2.5-fold increase when using 2 mM BTB when compared with 1 mM BTB. However, comparing 2 mM and 3 mM BTB, there was no significant difference in the absorbance signal (< 10% relative deviation), so 2 mM BTB was the concentration chosen.

The influence of the NaOH concentration in the slope of the calibration curve (device sensitivity) was also studied as an essential step for ammonium conversion to ammonia, to ensure diffusion through the hydrophobic membrane. Concentrations of 0.1, 0.5, 1, and 1.5 M NaOH were tested (Figure 5.5(B)), and although there was a significant increase in sensitivity when the concentration increased from 0.1 to 1 M, no significant difference was found between 1 and 1.5 M, so the concentration of 1 M was chosen.

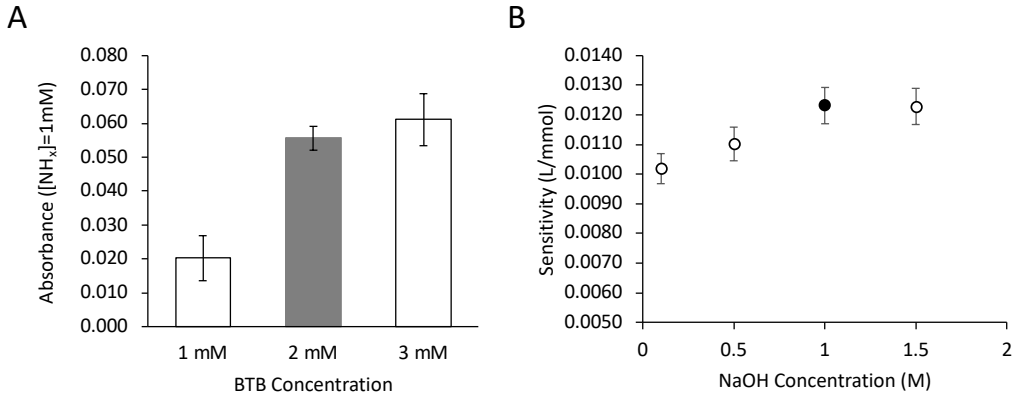

Figure 5.5 – Study of the concentrations of the reagents: (A) influence of BTB concentration in the absorbance signal obtained when using a 1 mM NH_x standard; the error bars correspond to the standard deviation of the respective absorbance measurement; the grey bar corresponds to the concentration chosen; (B) influence of NaOH concentration in the sensitivity of the calibration curve; the error bars correspond to a 5% deviation; the point in black corresponds to the chosen concentration.

5.3.1.5. Influence of Adhesive Tape – Biological Samples Handling

Because the developed device is intended for application to saliva samples, the covering of the sample hole after sample loading is a safety and security procedure for the operator.

As the µPAD for NHx determination involves the production and diffusion of the formed gaseous ammonia, it was especially important to evaluate the influence of applying adhesive tape over the sample holes. Two µPADs were prepared and ammonium standards were loaded; then, in one µPAD, the sample holes were covered with adhesive tape immediately after the standard insertion, and, in the other µPAD, the sample holes were not covered. No significant differences between the two calibration curves were observed. Still, due to the above mentioned safety reason, the covering with adhesive tape was employed.

5.3.2. Urea µPAD

In the µPAD for urea determination, the colour reaction was the same as in the NH_x µPAD, based upon the colour change of BTB in the bottom layer after the ammonia diffusion through the hydrophobic membrane. This meant that both the membrane layer and the BTB layer were kept from the optimization studies of the NH_x µPAD (section 5.3.1.).

5.3.2.1. Enzymatic Reaction

To achieve the urea determination, the enzymatic reaction that converts urea to ammonia using urease enzyme was chosen and then the formed ammonia would be determined following the process of the NH_x µPAD. In this context, the urease enzyme had to be incorporated into the µPAD assembly and several possible units alignment were tested (Figure 5.6).

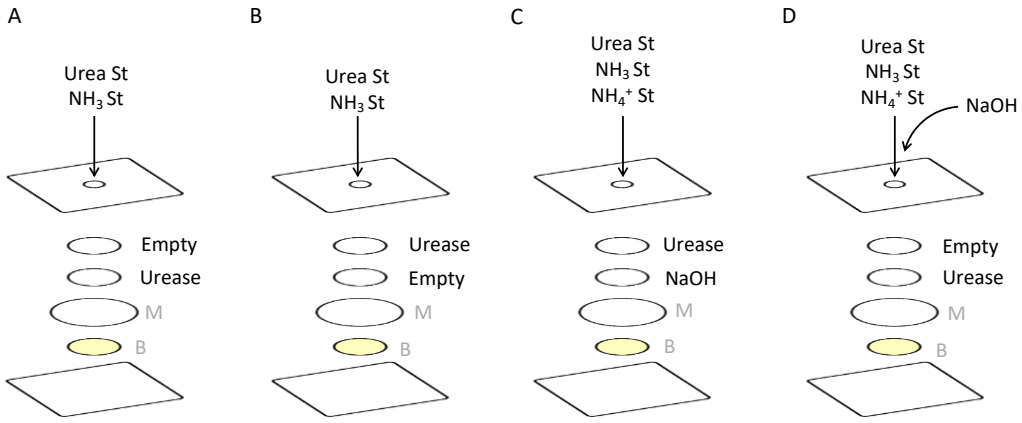

Figure 5.6 – Schematic representation of four different unit assemblies for the urea μPAD tested with indication of the different standard solutions tested; St, standards; M, hydrophobic membrane layer; B, BTB colour reagent layer.

First, the NaOH in the second layer was replaced by urease enzyme (Figure 5.6(A)) and this layout was tested with urease concentrations ranging from 0.1 – 100 U/mL.

However, when standards of urea were placed on the device, no colour was observed and consequently no signal was obtained from the scans. The same results were obtained when the urease was placed on the first layer (Figure 5.6(B)). To evaluate if the problem was due to the enzymatic reaction, standards of NH_3 were placed on these two layouts (Figure 5.6(A) and (B)) and it was expected that the NH_3 would reach the bottom layer and induce a change in pH which consequently would lead to a change in colour. However, that was not observed, which led us to conclude that the buffer used in the urease preparation was interfering with the NH_3/NH_4^+ equilibrium.

To fix this issue, a μPAD was prepared with urease on the first layer and NaOH on the second (Figure 5.6(C)). This would allow the urea conversion to NH_3/NH_4^+ and, with the NaOH in the second layer, the NH_3/NH_4^+ equilibrium would favor the presence of NH_3. Nevertheless, this layout also did not produce colour when standards of urea were inserted. Colour was only observed when standards of NH_3 or NH_4^+ were placed on the device, which indicated that the NaOH was allowing the NH_3 to reach the BTB layer but was interfering in the urease conversion efficiency.

The strategy found for the removal of this interference was to prepare a μPAD with just urease on the second layer (Figure 5.6(D)), to inject the standard/sample in the device, and allow the enzymatic reaction to occur for about 20 minutes and, only after, to insert the NaOH to convert the NH_4^+ formed to NH_3. This approach allowed the urea to be converted to NH_4^+ by the enzyme without any interference, after which the addition of the NaOH to the device led to its conversion to NH_3, causing the gradual increase of colour of the BTB layer.

5.3.2.2. Urease and NaOH Concentration

Several urease concentrations, in the range of 50 – 150 U/mL, were tested and the results showed that the sensitivity of the reaction (calibration curve slope) increased with the increase of urease concentration (Figure 5.7(A)). The increase was significant up to 125 U/mL but smaller when using 150 U/mL (relative deviation of the slope < 10 %) so 125 U/mL of urease was chosen to continue the studies.

The NaOH was now added after the sample/standard and to ensure the complete absorption into the μPAD the volume used was set at 10 μL. The concentration previously chosen of 1 M was revisited, hydroxide solutions of 0.5, 1, and 2 M of were tested. Still 1 M proved to be a better compromise choice of highest sensitivity and reagent consumption (Figure 5.7(B)).

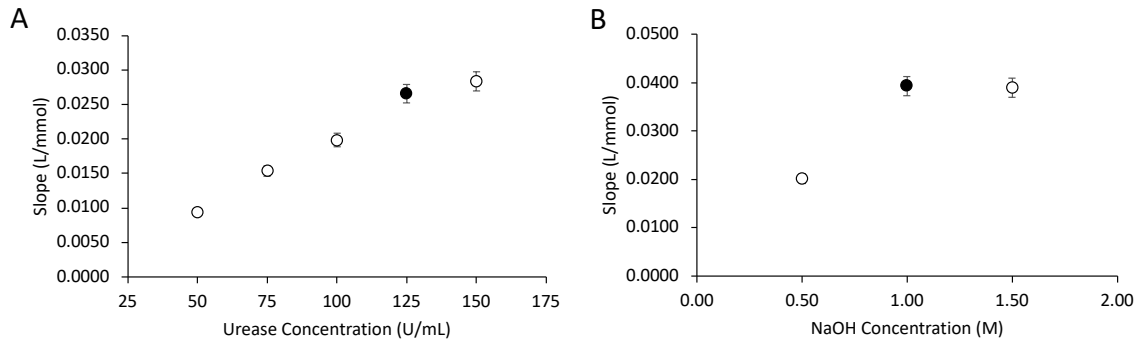

Figure 5.7 – Study of the influence of the Urease (A) and NaOH (B) concentrations in the μPADs calibration curve slope; the points in black represent the chosen values.

5.3.2.3. Time for the enzymatic and colour reaction

In the urea determination, both the enzymatic reaction time (ERT) and colour reaction time (CRT) was assessed in regarding the quantification sensitivity. Considering that the addition of hydroxide (loading NaOH) inactivated the enzyme and promoted the conversion of the formed ammonium to ammonia, the ERT corresponds to the time interval between the sample and the hydroxide loading. After the NaOH loading, when the ammonia is being formed, the time interval up to the device scanning corresponds to the CRT. For the urea quantification, a combined study of different ERT and CRT was carried out and calibration curves with different time intervals between sample and NaOH loading (ERT assessing) and between NaOH loading and device scanning (CRT assessing) were established. The calibration curves were compared to determine the best combination of ERT and CRT (Table 5.1). The established calibration curves, within the urea concentration range of 0.1 to 5 mM, presented two distinct slopes indicating two linear ranges: 0.1 – 1 mM and 1 – 5 mM.

Table 5.1 – Influence of both the enzymatic reaction time (ERT) and colour reaction time (CRT) on the calibration curve slope (sensitivity).

Urea dynamic range	ERT	CRT		
		10 min	*15 min*	*20 min*
0.1 – 1 mM	*10 min*	0.0517	0.0711	0.0856
	20 min	0.0530	**0.0740**	0.0969
	30 min	0.0568	0.0772	0.0943
1 – 5 mM	*10 min*	0.0150	0.0219	0.0196
	20 min	0.0225	**0.0226**	0.0260
	30 min	0.0194	0.0260	0.0212

In both defined concentration ranges, the sensitivity (calibration curve slope) increased with the increase of ERT from 10 to 20 minutes in all tested CRTs and, in most cases, it also increased from 20 to 30 minutes, but not for all the tested CRT.

Additionally, for a set ERT, the sensitivity also increased with the increase of the CRT. However, because the purpose of the device is to provide a fast measurement, a maximum combined time (ERT+CRT) of 35 minutes was established, as a compromise between sensitivity and analysis time. So, some combinations of analysis time (grey shadowed cells in Table 5.1) were discarded. The chosen combination was an ERT of 15 minutes and a CRT of 20 min since it presented a higher sensitivity in both concentration ranges (numbers in bold in Table 5.1).

5.3.3. Features of the Developed Devices

The main characteristics of both developed µPADs, such as dynamic range, average calibration curve, limit of detection (LOD) and quantification (LOQ), and relative standard deviation (RSD) are summarized in Table 5.2. In both determinations, the quantification range was divided in the linear dynamic ranges because of the difference in calibration curve slopes (Figure 5.8).

The limit of detection (LOD) and the limit of quantification (LOQ) were calculated as the concentration corresponding to three and 10 times the standard deviation of the intercept (n = 4), respectively, according to IUPAC recommendations (109). A difference between the LOD of urea determination and the LOD of NH_x determination can be explained by the addition of the enzymatic reaction and the extra steps in the quantification process.

The repeatability of the developed µPADs was evaluated calculating the relative standard deviation (RSD) of a sample measurement, obtained dividing the standard deviation of the sample measurements (n= 4) by the average of those values.

Table 5.2 – Features of the developed µPADs for the determination of NHx and urea; LOD, limit of detection; LOQ, limit of quantification; RSD, relative standard deviation.

Analyte	Dynamic Range, mM	Average Calibration Curve [a] A = S x [Conc] + b	Repeatability, RSD, % (Conc.)	LOD, [b] mM	LOQ, [b] mM
NH_x	0.105 – 1.0	Y = (0.087 ± 0.008) x [NH_x] + (0.003 ± 0.004) R^2 = 0.992 ± 0.004	5.5 (0.866 mM)	0.032	0.105
	1.0 – 5.0	Y = (0.018 ± 0.001) x [NH_x] + (0.064 ± 0.015) R^2 = 0.992 ± 0.009	4.7 (3.93 mM)		
Urea	0.163 – 1.0	y = (0.082 ± 0.001) x [Urea] + (0.003 ± 0.004) R^2 = 0.991 ± 0.004	3.2 (0.928 mM)	0.049	0.163
	1.0 – 5.0	Y = (0.016 ± 0.002) x [Urea] + (0.073 ± 0.001) R^2 = 0.992 ± 0.002	3.8 (4.32 mM)		

[a] n=3; [b] n=4

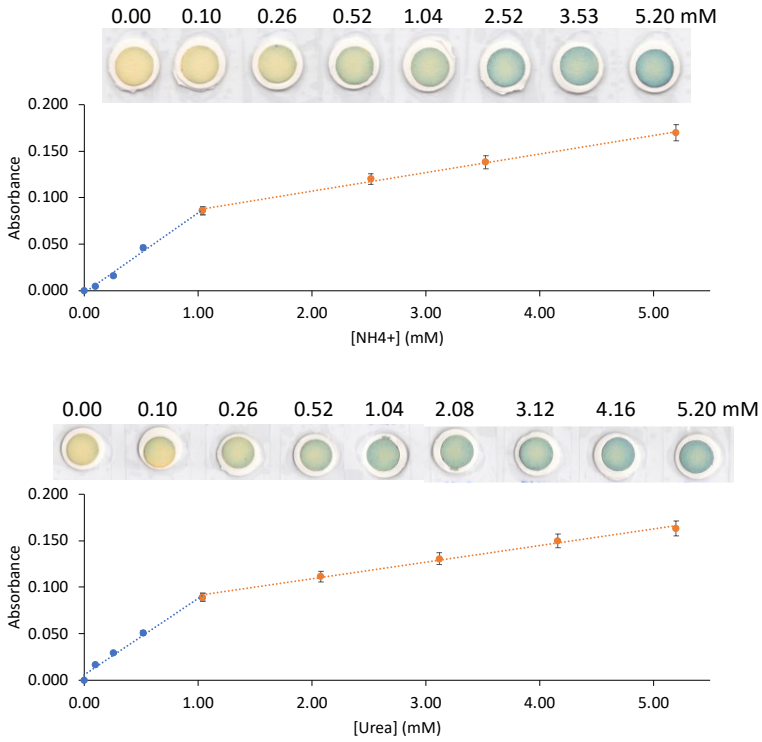

Figure 5.8 – Calibration curves of ammonium and urea determination, and colour chart of the respective device; the error bars correspond to a 5% deviation.

5.3.4. Devices Stability

Because μPADs are devices that typically are intended for on-hand, point-of-care application, it was vital to assess their stability both in storage before use, and after the coloured product formation, after sample analysis.

To assess the storage stability, μPADs were prepared and placed in clear plastic bags, shielded from light, under two different atmospheric conditions, air, and vacuum, for different periods of time. After each tested period, standards were loaded in the stored μPAD and the calibration curve obtained was compared with one obtained from freshly prepared μPADs, calculating the relative deviation between the slopes (RD < 10%, no significant differences).

The μPAD developed for NH_x determination showed to be stable for at least 2 months when stored in vacuum (RD -5%). On the other hand, the urea determination μPAD was stable for only 1 month in a vacuum atmosphere (RD 4%). Because enzymes are sensitive to temperature, additional studies were performed to evaluate the effect of the storage temperature on the device sensitivity. μPADs were prepared and stored in a vacuum atmosphere at room temperature (21 ^{o}C), 4 ^{o}C, and -20 ^{o}C. In all the storage conditions used, the devices were stable for 1 month. When storing for 2 months, a decrease in sensitivity was observed for all tested temperatures, -34% for 4 ^{o}C and -20 ^{o}C storage, and -90% in relative deviation of the slope for room temperature storage.

To study the stability of the coloured product, μPADs for each determination were prepared to obtain a calibration curve and then scanned several times, up to 3 hours. It was possible to conclude that the colour formed in the NH_x and urea μPADs was stable for 2 and 1 hour, respectively.

5.3.5. Application to Saliva Samples

The accuracy of the developed μPAD for NH_x determination was evaluated by comparing the results obtained from #15 saliva samples analysed with the developed device and with an ammonia selective electrode (ASE), as a reference method. A linear correlation between the two set of results was established (Figure 5.9).

The obtained equation $[NH_x]_{\mu PAD} = 0.974(\pm 0.078) \times [NH_x]_{ASE} + 0.065 (\pm 0.195)$, where the values in brackets corresponds to 95% confidence interval, proved that there was no statistically differences between the two sets of results because the slope and the intercept were not statistically different from 1 and 0, respectively.

Since in the urea determination, urea is converted into NH_4^+, and NH_3 is the analyte that is detected, the μPAD for urea determination is in fact the sum of NH_x and urea in the sample. Therefore, 11 saliva samples were analysed with both developed devices, and the results were compared with the ones obtained with a commercially available ammonia/urea determination kit (Table 5.3). The concentration of urea was obtained by calculating ($[Urea]_{calc}$) the difference between the concentration of NH_x ($[NH_x]_{\mu PAD}$) and of urea ($[NH_x+Urea]_{\mu PAD}$) obtained with the two μPADs, and the value compared with the kit measurement ($[Urea]_{kit}$).

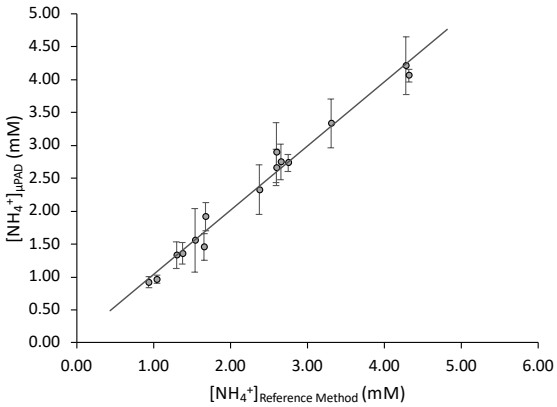

Figure 5.9 – Comparison between the results obtained for ammonia determination in saliva samples (#15) with the developed µPAD ($[NH_4^+]_{µPAD}$) and ammonia selective electrode (ASE) as the reference ($[NH_4^+]_{Reference\ Method}$); the full line represents the linear trendline between the two sets of results; the error bars represent the standard deviation.

Table 5.3 – Analysis of saliva samples with the developed µPADs and comparison of the results obtained with the measurements obtained with a commercially available kit; RD, relative deviation.

Saliva sample ID	Collection Method	NH_x determination			Urea determination				
		$[NH_x]_{µPAD}$ (mM)	$[NH_x]_{kit}$ (mM)	RD (%)	$[NH_x + Urea]_{µPAD}$ (mM)	$[NH_x]_{µPAD}$ (mM)	$[Urea]_{calc.}$ (mM)	$[Urea]_{kit}$ (mM)	RD (%)
S1	Gauze	1.42 ±0.08	1.53	-7.2%	2.47±0.12	1.42 ±0.08	1.04	1.16	-9.7%
S2	Gauze	1.18 ±0.13	1.29	-9.1%	2.73 ±0.20	1.18 ±0.13	1.56	1.50	3.6%
S3	Gauze	1.74 ±0.12	1.74	-0.2%	3.09 ±0.27	1.74 ±0.12	1.36	1.39	-2.4%
S4	Gauze	0.934 ±0.057	0.995	-6.2%	2.77 ±0.26	0.934 ±0.057	1.83	1.87	-2.0%
S5	Gauze	3.18 ±0.10	3.01	5.8%	3.97 ±0.33	3.18 ±0.10	0.788	0.780	1.0%
S6	Swishing	0.692 ±0.011	0.744	-7.0%	0.992 ±0.075	0.692 ±0.011	0.301	0.297	1.3%
S7	Swishing	1.11 ±0.18	1.22	-9.1%	1.29 ±0.09	1.11 ±0.18	0.181	<0.212	-
S8	Swishing	0.113 ±0.022	<0.384	-	0.301 ±0.012	0.113 ±0.022	0.188	<0.212	-
S9	Swishing	0.709 ±0.019	0.661	7.3%	0.873 ±0.047	0.709 ±0.019	0.164	<0.212	-
S10	Spiting	0.365 ± 0.016	<0.384	-	2.47 ±0.02	0.365 ±0.016	2.11	2.02	4.5%
S11	Spiting	0.193 ±0.007	<0.384	-	1.99±0.27	0.193 ±0.007	1.79	1.68	6.2%

5.3.5.1. Sampling Procedure

There are several methods of saliva collection already reported, so to develop a simple, user-friendly, point-of-care method of CKD biomarkers determination, it was also important to test different sampling processes. The three sampling procedures tested consisted of collection using a piece of gauze (26); collection by swishing with Milli-Q water (60); and collection by spitting (149). The quantification of urea and ammonium was effectively attained independently of the collection procedure used, so it is possible to conclude that the developed μPADs work with all three tested sampling methodologies. This can be an important feature due to some practical issues observed.

The use of gauze to collect saliva showed to be a simple and efficient procedure since it allowed the collection of higher amounts of saliva (1 to 3 mL) without altering the sample matrix. However, some children and elderly individuals did find the gauze collection procedure somewhat difficult and uncomfortable. The saliva collection procedure used with CKD patients was by spitting, and the samples were diluted with synthetic saliva (10-fold dilution), in order to maintain uniformity in the sample matrix. This saliva collection proved to be ineffective since in some cases less than 0.1 mL was obtained (in 5 minutes given to the patients). The use of synthetic saliva in the dilutions would be a good solution since it would minimize the changes in the sample matrix or viscosity.

The collection by swishing avoids some of the limitations of the other procedures since it was very simple and assessable to all age groups and would facilitate sampling from CKD patients with an incorporated dilution. However, that is its main drawback, the inability to control the dilution factor. Even though the each saliva sampling collection tested has advantages and limitations, they all can be used with the developed devices.

5.4. Conclusions

In this work, the determination of urea and NH_x in human saliva samples was accomplished in 35 and 15 minutes, respectively, with two newly developed microfluidic paper-based analytical devices (μPADs), which could be used as a tool in the diagnosis and monitoring of CKD. The NH_x determination μPAD was capable of quantifying ammonia in a range of 0.105-5.0 mM and provided limits of detection and quantification of 0.032 mM and 0.105 mM, respectively. The urea determination μPAD was capable of quantifying urea in a range of 0.163-5.0 mM and provided limits of detection and quantification of 0.049 mM and 0.163 mM, respectively.

The use of a gas-diffusion hydrophobic membrane and of the urease enzyme makes the developed μPADs very selective and efficient devices for determinations in human saliva samples, since it eliminates possible sample matrix interferences without requiring any pre-treatment. Moreover, the developed devices were successfully applied in human saliva samples of both healthy individuals and CKD patients.

Because the main application proposed for these devices was to facilitate health diagnosis in a very simple, on-hand, point-of-care manner, the stability of the developed devices was tested. The NH_x μPADs were stable for at least 2 months when stored in a vacuum, and the colour formed after placing the sample was stable for scanning for up to 2 hours. The urea μPADs, on the other hand, could remain in vacuum storage for just 1 month and, after placement of the sample, should be scanned within 1 hour.

Ammonia and urea are well-known biomarkers for several human health conditions (149), and there are some reports of paper-based devices developed for their determination. However, as far as we know, the μPAD developed in this work can be applied directly to saliva samples without any sample pretreatment and presents lower LOD and LOQ than a few others previously reported (145,150,151).

In addition to the advantages already mentioned, the developed devices are also disposable by incineration, which besides being environmentally friendly, is also important when handling biological samples. Furthermore, the use of several replicates and the possibility of removing outliers nearly eliminates the main downside of these types of manually assembled devices, which is the possible shifting of the discs during assembly and lamination, which can lead to uneven distribution and decreased reproducibility.

Chapter 6. Urease Activity in Saliva Samples

Chapter based on the paper published in

Biosensors

Volume 15, 48 (2025)

https://doi.org/10.3390/bios15010048

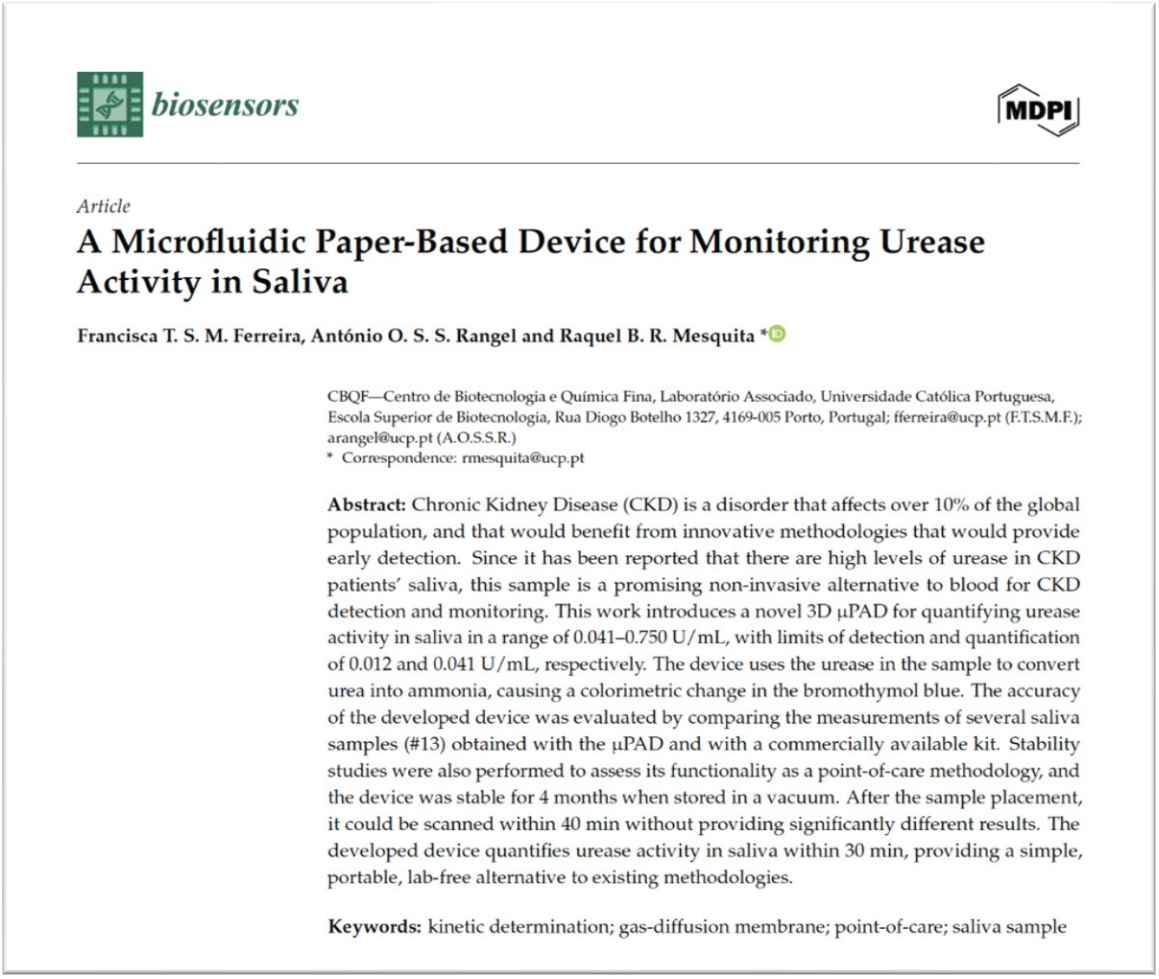

biosensors

MDPI

Article

A Microfluidic Paper-Based Device for Monitoring Urease Activity in Saliva

Francisca T. S. M. Ferreira, António O. S. S. Rangel and Raquel B. R. Mesquita *

CBQF—Centro de Biotecnologia e Química Fina, Laboratório Associado, Universidade Católica Portuguesa, Escola Superior de Biotecnologia, Rua Diogo Botelho 1327, 4169-005 Porto, Portugal; fferreira@ucp.pt (F.T.S.M.F.); arangel@ucp.pt (A.O.S.S.R.)
* Correspondence: rmesquita@ucp.pt

Abstract: Chronic Kidney Disease (CKD) is a disorder that affects over 10% of the global population, and that would benefit from innovative methodologies that would provide early detection. Since it has been reported that there are high levels of urease in CKD patients' saliva, this sample is a promising non-invasive alternative to blood for CKD detection and monitoring. This work introduces a novel 3D µPAD for quantifying urease activity in saliva in a range of 0.041–0.750 U/mL, with limits of detection and quantification of 0.012 and 0.041 U/mL, respectively. The device uses the urease in the sample to convert urea into ammonia, causing a colorimetric change in the bromothymol blue. The accuracy of the developed device was evaluated by comparing the measurements of several saliva samples (#13) obtained with the µPAD and with a commercially available kit. Stability studies were also performed to assess its functionality as a point-of-care methodology, and the device was stable for 4 months when stored in a vacuum. After the sample placement, it could be scanned within 40 min without providing significantly different results. The developed device quantifies urease activity in saliva within 30 min, providing a simple, portable, lab-free alternative to existing methodologies.

Keywords: kinetic determination; gas-diffusion membrane; point-of-care; saliva sample

Submission received: 24 November 2024

Revised: 4 January 2025

Accepted: 10 January 2025

Published: 15 January 2025

6.1. Introduction

Chronic Kidney Disease (CKD) is a condition that affects over 10% of the world's population and is characterized by kidney malfunction, which leads to inadequate blood filtration and build-up of harmful metabolic toxins and waste in the body (149,152–154). Early detection is crucial for slowing disease progression, preventing complications, and pre-serving patients' quality of life, especially since currently there is no cure for CKD (138,152,153). This need is especially pressing in economically vulnerable countries with limited healthcare access, where the prevalence is higher, and undiagnosed CKD can be life-threatening (152,153).

Although blood is the standardized sample for evaluating renal function, its collection process is inconvenient, painful, time-consuming, and invasive (145,149,154). Moreover, individuals with CKD face an elevated risk of contracting blood-borne illnesses, which elevates the importance of using alternative biological samples of non-invasive collection (139,152). Saliva emerges as a viable alternative sample due to its easy, quick, painless, and non-invasive collection method (152). Furthermore, several studies reported that the urea levels in saliva CKD patients are significantly higher than the ones of healthy individuals (139,148,154). With the increase of urea in saliva, a modification of the oral microbiota is expected to occur, particularly the proliferation of urease-producing microorganisms (149,154). This urease enzyme then converts the high levels of urea into ammonia, which gives the patients the characteristic ammonia breath (147,149,155).

In this work, a novel 3D structured microfluidic paper-based device was developed to determine urease activity in saliva samples as a potential aid in diagnosing and monitoring CKD. This determination relies on the enzymatic reaction involving urease, the conversion of urea to gaseous ammonia, which consequently diffuses through a hydrophobic membrane and generates a colorimetric change in the pH indicator bromothymol blue (BTB). This device provides a more straightforward, portable, lab equipment-free, point-of-care alternative to commercially available kits that normally require specific lab equipment and extra steps such as sample pre-treatment (156). To the best of our knowledge, only one other paper-based device for determining urease activity has been reported, but with an application to soil samples (157).

6.2. Materials and Methods

6.2.1. Reagents and Solutions

A 0.2 M phosphate-buffer solution was prepared by dissolving 4.5 g of $K_2HPO_4 \cdot 3H_2O$ (Merck) in 100 mL of water, and the pH was adjusted to 7. This solution was stored at 2–8 °C in the refrigerator.

The urease enzyme (from *Canavalia ensiformis* (Jack Bean), Sigma-Aldrich) stock solution of 100 U/mL was prepared by dissolving 5.0 mg of the lyophilized powder in 2 mL of phosphate buffer and was stored at −20 °C. A 10-fold dilution was prepared weekly, and standards in the range of 0.05–0.75 U/mL were prepared daily in synthetic saliva.

A standard stock solution of 8.4 mM of urea (Sigma-Aldrich) was prepared monthly by dissolving 10 mg of the previously dried solid (overnight at 100 °C) in 20 mL of water.

A 2.5 M sodium hydroxide stock solution was prepared by dissolving 10 g of the solid pellets (Panreac) in 100 mL of water. A twofold dilution was prepared weekly to a final concentration of 1.25 M.

The colour reagent, 4 mM bromothymol blue indicator (BTB) solution, was prepared by dissolving 25 mg of BTB powder (Merck) in 10 mL of ethanol (Panreac, 99.8% (v/v)). A dilution to 2 mM was prepared and the pH adjusted to 6.5. with NaOH 0.1 M (152).

6.2.2. Design of the Developed µPAD

In this work, the assembly of the µPAD consists of placing 32 detection units, in 4 columns and 8 lines distribution (Figure 6.1), inside a plastic laminating pouch (125 microns, A6 size, Leitz). These detection units were aligned under the 3 mm diameter sample insertion holes of the top sheet of the laminating pouch (L1 in Figure 6.1A). Each detection unit is composed of three layers: the first layer, the urea layer (U in Figure 6.1(A)); the middle layer (M in Figure 6.1(A)), the hydrophobic polyvinylidene fluoride (PVDF) membrane (1.27 cm diameter, Durapore, 0.45 µm porosity, HVHP09050, Merck); and the bottom layer, the BTB layer (BTB in Figure 6.1(A)).

The paper discs on the top layer (U in Figure 6.1A) consisted of Whatman filter paper Grade 4 (9.5 mm diameter), loaded with 15 µL of 8.4 M urea and dried for 20 min in a 50 °C oven. The discs on the bottom layer (BTB in Figure 6.1(A)), consisted of Whatman filter paper Grade 1 (9.5 mm diameter), loaded with 15 µL of 2 mM BTB (pH = 6.5) and dried in a 50 °C oven for 10 min. The oven temperature and time ensure the drying of the paper without over-drying. The plastic pouch with the aligned discs was then laminated to melt the plastic around each detection unit, creating a hydrophobic seal between the 32 units.

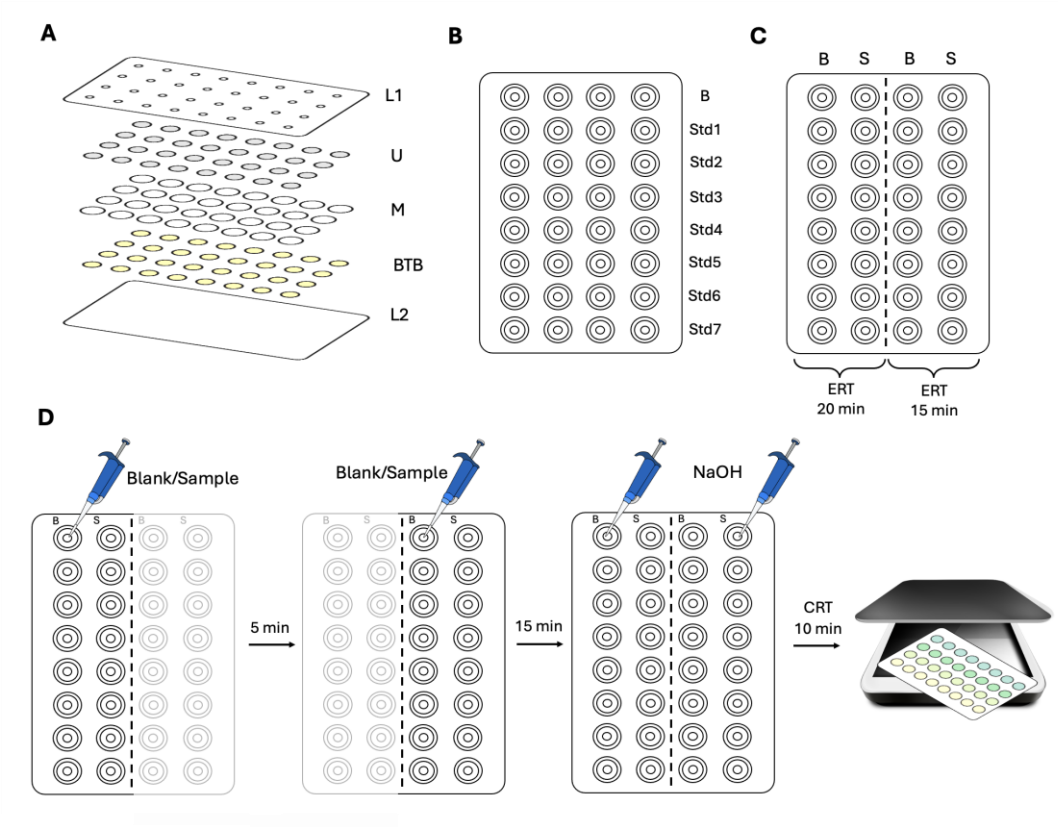

Figure 6.1 – Schematic representation of the developed μPADs (A) assembly structure; L1, top sheet of the laminating pouch; U, urea layer (15 μL per disc); M, hydrophobic membrane layer; BTB, bromothymol blue layer (15 μL per disc); L2, bottom sheet of the laminating pouch; (B) calibration curve structure; B, blank; Std, standard; (C) structure for sample and blank placement; B, blank; S, sample; ERT, enzymatic reaction time; (D) determination procedure; CRT, colour reaction time.

6.2.3. Determination Procedure

This work aimed to quantify the urease activity by combining the enzymatic reaction of urease with a colorimetric reaction of BTB with the formed product from the enzymatic reaction. The product of the enzymatic urease reaction is ammonia nitrogen, then hydroxide was added to quantitively convert it to gaseous ammonia which diffuses through a hydrophobic membrane. After the diffusion process, the gaseous ammonia alters the pH of the BTB solution causing a colour change. To eliminate the interference of the ammonium in the sample, the urease activity determination was attained by a ΔA calculated from two enzymatic reaction times. The enzymatic reaction, set to occur first, is stopped with the loading of the hydroxide at 15 and 20 min reaction times and then the colour change registered enabling the calculation of A_{20min} and A_{15min} to be used for the ΔA calculation.

To accomplish this in the preparation of the calibration curve (Figure 6.1(B)), two devices were prepared: one for a 15 min enzymatic reaction time (ERT) and the other for 20 min ERT, both reaction times followed by the colorimetric reaction involving the ammonium. So, 10 μL of blank and a set of standards were placed on the devices and, after the corresponding ERT, 4 μL of NaOH 1.25 M was loaded into the devices in order to promote the conversion of NH_4^+ to NH_3.

The ammonia diffuses through the hydrophobic membrane (M in Figure 6.1(A)) to reach the BTB layer (BTB in Figure 6.1(A)) causing the colour change. The urease concentration relates to its activity and correlates to subtracting the measurements obtained with the two ERTs, 20 and 15 min. This procedure also enables to account for the NH_4^+ already present in the sample, avoiding misleading results with the produced NH_4^+ by enzyme activity.

To accomplish the urease activity determination in a sample, a device was prepared and divided into two sections (Figure 6.1(C)), one for each ERT. A volume of 10 µL of synthetic saliva (blank) was loaded into #8 detection units (as illustrated in Figure 6.1(C)) together with 10 µL of sample loaded into #8 detection units each (Figure 6.1(C)). After 5 min, the same process was carried out on the right side of the µPAD (Figure 6.1(C)). Then, after the device has rested for 15 min, 4 µL of NaOH 1.25 M is placed in all the #32 detection units. To avoid the loss of the gaseous ammonia, the sample insertion holes were covered with adhesive tape immediately after the NaOH was completely absorbed. The scanning of the device is performed on the BTB side (opposite to the sample/standard insertion) 10 min after loading the NaOH, corresponding to the colour reaction time (CRT) (Figure 6.1(D)).

The colour change, from yellow to green, is registered by scanning the device and treating the acquired image with an image processing software, ImageJ. To establish the calibration curve, the absorbance signal was calculated for each standard as follows: $\Delta A = A_{20min} - A_{15min}$, in which ΔA is the variation in absorbance, A_{20min} is the absorbance of the standard with a 20 min ERT, and A_{15min} is the absorbance of the standard with a 15 min ERT. A linear relationship was established between ΔA and the urease concentration in the range of 0.05–0.75 U/mL.

6.2.4. Saliva Samples

Saliva samples from healthy volunteers were collected with their informed consent. The samples were spiked with 5 µL of a urease solution of 10 U/mL in 500 µL of sample and analysed on the same day of the collection.

6.2.5. Comparison Method – Validation Procedure

The accuracy of the developed device was assessed by analysing saliva samples with the developed µPAD and comparing the results obtained with a commercially available Urease Activity Assay Kit (MAK120, Sigma-Aldrich). For this, #13 saliva samples were spiked with 0.1 U/mL urease.

6.3. Results and Discussion

The development of the urease activity μPAD was based on a previously developed device for urea determination using the enzymatic reaction of urease (152). In that determination, urea was converted into ammonium by urease, and then ammonium was converted into ammonia by adding hydroxide. The formed ammonia diffused through a hydrophobic membrane to a pH indicator layer, causing a colour change. In the end, the described device was composed of four layers: a top layer consisting of an empty paper disc; a second layer of a paper disc with urease; a third layer corresponding to the hydrophobic membrane; and a bottom layer with the pH indicator paper disc. The top layer consists of an empty paper disc intended to be a physical protective barrier of the urease enzyme layer.

A similar structure was used to perform the urease determination, replacing the urease with a urea standard of 2 mM on the second paper layer. An initial calibration curve was obtained loading urease standards ranging from 10 to 150 U/mL (slope about 3.1×10^{-4} mL/U).

6.3.1. Number of Layers

The first optimization study aimed to evaluate the need for the top empty layer, and two devices were prepared, one with the empty paper disc and another without (shown in Figure 6.2(A)). Because the absorption capacity of the μPAD decreases when one layer of paper discs is removed, the volume of sample placed in the three layers μPAD was reduced to half (10 μL) of the 20 μL used in the four layers μPAD.

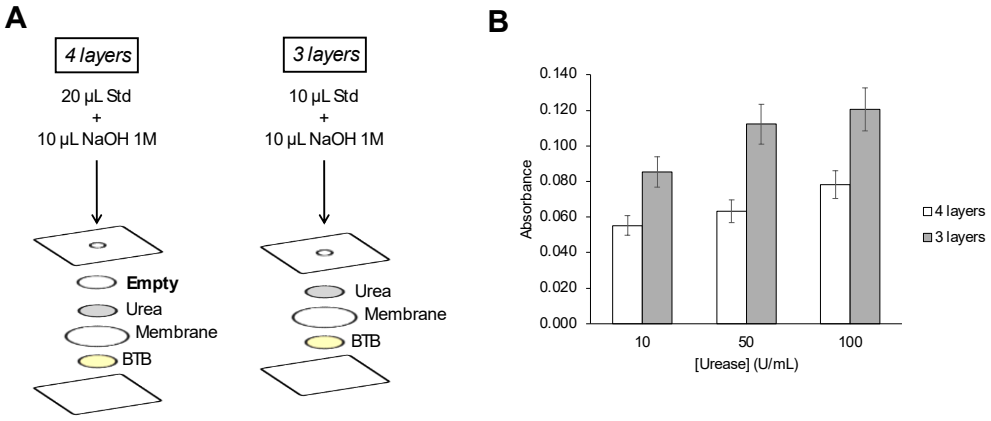

Figure 6.2 – (A) Schematic representation of both studied device structures and (B) resulting absorbance values obtained from placing urease standards of 10, 50 and 100 U/mL in each studied structure; Std, standard; BTB, bromothymol blue; the error bars correspond to a 10% deviation.

It was observed (Figure 6.2(B)) that, even with a lower amount of standard, the three-layer structure provided not only higher values of absorbance for each standard (> 50%) but also significantly higher overall sensitivity (calibration curve slope > 40%).

This can be explained as in the four-layer assembly, despite the higher volume, part of the urease gets dispersed/retained in the top empty layer, never reaching the urea layer, and consequently not producing ammonia. Thus, there is less ammonia to diffuse through the hydrophobic membrane and reach the BTB layer for colour change, resulting in lower absorbance values and lower sensitivity. Therefore, the three-layer structure was chosen.

6.3.2. Urea Concentration

Next, the influence of urea concentration on the sensitivity of the calibration curve was evaluated. Standard urea solutions ranging from 1.12 to 11.2 mM were prepared and loaded in the first paper layer of the developed devices (U in Figure 6.1(A)). Then, calibration curves with urease standards (volume of 15 µL) were established. The results (Figure 6.3(A)) showed that when using concentrations of 1.12 and 2.24 mM, there was no significant difference (relative deviation of the slopes < 10%) in the sensitivity of the calibration curve. However, when the urea concentration was increased to 8.4 mM, there was an increase in sensitivity of over 380%. The results also showed no significant difference between using 8.4 and 11.2 mM of urea (relative deviation of the slopes < 10%), and, therefore, 8.4 mM was the concentration of urea chosen for the remaining studies.

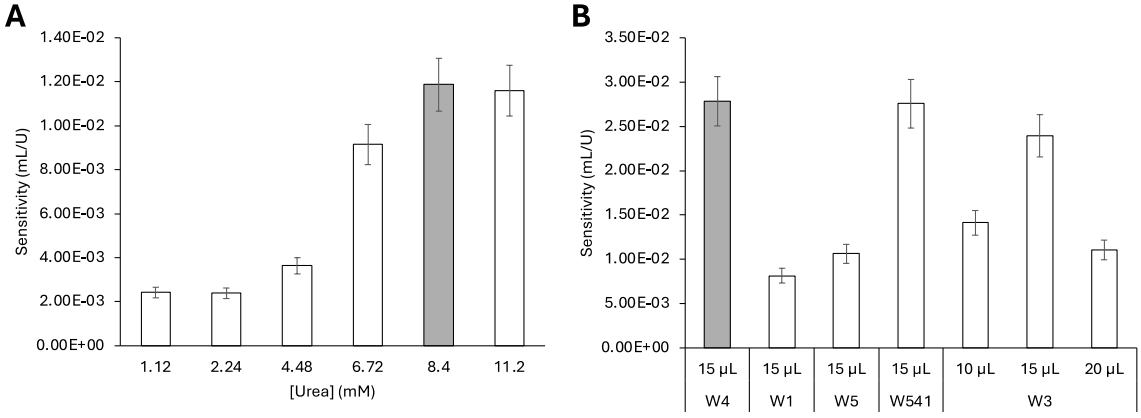

Figure 6.3 – Influence of the (A) urea concentration (mM) and (B) filter paper type (and correspondent sample volume) on the sensitivity of the calibration curve; W4, Whatman Grade 4 filter paper; W1, Whatman Grade 1 filter paper; W5, Whatman Grade 5 filter paper; W541, Whatman Grade 541 filter paper; W3, Whatman Grade 3 filter paper; the grey bars correspond to the chosen condition; the error bars correspond to a 10% deviation.

6.3.3. Type of Paper

The type of paper used was the next optimization study performed since it can significantly interfere with the sensitivity of the device. A variety of filter papers were studied: Whatman Grade 4 (W4), Whatman Grade 1 (W1), Whatman Grade 3 (W3), Whatman Grade 5 (W5), and Whatman Grade 541 (W541).

These vary in paper porosity: 2.5 µm (W5), 6 µm (W3), 11 µm (W1), and 20–25 µm (W4 and W541); and in paper treatment: Qualitative (W1, W3, W4, W5) and Hardened Ashless (W541). For this study, a device was prepared with each type of paper and 15 µL of urease standards was placed to obtain a calibration curve. Because W3 has a higher thickness and, therefore, a higher absorption capacity, the standard volumes of 10 and 20 µL when using W3 were included in this study. The sensitivities of the calibration curves were compared (Figure 6.3(B)), and the papers that provided a higher calibration curve sensitivity were W4 and W541.

Because there was no significant difference between the sensitivities provided by these two types of paper, and since W541 is more expensive, W4 was the filter paper chosen for the developed device.

6.3.4. Enzymatic Reaction Time

As previously mentioned, the urease quantification device is based on the corresponding enzymatic conversion of urea into ammonia nitrogen. For the quantification, the ammonium present must then be converted to ammonia with the addition of hydroxide, which stops the urease reaction. Because enzymatic reactions are usually highly time-dependent, the next study was performed to assess the influence of different enzymatic reaction times (ERT). Periods of 10, 15, and 20 min between loading the standard and the NaOH were tested, for colour reaction times between 5 and 20 min (Figure 6.4).

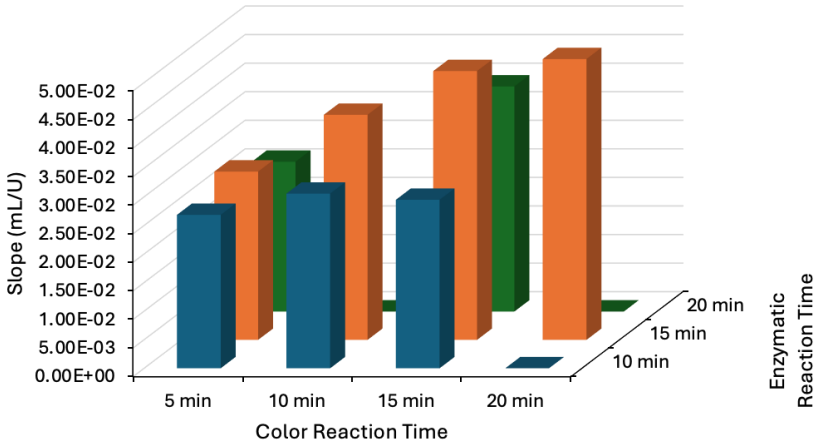

Figure 6.4 – Slope of the calibration curves obtained in the combination study of the influence of the enzymatic reaction time (10, 15, 20 minutes), and of the colour reaction time (5, 10, 15 and 20 minutes) in the developed device.

It was possible to observe that the increase in ERT from 10 to 15 min always resulted in an increase in the sensitivity (calibration curve slope increase > 30%) for all the tested colour reaction times 5, 10, and 15 min.

However, when the ERT was increased to 20 min, the sensitivity of the calibration curve was not statistically different from the sensitivity at 15 min, even showing a slight decrease for both tested colour reaction times (average 19%). This could be explained due to the extended time in contact with air and consequent evaporation affecting the necessary downward vertical flow within the device. As the highest sensitivity was obtained with an ERT of 15 min and colour reaction of 15 min, these were the chosen intervals.

6.3.5. Sodium Hydroxide

Then, the influence of the amount of NaOH on the calibration curve was assessed. The amount of NaOH ranging from 2 to 10 µmol was studied (Figure 6.5(A)), and it was possible to conclude that the highest sensitivity of the calibration curve was obtained with amounts of 5 and 10 µmol of NaOH. Since there was no significant difference in the sensitivity between these two amounts, 5 µmol was chosen. Then, maintaining the final amount of 5 µmol NaOH, different proportions of volume and concentration were tested (Figure 6.5(B)).

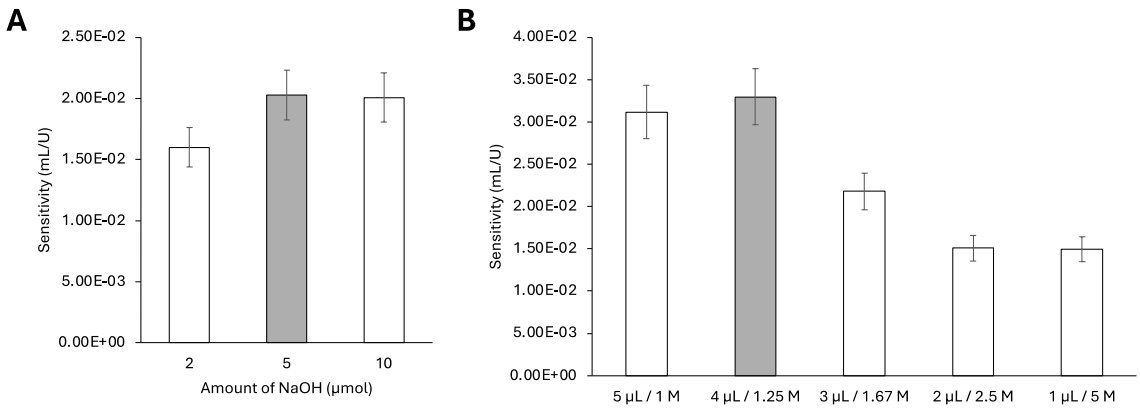

Figure 6.5 – Influence of the (A) amount of NaOH (µmol) and (B) influence of different proportions of volume/concentration of NaOH, maintaining a final amount of 5 µmol; the grey bars correspond to the chosen condition; the error bars correspond to a 10% deviation.

The results showed that the proportions that provided the higher sensitivity of the calibration curve were 5 µL of 1 M and 4 µL of 1.25 M. However, because the volume of 4 µL showed an easier absorption into the device, the chosen optimal condition was 4 µL of NaOH 1.25 M.

6.3.6. Matrix Influence

Because the developed device aimed to quantify urease in saliva samples, evaluating the potential interference from the saliva matrix composition was important. Two devices were prepared, and calibration curves were established using two sets of standards, one prepared in phosphate buffer (recommended by the manufacturer for the stability of the enzyme), and another set prepared in synthetic saliva (107).

The sensitivity of the calibration curves obtained was compared and it was possible to observe that there was an enormous increase (over six-fold) in the sensitivity when using standards prepared in the synthetic saliva. This can happen due to the presence of several compounds that can act as buffer in the reaction, favouring the enzyme activity, and consequently increasing the sensitivity of the device. The final decision was to continue the optimization studies using standards prepared in synthetic saliva.

6.3.7. Kinetic Determination

As mentioned before, the quantification of urease in the developed μPAD is based on the enzymatic conversion of urea to ammonia nitrogen, diffusion, and consequent change in the BTB colour (pH indicator). Saliva samples have already a considerable amount of ammonium (62,149,152). This should not present an interference since this determination is dependent on the kinetic properties of the enzyme. The idea was to perform the measurements at two different ERTs and calculate the variation in the absorbance signal obtained. If the sample contained urease, the signal was expected to increase with the increase in the time allowed for the enzymatic reaction (ERT), since the enzyme would convert more urea to ammonia nitrogen. On the other hand, the ammonium that could already be present in the sample would provide the same signal in both ERTs and therefore be suppressed when calculating the ΔA.

To test this hypothesis, devices were prepared, and two periods of time between standard and NaOH placement (ERTs) were established to calculate the ΔA: absorbance calculation between 10 and 15 min and absorbance calculation between 15 and 20 min (Table 6.1). The choice of these ERTs is justified by the results obtained in previous tests (Section 6.3.4) always using the optimum time of 15 min. A couple of urease standards were loaded and the variation in the absorbance (ΔA) values between the two ERTs calculated: (i) $\Delta A = A_{15min} - A_{10min}$, where A_{15min} is the absorbance of one standard with a 15 min ERT, and A_{10min} is the absorbance of the same standard with a 10 min ERT; (ii) $\Delta A = A_{20min} - A_{15min}$, where A_{20min} is the absorbance of one standard with a 20 min ERT, and A15min is the absorbance of the same standard with a 15 min ERT (Table 6.1).

Table 6.1 – Preliminary assessment of the effectiveness of the kinetic determination; variation of the absorbance reading in different time intervals for two urease standards (0.1 and 0.5 U/mL) and one sample without any addition (Sample), with addition of NH_4^+(Sample_NH_4^+), and with addition of Urease (Sample_Urease).

	ΔA	
	[10-15] min	*[15-20] min*
0.1 U/mL	0.009	0.005
0.5 U/mL	0.022	0.037
Sample	0.003	0.002
Sample_NH_4^+	0.003	0.004
Sample_Urease	0.041	0.035

To further assess the effectiveness of the hypothesis, one human saliva sample was also loaded in the same conditions and spiked with ammonium and with urease. Comparing the absorbance signals of the sample and the sample spiked with NH_4^+, no significant difference was observed, indicating that the presence of NH_4^+ in the sample did not influence the quantification when the signal obtained is the ΔA. On the other hand, when comparing the signal of the sample and the sample spiked with urease, the signal from the urease-spiked sample was significantly higher, as expected. This validates our hypothesis that the kinetic determination allows the quantification of urease and suppresses the influence of NH_X already present in the samples.

6.3.7.1. Enzymatic Reaction Kinetics

The two different ERTs used in the kinetic determination were reevaluated by testing different combinations. The intervals of [10;15] min, [15;20] min and [10;20] min were tested (Figure 6.6) and it was possible to conclude that [15;20] min was the optimal interval since it provided a calibration curve with a significantly higher sensitivity when compared to the intervals [10;15] min (RD=-47%) and [10;20] min (RD=-87%).

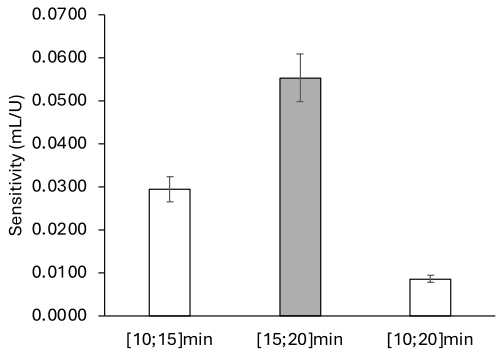

Figure 6.6 – Influence of the enzymatic reaction time interval (in minutes) in the sensitivity of the developed device; the error bars correspond to a 10% deviation.

6.3.8. Features of the Developed Device

The main features of the developed μPAD, such as the dynamic range, the limit of detection and quantification, and the repeatability, both intraday and interday, are summarized in Table 6.2.

Table 6.2 – Features of the developed μPAD for urease determination; LOD, limit of detection; LOQ, limit of quantification; RSD, relative standard deviation.

Dynamic Range (U/mL)	Calibration Curve [a] ΔA = S × [Urease] + b	LOD [a] (U/mL)	LOQ [a] (U/mL)	Repeatability, RSD	
				Intraday [a]	*Interday* [a]
0.041 - 0.750	ΔA = 0.0531(±0.0018) x [Urease] + 0.0142(±0.0002) R^2 = 0.9969(±0.0023)	0.012	0.041	4%	3%

[a] n=4.

The limit of detection (LOD) and the limit of quantification (LOQ) were calculated as the concentration corresponding to three times (LOD) and ten times (LOQ) the standard deviation of the intercept of the calibration curves (n = 4), according to IUPAC recommendations (109). The intraday repeatability of the developed device was assessed by calculating the relative standard deviation (RSD) of four replicas of a sample on the same day and same device. The interday repeatability of the developed device was assessed by calculating the relative standard deviation (RSD) of four calibration curve slopes on consecutive days.

6.3.9. Stability Studies

Stability studies were performed to evaluate the performance and robustness of the developed μPAD, not only when stored (before the sample insertion), but also the stability of the coloured product.

The storage stability was evaluated by preparing devices and storing them for different periods under two different atmospheric conditions: in contact with air and in vacuum. The storage devices were wrapped in aluminium foil to be protected from light, and the ones in contact with air were placed inside a clear plastic zip lock bag, while the ones in vacuum were placed in a clear vacuum bag. The vacuum atmosphere was achieved using a vacuum packaging machine. The devices were stored at room temperature (approximately 21 °C).

After each tested period, a set of urease standards was loaded into the stored μPADs and into freshly prepared ones, and the calibration curve slopes were compared by calculating the relative deviation (RD), considering that < 10% means there were no differences. After analysing the results (Figure 6.7(A)), it was possible to conclude that the storage in the air atmosphere was not able to maintain the sensitivity of the device in any of the periods tested (RD > 10%). When the μPADs were stored in a vacuum atmosphere, it was possible to observe that the devices were stable (RD < 10%) for at least 4 months.

To assess the stability of the coloured product formed on the developed μPADs, a calibration curve was prepared, and the evolution of the colour in the devices was registered with a scanner at several colour reaction times (CRTs) from the 10 min (used up until this study) to 120 min. CRTs lower than 10 min were not studied since 10 min was the minimum time required for the device to fully absorb the NaOH, to place the adhesive tape and then perform the scan. The results (Figure 6.7(B)) showed that the coloured product on developed μPAD was stable for at least 40 min since there was no significant decrease (RD < 10%) in the sensitivity of the obtained calibration curve.

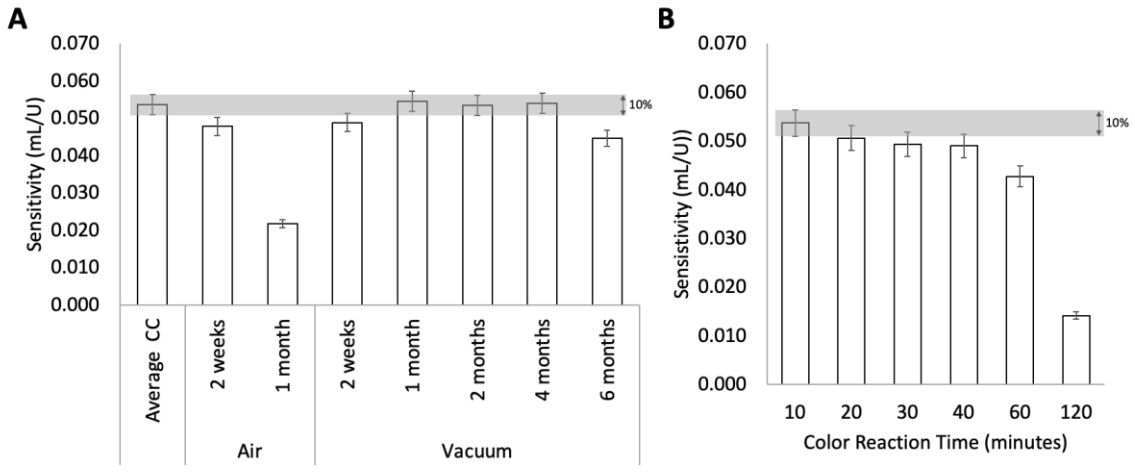

Figure 6.7 – Stability assessment by comparison of the sensitivity of the calibration curves: (A) storage stability of the developed device under different atmospheric conditions and periods of time; the grey area represent the 10% deviation of an average calibration curve slope; the error bars correspond to a 5% deviation; (B) stability of the coloured product formed on the device under different colour reaction times (CRT); the grey area represent the 10% deviation of a calibration curve slope obtained with a colour reaction time of 10 min. The error bars correspond to a 5% deviation.

6.3.10. Validation

To evaluate the accuracy of the urease quantification by the developed μPAD, 13 spiked saliva samples were tested on the device, and the results obtained were compared with the measurements from a commercially available urease activity determination kit (Table 6.3). A linear relationship was established (Figure 6.8) between the two sets of results, and the following equation was obtained: $[Urease]_{\mu PAD} = 0.993\ (\pm 0.067) \times [Urease]_{Kit} + 0.003(\pm 0.012)$. Since the slope was not statistically different from 1 and the intercept was not statistically different from 0, it was possible to conclude that there were no statistically significant differences between the two sets of results.

Table 6.3 – Analysis of saliva samples with the developed μPADs and comparison of the results obtained with the measurements obtained with the commercially available glucose determination kit; RE, relative error.

Sample ID	$[Urease]_{Kit}$ (U/mL)	$[Urease]_{\mu PAD}$ (U/mL)	RE (%)
1	0.125	0.130	4.2
2	0.140	0.145	3.8
3	0.105	0.095	-9.4
4	0.198	0.189	-4.5
5	0.110	0.116	5.1
6	0.179	0.187	3.9
7	0.234	0.220	-5.9
8	0.114	0.122	7.0
9	0.124	0.133	7.5
10	0.165	0.178	7.6
11	0.363	0.372	2.7
12	0.155	0.141	-8.8
13	0.084	0.092	9.2

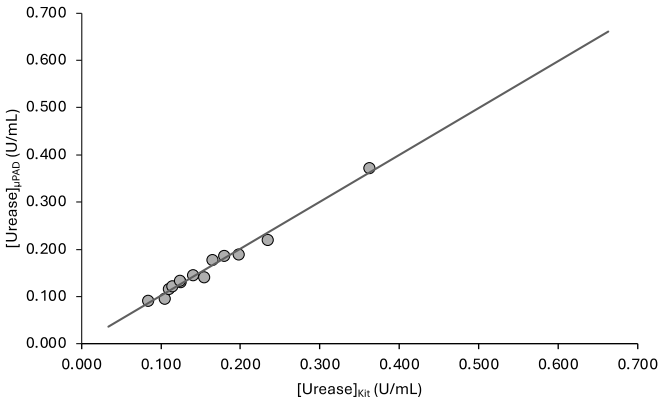

Figure 6.8 – Linear relationship between the measurements obtained with the developed μPAD and the measurements obtained with the commercially available kit.

6.4. Conclusion

In this work, a novel microfluidic paper-based device was developed for the de-termination of urease activity in saliva samples. Considering both the enzymatic reaction (20 min) and the colorimetric reaction (10 min), this determination is accomplished within 30 min and could be potentially used as an aiding tool in the diagnosis and monitoring of CKD. The urease activity determination was performed in the range of 0.041–0.750 U/mL, with limits of detection and quantification of 0.012 U/mL and 0.041 U/mL, respectively.

The developed μPAD is composed of three layers of stacked filter paper/membrane discs, resulting in a 3D structure that uses both lateral and vertical flow through the layers. The analytical determination within is based on the enzymatic reaction of urease, that converts urea into ammonia nitrogen, and on the colorimetric detection of the BTB pH indicator. The hydrophobic gas-diffusion membrane included in the device, not only enhances the selectivity and efficiency of the developed method, but it also eliminates potential interferences from the sample matrix without requiring sample pre-treatment. This was supported by the successful validation of the device with 13 saliva samples from healthy individuals.

To further ensure the robustness of the developed device, stability studies were performed, taking into consideration the storage conditions and the stability of the coloured product formed on the device. The results showed that the developed μPAD would maintain its sensitivity for at least 4 months when stored and protected from light in a vacuum atmosphere. After placing the sample and NaOH on the device, the colour formed can be captured by scanning the μPAD up to 40 min without any significant sensitivity decrease. Additionally, to considerably reduce the common drawback of manually assembled devices (low reproducibility due to potential shifting of discs during assembly and lamination), the developed methodology incorporates the possibility of performing multiple replicates and removing outliers if needed.

To conclude, the developed μPAD is an innovative device that provides a simple, easy-to-use alternative to the classical techniques available for this determination, in addition to being portable, lab equipment-free, and disposable via incineration, offering relative environmental friendliness and simplifying biological sample handling. According to our search, only one other paper-based device for urease activity determination has been reported previously (157), but with an application to soil samples. To the best of our knowledge, there are no other reports of paper-based devices for the determination of urease activity in human saliva.

Chapter 7. Glucose in Saliva Samples

Alternative diabetes monitorization tool: development of a microfluidic paper-based device for glucose determination in saliva samples.

In preparation for submission

7.1. Introduction

Glucose plays a critical role in human health, serving as a primary energy source for the body's cells (158,159). In human blood, the concentration of glucose is expected to be within the range of 68.0 – 124.0 mg/dL (3.8 – 6.9 mM) (158). Maintaining appropriate glucose levels is essential for metabolic balance, and disruptions in glucose homeostasis can lead to serious health conditions, such as diabetes. Diabetes mellitus is a chronic disease characterized by the body's inability to regulate blood glucose levels, leading to hyperglycemia (158,159). This occurs due to either the inability to produce insulin or the production of a form of insulin that is ineffective (158,160). According to the World Health Organization (WHO), the number of diabetes patients has surged significantly and it is expected to reach 693 million by 2045 (158). Currently, there is no definitive cure for this disease, and effective management relies heavily on regular monitoring of glucose levels, which traditionally involves invasive methods such as blood sampling (160). Even though conventional blood glucose monitoring techniques are effective and extensively studied, they still present several challenges. These methods can be not only uncomfortable, leading to poor patient compliance, especially in the case of frequent testing, but also the invasive nature of blood sampling increases the risk of infections and may not be suitable for certain patient populations (152). As a result, there is a growing need for alternative, non-invasive methods for glucose monitoring.

In this work, a novel μPAD designed specifically for the non-invasive quantification of glucose in saliva samples was developed. This device uses the enzymatic reaction of glucose oxidase that converts glucose in gluconic acid with the release of hydrogen peroxide (Scheme 7.1). The peroxidase enzyme then catalyses the release of oxygen from hydrogen peroxide, which interacts with o-dianisidine, oxidizing it into a red chromophore product (161) (Scheme 7.2). This approach not only addresses the limitations of blood-based monitoring by utilizing saliva as the sample but also takes advantage of the rapid and efficient point-of-care analysis offered by μPADs, making it a valuable aiding tool for diabetes monitoring.

Scheme (7.1) $\text{Glucose} \xrightarrow{\text{Glucose Oxidase}} \text{Gluconic Acid} + H_2O_2$

Scheme (7.2) $\underset{\text{(Reduced - Colourless)}}{\text{o-Dianisidine} + H_2O_2} \xrightarrow{\text{Peroxidase}} \underset{\text{(Oxidized - Pink)}}{\text{o-Dianisidine} + 2H_2O}$

7.2. Methods and Materials

7.2.1. Reagents and Solutions

A standard stock solution of 5 mM of glucose was prepared monthly by dissolving 4.5 mg of D(+)-glucose anidro (Merck) in 5 mL of water. The working glucose standards were prepared daily from the stock solution in the range of 0.1–1.0 mM.

The acetate buffered solution of 0.1 M was prepared by dissolving 85 mg of CH_3COONa (Merck) in 10 mL of water and the pH was adjusted to 5.0. A two-fold dilution of this acetate buffer solution was also prepared. All buffer solutions were stored in the refrigerator when not in use.

A glucose oxidase (GOx) stock solution (from Aspergillus niger, Type VII, Sigma-Aldrich) of 750 U/mL was prepared by dissolving 3 mg of the enzyme powder in 1 mL of acetate buffer 50 mM, and then stored in the freezer, as recommended by the manufacturer. A dilution was performed daily to a concentration of 158 U/mL.

The buffered solution of phosphate 0.1 M was prepared by dissolving 50 mg of $K_2HPO_4 \cdot 3H_2O$ (Merck) in 2 mL of water and the pH was adjusted to 6.0.

The peroxidase (Pox) stock solution (from Horseradish, Type I, Sigma-Aldrich) of 800 U/mL was prepared by dissolving 9 mg of the enzyme powder in 1 mL of phosphate buffer 0.1 M, as recommended by the manufacturer. A dilution with acetate buffer 50 mM was performed daily to a concentration of 165 U/mL.

The enzymatic mixture placed on the device was prepared immediately before the assembly by mixing GOx 158 U/mL, Pox 165 U/mL and acetate buffer 100 mM in a 1:1:1 ratio.

A o-dianisidine stock solution of 4 mM was prepared monthly by dissolving 10 mg of the o-dianisidine power (Sigma-Aldrich) in 10 mL of ethanol 96%. A dilution in water was prepared every two weeks to a final concentration of 1 mM (24% ethanol).

7.2.2. Design of the Developed µPAD

To assemble the device, 24 detection units were placed inside the plastic laminating pouch (L1, L2 Figure 7.1(A)), aligned in a 4 column and 6 row distribution (horizontal orientation) under the 3 mm holes of the top sheet of the laminating pouch (L1, Figure 7.1(A)). Each detection units consisted in two layers (Figure 7.1(A)): the top layer, E, consisted of a Whatman Grade 42 filter paper disc with 9.5 mm diameter ,loaded with 15 µL of enzymatic mixture (GOx, Pox and buffer); and the bottom layer, D, consists of a Whatman Grade 50 filter paper disc with 12.7 mm diameter loaded with 18 µL of o-dianisidine 1 mM. Both paper disc layers were placed in a 50 ^oC oven for 10 minutes to dry before assembly.

After the alignment of the detection units, the laminating pouches were passed through the laminator, which forces the plastic pouch to melt and seal around the units, creating an hydrophobic separation between the units. After the lamination, the µPADs were ready to be used.

The lamination phase stands out as the most delicate stage in the assembly process, since an improper unit distribution can lead to diminished reproducibility. Preventing disc and unit displacement is crucial, yet it remains susceptible to occurrence. Hence, it was incorporated four to six units per standard/sample (depending of device orientation) and gathered data from only three/four replicates to accommodate potential outliers.

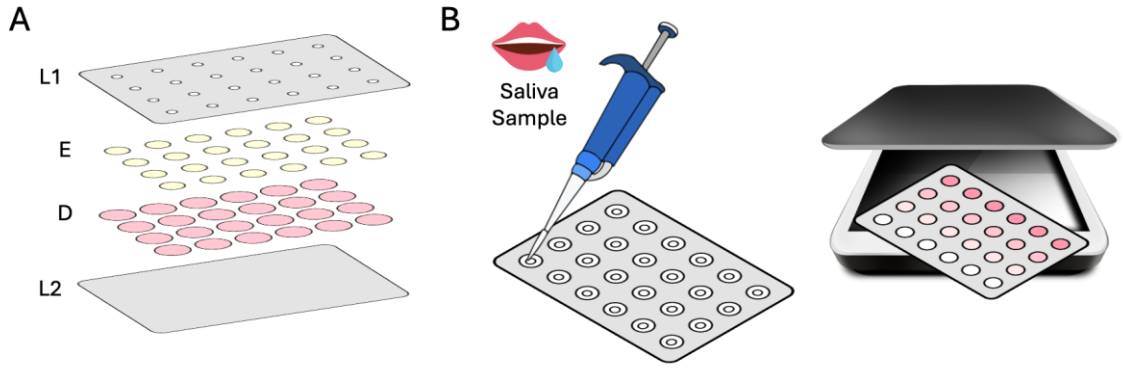

Figure 7.1 – Schematic representation of the (A) μPAD structure and (B) the procedure for the glucose determination; L1, top layer of the laminating pouch; L2, bottom layer of the laminating pouch; E, enzymatic mixture layer (15 μL per disc); D, o-dianisidine layer (18 μL per disc).

7.2.3. Determination Procedure

To measure the concentration of glucose in saliva samples, 20 μL of standard/sample was placed through the insertion hole of the assembled μPAD (Figure 7.1(B)). The glucose present in the sample/standard interacts with the glucose oxidase enzyme and is converted to peroxide and gluconic acid. Then, the peroxidase enzyme catalyses the release of oxygen from hydrogen peroxide, which then interacts with o-dianisidine, oxidizing it into a red chromophore product (161).

After the complete absorption of the sample/standard, the holes were covered with adhesive tape to prevent evaporation and possible contaminations. The intensity of the colour was measured by scanning the bottom layer of the μPADs. The time elapsed between the sample/standard insertion and the scanning was set to 25 min and named time-to-scan (TTS).

The scanned images underwent processing in ImageJ where they were converted into RGB plots. Subsequently, a green filter was applied before measuring intensity, since the colour product of the oxidized o-dianisidine is red-orange (with green being its complementary colour). Intensity values were later converted into absorbance values.

As mentioned in section 7.2.2., four to six measurements were taken for each reading of the blank or standard/sample, with outliers being discarded as necessary. The remaining replicates were used to enable calculation of an average absorbance. Subsequently, a calibration curve was established plotting the calculated average absorbance obtained when placing different standard solutions against the glucose concentration of those standards.

7.2.4. Biological Samples

The saliva samples used in the validation of this work were all blind samples collected from healthy volunteers. These samples were stored at −18 °C for later use.

To evaluate the applicability of the developed device to the monitorization of diabetes, saliva samples were also collected from diabetic patients together with their blood glucose concentration, and a correlation between the two values was established. The collection procedure, obtained with their informed consent, was similar to the one described for the healthy volunteers and detailed in Chapter 2.

7.2.5. Comparison Method – Validation Procedure

In order to assess the accuracy of measurements and validate the developed μPAD for glucose determination, a comparison was made between the results obtained with the developed μPAD for #8 saliva samples and the results obtained for the same samples by the reference procedure with Dinitrosalicylic Acid Reagent for Determination of Reducing Sugar (162). To perform the latter all solutions were also prepared accordingly.

For further accuracy assessment, #6 saliva samples were analysed with the developed μPAD and with a commercially available kit for glucose determination (K-GLUHK-110A; Megazyme). The results were compared by calculating the relative error.

7.3. Results and Discussion

7.3.1. Preliminary Studies

As previously mentioned, this work is based on two enzymatic reactions: the oxidation of glucose to gluconic acid and peroxide conducted by glucose oxidase enzyme, and the oxidation of o-dianisidine into a red chromophore product by using peroxide and peroxidase enzyme. These reactions were tested in a batchwise procedure based on the enzymatic assay protocol of glucose oxidase of Merck (163).

A few parameters such as enzymatic concentrations, reagents volumes, temperature and choice of buffer were tested during these batch preliminary studies. However, these studies were revisited in the developed μPAD. Still, some of the most significant conclusions were the possibility of mixing the two enzymes and buffer prior to the analysis without significant loss of sensitivity and also no need to maintain a set temperature of 35 ºC, as recommended by the manufacturer, in order to be able to accomplish the glucose determination.

After pre-optimizing the reactions in batch, a scale-down to the μPAD was performed. The volumes were reduced by about 100 times, but in order to maintain the amounts of each reagent, the concentration of these solutions was increased in the same proportion.

The first prototype of the device was composed of 2 layers of Whatman 1 paper discs with 9.5 mm diameter. The top layer was embedded with a mixture of GOx 108 U/mL, Pox 1280 U/mL, and sodium acetate buffer 100 mM in a 1:1:1 proportion, and the bottom layer was embedded in o-dianisidine 0.25 mM.

7.3.2. Peroxidase and Glucose Oxidase Concentrations

The first parameters evaluated and optimised in the developed µPAD were the concentrations of both peroxidase and glucose oxidase. The influence of the peroxidase concentration in a calibration curve was tested in a range of 82 – 1318 U/mL as shown in Figure 7.2(A), and it was possible to conclude that a concentration of 165 U/mL enabled a significantly higher sensitivity (RD > 10%).

As for the glucose oxidase concentration, a range of 54 – 158 U/mL was studied (Figure 7.2(B)), and a higher sensitivity was obtained when using 127 U/mL and 158 U/mL. Even though there is no statistically significant difference between these two concentrations, 158 U/mL was chosen as optimal GOx concentration for the developed device, to ensure the best sensitivity possible.

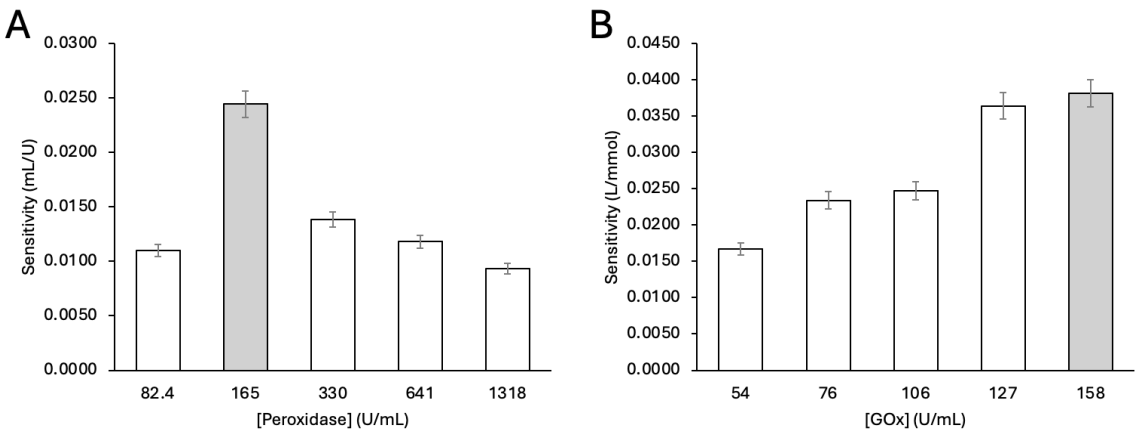

Figure 7.2 – Influence of the (A) peroxidase concentration and of the (B) glucose oxidase concentration in the sensitivity of the calibration curves in the developed device; the grey bars represent the chosen concentrations, and the error bars correspond to the 5% relative error.

7.3.3. Type of Filter Paper – Top Layer

To continue the optimization of the top layer of the device, the treatment and porosity of the filter papers used for the discs in the top layer were tested. The filter papers studied were Whatman Grades 1, 4, 5, 42, 50 and 542 (Figure 7.3), which vary in treatment and porosity (Appendix B).

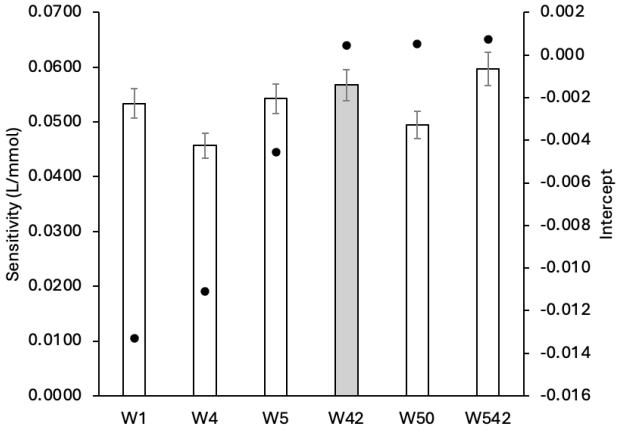

Figure 7.3 – Influence of the type of filter paper (top layer of device) in the sensitivity (bars) and intercept (bullets) of the calibration curve; the grey bar represents the chosen paper, and the error bars correspond to the 5% relative error.

After analysing the results (Figure 7.3) it was possible to see that the filter papers that led to a calibration curve with the highest sensitivity and intercept closer to zero were Whatman Grade 42 (W42) and Whatman Grade 542 (W542). Because there was no significant difference between the two papers and W542 has a more complex treatment, making it a more expensive filter paper, W42 was the paper chosen for the top layer of the device.

7.3.4. O-Dianisidine Concentration

Next, the influence of the concentration of o-dianisidine in the sensitivity of the calibration curve was evaluated. Concentrations in a range of 0.25 – 2.00 mM were tested (Figure 7.4), and it was possible to conclude that the concentration that originated a calibration curve with the highest sensitivity was 1.00 mM of o-dianisidine, therefore this was the concentration chosen for the remaining studies.

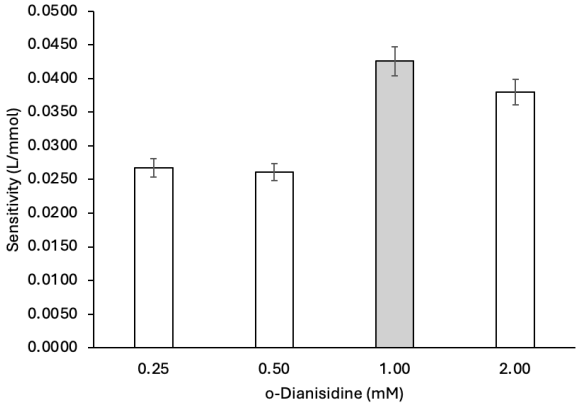

Figure 7.4 – Influence of the concentration of o-dianisidine in the sensitivity of the calibration curve; the grey bar represents the chosen concentration, and the error bars correspond to the 5% relative error.

7.3.5. Type of Filter Paper – Bottom Layer

To conclude the optimization studies on the bottom layer of the device, the influence of the type of filter paper was also evaluated. The filter papers studied were Whatman Grades 1, 4, 5, 42, 50 and 542 (Figure 7.5), that vary in treatment and porosity (Appendix B).

After analysing the results (Figure 7.5) it was possible to see that the filter paper that led to a calibration curve with the highest sensitivity and correlation was Whatman Grade 50 (W50), therefore this was the filter paper chosen for the remaining of the studies.

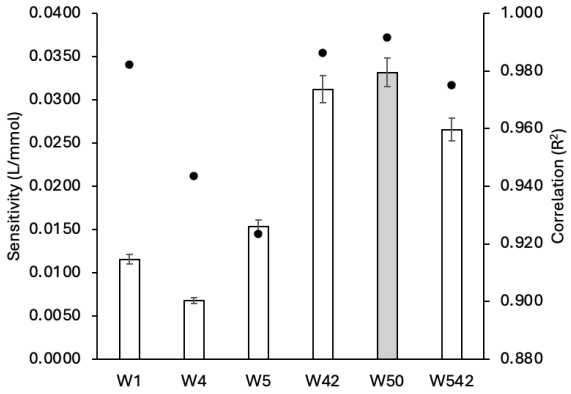

Figure 7.5 – Influence of the type of filter paper (bottom layer of device) in the sensitivity (bars) and correlation (bullets) of the calibration curve; the grey bar represents the chosen paper, and the error bars correspond to the 5% relative error.

7.3.6. Sample Volume

Finally, the volume of sample placed on the device was also studied. Volumes ranging from 10 to 20 µL were tested (Figure 7.6(A)). For each volume studied, the device was also scanned at two different TTS (time elapsed between the sample/standard insertion and the scanning).

When inserting 10 or 12 µL, sample/standard was completely absorbed into the device in under 20 minutes which allowed the scanning of the device as early as 20 minutes. But the placement of 15 µL did not allow the complete absorption of the sample/standard within 20 minutes, therefore the device was only scanned at 30 minutes. When placing 20 µL, it was not possible to scan the device since the sample/standard was not absorbed in the 30 minutes period set for this study.

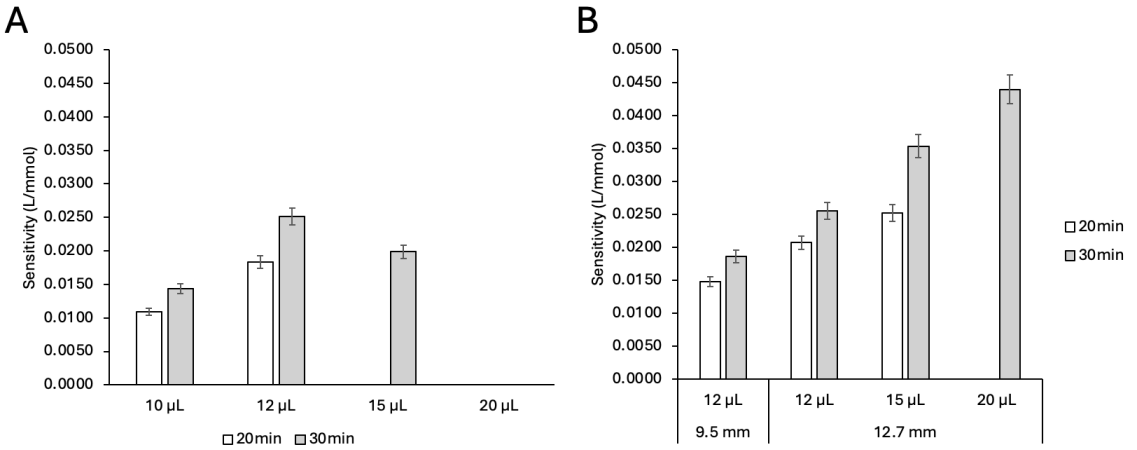

Figure 7.6 – Influence of the (A) sample volume and (B) of its combination with different diameters of the bottom filter paper discs, in the sensitivity of the calibration curves obtained with the developed device; the white bars represent the TTS of 20 minutes; the grey bars represent the TTS of 30 minutes; the error bars correspond to the 5% relative error.

With the goal of further increasing the sensitivity of the device, the combination of the different sample volumes and larger sizes (diameter) of the bottom layer disc (12.7 mm) was studied. As shown in Figure 7.6(B), the increase in the size of the filter paper disc allowed the accommodation of higher volumes of sample within a shorter time, consequently providing higher sensitivities of the device. The highest sensitivity obtained was with 20 µL of sample/standard and a 12.7 mm diameter disc in the bottom layer of the device, so these were the conditions kept for the remaining studies.

7.3.7. Stability Studies

Paper-based devices offer significant advantages in field applications and, to ensure their effectiveness outside of the lab, it is important to thoroughly assess both the long-term storage stability of the µPADs before use and the stability of the coloured product that develops after the sample/standard placement. This dual assessment is vital because any degradation in the device or the formed product could compromise the accuracy and reliability of the results obtained in the field.

To evaluate the colour product stability in the developed µPAD, a calibration curve was prepared and the µPADs scanned at several TTS from the moment the device completely absorbs the standards (25 minutes) up to 24 hours (1440 minutes) (Figure 7.7). The calibration curve slopes obtained with the different TTS times were compared and it was possible to observe that the sensitivity significantly increased up to 2 hours and only then started to stabilize. No decrease in sensitivity was observed within the 24-hour period tested. A choice was made to consider 25 minutes of the standardized TTS in order to provide a rapid method. However, the device can be used to quantify glucose in saliva samples with a different TTS as long as the equivalent calibration curve is used.

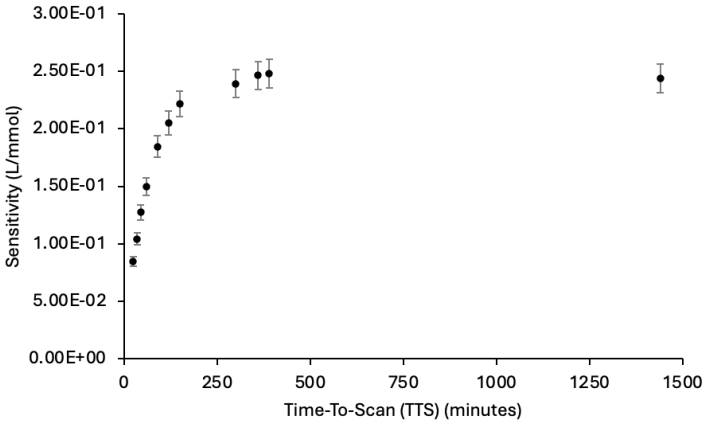

Figure 7.7 – Evolution of the stability of the coloured product in the developed μPAD from 25 minutes to 24 hours (1440 minutes); the error bars correspond to the 5% relative error.

To assess the storage stability of the μPADs, several devices were prepared and stored in plastic bags protected from light. Testing was conducted under two different temperatures (21 °C and -18 °C) and two atmospheric conditions: air and vacuum. The vacuum condition was achieved using a vacuum packaging machine. Each condition was studied over varying time periods, ranging from 2 days to 1 month. At each time, the stored μPAD was used to create a calibration curve, which was then compared to the calibration curve of a freshly assembled μPAD prepared using the same set of standards. A relative deviation of less than 10% was considered non-significant. From the results (Figure 7.8) it was possible to conclude that the devices were not stable at 21 ºC in both atmospheric conditions, even for 2 days. At -18 ºC using an air atmosphere, the developed μPAD was stable for only 1 week. On the other hand, the vacuum atmosphere at the same temperature allowed the device to remain stable for at least 2 weeks before use.

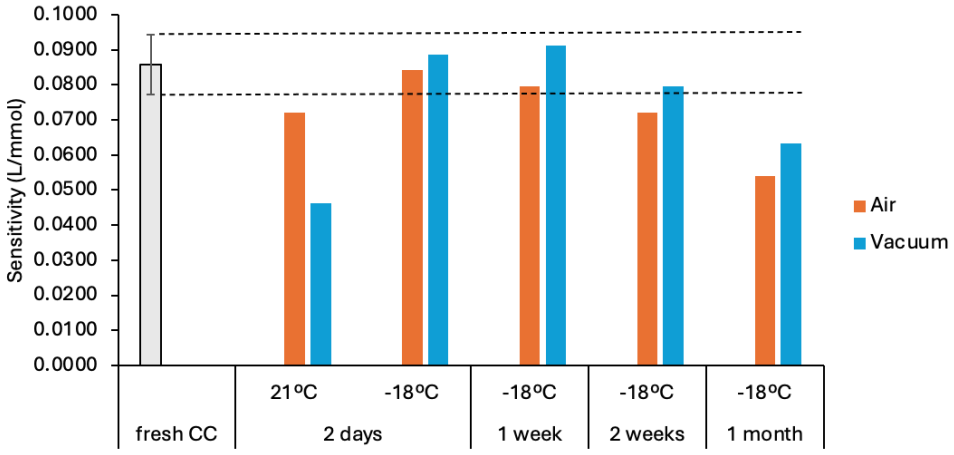

Figure 7.8 – Stability of the developed device under different storage conditions, namely different temperatures and different atmospheres.

7.3.8. Matrix Interferences

Given that the devices were designed for application to saliva samples, it was important to evaluate the potential interference of the saliva matrix in the glucose determination. This assessment was performed by preparing two μPADs to obtain two calibration curves, one using glucose standards dissolved in water and another using glucose standards dissolved in synthetic saliva.
The results showed that there was no statistically significant difference (RD < 10%) between the sensitivity of the two calibration curves, thus indicating that the remaining components of saliva would not interfere with the quantification of glucose.

7.3.9. Features of the Developed Device

The main characteristics of the developed μPAD are summarized in Table 7.1, including the dynamic range, the limit of detection (LOD), the limit of quantification (LOQ), and the repeatability, intraday and interday.

Table 7.1 – Features of the developed μPAD for glucose quantification; LOD, limit of detection; LOQ, limit of quantification; RSD, relative standard deviation.

Dynamic Range (mM)	**Average Calibration Curve [a] A = S × [Glucose] + b**	**LOD (mM)**	**LOQ (mM)**	**Repeatability, RSD [a]**	
				Intraday	Interday
0.095 – 1.1	A = 0.0846(±0.0034) x [Glucose] - 0.0048(±0.0008) R^2 = 0.997(±0.003)	0.028	0.095	3.8%	4.0%

[a]n=4.

The limits of detection and quantification were calculated according to IUPAC recommendations as the concentration corresponding to three times (LOD) and ten times (LOQ) the standard deviation of the intercept (n = 4), respectively. (109,162) The μPAD repeatability was assessed by calculating the relative standard deviation (RSD) of four calibration curves in the same day, (intraday) and four calibration curves in consecutive days (interday).

7.3.10. Validation

To assess the accuracy of the developed μPAD for glucose quantification in saliva, several samples (#8) were analysed with the developed device and the results compared to those obtained by the reference procedure of “Dinitrosalicylic Acid Reagent for Determination of Reducing Sugar” (162). A linear relationship between the two set of results (Figure 7.9) was established: $[Glucose]_{\mu PAD}$ = 1.017 (± 0.219) × $[Glucose]_{Ref}$ + 0.003 (± 0.144), where the values in brackets correspond to the 95% confidence interval. As the slope and the intercept were not statistically different from 1 and 0, respectively, there is no difference between the two sets of results and, consequently, between the two methods.

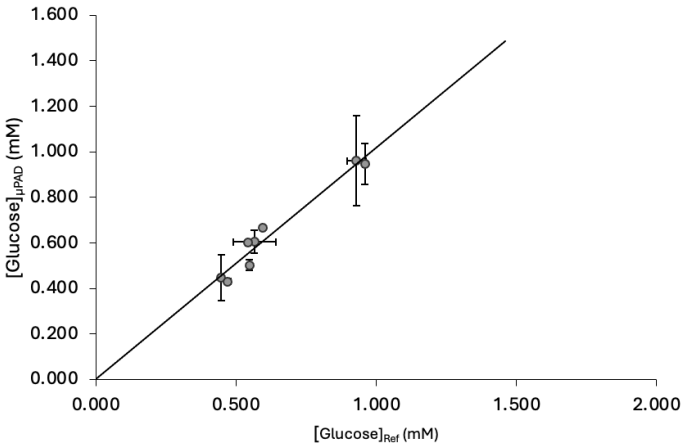

Figure 7.9 – Comparison between the results obtained for glucose determination in saliva samples (#8) with the developed µPAD and the reference procedure of dinitrosalicylic acid; the full line represents the linear trendline between the two sets of results.

Additionally, #6 saliva samples were analysed with the developed device and with a commercially available glucose determination kit, and the relative deviation between the results obtained were all below 10%, thus indicating there was no significant difference between the measurements from the developed µPAD and the measurements obtained with the kit (Table 7.2).

Table 7.2 – Comparison between the results obtained for glucose determination in saliva samples (#6) with the developed µPAD and a commercially available kit; RD%, relative deviation.

Sample ID	$[Glucose]_{\mu PAD}$ (mM)	$[Glucose]_{Kit}$ (mM)	RD%
S1	0.201	0.201	0.0
S2	0.453	0.440	3.0
S3	0.289	0.280	3.2
S4	0.195	0.195	-0.3
S5	0.949	0.960	-1.2
S6	0.782	0.735	0.0

So, the results obtained with the developed µPAD proved not only to be comparable to the dinitrosalicylic acid method, but also with the commercially available kit, therefore demonstrating the accuracy of the developed device and the adequacy of the working range for the analysis of the target samples.

7.3.11. Saliva/Blood Correlation

To evaluate the correlation between the concentrations of glucose in saliva and in blood, #5 saliva samples were collected from diabetic patients while measuring the glucose concentration in the blood using a glucometer. According to the results obtained, shown in Table 7.3, it was possible to conclude that the concentration of glucose in saliva would correspond to an average of 1.9% of the glucose concentration in blood, with a standard deviation of 0.1%. Because the variation coefficient (the ratio between the standard deviation and the average) was 5.1% (< 10%), it was possible to conclude that there was no statistically significant difference between measurements.

Table 7.3 – Evaluation of the correlation between the concentration of glucose in saliva and in blood using diabetic patients' samples.

Sample ID	$[Glucose]_{Blood}$ (mg/dL)	$[Glucose]_{Blood}$ (mM)	$[Glucose]_{Saliva}$ (mM)	$\frac{[Glucose]_{Saliva}}{[Glucose]_{Blood}}$
DP1	180	9.99	0.186	1.9%
DP2	291	16.2	0.305	1.9%
DP3	150	8.33	0.147	1.8%
DP4	155	8.60	0.173	2.0%
DP5	161	8.94	0.161	1.8%

Additionally, based on this 1.9% ratio, the concentration of glucose expected in blood was calculated from the salivary glucose measured with the device and it was compared with the real glucose concentration in blood (Figure 7.10). No significant difference between the two sets of measurements was observed.

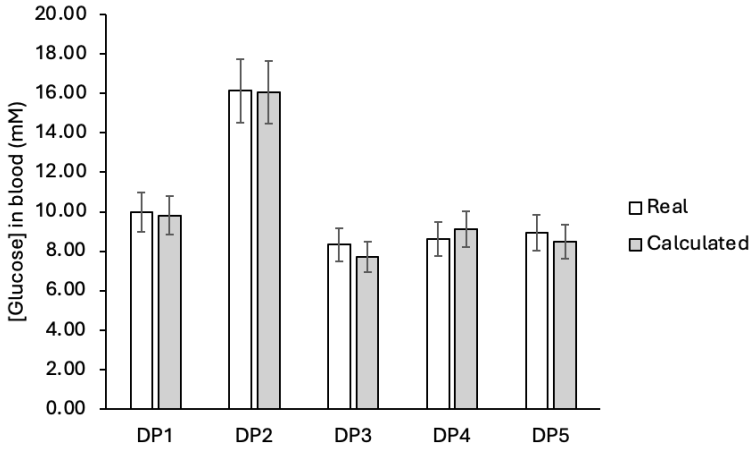

Figure 7.10 – Comparison between the real concentration of glucose in the blood of (#5) diabetic patients measured with a glucometer and the expected blood concentration calculated from the concentration of glucose in saliva. The error bars correspond to 10 % deviation.

7.4. Conclusions

In this work, a microfluidic paper-based analytical device was designed and optimized for the monitorization of diabetes, by quantification of glucose in saliva samples. This quantification is achieved by two consecutive enzymatic reactions. First, glucose oxidase converts glucose into gluconic acid, releasing hydrogen peroxide. Then, peroxidase catalyses the release of oxygen from hydrogen peroxide, which interacts with o-dianisidine, causing a change of colour that is recorded by scanning the device. After optimization, it was possible to obtain a device capable of performing the quantification of glucose in 25 minutes with limits of detection and quantification of 0.028 mM and 0.095 mM, respectively. Furthermore, the range of 0.095 to 1.1 mM of glucose proved suitable for all the analysed samples and comparable to the determination both with the commercially available kit and with the reference method of "Dinitrosalicylic Acid Reagent for Determination of Reducing Sugar".

Because the developed µPAD was envisioned to aid in health diagnosis, not only in healthcare facilities but also in field applications, stability studies were performed. Results showed that the device was stable for at least 2 weeks when stored in a vacuum at -18 ^{o}C. After placing the sample, the sensitivity of the µPAD significantly increased up to 2 hours and only then started to stabilize. This implies that if a TTS different than 25 min is used, then the calculations of the glucose concentration must be performed with a calibration curve of equivalent TTS, in order to obtain accurate results.

Additionally, a correlation between the concentration of glucose in saliva and in blood was established using #5 saliva samples of diabetic patients. Comparing the concentration of glucose in blood obtained with a glucometer and the concentration of glucose in saliva using the µPAD, it was possible to conclude that the concentration of glucose in saliva corresponds to approximately 2% of the blood glucose levels.

To the best of our knowledge, only two other microfluidic paper-based devices have been reported for the quantification of glucose in saliva samples, as shown in Table 7.4. While Chiang et al report the use of glucose oxidase (GOx) and horseradish peroxidase (HRP) to achieve the glucose quantification, Khachornsakkul et al uses gold and silver nanoparticles to mimic the enzymatic activity. (158,164) Nevertheless, the developed device proposed in this work, not only provides a lower limit of detection, but also features a linear range that closer resembles the glucose levels in saliva, therefore being a valuable aiding tool for diabetes monitoring.

Table 7.4 – Summary of the characteristics of the developed µPAD in comparison with previously described devices; LOD, limit of detection.

Method	Samples	Linear Range (mM)	LOD (mM)	Reference
GOx/HRP	Saliva	0.095 – 1.1	0.095	This work
AuNPs/AgNPS	Saliva/Urine/Serum	0.5 – 10.0	0.340	(158)
GOx/HRP	Urine/Saliva	0.5 – 4.5	0.3	(164)

Chapter 8. Lateral Flow Strip for Escherichia Coli Detection

Newly designed lateral flow strips for a semi-quantitative analysis of *E. coli*.

In preparation for submission

8.1. Introduction

Escherichia coli (*E. coli*), is a rod-shaped, Gram-negative bacterium typically found in the lower intestinal track of warm-blood animals, including Humans (165–167). While most strains are of commensal nature, some can cause severe illness, especially in immunocompromised hosts or when gastrointestinal barriers are compromised (168,169). Furthermore, the presence of *E. coli* in environmental waters is widely used as an indicator of fecal contamination, suggesting that pathogenic microorganisms may also be present (165,167,170).

Quantifying *E. coli* in environmental waters is crucial for several reasons, but most of all it helps in assessing the microbiological quality of water bodies for water use, such as recreational purposes, drinking water sources, and agricultural irrigation (165,171). This justifies why the current legislation is based solely in the fecal contamination for quality evaluation of water bodies (172,173). High concentrations of *E. coli* are and indicator of recent fecal contamination which not only affects human health but can also have economic implications, such as costs associated with healthcare, water treatment, and the loss of tourism and recreational activities. Regular monitoring of *E. coli* levels in water bodies enables public health authorities to identify contamination events early and take necessary actions. Additionally, data on *E. coli* concentrations can help identify trends and sources of contamination, facilitating the development of targeted strategies to prevent and mitigate pollution (174). Currently, there is an upward trend in antibiotic resistance in *E. coli*, ranked third among a group of 12 priority-pathogens with antibiotic resistance, as classified by the World Health Organization (175,176). Effective water management practices, public education, and robust regulatory frameworks are essential to minimize the public health risks associated with *E. coli* in environmental waters and ensure safe and clean water for all uses.

DNA-based assays are extensively employed for detecting bacteria pathogens because these contain unique genes/traits that serve as dependable biomarkers for identification (177). These techniques typically incorporate DNA fragments amplification technologies, based on the polymerase chain reaction (PCR). However, PCR has a few drawbacks such as the need of sequential heating and cooling cycles performed by expensive equipment (178). Loop-mediated isothermal amplification (LAMP), first developed by Notomi in 2000, aims to tackle some of the PCR drawbacks (177–179). LAMP not only allows the amplification of DNA at a constant temperature but also uses 4 to 6 primers that target 6 to 8 regions therefore providing high sensitivity and specificity (178,180–182). This primer set includes two inner primers (Forward Inner Primer (FIP) and Backward Inner Primer (BIP)) and two outer primers (F3 and B3) (178). The inner primers have two distinct sequences: one complementary to the target strand and another to the newly synthesized strand, facilitating loop formation. Bst polymerase, the enzyme used in LAMP, has a strand displacement activity, which means it can synthesize new DNA strands while displacing the existing strands. This allows for continuous amplification without the need for denaturation steps. The primers initiate the synthesis of new DNA strands, and the strand displacement activity of the polymerase leads to the formation of loop structures (Figure 8.1). These loops serve as templates for further amplification, resulting in a large amount of DNA being produced in a short time (178).

The amplified DNA can be detected by various methods, such as turbidity measurement (due to the formation of magnesium pyrophosphate crystals), fluorescence detection (using fluorescent probes), gel electrophoresis, or even by visual detection of a visible precipitate or colour change (183). This makes LAMP a powerful tool for rapid and specific DNA detection, particularly useful in resource-limited settings.

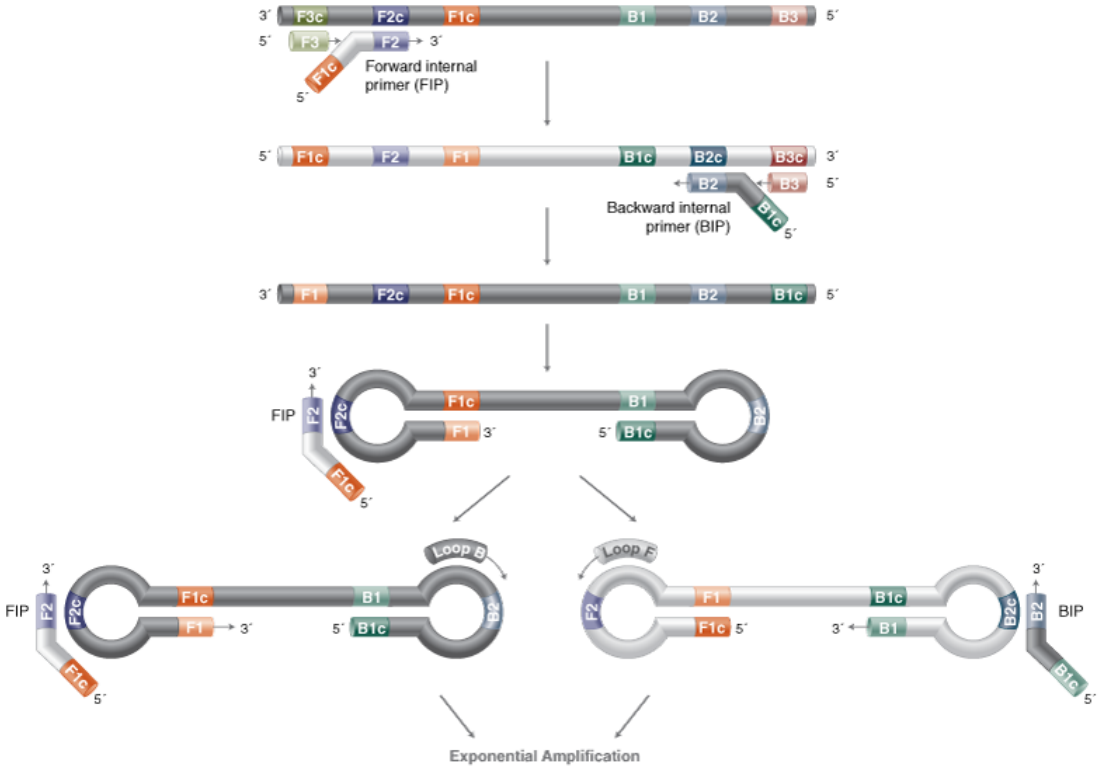

Figure 8.1 – Schematic representation of the DNA amplification process in a loop-mediated isothermal amplification technique (image from (183)).

Lateral Flow Assays (LFAs) are a widely used diagnostic tool in the detection of infectious diseases (22,184). These offer the advantage of being rapid, cost-effective, and user-friendly, requiring minimal training and no need for complex equipment. This makes them particularly suitable for point-of-care testing and in situations where immediate results are crucial, especially when coupled with an amplification technique such as LAMP (22,184).

In lateral flow assays for nucleic acid detection, amplicons generated by LAMP are usually labeled with two distinct biomolecules incorporated into the primers. (184) One biomolecule serves to immobilize the amplicons on the surface of the test strip, while the other interacts with a labeled antibody to provide a visible result, indicating the presence of the target nucleic acid fragment/sequence (22,184). Commonly used labels for immobilization include biotin or digoxigenin, with fluorescein isothiocyanate (FITC) often used for detection, allowing the result to be optically observed (184).

The objective of this work was to develop a new lateral flow assay that would allow the semi-quantitative detection of *E. coli* on lateral flow strips. This detection was possible by using LAMP as the DNA amplification technique. Several LAMP amplification parameters, such as temperature and primer concentrations, were studied and optimized. The strategy for semi-quantitative analysis was to obtain "flattened" amplification curves in which it would be possible to differentiate different concentrations of DNA at one specific incubation time (Figure 8.2), and consequently originate different signals in the lateral flow strips. To achieve this goal a new design of lateral flow strip was also studied.

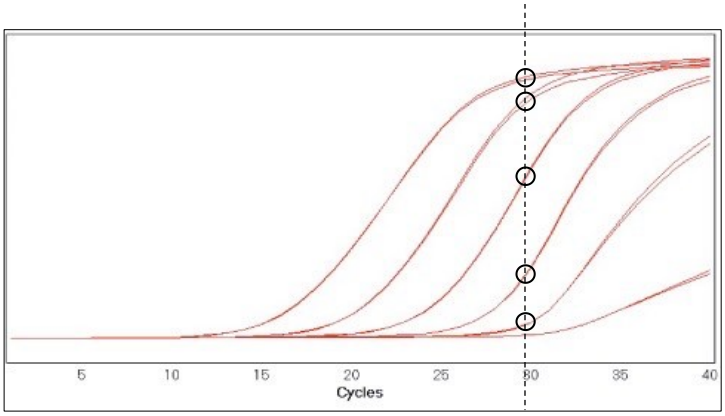

Figure 8.2 – Schematic representation of the "flattened" amplification curves with the differentiation of several DNA concentrations at one specific cycle; The red lines represent the amplification curves for different DNA concentrations templates.

8.2. Materials and Methods

8.2.1. Reagents and Solutions

UltraPure Distilled DNase/RNase-free water was used to prepare all aqueous solutions.

E. coli K12 was grown in liquid culture in LB broth overnight. DNA was extracted (during its exponential stage of growth) and purified using a commercial DNA extraction kit (MagaZorb® DNA Mini-Prep Kit, Promega). The concentration of the obtained DNA was quantified using Nanodrop spectrophotometer (Thermo). Decimal dilutions were prepared from the obtained DNA standard and used as template in the LAMP reaction.

8.2.2. LAMP Assay and Product Detection

The LAMP reaction was performed in 25 µL, containing 5 µL of DNA template, 5 µL of a primer mix and 15 µL of LAMP Isothermal Mastermix (ISO-004, OptiGene).

The LAMP Isothermal Mastermix provided DNA polymerase, inorganic pyrophosphatase, reaction buffer, $MgSO_4$ and deoxyribonucleotide triphosphates (dNTPs).

The final concentrations in the LAMP reaction were of 0.8 µM of forward inner primer (FIP), 0.72 µM backward inner primer (BIP), 0.08 µM backward inner primer labelled with Biotin (BIP*), 0.2 µM of outer primers (Forward 3 and Backward 3), 1.0 µM of Loop Forward primer, 0.9 µM of Loop Backward primer and 0.1 µM Loop Backward labelled with FITC (LF*). The primer sets used in the LAMP assay were all purchased from Eurofins and the sequences are provided in (185).

The reaction was performed at 70 °C for 80 minutes (80 cycles; 1 minute of incubation per cycle) in a QuantStudio™ 5 Real-Time PCR System using the SYGR green setting for fluorescence signal detection every minute for real-time monitoring. We used 70 °C instead of, the more efficient, lower temperatures generally accepted in LAMP reactions (between 60 – 65 °C) to decrease efficiency and flatten the curves. A reaction volume of 25 µL was then placed on a nucleic acid detection strip (Ustar) and the results were captured with a smartphone camera.

8.2.3. Lateral Flow Strips

The initial nucleic acid detection strips (Ustar) were modified by using a dispensing system (BioSpot BT 600 Workstation, BioFluidix) to place extra test lines, with different concentrations of FITC antibodies, on the commercially available strips.

8.3. Results and Discussion

8.3.1. Preliminary Studies

In order to distinguish different concentrations of DNA in the amplification curves at a specific incubation time and therefore be able to achieve a semi-quantitative determination of *E. coli*, an optimization of the LAMP assay was necessary (akin to a “de-optimization”, making the reaction less efficient). First, LAMP assay was performed following the recommended standard guidelines.

The assay was performed at 65 ^{o}C using unlabeled primers in the concentrations of 0.2 µM (F3/B3), 1.0 µM (LF/LB) and 0.8 µM (FIP/BIP). Two concentrations of *E. coli* DNA were tested (107 and 105 copies/µL) and the results are shown in Figure 8.3. The higher initial DNA template (10^7 copies/µL) was detected earlier since it also achieved the exponential phase earlier, which was expected, and indicates a typical amplification.

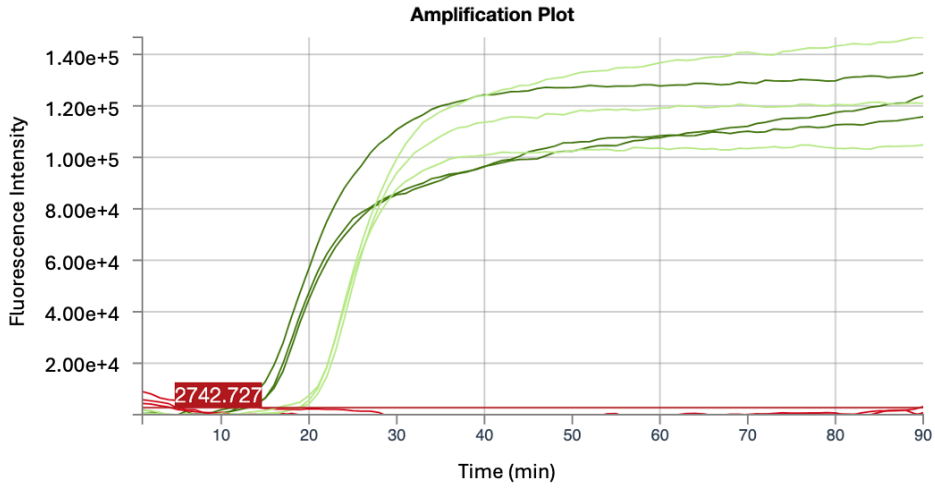

Figure 8.3 – Amplification curve of standard LAMP assay using 2 dilutions of *E. coli* DNA, 10^7 (dark green) and 10^5 (light green) copies/µL; in red is represented the negative control.

8.3.2. LAMP Assay Optimal Temperature

The first parameter studied for the optimization of the LAMP assay was the temperature. Since 65 ºC is the standardized temperature for this assay, 65 ºC, 67.5 ºC and 70 ºC were evaluated/assessed.

As shown in Figure 8.4, with the increase in the assay temperature, for the same DNA template concentration, not only the beginning of the amplification detection was delayed, but also the amplification efficiency decreased, which leads to an overall more “flattened” amplification curves. Since this “flattened” shape is necessary to widen the range of the semi-quantitative determination approach, the temperature chosen for this LAMP assay was 70 ºC.

Higher temperatures were not tested since the increase in temperature also leads to a more delayed amplification which would defeat the purpose of a fast point-of-care test.

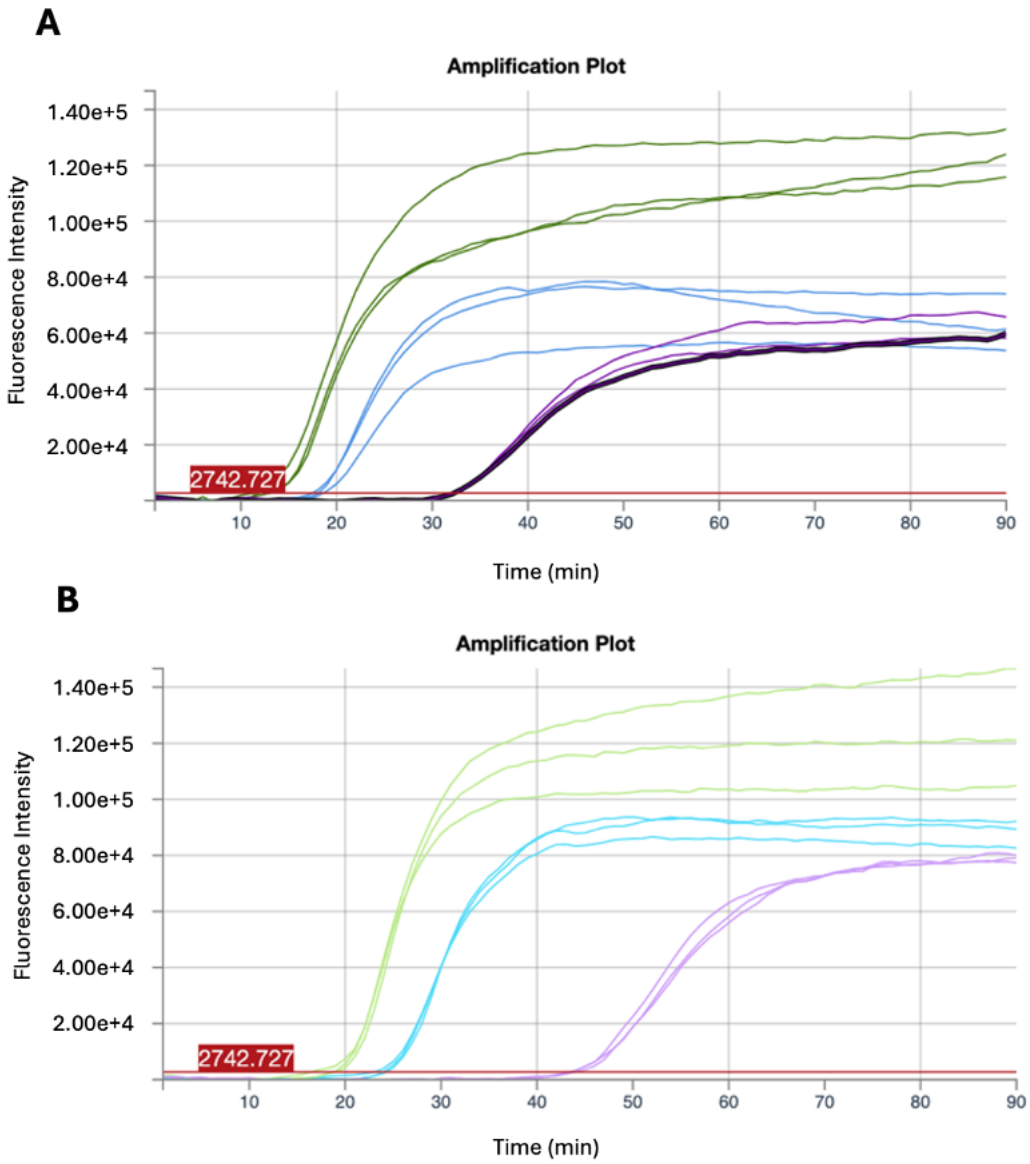

Figure 8.4 – Amplification curves of LAMP assay using two dilutions of *E. coli* DNA, (A) 10^7 and (B) 10^5 copies/µL, and 3 different assay temperatures, 65 ºC (green), 67.5 ºC (blue) and 70 ºC (purple), in red is represented the negative control.

8.3.3. LAMP Assay Optimal Primers Concentration

Next, the concentration of the primers used in the assay was tested. Three different mixtures were prepared (Mix 1, Mix 2, Mix 3) as shown in Figure 8.5, in which Mix 1 represents the recommended concentrations by the supplier for a standard LAMP assay and Mix 3 the recommended concentrations for a faster LAMP reaction (186). Increasing the concentrations of primers leads to an earlier amplification detection (Figure 8.5). However, because the aim is to obtain a “flattened” amplification curve, the mixture chosen was Mix 1.

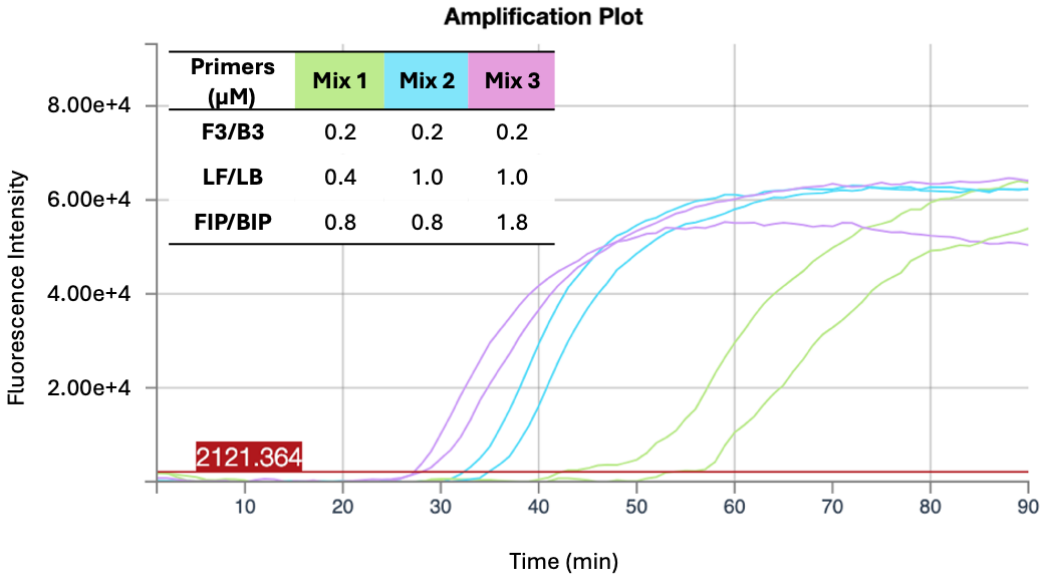

Figure 8.5 – Amplification curves of LAMP assay using three mixtures with different primer concentrations, Mix 1 (green), Mix 2 (blue) and Mix3 (purple), and in red is represented the negative control.

8.3.4. LAMP Assay Labelled/Unlabelled Primers Proportions

The proportion of labelled primers is directly related to the amount of amplicons that can bind to the capture probes onto the lateral flow strips, enabling us to optimise line intensity and consequently the range of quantification. However labelled primers can sometimes influence the LAMP reaction due to the steric influence of the label. We first verified the impact of different proportions on the reaction (Table 8.1 and Figure 8.6).

Table 8.1 – Different proportions of labelled and unlabelled primers studied in the LAMP assay.

	Unlabelled Primers	Labelled Primers
Condition 1	100%	0%
Condition 2	90%	10%
Condition 3	75%	25%
Condition 4	50%	50%
Condition 5	0%	100%

Of all the conditions tested, condition 2 which describes the proportion of 90%/10% of unlabeled/labeled primers, was the one that provided the best results since it allowed the differentiation between three concentrations of DNA with an incubation time of 80 minutes (80 cycles) (Figure 8.6), therefore possibly allowing a semi-quantitative analysis.

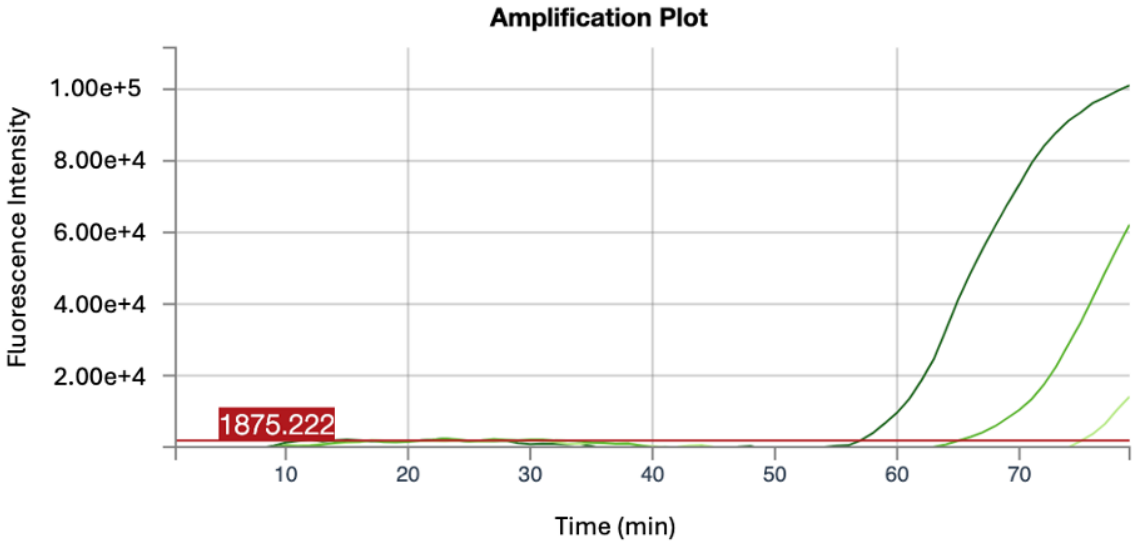

Figure 8.6 – Amplification curve of LAMP assay performed with 90% unlabelled primers and 10% labelled primers, using 3 dilutions of *E. coli* DNA, 10^6 (dark green), 10^5 (medium green) and 10^4 (light green) copies/µL; in red is represented the negative control.

8.3.5. Lateral Flow Strip Design

After the optimization of the LAMP assay, the lateral flow strips design was studied. The strategy to obtain a semi-quantitative analysis was to couple the optimized LAMP assay with a novel design of lateral flow strips (LFS). The initial idea for the design was to have a LFS with multiple test lines that would sequentially appear with increasing concentration, as represented in Figure 8.7(A).

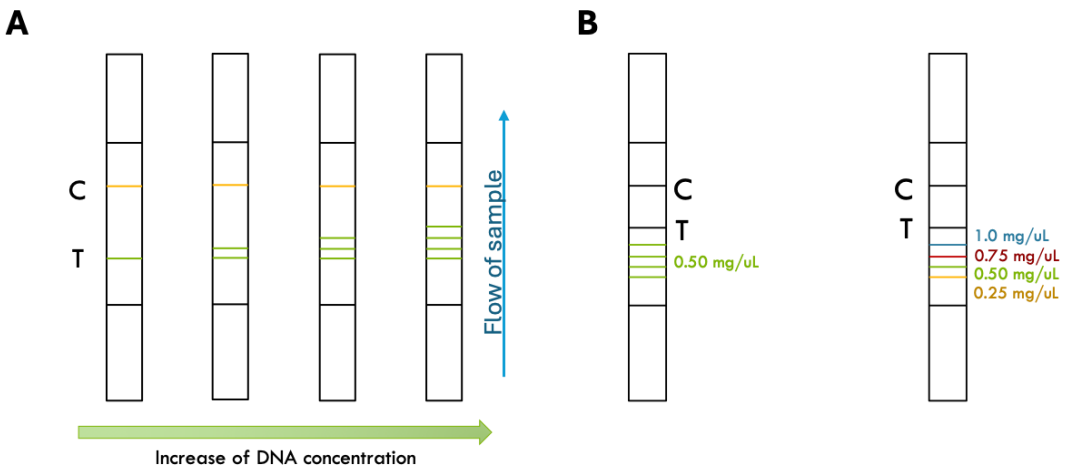

Figure 8.7 – Schematic representation of the (A) initial strategy to achieve the semi-quantitative analysis, and of the (B) two variations of LFS prepared and tested; C, control line; T, test line(s).

To test this approach, two different variations of designed strips were prepared. One set of LFS was printed with four lines of the FITC antibody solution of 0.50 mg/µL, and another with four lines with different concentrations of FITC antibody ranging from 0.25 to 1.0 mg/µL on each line, as showed in Figure 8.7(B).

Figure 8.8 shows the results obtained with the two designs when placing three different concentrations (10^4, 10^5 and 10^6 copies/µL). As it is possible to observe, the intended sequential display of lines according to the concentration did not happen. However, it was possible to distinguish with naked eye the intensity of colour of the test lines between 10^4 and 10^5 copies/µL in both variations of the LFS prepared.

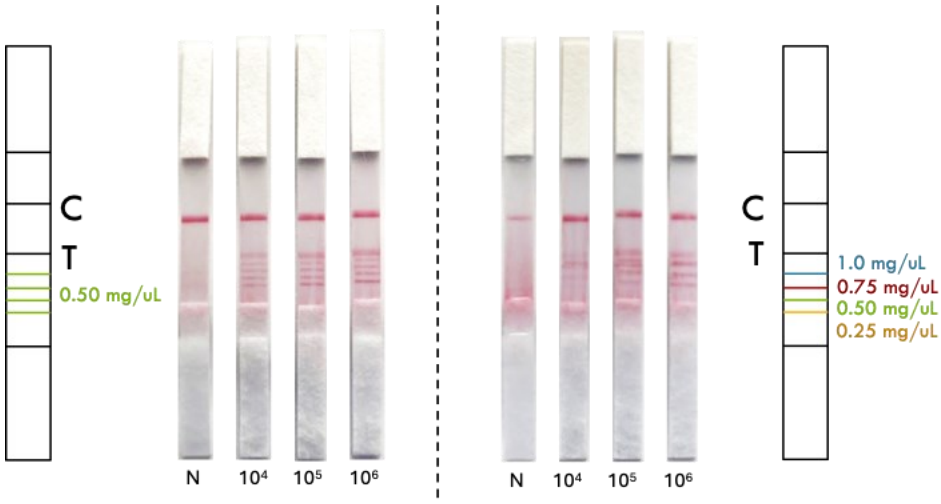

Figure 8.8 – Results obtained by placing different concentrations (10^4, 10^5 and 10^6 copies/µL) of amplified *E. coli* DNA in the two variations of LFS prepared; N, negative control; C, control line; T, test lines.

To better evaluate the signals obtained in the designed strips, the images were processed using an image processing software (Image J). A schematic representation of this procedure for image analysis is shown in Figure 8.9.

First, the RGB images were separated in its three components: red, green and blue, and the green filter was chosen since it is the closest complementary colour of the red colour of the control and test lines (Figure 8.9(A)) and allowed a better visibility of them. Then, a rectangular selection tool was used to select the area for analysis (yellow rectangle in Figure 8.9(B)) and a profile plot of the intensity of colour throughout the reading area of the strip was generated (Figure 8.9(B)).

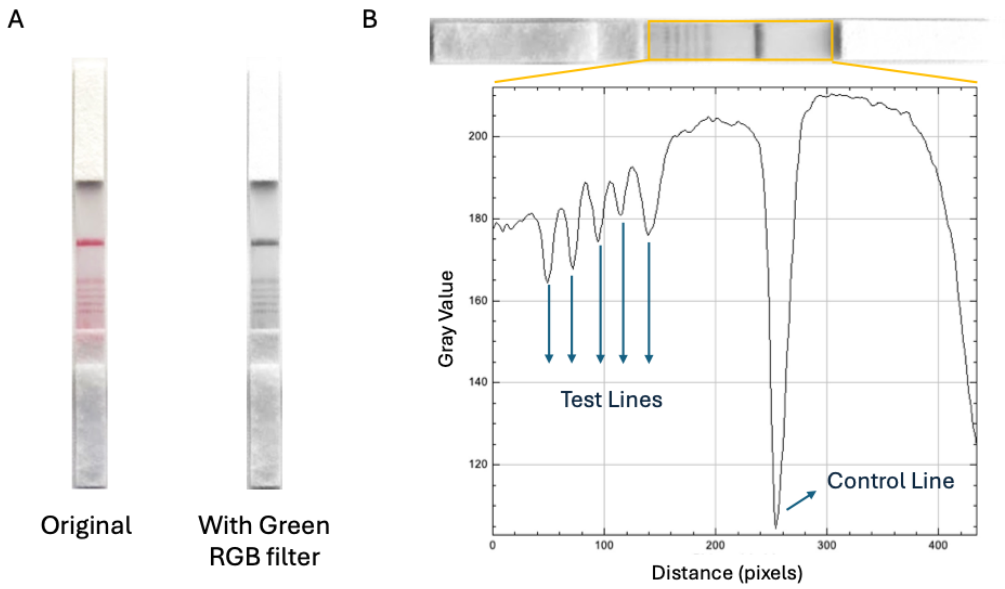

Figure 8.9 – Schematic representation of the image processing and analysis procedure; (A) application of a green filter to the original RGB image; (B) exemplification of a profile of the intensity of colour throughout the strip.

The results obtained from the image analysis of the strips designed with the same concentration of antibodies in each line is presented in Figure 8.10. It was possible to observe an increase in the colour intensity of the test lines with the increased concentration of amplified *E. coli* DNA, particularly in the first test line dispensed on the strip with 0.50 mg/µL of antibodies and in the fifth test line, which corresponds to the one already present in the commercially available strips used. The logarithmic correlation between the intensity of colour (gray values) and the DNA concentrations is shown in Figure 8.10(C). Furthermore, the decrease of intensities of colour from the first test line to the last one drawn on the strip (fourth line) is a promising result to achieve the intended semi-quantitative determination.

When using the strips prepared with four test lines with different concentrations of antibodies (Figure 8.11(A)), the difference between profiles of the strips with different concentrations of amplified *E. coli* DNA was less clear (Figure 8.11(B)).

It was possible to observe in both images and in the intensities profile, that there was overlapping of test lines, a consequence of the fabrication step, which severely impacted the readability of the strips. This variability of the dispensing of the test lines, could be due to the need to switch the solution in the dispensing needle for dispensing of each test line, slightly altering the position of it in relation to the strips. These initial studies show that the lateral flow strips with the same concentration of antibodies in each test line, present an advantage with regard to the repeatability of the analysis, when compared with the other design.

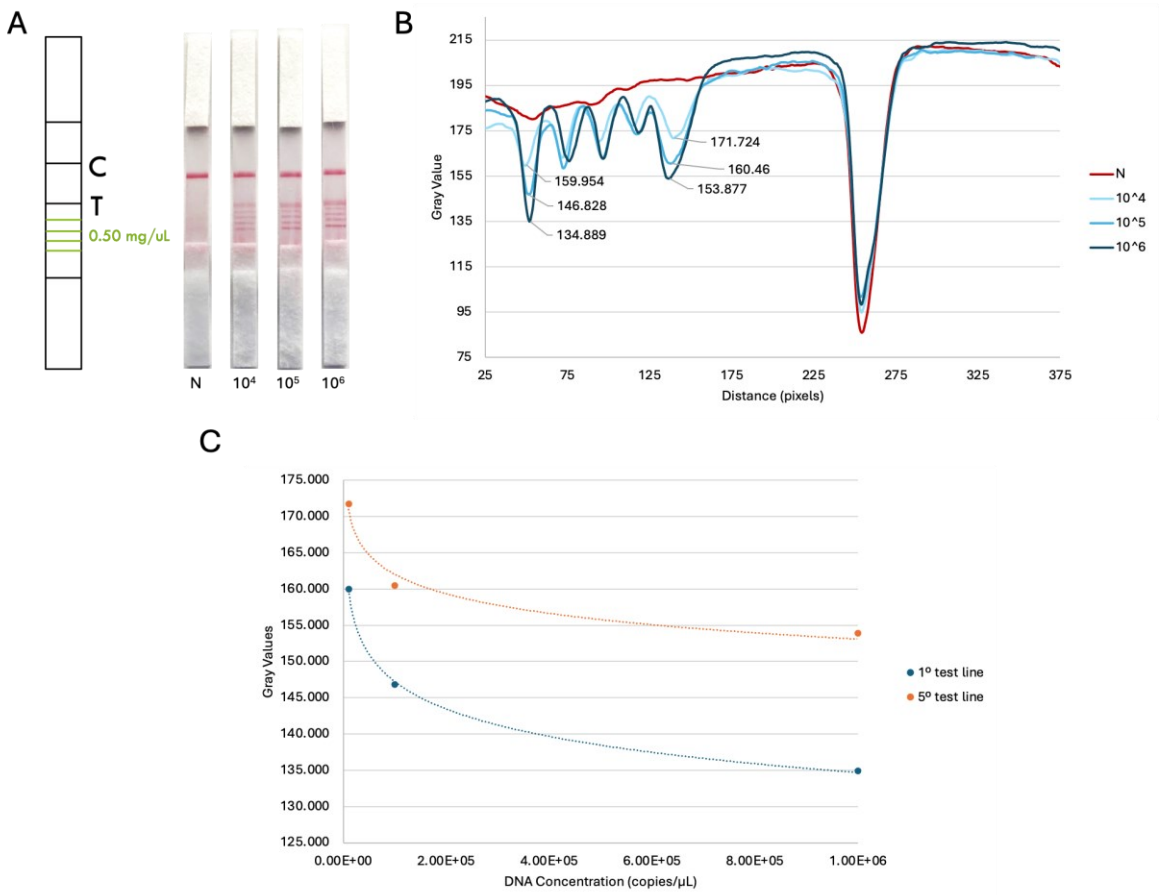

Figure 8.10 – Results obtained by placing different concentrations (10^4, 10^5 and 10^6 copies/µL) of amplified *E. coli* DNA in the LFS prepared with the same concentration of antibodies in each line; (A) Schematic representation of the design and original photo images of the strips; (B) profile of intensity of colour throughout the four strips; (C) Logarithmic correlation between the DNA concentration and the intensity of colour in the lines; N, negative control; C, control line; T, test lines.

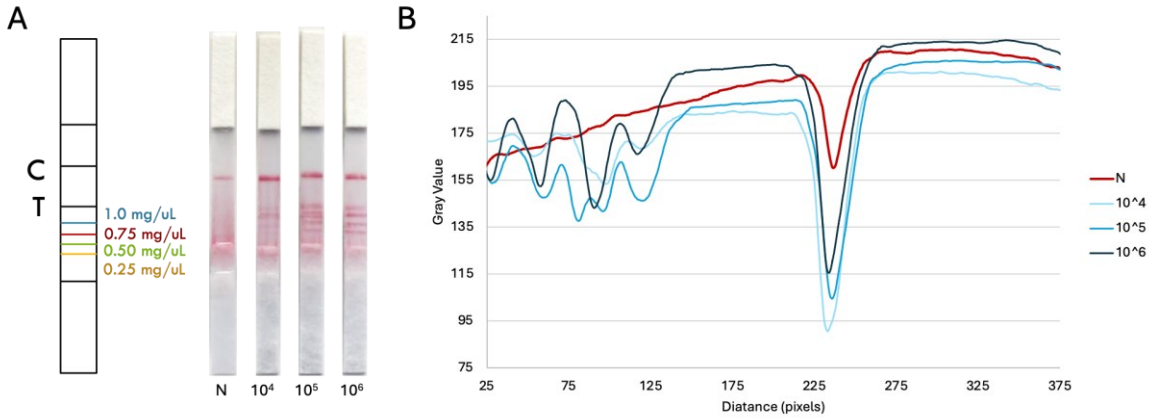

Figure 8.11 – Results obtained by placing different concentrations (10^4, 10^5 and 10^6 copies/µL) of *amplified E. coli* DNA in the LFS prepared with the different concentrations of antibodies in each line; (A) Schematic representation of the design and original photo images of the strips; (B) profile of intensity of colour throughout the four strips; N, negative control; C, control line; T, test lines.

The initial goal of designing a strip capable of sequential display of lines according to the concentration was not achieved at this point in the design optimization. A possible explanation could be that the amount of FITC antibody was not enough to capture all the copies in the lowest concentration (10^4 copies/µL). Additionally, since the test lines are placed on the strips by dispensing dots in a line side by side, it is possible that there was not a complete connection between the dots and some of the sample flowed through the reaction membrane in-between the dots of antibodies that formed the test line. So, more studies are needed to further optimize the LFS, such as increase the concentration of antibodies in the test lines, decrease the distance in-between the dots while dispensing the antibodies on the test lines, increasing the volume dispensed in each dot, increasing distance between the test lines, and also designing a strip with different concentrations of antibodies but from the highest concentration in the first test line to the lowest concentration on the last test line.

8.4. Conclusions

In this work, a lateral flow assay for the semi-quantitative detection of *E. coli* was developed, leveraging the Loop-Mediated Isothermal Amplification (LAMP) technique for DNA amplification. Through the optimization of key LAMP parameters, including temperature and primer concentrations, we were able to obtain "flattened" amplification curves. These curves enabled the differentiation of different DNA concentrations at a specific time, which consequently translated into distinguishable signals on the lateral flow strips. This crucial step ensured that the assay could reliably indicate the presence of different levels of *E. coli*, thus enhancing its semi-quantitative capabilities.

Additionally, an innovative lateral flow strip tailored to boost the semi-quantitative detection capabilities was designed and studied. Two sets of lateral flow strips (LFS) were designed and printed, and despite observing a visual difference between the dilutions of 10^4 and 10^5 copies/µL, further optimization is necessary to widen the range and capabilities of the approach. Future work will therefore focus on exploring other designs, testing higher concentrations of antibodies in the test lines, and increasing the space between them, to improve the resolution and accuracy of the assay.

Despite needing further refinement, the optimized assay demonstrated reliable performance across various settings. This makes it a valuable tool for detecting *E. coli*, providing a rapid and cost-effective diagnostic method, that not only is particularly useful in resource-limited environments, but that also allows an initial triage of the samples and identification of the ones that need more complex (and expensive) testing. Moreover, this advancement lays a robust foundation for the development of similar assays aimed at detecting other pathogens. By continuing to refine and adapt this technology, we can enhance public health surveillance and response strategies, ensuring that accurate, timely diagnostic tools are available where they are needed most.

Chapter 9. General Conclusions

9.1. General Conclusions

In this thesis, several innovative point-of-care devices were successfully designed based on the microfluidic paper-based device approach for the determination of several health-related parameters, that could serve as an adding tool in the diagnosis and monitoring of several health conditions. In the development of these devices, multiple parameters and conditions were tested and optimized in order to obtain a suitable sensitivity for the expected concentration levels in the proposed samples.

Table 9.1 shows a summary of the work presented in this thesis, including the target analyte the type of device, the number of layers in the device, the sample it was applied to and also its main features.

From Chapters 3 to 7, the point-of-care devices were developed using the 3D microfluidic paper-based analytical device approach. This type of point-of-care tests is affordable, portable, rapid, simple to use, and does not require specific training or complex equipment. Additionally, the 3D structure facilitates more complex multi-step analysis, better control of the fluids flow and also allows the possibility of introducing pre-treatment steps in the devices. Since, the developed µPAD were envisioned to aid in health diagnosis, not only in healthcare facilities, but also in field applications that involve remote areas, stability studies were performed both regarding storage of the devices and of the coloured product formed after the devices were used. To validate the results provided by the developed devices, several samples were tested with them and compared with the measurements obtained with a reference method.

Chapter 3 reports the development of a µPAD for iron determination in urine samples. This device was capable of fast, on-hand measurements of total iron in human urine samples without requiring pre-treatments steps. A range of 0.07 to 1.2 mg/L of iron, with a detection limit of 20 µg/L, proved suitable for all the analysed samples (#26) and comparable to the determination by atomic absorption spectrometry. Additionally, stability studies showed the developed µPAD was stable for 15 days while stored and, after loading the sample, it could be scanned within 3 hours. The low stability of the device while stored could be related to the reagents layer being in contact with the outside through the sample insertion hole, therefore being more exposed and susceptible to degradation. Due to the intrinsic colour of urine, and since the colorimetric detection was performed on the top layer of the device, a part of it was prepared without the colour reagent to perform a sample blank. The intrinsic absorption obtained with the urine itself was subtracted to the calculated absorption obtained with the colour reagent, to allow an accurate measurement of the colour formed in analytical determination.

The µPAD developed for the quantification of nitrate, reported in Chapter 4, was also applied to urine samples. However, this device contained a hydrophilic membrane with low porosity (0.20 µm) that, not only delayed the flow of the fluids to allow a higher enzymatic reaction time, but also filtered the sample and retained most of the bigger molecules that could possibly interfere in the colorimetric reaction. One of the interferences that was minimized due to the existence of the membrane was the intrinsic colour of urine samples.

Table 9.1 – Summary of the characteristics of all the point-of-care devices developed.

Chapter	Analyte	Type of Device	Number of Layers	Sample	Main Features
3	Iron	3D µPAD	2	Urine	- Range: 0.07 – 1.2 mg/L - LOD: 20 µg/L - Storage Stability: 15 days - Colour Stability: 3 hours - Validation: 26 samples - Interference of urine colour minimized
4	Nitrate	3D µPAD	3	Urine	- Range: 0.14 – 1.0 mM - LOD: 0.04 mM - Storage Stability: 30 days in vacuum at -20ºC - Colour Increases until 1 hour - Validation: 4 certified samples and recovery studies - Flow of fluids regulated with membrane - Interference of urine colour minimized
5	NH_x	3D µPAD	4	Saliva	- Range: 0.105 – 5.0 mM - LOD: 0.032 mM - Storage Stability: 2 months in vacuum - Colour Stability: 2 hours - Validation: 15 samples - Gas-diffusion hydrophobic membrane
5	Urea	3D µPAD	4	Saliva	- Range: 0.163 – 5.0 mM - LOD: 0.049 mM - Storage Stability: 1 month in vacuum - Colour Stability: 1 hour - Validation: 11 samples - Gas-diffusion hydrophobic membrane
6	Urease	3D µPAD	3	Saliva	- Range: 0.041 – 0.750 U/mL - LOD: 0.012 U/mL - Storage Stability: 4 months in vacuum - Colour Stability: 40 min - Validation: 13 samples - Gas-diffusion hydrophobic membrane - Kinetic determination
7	Glucose	3D µPAD	2	Saliva	- Range: 0.095 – 1.1 mM - LOD: 0.028 mM - Storage Stability: 2 weeks in vacuum at -20ºC - Colour Increases until 2 hours - Validation: 14 samples - Two enzymatic reactions in the device - Correlation between saliva and blood levels confirmed
8	*E. coli*	Lateral Flow Strip	1	Water	- Range detected: 10^4 – 10^6 copies/µL - Duration of LAMP assay: 80 min - Semi-quantitative analysis - Tool for monitoring water safety

Because of the small pore size of this membrane, the compounds that contribute to the urine colour did not reach the bottom layer where the colorimetric reaction occurs, therefore not interfering in the detection. This device proved to be able to quantify nitrate in urine samples in a range of 0.14 – 1.0 mM with a limit of detection of 0.04 mM. Furthermore, the accuracy of the device was validated with four certified samples and with recovery studies (#7 urine samples). In terms of stability, the μPAD showed to be stable for 30 days when stored in vacuum at -20 ºC. After being used, colour formed in the device increases up until 1 hour, after which it stabilizes.

In Chapters 5 and 6, three devices were developed for the quantifications of NH_x, urea and urease in saliva samples. All these determinations relied on the production of ammonia causing a change in the pH of bromothymol blue, and consequent change of colour. Because the ammonia produced was in a gaseous state, a gas-diffusion membrane was used in the devices. Due to the hydrophobicity of this membrane, the aqueous sample did not reach the colour reagent, eliminating possible interferences of the saliva sample in the colorimetric reaction. The devices reported in Chapter 5 were capable to quantify ammonia/ammonium (NH_x) and urea in saliva samples in a range of 0.105 - 5.0 mM and 0.163 - 5.0 mM, with limits of detection of 0.032 mM and 0.049 mM, respectively. While the NH_x μPADs were stable for at least 2 months when stored in vacuum and the colour formed could be scanned up to 2 hours, the urea μPADs, on the other hand, maintained is performance for only 1 month in vacuum storage and, after reaction with the sample, should be scanned within 1 hour. The decrease in stability of the urea determination μPAD when compared with the NH_x determination μPAD, could be justified by the presence of an enzyme immobilized in the paper discs inside the devices. Even though enzymes are a very useful tool to increase sensitivity and selectivity, it also makes it more difficult to ensure the stability of the devices in long term. Both devices were also validated successfully with measurements with more than human saliva samples of both healthy individuals and CKD patients. The NH_x determination device was validated by comparison with an ammonia selective electrode, while the measurements obtained with the urea determination μPAD was compared with the measurements obtained with a commercially available kit.

Although the urease activity μPAD, reported in Chapter 6, used a similar approach to the devices reported in Chapter 5, both in terms of reactions and structure, the determination itself was achieved using the kinetic capabilities of the urease enzyme. The reactions were performed at two different enzymatic reaction times (15 and 20 min), and the variation of signal between these two ERT's was correlated to the urease activity. This approach not only allowed a more accurate quantification of the salivary urease, but also suppressed the influence of NH_X already present in the samples. With the developed device it was possible to quantify the urease activity in saliva samples in a range of 0.041 – 0.750 U/mL with a limit of detection of 0.012 U/mL. These features proved to be suitable for all the samples analysed (#13) and comparable to the determination using a commercially available kit.

Chapter 7 reports the development of μPAD for the quantification of glucose in saliva samples. This quantification was achieved by using two consecutive enzymatic reactions. In the first, glucose oxidase converts glucose in gluconic acid, releasing hydrogen peroxide.

Then, peroxidase catalyses the release of oxygen from hydrogen peroxide, which interacts with o-dianisidine, causing a change of colour that is recorded by scanning the device. The quantification of glucose in saliva was achieved within a range of 0.095 to 1.1 mM of glucose, with a limit of detection of 0.028 mM. The accuracy of the devices was confirmed by comparing the measurements of #14 saliva samples with the developed device and with the reference method of "Dinitrosalicylic Acid Reagent for Determination of Reducing Sugar". The stability of this µPAD was also studied and results showed that the device could be stored for 2 weeks in vacuum at -20 ºC, without decreasing its sensitivity, and after being used, the colour formed increased in the first 2 hours, only stabilizing after that period. To ensure the device could be used as an aiding tool in the monitoring of diabetes, a correlation between the concentration of glucose in saliva and in blood was studied using #5 saliva samples of diabetic patients. Results showed that there is a correlation of 2% between the concentration of glucose in saliva and in blood, confirming that this device could provide an accurate analysis of the glucose levels in saliva and therefore be a tool for diabetes monitoring.

In summary, the developed µPADs reported in Chapters 3 to 7 are innovative devices that provide a simple, easy-to-use alternative to the classical techniques that are currently available, in addition to being portable, lab equipment-free, and disposable via incineration, offering environmental friendliness and simplifying biological sample handling. The main drawback found using this type of fabrication and assembly of paper-based devices was the manual and laborious assembly, and delicate lamination process (avoiding the shifting of the discs), which could lead for an uneven distribution and decreased reproducibility. In the work carried out and presented in this thesis, this problem was minimized by using several replicates for each measurement and removing outliers if necessary.

In Chapter 8, a different approach to the one described so far was adopted. This chapter reports the development of a lateral flow assay for the semi-quantitative detection of *E. coli*. To perform the amplification of the DNA in the sample, the Loop-Mediated Isothermal Amplification (LAMP) technique was used since it can be performed at a constant temperature and provides high sensitivity and specificity of results, due to the use of four to six primers that target six to eight regions. The LAMP assay was optimized in order to obtain "flattened" amplification curves that would allow the differentiation of different DNA concentrations at a specific time, enabling a semi-quantitative analysis. The detection was achieved using a newly designed and innovative lateral flow strip that consisted of five test lines, instead of the traditionally found strip with only one test line. The objective was to design barcode-style lateral flow strip, where the number of visible lines would be related to the concentration of *E. coli* DNA in the sample. Even though it was possible to visually distinguish between the dilutions of 10^4 and 10^5 copies/µL with the designed presented, further optimization is necessary to widen the range and capabilities of the approach. Despite needing further improvement, the assay demonstrated reliable performance across several settings, making it a potentially valuable tool for detecting *E. coli* and providing a rapid and cost-effective diagnostic method, that not only is particularly useful in resource-limited environments, but that also allows an initial triage of the samples that could need more complex (and expensive) testing.

Chapter 9. *General Conclusions*

Overall, this thesis has demonstrated the potential of microfluidic paper-based analytical devices and lateral flow assays as innovative, cost-effective, and affordable diagnostic tools. The developed devices successfully addressed key challenges associated with point-of-care testing, such as sample complexity, reagent stability, and measurement accuracy. Despite some limitations in fabrication and reproducibility, the optimization strategies implemented throughout this thesis have contributed to improving their reliability and accuracy. Ultimately, these advancements lay the foundation for further innovation in point-of-care diagnostics, with the potential to enhance disease detection and health monitoring in both clinical and non-clinical settings.

List of Publications

Publications in International Scientific Periodicals with Peer Review

[4] F. T. S. M. Ferreira, A. O. S. S. Rangel, R. B. R. Mesquita, A Microfluidic Paper-Based Device for Monitoring Urease Activity in Saliva, Biosensors (2025) DOI: https://doi.org/10.3390/bios15010048

[3] F. T. S. M. Ferreira, R. B. R. Mesquita, A. O. S. S. Rangel, On-hand tool for ammonium and urea determination in saliva to monitor chronic kidney disease – Design of a couple of microfluidic paper-based devices, Microchemical Journal (2023) DOI: https://doi.org/10.1016/j.microc.2023.109102

[2] F. T. S. M. Ferreira, R. B. R. Mesquita, A. O. S. S. Rangel, Design and Functionalization of a PAD for the Enzymatic Determination of Nitrate in Urine, Molecules (2021) DOI: https://doi.org/10.3390/molecules26216355

[1] F. T. S. M. Ferreira, K. A. Catalão, R. B. R. Mesquita, A. O. S. S. Rangel, New microfluidic paper-based analytical device for iron determination in urine samples, Analytical and Bioanalytical Chemistry (2021) DOI: https://doi.org/10.1007/s00216-021-03706-9

Oral Communications

[6] F. T. S. M. Ferreira, A. O. S. S. Rangel, R. B. R. Mesquita, design of paper-based analytical devices for chemical and biochemical assays of biomarkers in biological fluids of non-invasive collection., QA7, XXVIII Encontro Galego-Portugués de Química, Vigo, Spain (2024).

[5] F. T. S. M. Ferreira, R. B. R. Mesquita, A. O. S. S. Rangel, Point-of-care enzymatic quantification of glucose in saliva with a newly designed microfluidic paper-based device., YSOP6, 11th Meeting of the Analytical Chemistry Division, Porto, Portugal (2024).

[4] F. T. S. M. Ferreira, P. Jajesniak, J. Huang, X. Yan, A. O. S. S. Rangel, R. B. R. Mesquita, J. Reboud, Microfluidic sensor for semi-quantitative E. coli monitoring in water samples, QA7, XXVII Encontro Luso Galego De Química, Porto, Portugal (2023).

[3] F. T. S. M. Ferreira, R. B. R. Mesquita, A. O. S. S. Rangel, On-hand tool for CKD monitoring – design of a couple of μPADs for ammonium and urea determination in saliva, YSP6, 15th International Conference on Flow Analysis - Flow Analysis XIV, Krakow, Poland (2022).

[2] F. T. S. M. Ferreira, K. A. Catalão, R. B. R. Mesquita, A. O. S. S. Rangel, Novel microfluidic paper-based analytical device for the colorimetric determination of iron in urine samples, YS-7, V4 Symposium Flow Analysis & Capillary Electrophoresis, online, Poland (2021).

[1] F. T. S. M. Ferreira, K. A. Catalão, R. B. R. Mesquita, A. O. S. S. Rangel, Determination of urinary iron by colorimetric detection with a novel microfluidic paper-based analytical device, OC 8, 10^{o} Encontro da Divisão de Química Analítica, online, Portugal (2020).

Poster Presentations

[2] F. T. S. M. Ferreira, A. O. S. S. Rangel, R. B. R. Mesquita, Application of a microfluidic paper-based device to the enzymatic quantification of glucose in saliva, P54, 23rd International Conference on Flow Injection Analysis and Related Techniques, Chiang Mai, Thailand (2024).

[1] F. T. S. M. Ferreira, R. B. R. Mesquita, A. O. S. S. Rangel, Urease Quantification with a Newly Designed Microfluidic Device, P30, 22nd International Conference on Flow Injection Analysis and Related Techniques, Marseille, France (2023).

References

References

1. Alexander Fleming Discovery and Development of Penicillin - Landmark - American Chemical Society [Internet]. [cited 2025 Feb 7]. Available from: https://www.acs.org/education/whatischemistry/landmarks/flemingpenicillin.html
2. Al Fayez N, Nassar MS, Alshehri AA, Alnefaie MK, Almughem FA, Alshehri BY, et al. Recent Advancement in mRNA Vaccine Development and Applications. Pharmaceutics [Internet]. 2023 Jul 1 [cited 2025 Feb 7];15(7):1972. Available from: https://pmc.ncbi.nlm.nih.gov/articles/PMC10384963/
3. Word Health Organization. Standing up for the right to health [Internet]. 2018 [cited 2019 Feb 22]. Available from: https://www.who.int/news-room/feature-stories/detail/standing-up-for-the-right-to-health
4. World Health Organization. Billions left behind on the path to universal health coverage [Internet]. 2023 [cited 2024 Nov 10]. Available from: https://www.who.int/news/item/18-09-2023-billions-left-behind-on-the-path-to-universal-health-coverage
5. United Nations. THE 17 GOALS | Sustainable Development [Internet]. [cited 2024 Feb 6]. Available from: https://sdgs.un.org/goals
6. Wang J, Tan F, Wang Z, Yu Y, Yang J, Wang Y, et al. Understanding Gaps in the Hypertension and Diabetes Care Cascade: Systematic Scoping Review. JMIR Public Health Surveill [Internet]. 2024 [cited 2025 Feb 7];10(1):e51802. Available from: https://pmc.ncbi.nlm.nih.gov/articles/PMC10907944/
7. Singh K, Brož J, Larissa Aviles-Santa M, Karachaliou F, Simatos G, Simatou A. The Challenges in the Development of Diabetes Prevention and Care Models in Low-Income Settings. Front Endocrinol (Lausanne) [Internet]. 2020 Aug 13 [cited 2025 Feb 7];11:518. Available from: https://pmc.ncbi.nlm.nih.gov/articles/PMC7438784/
8. World Health Organization. Sexual and Reproductive Health and Research (SRH) [Internet]. [cited 2024 Oct 13]. Available from: https://www.who.int/teams/sexual-and-reproductive-health-and-research-(srh)/areas-of-work/sexual-health/sexually-transmitted-infections/point-of-care-tests
9. Kumari S, Islam M, Gupta A. Paper-based multiplex biosensors for inexpensive healthcare diagnostics: a comprehensive review. Biomedical Microdevices 2023 25:2 [Internet]. 2023 May 3 [cited 2024 Oct 13];25(2):1–17. Available from: https://link.springer.com/article/10.1007/s10544-023-00656-0
10. Land KJ, Boeras DI, Chen XS, Ramsay AR, Peeling RW. REASSURED diagnostics to inform disease control strategies, strengthen health systems and improve patient outcomes. Nature Microbiology 2018 4:1 [Internet]. 2018 Dec 13 [cited 2024 Dec 9];4(1):46–54. Available from: https://www.nature.com/articles/s41564-018-0295-3
11. Zhang H, Fink G, Cohen J. Malaria Rapid Tests, Febrile Illness Management, and Child Mortality Across Sub-Saharan African Countries. JAMA [Internet]. 2024 Oct 15 [cited 2025 Feb 7];332(15):1270–81. Available from: https://pubmed.ncbi.nlm.nih.gov/39292453/

References

12. Oyegoke OO, Maharaj L, Akoniyon OP, Kwoji I, Roux AT, Adewumi TS, et al. Malaria diagnostic methods with the elimination goal in view. Parasitol Res [Internet]. 2022 Jul 1 [cited 2025 Feb 7];121(7):1867. Available from: https://pmc.ncbi.nlm.nih.gov/articles/PMC9033523/
13. United Nations. World Social Report 2023: Leaving No One Behind In An Ageing World | DESA Publications [Internet]. 2023 [cited 2025 Feb 7]. Available from: https://desapublications.un.org/publications/world-social-report-2023-leaving-no-one-behind-ageing-world
14. Khan AR, Hussain WL, Shum HC, Hassan SU. Point-of-care testing: a critical analysis of the market and future trends. Frontiers in Lab on a Chip Technologies. 2024 May 13;3:1394752.
15. Pour SRS, Calabria D, Emamiamin A, Lazzarini E, Pace A, Guardigli M, et al. Electrochemical vs. Optical Biosensors for Point-of-Care Applications: A Critical Review. Chemosensors 2023, Vol 11, Page 546 [Internet]. 2023 Oct 21 [cited 2024 Oct 13];11(10):546. Available from: https://www.mdpi.com/2227-9040/11/10/546/htm
16. Chen L, Guo X, Sun X, Zhang S, Wu J, Yu H, et al. Porous Structural Microfluidic Device for Biomedical Diagnosis: A Review. Micromachines 2023, Vol 14, Page 547 [Internet]. 2023 Feb 26 [cited 2024 Oct 13];14(3):547. Available from: https://www.mdpi.com/2072-666X/14/3/547/htm
17. Chen C, Tian L, Li W, Wang K, Yang Q, Lin J, et al. Recent Advances and Perspectives Regarding Paper-Based Sensors for Salivary Biomarker Detection. Chemosensors 2023, Vol 11, Page 383 [Internet]. 2023 Jul 7 [cited 2024 Oct 13];11(7):383. Available from: https://www.mdpi.com/2227-9040/11/7/383/htm
18. Singh S, Hasan MR, Jain A, Pilloton R, Narang J. LFA: The Mysterious Paper-Based Biosensor: A Futuristic Overview. Chemosensors 2023, Vol 11, Page 255 [Internet]. 2023 Apr 19 [cited 2024 Oct 13];11(4):255. Available from: https://www.mdpi.com/2227-9040/11/4/255/htm
19. Hajam MI, Khan MM. Microfluidics: a concise review of the history, principles, design, applications, and future outlook. Biomater Sci [Internet]. 2024 Jan 16 [cited 2024 Oct 13];12(2):218–51. Available from: https://pubs.rsc.org/en/content/articlehtml/2024/bm/d3bm01463k
20. Koczula KM, Gallotta A. Lateral flow assays. Essays Biochem [Internet]. 2016 Jun 30 [cited 2024 Nov 18];60(1):111–20. Available from: /essaysbiochem/article/60/1/111/78237/Lateral-flow-assays
21. Budd J, Miller BS, Weckman NE, Cherkaoui D, Huang D, Decruz AT, et al. Lateral flow test engineering and lessons learned from COVID-19. Nature Reviews Bioengineering 2023 1:1 [Internet]. 2023 Jan 19 [cited 2024 Dec 10];1(1):13–31. Available from: https://www.nature.com/articles/s44222-022-00007-3
22. Omidfar K, Riahi F, Kashanian S. Lateral Flow Assay: A Summary of Recent Progress for Improving Assay Performance. Biosensors 2023, Vol 13, Page 837 [Internet]. 2023 Aug 23 [cited 2024 Dec 30];13(9):837. Available from: https://www.mdpi.com/2079-6374/13/9/837/htm

References

23. Sachdeva S, Davis RW, Saha AK. Microfluidic Point-of-Care Testing: Commercial Landscape and Future Directions. Front Bioeng Biotechnol [Internet]. 2021 Jan 15 [cited 2025 Jan 12];8:602659. Available from: www.frontiersin.org
24. Di Nardo F, Chiarello M, Cavalera S, Baggiani C, Anfossi L. Ten Years of Lateral Flow Immunoassay Technique Applications: Trends, Challenges and Future Perspectives. Sensors (Basel) [Internet]. 2021 Aug 1 [cited 2025 Jan 3];21(15):5185. Available from: https://pmc.ncbi.nlm.nih.gov/articles/PMC8348896/
25. Parolo C, Sena-Torralba A, Bergua JF, Calucho E, Fuentes-Chust C, Hu L, et al. Tutorial: design and fabrication of nanoparticle-based lateral-flow immunoassays. Nature Protocols 2020 15:12 [Internet]. 2020 Oct 23 [cited 2025 Jan 3];15(12):3788–816. Available from: https://www.nature.com/articles/s41596-020-0357-x
26. Ferreira FTSM, Mesquita RBR, Rangel AOSS. Novel microfluidic paper-based analytical devices (μPADs) for the determination of nitrate and nitrite in human saliva. Talanta [Internet]. 2020;219(May):121183. Available from: https://doi.org/10.1016/j.talanta.2020.121183
27. Noviana E, Carrão DB, Pratiwi R, Henry CS. Emerging applications of paper-based analytical devices for drug analysis: A review. Anal Chim Acta. 2020 Jun 15;1116:70–90.
28. Kumari S, Islam M, Gupta A. Paper-based multiplex biosensors for inexpensive healthcare diagnostics: a comprehensive review. Biomedical Microdevices 2023 25:2 [Internet]. 2023 May 3 [cited 2025 Jan 12];25(2):1–17. Available from: https://link.springer.com/article/10.1007/s10544-023-00656-0
29. Boobphahom S, Ly MN, Soum V, Pyun N, Kwon OS, Rodthongkum N, et al. Recent Advances in Microfluidic Paper-Based Analytical Devices toward High-Throughput Screening. Molecules 2020, Vol 25, Page 2970 [Internet]. 2020 Jun 28 [cited 2025 Jan 12];25(13):2970. Available from: https://www.mdpi.com/1420-3049/25/13/2970/htm
30. Nishat S, Jafry AT, Martinez AW, Awan FR. Paper-based microfluidics: Simplified fabrication and assay methods. Sens Actuators B Chem. 2021 Jun;336:129681.
31. Ozer T, McMahon C, Henry CS. Advances in Paper-Based Analytical Devices. Annual Review of Analytical Chemistry. 2020;13:85–109.
32. Mishra A, Patra S, Srivastava V, Uzun L, Mishra YK, Syväjärvi M, et al. Progress in paper-based analytical devices for climate neutral biosensing. Biosens Bioelectron X. 2022 Sep 1;11:100166.
33. Asano H, Shiraishi Y. Development of paper-based microfluidic analytical device for iron assay using photomask printed with 3D printer for fabrication of hydrophilic and hydrophobic zones on paper by photolithography. Anal Chim Acta. 2015 Jul 9;883:55–60.
34. Paper microfluidic devices : A review 2017 - Elveflow [Internet]. [cited 2025 Jan 19]. Available from: https://www.elveflow.com/microfluidic-reviews/general-microfluidics/paper-microfluidic-devices-a-review-2017/
35. Visão geral abrangente da flexografia [Internet]. [cited 2025 Jan 19]. Available from: https://flexopedia.net/comprehensive-overview-of-flexography/

36. Noviana E, Ozer T, Carrell CS, Link JS, McMahon C, Jang I, et al. Microfluidic Paper-Based Analytical Devices: From Design to Applications. Chem Rev [Internet]. 2021 Oct 13 [cited 2025 Jan 19];121(19):11835–85. Available from: https://pubs.acs.org/doi/abs/10.1021/acs.chemrev.0c01335
37. Ebrahimi G, Pakchin PS, Mota A, Omidian H, Omidi Y. Electrochemical microfluidic paper-based analytical devices for cancer biomarker detection: From 2D to 3D sensing systems. Talanta. 2023 May 15;257:124370.
38. Tseng CC, Kung C Te, Chen RF, Tsai MH, Chao HR, Wang YN, et al. Recent advances in microfluidic paper-based assay devices for diagnosis of human diseases using saliva, tears and sweat samples. Sens Actuators B Chem [Internet]. 2021;342(May):130078. Available from: https://doi.org/10.1016/j.snb.2021.130078
39. Sun K, Fan Y, Hebda M, Zhang Y. Origami Microfluidics: A Review of Research Progress and Biomedical Applications. Biomedical Materials and Devices [Internet]. 2023 Mar 1 [cited 2025 Jan 19];1(1):388–401. Available from: https://link.springer.com/article/10.1007/s44174-022-00007-2
40. Zheng W, Wang K, Xu H, Zheng C, Cao B, Qin Q, et al. Strategies for the detection of target analytes using microfluidic paper-based analytical devices. Anal Bioanal Chem. 2021;413(9):2429–45.
41. García-Azuma R, Werner K, Revilla-Monsalve C, Trinidad O, Altamirano-Bustamante NF, Altamirano-Bustamante MM. Unveiling the state of the art: a systematic review and meta-analysis of paper-based microfluidic devices. Front Bioeng Biotechnol. 2024 Aug 21;12:1421831.
42. Aryal P, Henry CS. Advancements and challenges in microfluidic paper-based analytical devices: design, manufacturing, sustainability, and field applications. Frontiers in Lab on a Chip Technologies [Internet]. 2024 Dec 20 [cited 2025 Feb 9];3:1467423. Available from: https://www.frontiersin.org/articles/10.3389/frlct.2024.1467423/full
43. Han T, Jin Y, Geng C, Aziz A ur R, Zhang Y, Deng S, et al. Microfluidic Paper-based Analytical Devices in Clinical Applications. Chromatographia [Internet]. 2020 Jun 1 [cited 2025 Jan 26];83(6):693–701. Available from: https://link.springer.com/article/10.1007/s10337-020-03892-1
44. Yeasmin S, Ammanath G, Onder A, Yan E, Yildiz UH, Palaniappan A, et al. Current trends and challenges in point-of-care urinalysis of biomarkers in trace amounts. TrAC Trends in Analytical Chemistry. 2022 Dec 1;157:116786.
45. RGB color model - Wikipedia [Internet]. [cited 2025 Jan 26]. Available from: https://en.wikipedia.org/wiki/RGB_color_model
46. Xie Y, Zhi X, Su H, Wang K, Yan Z, He N, et al. A Novel Electrochemical Microfluidic Chip Combined with Multiple Biomarkers for Early Diagnosis of Gastric Cancer. Nanoscale Res Lett. 2015 Dec 1;10(1):1–9.
47. Narasimhan A, Jain H, Muniandy K, Chinnappan R, Mani NK. Bio-analysis of Saliva Using Paper Devices and Colorimetric Assays. Journal of Analysis and Testing 2023 8:1 [Internet].

2023 Dec 13 [cited 2025 Jan 27];8(1):114–32. Available from: https://link.springer.com/article/10.1007/s41664-023-00282-y

48. Pittman TW, Decsi DB, Punyadeera C, Henry CS. Saliva-based microfluidic point-of-care diagnostic. Theranostics [Internet]. 2023 [cited 2025 Jan 27];13(3):1091. Available from: https://pmc.ncbi.nlm.nih.gov/articles/PMC9925318/
49. Khan RS, Khurshid Z, Asiri FYI. Advancing Point-of-Care (PoC) Testing Using Human Saliva as Liquid Biopsy. Diagnostics [Internet]. 2017 Sep 1 [cited 2025 Jan 27];7(3):39. Available from: https://pmc.ncbi.nlm.nih.gov/articles/PMC5617939/
50. Aguiar JIS, Rangel AOSS, Mesquita RBR. Salivary calcium determination with a specially developed microfluidic paper-based device for point-of-care analysis. Talanta Open. 2023 Dec 1;8:100254.
51. Aguiar JIS, Silva MTS, Ferreira HAG, Pinto ECB, Vasconcelos MW, Rangel AOSS, et al. Development of a microfluidic paper-based analytical device for magnesium determination in saliva samples. Talanta Open. 2022 Dec 1;6:100135.
52. Anatomy of the Urinary System | Johns Hopkins Medicine [Internet]. [cited 2025 Feb 9]. Available from: https://www.hopkinsmedicine.org/health/wellness-and-prevention/anatomy-of-the-urinary-system
53. Balhara N, Devi M, Balda A, Phour M, Giri A. Urine; a new promising biological fluid to act as a non-invasive biomarker for different human diseases. URINE. 2023 Jan 1;5:40–52.
54. Sequeira-Antunes B, Ferreira HA. Urinary Biomarkers and Point-of-Care Urinalysis Devices for Early Diagnosis and Management of Disease: A Review. Biomedicines 2023, Vol 11, Page 1051 [Internet]. 2023 Mar 29 [cited 2025 Feb 9];11(4):1051. Available from: https://www.mdpi.com/2227-9059/11/4/1051/htm
55. Khachornsakkul K, Tiangtrong A, Suwannasom A, Sangkharoek W, Jamjumrus O, Dungchai W. Distance-based β-amyloid protein detection on PADs for the scanning and subsequent follow-up of Alzheimer's disease in human urine samples. Analyst [Internet]. 2022 Feb 14 [cited 2025 Jan 31];147(4):695–703. Available from: https://pubs.rsc.org/en/content/articlehtml/2022/an/d1an01605a
56. Martins G V., Marques AC, Fortunato E, Sales MGF. Paper-based (bio)sensor for label-free detection of 3-nitrotyrosine in human urine samples using molecular imprinted polymer. Sens Biosensing Res. 2020 Jun 1;28:100333.
57. Lu C, Xu L, Jiang Y, Liao C, Li Y, Tang Y, et al. Sensitive and accurate monitoring of urinary albumin and point-of-care testing using a fluorescent probe with anti-interference capacity against exogenous drugs. Talanta. 2024 Nov 1;279:126575.
58. Yomthiangthae P, Chailapakul O, Siangproh W. Rapid urinary albumin detection using a simple redox cycling process coupled with a paper-based device. Journal of Electroanalytical Chemistry. 2022 Apr 15;911:116230.
59. Hiraoka R, Kuwahara K, Wen YC, Yen TH, Hiruta Y, Cheng CM, et al. Paper-Based Device for Naked Eye Urinary Albumin/Creatinine Ratio Evaluation. ACS Sens [Internet]. 2020 Apr

24 [cited 2025 Feb 3];5(4):1110–8. Available from: https://pubs.acs.org/doi/full/10.1021/acssensors.0c00050

60. Ramdzan AN, Almeida MIGS, McCullough MJ, Kolev SD. Development of a microfluidic paper-based analytical device for the determination of salivary aldehydes. Anal Chim Acta. 2016;919:47–54.
61. Wang D, Mao X, Liang Y, Cai Y, Tu T, Zhang S, et al. Multi-Parameter Detection of Urine Based on Electropolymerized PANI: PSS/AuNPs/SPCE. Biosensors (Basel) [Internet]. 2023 Feb 1 [cited 2025 Jan 31];13(2):272. Available from: https://www.mdpi.com/2079-6374/13/2/272/htm
62. Thepchuay Y, Mesquita RBR, Nacapricha D, Rangel AOSS. Micro-PAD card for measuring total ammonia nitrogen in saliva. Anal Bioanal Chem. 2020;3167–76.
63. Nontawong N, Amatatongchai M, Wuepchaiyaphum W, Chairam S, Pimmongkol S, Panich S, et al. Fabrication of a three-dimensional electrochemical paper-based device (3D-ePAD) for individual and simultaneous detection of ascorbic acid, dopamine and uric acid. Int J Electrochem Sci. 2018 Jul 1;13(7):6940–57.
64. Edachana RP, Kumaresan A, Balasubramanian V, Thiagarajan R, Nair BG, Thekkedath Gopalakrishnan SB. Paper-based device for the colorimetric assay of bilirubin based on in-situ formation of gold nanoparticles. Microchimica Acta [Internet]. 2020 Jan 1 [cited 2025 Feb 3];187(1):1–9. Available from: https://link.springer.com/article/10.1007/s00604-019-4051-z
65. Conrado JAM, Araújo DAG, Petruci JF da S. Combination of headspace single-drop microextraction (HS-SDME) with a nickel-embedded paper-based analytical device for cyanide quantification. Anal Chim Acta. 2023 Nov 15;1281:341882.
66. Janrod M, Srisa-Art M. Simultaneous colorimetric detection of nephrolithiasis biomarkers using a microfluidic paper-based analytical device. Analytical Methods [Internet]. 2023 Feb 9 [cited 2025 Jan 31];15(6):752–61. Available from: https://pubs.rsc.org/en/content/articlehtml/2023/ay/d2ay01648f
67. Abdollahiyan P, Heidari H, Hassanzadeh S, Hasanzadeh M, Seidi F, Pashazadeh-Panahi P. Providing multicolor plasmonic patterns with graphene quantum dots functionalized d-penicillamine for visual recognition of V(V), Cu (II), and Fe(III): Colorimetric fingerprints of GQDs-DPA for discriminating ions in human urine samples. Journal of Molecular Recognition [Internet]. 2021 Dec 1 [cited 2025 Feb 3];34(12):e2936. Available from: https://onlinelibrary.wiley.com/doi/full/10.1002/jmr.2936
68. Abdollahiyan P, Hasanzadeh M, Seidi F, Pashazadeh-Panahi P. An innovative colorimetric platform for the low-cost and selective identification of Cu(II), Fe(III), and Hg(II) using GQDs-DPA supported amino acids by microfluidic paper-based (μPADs) device: Multicolor plasmonic patterns. J Environ Chem Eng. 2021 Oct 1;9(5):106197.
69. Melo MMP, Machado A, Rangel AOSS, Mesquita RBR. Disposable Microfluidic Paper-Based Device for On-Site Quantification of Urinary Creatinine. Chemosensors [Internet]. 2023 Jul 1 [cited 2025 Jan 31];11(7):368. Available from: https://www.mdpi.com/2227-9040/11/7/368/htm

70. Shariati S, Khayatian G. A new method for selective determination of creatinine using smartphone-based digital image. Microfluid Nanofluidics [Internet]. 2022 Apr 1 [cited 2025 Jan 31];26(4):1–9. Available from: https://link.springer.com/article/10.1007/s10404-022-02538-y
71. Lewińska I, Speichert M, Granica M, Tymecki Ł. Colorimetric point-of-care paper-based sensors for urinary creatinine with smartphone readout. Sens Actuators B Chem. 2021 Aug 1;340:129915.
72. Shojaeifard Z, Bordbar MM, Aseman MD, Nabavizadeh SM, Hemmateenejad B. Collaboration of cyclometalated platinum complexes and metallic nanoclusters for rapid discrimination and detection of biogenic amines through a fluorometric paper-based sensor array. Sens Actuators B Chem. 2021 May 1;334:129582.
73. Mathaweesansurn A, Thongrod S, Khongkaew P, Phechkrajang CM, Wilairat P, Choengchan N. Simple and fast fabrication of microfluidic paper-based analytical device by contact stamping for multiple-point standard addition assay: Application to direct analysis of urinary creatinine. Talanta. 2020 Apr 1;210:120675.
74. Cincotto FH, Fava EL, Moraes FC, Fatibello-Filho O, Faria RC. A new disposable microfluidic electrochemical paper-based device for the simultaneous determination of clinical biomarkers. Talanta. 2019 Apr 1;195:62–8.
75. Rossini EL, Milani MI, Carrilho E, Pezza L, Pezza HR. Simultaneous determination of renal function biomarkers in urine using a validated paper-based microfluidic analytical device. Anal Chim Acta. 2018 Jan 2;997:16–23.
76. Talalak K, Noiphung J, Songjaroen T, Chailapakul O, Laiwattanapaisal W. A facile low-cost enzymatic paper-based assay for the determination of urine creatinine. Talanta. 2015 Nov 1;144:915–21.
77. Razavi F, Khajehsharifi H. A colorimetric paper-based sensor with nanoporous SBA-15 for simultaneous determination of histidine and cysteine in urine samples. Chemical Papers [Internet]. 2021 Jul 1 [cited 2025 Feb 3];75(7):3401–10. Available from: https://link.springer.com/article/10.1007/s11696-021-01548-4
78. Bahavarnia F, Kohansal F, Hasanzadeh M. One-drop chemosensing of dapoxetine hydrochloride using opto-analysis by multi-channel μPAD decorated silver nanoparticles: introducing a paper-based microfluidic portable device/sensor toward naked-eye pharmaceutical analysis by lab-on-paper technology. RSC Adv [Internet]. 2024 Jan 10 [cited 2025 Jan 31];14(4):2610–20. Available from: https://pubs.rsc.org/en/content/articlehtml/2024/ra/d3ra06752a
79. Narang J, Singhal C, Mathur A, Khanuja M, Varshney A, Garg K, et al. Lab on paper chip integrated with Si@GNRs for electroanalysis of diazepam. Anal Chim Acta. 2017 Aug 8;980:50–7.
80. Khachornsakkul K, Del-Rio-Ruiz R, Creasey H, Widmer G, Sonkusale SR. Gold Nanomaterial-Based Microfluidic Paper Analytical Device for Simultaneous Quantification of Gram-Negative Bacteria and Nitrite Ions in Water Samples. ACS Sens [Internet]. 2023 Nov

24 [cited 2025 Jan 31];8(11):4364–73. Available from: https://pubs.acs.org/doi/full/10.1021/acssensors.3c01769

81. Srisomwat C, Bawornnithichaiyakul N, Khonyoung S, Tiyapongpattana W, Butcha S, Youngvises N, et al. Unveiling the potential of the capillary-driven microfluidic paper-based device integrated with smartphone-based for simultaneously colorimetric salivary ethanol and △9-tetrahydrocannabinol analysis. Talanta. 2024 Dec 1;280:126770.
82. Li W, Zhang X, Miao C, Li R, Ji Y. Fluorescent paper–based sensor based on carbon dots for detection of folic acid. Anal Bioanal Chem [Internet]. 2020 May 1 [cited 2025 Feb 3];412(12):2805–13. Available from: https://link.springer.com/article/10.1007/s00216-020-02507-w
83. Ortiz-Gómez I, Toral-López V, Romero FJ, de Orbe-Payá I, García A, Rodríguez N, et al. In situ synthesis of fluorescent silicon nanodots for determination of total carbohydrates in a paper microfluidic device combined with laser prepared graphene heater. Sens Actuators B Chem. 2021 Apr 1;332:129506.
84. Jin C, Yang S, Zheng J, Chai F, Tian M. Smartphone-assisted portable paper-based biosensors for rapid and sensitive detection of biomarkers in urine. Microchemical Journal. 2024 Sep 1;204:110982.
85. Song K, Liu C, Chen G, Zhao W, Tian S, Zhou Q. Paper-based ratiometric fluorescent sensing platform based on mixed quantum dots for the detection of glucose in urine. RSC Adv [Internet]. 2024 Jan 2 [cited 2025 Jan 31];14(2):1207–15. Available from: https://pubs.rsc.org/en/content/articlehtml/2024/ra/d3ra07082d
86. Safiabadi Tali SH, Hajimiri H, Sadiq Z, Jahanshahi-Anbuhi S. Engineered detection zone to enhance color uniformity on paper microfluidics fabricated via Parafilm®-heating-laser-cutting. Sens Actuators B Chem. 2023 Apr 1;380:133324.
87. He Y, Wang P, Chen X, Li Y, Wei J, Cai G, et al. Facile preparation of Fe3O4@Pt nanoparticles as peroxidase mimics for sensitive glucose detection by a paper-based colorimetric assay. R Soc Open Sci [Internet]. 2022 Sep 28 [cited 2025 Jan 31];9(9). Available from: https://royalsocietypublishing.org/doi/10.1098/rsos.220484
88. Feng LX, Tang C, Han XX, Zhang HC, Guo FN, Yang T, et al. Simultaneous and sensitive detection of multiple small biological molecules by microfluidic paper-based analytical device integrated with zinc oxide nanorods. Talanta. 2021 Sep 1;232:122499.
89. Manbohi A, Ahmadi SH. Chitosan–Fe3O4 nanoparticle enzymatic electrodes on paper as an efficient assay for glucose and uric acid detection in biological fluids. Chemical Papers [Internet]. 2020 Aug 1 [cited 2025 Feb 3];74(8):2675–87. Available from: https://link.springer.com/article/10.1007/s11696-020-01105-5
90. Santana-Jiménez LA, Márquez-Lucero A, Osuna V, Estrada-Moreno I, Dominguez RB. Naked-Eye Detection of Glucose in Saliva with Bienzymatic Paper-Based Sensor. Sensors 2018, Vol 18, Page 1071 [Internet]. 2018 Apr 3 [cited 2025 Feb 3];18(4):1071. Available from: https://www.mdpi.com/1424-8220/18/4/1071/htm

91. Yao Y, Zhang C. A novel screen-printed microfluidic paper-based electrochemical device for detection of glucose and uric acid in urine. Biomed Microdevices [Internet]. 2016 Oct 1 [cited 2025 Feb 3];18(5):1–9. Available from: https://link.springer.com/article/10.1007/s10544-016-0115-6
92. Cai L, Xu C, Lin SH, Luo J, Wu M, Yang F. A simple paper-based sensor fabricated by selective wet etching of silanized filter paper using a paper mask. Biomicrofluidics [Internet]. 2014 Oct 9 [cited 2025 Feb 3];8(5). Available from: /aip/bmf/article/8/5/056504/386118/A-simple-paper-based-sensor-fabricated-by
93. Rahbar M, Zou S, Baharfar M, Liu G. A customized microfluidic paper-based platform for colorimetric immunosensing: Demonstrated via hcg assay for pregnancy test. Biosensors (Basel) [Internet]. 2021 Dec 1 [cited 2025 Jan 31];11(12):474. Available from: https://www.mdpi.com/2079-6374/11/12/474/htm
94. Razavi F, Khajehsharifi H. Paper-based electrochemical sensor with a commercial glucose meter to determine L-cysteine by graphene electrode and Ag-doped silica nanoporous SBA-16. Journal of the Iranian Chemical Society [Internet]. 2022 Nov 1 [cited 2025 Jan 31];19(11):4349–57. Available from: https://link.springer.com/article/10.1007/s13738-022-02596-7
95. Wang W, Ding S, Wang Z, Lv Q, Zhang Q. Electrochemical paper-based microfluidic device for on-line isolation of proteins and direct detection of lead in urine. Biosens Bioelectron. 2021 Sep 1;187:113310.
96. Tseng WT, Tseng HY, Chou YY, Wang YC, Tseng TN, Ho LI, et al. Quantitative urinary tract infection diagnosis of leukocyte esterase with a microfluidic paper-based device. Dalton Transactions [Internet]. 2021 Jul 13 [cited 2025 Feb 3];50(27):9417–25. Available from: https://pubs.rsc.org/en/content/articlehtml/2021/dt/d1dt01541a
97. Fakhri N, Abarghoei S, Dadmehr M, Hosseini M, Sabahi H, Ganjali MR. Paper based colorimetric detection of miRNA-21 using Ag/Pt nanoclusters. Spectrochim Acta A Mol Biomol Spectrosc. 2020 Feb 15;227:117529.
98. Sun B, Wang Z, Wang X, Qiu M, Zhang Z, Wang Z, et al. Paper-based biosensor based on phenylalnine ammonia lyase hybrid nanoflowers for urinary phenylalanine measurement. Int J Biol Macromol. 2021 Jan 1;166:601–10.
99. Amatatongchai M, Sitanurak J, Sroysee W, Sodanat S, Chairam S, Jarujamrus P, et al. Highly sensitive and selective electrochemical paper-based device using a graphite screen-printed electrode modified with molecularly imprinted polymers coated Fe3O4@Au@SiO2 for serotonin determination. Anal Chim Acta. 2019 Oct 24;1077:255–65.
100. Pena-Pereira F, Lavilla I, Bendicho C. Paper-based analytical device for instrumental-free detection of thiocyanate in saliva as a biomarker of tobacco smoke exposure. Talanta. 2016 Jan 15;147:390–6.
101. Zhang WY, Zhang CY, Zhou HY, Tian T, Chen H, Zhang H, et al. Paper-based sensor depending on the Prussian blue pH sensitivity: Smartphone-assisted detection of urea. Microchemical Journal. 2022 Oct 1;181:107783.

102. Tong X, Li G, Guo Q, Hu J, Zhang B, Liu S, et al. Fe/Pt-doped carbon nanoparticles with peroxidase-like activity for point-of-care determination of uric acid. Microchimica Acta [Internet]. 2025 Jan 1 [cited 2025 Jan 30];192(1):1–10. Available from: https://link.springer.com/article/10.1007/s00604-024-06861-9
103. Wang W, Ding SN, Chen FF, Zhang Q. Electrochemical paper-based analytical device for flow injection analysis based on locally enhanced evaporation. Sens Actuators B Chem. 2022 Nov 15;371:132517.
104. University of Rochester Medical Center. Creatinine (Urine) [Internet]. [cited 2025 Feb 8]. Available from: https://www.urmc.rochester.edu/encyclopedia/content?contenttypeid=167&contentid=creatinine_urine
105. MedlinePlus. Glucose in Urine Test [Internet]. [cited 2025 Feb 8]. Available from: https://medlineplus.gov/lab-tests/glucose-in-urine-test/
106. University of Rochester Medical Center. Uric Acid (Urine) [Internet]. [cited 2025 Feb 8]. Available from: https://www.urmc.rochester.edu/encyclopedia/content?ContentTypeID=167&ContentID=uric_acid_urine
107. Wiegand A, Batista GR, Torres CRG, Sener B, Attin T. Artificial Saliva Formulations versus Human Saliva Pretreatment in Dental Erosion Experiments. Caries Res. 2016;50(1):78–86.
108. Machado A, Mesquita RBR, Oliveira S, Bordalo AA. Development of a robust, fast screening method for the potentiometric determination of iodide in urine and salt samples. Talanta [Internet]. 2017;167(January):688–94. Available from: http://dx.doi.org/10.1016/j.talanta.2017.03.017
109. Currie LA. Nomenclature in Evaluation of Analytical Methods Including Detection and Quantification Capabilities. International Union of Pure and Applied Chemistry. 1995;67(10):1699–723.
110. Miller JC, Miller JN. Statistics for Analytical Chemistry. 3rd ed. New York: Ellis Horwood PTR Prentice Hall; 1993.
111. Burns DT, Danzer K, Townshend A. Use of the term “recovery” and “apparent recovery” in analytical procedures (IUPAC Recommendations 2002). Pure and Applied Chemistry [Internet]. 2002 Jan 1;74(11):2201–5. Available from: http://www.degruyter.com/view/j/pac.2002.74.issue-11/pac200274112201/pac200274112201.xml
112. Linus Pauling Institute | Oregon State University. Iron [Internet]. [cited 2020 Sep 7]. Available from: https://lpi.oregonstate.edu/mic/minerals/iron
113. Nakatani S, Nakatani A, Ishimura E, Toi N, Tsuda A, Mori K, et al. Urinary Iron Excretion is Associated with Urinary Full-Length Megalin and Renal Oxidative Stress in Chronic Kidney Disease. Kidney Blood Press Res [Internet]. 2018 Jun 1 [cited 2025 Feb 14];43(2):458–70. Available from: https://dx.doi.org/10.1159/000488470

114. Marshfield Labs. Iron, Urine [Internet]. [cited 2020 Sep 7]. Available from: https:// www. marsh field labs. org/ sites/ ltrm/ Human/ Pages/ 22804. aspx
115. Iron, Urine [Internet]. [cited 2020 Sep 17]. Available from: http:// www.labnet.health.nz/testmanager/index. php?fuseaction=main.DisplayTest&testid=284
116. NMS Labs. Iron, Urine [Internet]. [cited 2020 Sep 17]. Available from: https://www.nmslabs.com/tests/iron-urine-2430u
117. Yiannikourides A, Latunde-Dada GO. A Short Review of Iron Metabolism and Pathophysiology of Iron Disorders. Medicines 2019, Vol 6, Page 85 [Internet]. 2019 Aug 5 [cited 2025 Feb 14];6(3):85. Available from: https://www.mdpi.com/2305-6320/6/3/85/htm
118. Ems T, Lucia KS, Huecker MR. Biochemistry, Iron Absorption. StatPearls [Internet]. 2023 Apr 17; Available from: https://www.ncbi.nlm.nih.gov/books/NBK448204/
119. Moniz T, Bassett CR, Almeida MIGS, Kolev SD, Rangel M, Mesquita RBR. Use of an ether-derived 3-hydroxy-4-pyridinone chelator as a new chromogenic reagent in the development of a microfluidic paper-based analytical device for Fe(III) determination in natural waters. Talanta. 2020 Jul 1;214:120887.
120. Ogawa K, Kaneta T. Determination of iron ion in the water of a natural hot spring using microfluidic paper-based analytical devices. Analytical Sciences [Internet]. 2016 Jan 10 [cited 2025 Feb 14];32(1):31–4. Available from: https://link.springer.com/article/10.2116/analsci.32.31
121. Shrivas K, Monisha, Kant T, Karbhal I, Kurrey R, Sahu B, et al. Smartphone coupled with paper-based chemical sensor for on-site determination of iron(III) in environmental and biological samples. Anal Bioanal Chem [Internet]. 2020 Mar 1 [cited 2025 Feb 14];412(7):1573–83. Available from: https://link.springer.com/article/10.1007/s00216-019-02385-x
122. Hirayama T, Nagasawa H. Chemical tools for detecting Fe ions. J Clin Biochem Nutr. 2017 Jan 1;60(1):39–48.
123. Marczenko Z, Balcerzak M. Separation, preconcentration, and spectrophotometry in inorganic analysis, Volume 10. Kloczko E, editor. 2000;3–521.
124. APHA, AWWA, WEF. Standard Methods for the Examination of Water and Wastewater. 20th ed. Washington, DC; 1998.
125. Santos IC, Mesquita RBR, Bordalo AA, Rangel AOSS. Iodine speciation in coastal and inland bathing waters and seaweeds extracts using a sequential injection standard addition flow-batch method. Talanta. 2015 Feb 1;133:7–14.
126. Nitrites in Urine: Causes, Symptoms, and Treatments [Internet]. [cited 2021 Sep 13]. Available from: https://www.healthline.com/health/nitrites-in-urine
127. Zhang P, Lee J, Kang G, Li Y, Yang D, Pang B, et al. Disparity of nitrate and nitrite in vivo in cancer villages as compared to other areas in Huai River Basin, China. Science of The Total Environment. 2018 Jan 15;612:966–74.
128. Zhang XX, Song YZ, Fang F, Wu ZY. Sensitive paper-based analytical device for fast colorimetric detection of nitrite with smartphone. Anal Bioanal Chem [Internet]. 2018 Apr 1

[cited 2025 Feb 14];410(11):2665–9. Available from: https://link.springer.com/article/10.1007/s00216-018-0965-2

129. Healthline. Methemoglobinemia: Causes, Diagnosis, and Treatment [Internet]. [cited 2021 Sep 13]. Available from: https://www.healthline.com/health/methemoglobinemia
130. MedlinePlus. Nitrites in Urine: MedlinePlus Medical Test [Internet]. [cited 2021 Sep 13]. Available from: https://medlineplus.gov/lab-tests/nitrites-in-urine/
131. Hooda V, Sachdeva V, Chauhan N. Nitrate quantification: Recent insights into enzyme-based methods. Rev Anal Chem [Internet]. 2016 Sep 1 [cited 2025 Feb 14];35(3):99–114. Available from: https://www.degruyter.com/document/doi/10.1515/revac-2016-0002/html
132. Campbell WH. Nitrate reductase structure, function and regulation: Bridging the gap between biochemistry and physiology. Annu Rev Plant Biol [Internet]. 1999 Jun 1 [cited 2025 Feb 14];50(Volume 50, 1999):277–303. Available from: https://www.annualreviews.org/content/journals/10.1146/annurev.arplant.50.1.277
133. Teixeira CFCP, Segundo RLA, Rangel AOSS, Mesquita RBR, Ferreira MTSOB, Bordalo AA. Development of a sequential injection system for the determination of nitrite and nitrate in waters with different salinity: Application to estuaries in NW Portugal. Analytical Methods. 2009;1(3):195–202.
134. Nadar SS, Patil PD, Tiwari MS, Ahirrao DJ. Enzyme embedded microfluidic paper-based analytic device (μPAD): a comprehensive review. Crit Rev Biotechnol [Internet]. 2021;0(0):1–39. Available from: https://doi.org/10.1080/07388551.2021.1898327
135. Jayawardane BM, Wei S, McKelvie ID, Kolev SD. Microfluidic Paper-Based Analytical Device for the Determination of Nitrite and Nitrate. Anal Chem [Internet]. 2014 Aug 5 [cited 2018 Jun 20];86(15):7274–9. Available from: http://pubs.acs.org/doi/10.1021/ac5013249
136. Teepoo S, Arsawiset S, Chanayota P. One-Step Polylactic Acid Screen-Printing Microfluidic Paper-Based Analytical Device: Application for Simultaneous Detection of Nitrite and Nitrate in Food Samples. Chemosensors. 2019;7(3):44.
137. Thongkam T, Hemavibool K. An environmentally friendly microfluidic paper-based analytical device for simultaneous colorimetric detection of nitrite and nitrate in food products. Microchemical Journal [Internet]. 2020;159(May):105412. Available from: https://doi.org/10.1016/j.microc.2020.105412
138. CDC - Center for Disease Control and Prevention. Chronic Kidney Disease Basics [Internet]. [cited 2024 Feb 6]. Available from: https://www.cdc.gov/kidneydisease/basics.html
139. Lasisi TJ, Raji YR, Salako BL. Salivary creatinine and urea analysis in patients with chronic kidney disease: A case control study. BMC Nephrol [Internet]. 2016 Jan 16 [cited 2022 Mar 21];17(1):1–6. Available from: https://bmcnephrol.biomedcentral.com/articles/10.1186/s12882-016-0222-x
140. Smith D, Siemens Healthineers. Chronic Kidney Disease: A Global Crisis [Internet]. 2018 [cited 2022 Mar 21]. Available from: https://www.siemens-healthineers.com/pt/news/chronic-kidney-disease.html

141. Carney EF. The impact of chronic kidney disease on global health. Nature Reviews Nephrology 2020 16:5 [Internet]. 2020 Mar 6 [cited 2022 Mar 21];16(5):251–251. Available from: https://www.nature.com/articles/s41581-020-0268-7
142. Weiner ID, Mitch WE, Sands JM. Urea and Ammonia Metabolism and the Control of Renal Nitrogen Excretion. Clin J Am Soc Nephrol [Internet]. 2015 Aug 7 [cited 2022 Mar 21];10(8):1444. Available from: /pmc/articles/PMC4527031/
143. Barmore W, Azad F, Stone WL. Physiology, Urea Cycle. StatPearls [Internet]. 2021 May 19 [cited 2022 Mar 21]; Available from: https://www.ncbi.nlm.nih.gov/books/NBK513323/
144. Pundir CS, Jakhar S, Narwal V. Determination of urea with special emphasis on biosensors: A review. Biosens Bioelectron [Internet]. 2019;123(July 2018):36–50. Available from: https://doi.org/10.1016/j.bios.2018.09.067
145. Sheini A. A paper-based device for the colorimetric determination of ammonia and carbon dioxide using thiomalic acid and maltol functionalized silver nanoparticles: application to the enzymatic determination of urea in saliva and blood. Microchimica Acta. 2020;187(10).
146. Choi CK, Shaban SM, Moon BS, Pyun DG, Kim DH. Smartphone-assisted point-of-care colorimetric biosensor for the detection of urea via pH-mediated AgNPs growth. Anal Chim Acta [Internet]. 2021;1170:338630. Available from: https://doi.org/10.1016/j.aca.2021.338630
147. Wang KH, Hsieh JC, Chen CC, Zan HW, Meng HF, Kuo SY, et al. A low-cost, portable and easy-operated salivary urea sensor for point-of-care application. Biosens Bioelectron. 2019;132(December 2018):352–9.
148. Bagalad BS, Mohankumar KP, Madhushankari GS, Donoghue M, Kuberappa PH. Diagnostic accuracy of salivary creatinine, urea, and potassium levels to assess dialysis need in renal failure patients. Dent Res J (Isfahan). 2017;14(1):13–8.
149. Thepchuay Y, Costa CFA, Mesquita RBR, Sampaio-Maia B, Nacapricha D, Rangel AOSS. Flow-based method for the determination of biomarkers urea and ammoniacal nitrogen in saliva. Bioanalysis. 2020;12(7):455–65.
150. Zhang H, Yang FQ. Equipment-free quantitative determination of urea based on paper-based sensor via urease-mediated chitosan viscosity change. Enzyme Microb Technol. 2021 Aug 1;148:109830.
151. Soni A, Surana RK, Jha SK. Smartphone based optical biosensor for the detection of urea in saliva. Sens Actuators B Chem. 2018 Sep 15;269:346–53.
152. Ferreira FTSM, Mesquita RBR, Rangel AOSS. On-hand tool for ammonium and urea determination in saliva to monitor chronic kidney disease – Design of a couple of microfluidic paper-based devices. Microchemical Journal [Internet]. 2023 Jul;109102. Available from: https://linkinghub.elsevier.com/retrieve/pii/S0026265X2300721X
153. Kovesdy CP. Epidemiology of chronic kidney disease: an update 2022. Kidney Int Suppl (2011). 2022 Apr;12(1):7–11.
154. Costa CFFA, Merino-Ribas A, Ferreira C, Campos C, Silva N, Pereira L, et al. Characterization of Oral Enterobacteriaceae Prevalence and Resistance Profile in Chronic

Kidney Disease Patients Undergoing Peritoneal Dialysis. Front Microbiol. 2021;12(December).

155. Fresenius Kidney Care. What is Ammonia Breath and Is It a Symptom of CKD? [Internet]. [cited 2024 Feb 8]. Available from: https://www.freseniuskidneycare.com/thrive-central/ammonia-breath
156. Chang Y, Park TE, Lee SW, Lee EH. Colorimetric Detection of Urease-Producing Microbes Using an Ammonia-Responsive Flexible Film Sensor. Biosensors (Basel). 2022;12(10).
157. Tavares MC, Oliveira KA, de Fátima Â, Coltro WKT, Santos JCC. Paper-based analytical device with colorimetric detection for urease activity determination in soils and evaluation of potential inhibitors. Talanta. 2021 Aug;230:122301.
158. Khachornsakkul K, Rybicki FJ, Sonkusale S. Nanomaterials integrated with microfluidic paper-based analytical devices for enzyme-free glucose quantification. Talanta. 2023 Aug 1;260:124538.
159. Zheng J, Zhu M, Kong J, Li Z, Jiang J, Xi Y, et al. Microfluidic paper-based analytical device by using Pt nanoparticles as highly active peroxidase mimic for simultaneous detection of glucose and uric acid with use of a smartphone. Talanta. 2022 Jan 15;237:122954.
160. Mitra S, Basak M, Biswas S, Gooh Pattader PS. Digital electronic based portable device for colorimetric quantification of ketones and glucose level in human urine. Measurement. 2023 Jun 15;214:112848.
161. Sreeranjit CVK, Lal JJ. GLUCOSE | Properties and Analysis. Encyclopedia of Food Sciences and Nutrition. 2003 Jan 1;2898–903.
162. Miller GL. Use of Dinitrosalicylic Acid Reagent for Determination of Reducing Sugar. Anal Chem [Internet]. 1959 Mar 1 [cited 2024 Aug 12];31(3):426–8. Available from: https://pubs.acs.org/doi/abs/10.1021/ac60147a030
163. Enzymatic Assay: Glucose Oxidase [Internet]. [cited 2024 Aug 12]. Available from: https://www.sigmaaldrich.com/PT/en/technical-documents/protocol/protein-biology/enzyme-activity-assays/enzymatic-assay-of-glucose-oxidase?srsltid=AfmBOoo-Q_WJKeK8L5aEi3KermaN-7_fHwAxLF00I59CZ3kcgM_ZDLaq
164. Chiang CK, Kurniawan A, Kao CY, Wang MJ. Single step and mask-free 3D wax printing of microfluidic paper-based analytical devices for glucose and nitrite assays. Talanta [Internet]. 2019 Mar;194(October 2018):837–45. Available from: https://doi.org/10.1016/j.talanta.2018.10.104
165. Jang J, Hur HG, Sadowsky MJ, Byappanahalli MN, Yan T, Ishii S. Environmental Escherichia coli: ecology and public health implications—a review. J Appl Microbiol [Internet]. 2017 Sep 1 [cited 2024 Jul 23];123(3):570–81. Available from: https://onlinelibrary.wiley.com/doi/full/10.1111/jam.13468
166. Onyeaka HN, Nwabor OF. Microbial food contamination and foodborne diseases. Food Preservation and Safety of Natural Products. 2022 Jan 1;19–37.

167. Basavaraju M, Gunashree BS, Basavaraju M, Gunashree BS. Escherichia coli: An Overview of Main Characteristics. Escherichia coli - Old and New Insights [Internet]. 2022 Nov 11 [cited 2024 Jul 23]; Available from: https://www.intechopen.com/chapters/84764
168. Nataro JP, Kaper JB. Diarrheagenic Escherichia coli. Clin Microbiol Rev [Internet]. 1998 [cited 2024 Sep 5];11(1):142–201. Available from: https://journals.asm.org/doi/10.1128/cmr.11.1.142
169. Kaper JB, Nataro JP, Mobley HLT. Pathogenic Escherichia coli. Nature Reviews Microbiology 2004 2:2 [Internet]. 2004 Feb [cited 2024 Sep 5];2(2):123–40. Available from: https://www.nature.com/articles/nrmicro818
170. Offenbaume KL, Bertone E, Stewart RA. Monitoring Approaches for Faecal Indicator Bacteria in Water: Visioning a Remote Real-Time Sensor for E. coli and Enterococci. Water 2020, Vol 12, Page 2591 [Internet]. 2020 Sep 16 [cited 2024 Sep 5];12(9):2591. Available from: https://www.mdpi.com/2073-4441/12/9/2591/htm
171. Lewis L. E. Coli - Health Implications in Recreational and Drinking Water [Internet]. [cited 2024 Jul 23]. Available from: https://thewaterproject.org/water-scarcity/health-implications-of-e-coli
172. Directive - 2006/7 - EN - EUR-Lex [Internet]. [cited 2024 Sep 11]. Available from: https://eur-lex.europa.eu/eli/dir/2006/7/oj
173. Directive - 2020/2184 - EN - EUR-Lex [Internet]. [cited 2024 Sep 11]. Available from: https://eur-lex.europa.eu/eli/dir/2020/2184/oj
174. Carlos C, Pires MM, Stoppe NC, Hachich EM, Sato MIZ, Gomes TAT, et al. Escherichia coli phylogenetic group determination and its application in the identification of the major animal source of fecal contamination. BMC Microbiol [Internet]. 2010 Jun 1 [cited 2024 Sep 5];10(1):1–10. Available from: https://bmcmicrobiol.biomedcentral.com/articles/10.1186/1471-2180-10-161
175. Cassini A, Högberg LD, Plachouras D, Quattrocchi A, Hoxha A, Simonsen GS, et al. Attributable deaths and disability-adjusted life-years caused by infections with antibiotic-resistant bacteria in the EU and the European Economic Area in 2015: a population-level modelling analysis. Lancet Infect Dis [Internet]. 2019 Jan 1 [cited 2024 Sep 11];19(1):56–66. Available from: http://www.thelancet.com/article/S1473309918306054/fulltext
176. World Health Organization. Prioritization of pathogens to guide discovery, research and development of new antibiotics for drug-resistant bacterial infections, including tuberculosis [Internet]. 2017 [cited 2024 Sep 11]. Available from: https://iris.who.int/handle/10665/311820
177. Foo PC, Nurul Najian AB, Muhamad NA, Ahamad M, Mohamed M, Yean Yean C, et al. Loop-mediated isothermal amplification (LAMP) reaction as viable PCR substitute for diagnostic applications: A comparative analysis study of LAMP, conventional PCR, nested PCR (nPCR) and real-time PCR (qPCR) based on Entamoeba histolytica DNA derived from faecal sample. BMC Biotechnol [Internet]. 2020 Jun 22 [cited 2024 Jul 23];20(1):1–15. Available from: https://bmcbiotechnol.biomedcentral.com/articles/10.1186/s12896-020-00629-8

178. Panno S, Matić S, Tiberini A, Caruso AG, Bella P, Torta L, et al. Loop Mediated Isothermal Amplification: Principles and Applications in Plant Virology. Plants 2020, Vol 9, Page 461 [Internet]. 2020 Apr 6 [cited 2024 Jul 23];9(4):461. Available from: https://www.mdpi.com/2223-7747/9/4/461/htm

179. Notomi T, Okayama H, Masubuchi H, Yonekawa T, Watanabe K, Amino N, et al. Loop-mediated isothermal amplification of DNA. Nucleic Acids Res [Internet]. 2000 Jun 15 [cited 2024 Jul 23];28(12):e63–e63. Available from: https://dx.doi.org/10.1093/nar/28.12.e63

180. Witkowska McConnell W, Davis C, Sabir SR, Garrett A, Bradley-Stewart A, Jajesniak P, et al. Paper microfluidic implementation of loop mediated isothermal amplification for early diagnosis of hepatitis C virus. Nature Communications 2021 12:1 [Internet]. 2021 Nov 30 [cited 2024 Jul 23];12(1):1–8. Available from: https://www.nature.com/articles/s41467-021-27076-z

181. Xu G, Gunson RN, Cooper JM, Reboud J. Rapid ultrasonic isothermal amplification of DNA with multiplexed melting analysis – applications in the clinical diagnosis of sexually transmitted diseases. Chemical Communications [Internet]. 2015 Jan 29 [cited 2024 Jul 24];51(13):2589–92. Available from: https://pubs.rsc.org/en/content/articlehtml/2015/cc/c4cc08389j

182. Loop-Mediated Isothermal Amplification | NEB [Internet]. [cited 2024 Jul 24]. Available from: https://www.neb.com/en/applications/dna-amplification-pcr-and-qpcr/isothermal-amplification/loop-mediated-isothermal-amplification-lamp

183. Saifuddin SA, Rashid R, Nor Azmi NJ, Mohamad S. Colorimetric strategies applicable for loop-mediated isothermal amplification. J Microbiol Methods. 2024 Aug 1;223:106981.

184. Warmt C, Nagaba J, Henkel J. Comparison of pre-labelled primers and nucleotides as DNA labelling method for lateral flow detection of Legionella pneumophila amplicons. Scientific Reports 2024 14:1 [Internet]. 2024 Feb 29 [cited 2024 Jul 24];14(1):1–11. Available from: https://www.nature.com/articles/s41598-024-55703-4

185. Hill J, Beriwal S, Chandra I, Paul VK, Kapil A, Singh T, et al. Loop-mediated isothermal amplification assay for rapid detection of common strains of Escherichia coli. J Clin Microbiol [Internet]. 2008 Aug [cited 2025 Jan 18];46(8):2800–4. Available from: https://journals.asm.org/doi/10.1128/jcm.00152-08

186. Optigene. LAMP User Guide-Assay Design & Primers [Internet]. 17AD [cited 2025 Jan 18]. Available from: https://www.optigene.co.uk/wp-content/uploads/2012/06/OptiGene-LAMP-User-Guide-Assay-Design-Primers-1.pdf

Appendix

Appendix A – Web of Science Search Parameters

Searches:

1: "microfluidic paper-based analytical device" (All Fields) Date Run: Thu Jan 30 2025 15:19:35 GMT+0000 (Western European Standard Time) Results: 399

2: "microfluidic paper-based device" (All Fields) Date Run: Thu Jan 30 2025 15:19:48 GMT+0000 (Western European Standard Time) Results: 68

3: "paper-based device" (All Fields) Date Run: Thu Jan 30 2025 15:20:32 GMT+0000 (Western European Standard Time) Results: 612

4: "paper-based biosensor" (All Fields) Date Run: Thu Jan 30 2025 15:20:42 GMT+0000 (Western European Standard Time) Results: 166

5: "paper-based sensor" (All Fields) Date Run: Thu Jan 30 2025 15:20:50 GMT+0000 (Western European Standard Time) Results: 626

6: #5 OR #4 OR #3 OR #2 OR #1 Date Run: Thu Jan 30 2025 15:21:46 GMT+0000 (Western European Standard Time) Results: 1695

7: "non invasive sample" (All Fields) Date Run: Thu Jan 30 2025 15:23:45 GMT+0000 (Western European Standard Time) Results: 180

8: "non invasive samples" (All Fields) Date Run: Thu Jan 30 2025 15:23:50 GMT+0000 (Western European Standard Time) Results: 292

9: "non invasive collection samples" (All Fields) Date Run: Thu Jan 30 2025 15:23:57 GMT+0000 (Western European Standard Time) Results: 0

10: "non invasive collection sample" (All Fields) Date Run: Thu Jan 30 2025 15:24:03 GMT+0000 (Western European Standard Time) Results: 0

11: "saliva sample" (All Fields) Date Run: Thu Jan 30 2025 15:24:14 GMT+0000 (Western European Standard Time) Results: 1101

12: "saliva samples" (All Fields) Date Run: Thu Jan 30 2025 15:24:18 GMT+0000 (Western European Standard Time) Results: 10583

13: "urine samples" (All Fields) Date Run: Thu Jan 30 2025 15:24:30 GMT+0000 (Western European Standard Time) Results: 46808

14: "urine sample" (All Fields) Date Run: Thu Jan 30 2025 15:24:35 GMT+0000 (Western European Standard Time) Results: 6904

15: "sample of urine" (All Fields) Date Run: Thu Jan 30 2025 15:24:43 GMT+0000 (Western European Standard Time) Results: 166

16: "samples of urine" (All Fields) Date Run: Thu Jan 30 2025 15:24:48 GMT+0000 (Western European Standard Time) Results: 644

17: "samples of saliva" (All Fields) Date Run: Thu Jan 30 2025 15:24:54 GMT+0000 (Western European Standard Time) Results: 310

18: "sample of saliva" (All Fields) Date Run: Thu Jan 30 2025 15:24:57 GMT+0000 (Western European Standard Time) Results: 49

19: #18 OR #17 OR #16 OR #15 OR #14 OR #13 OR #12 OR #11 OR #10 OR #9 OR #8 OR #7 Date Run: Thu Jan 30 2025 15:25:53 GMT+0000 (Western European Standard Time) Results: 63945

20: #6 AND #19 Date Run: Thu Jan 30 2025 15:26:06 GMT+0000 (Western European Standard Time) Results: 75

Appendix B – Whatman Filter Paper Characteristics

Treatment	*Grade*	*Particle Retention Liquid (µm)*	*Typical Thickness (µm)*
Qualitative	1	11	180
	3	6	390
	4	20-25	205
	5	2.5	200
Ashless Quantitative	40	8	210
	41	20-25	215
	42	2.5	200
Hardened Low Ash Quantitative	50	2.7	115
	52	7	175
	54	20-25	185
Hardened Ashless Quantitative	540	8	160
	541	20-25	155
	542	2.7	150